UNIVERSITY OF LONDON THESIS

Degree PhD Year 2007 Name of Author JULIA LOUISE PENDRED

COPYRIGHT

This is a thesis accepted for a Higher Degree of the University of London. It is an unpublished typescript and the copyright is held by the author. All persons consulting the thesis must read and abide by the Copyright Declaration below.

COPYRIGHT DECLARATION

I recognise that the copyright of the above-described thesis rests with the author and that no quotation from it or information derived from it may be published without the prior written consent of the author.

LOAN

Theses may not be lent to individuals, but the University Library may lend a copy to approved libraries within the United Kingdom, for consultation solely on the premises of those libraries. Application should be made to: The Theses Section, University of London Library, Senate House, Malet Street, London WC1E 7HU.

REPRODUCTION

University of London theses may not be reproduced without explicit written permission from the University of London Library. Enquiries should be addressed to the Theses Section of the Library. Regulations concerning reproduction vary according to the date of acceptance of the thesis and are listed below as guidelines.

A. Before 1962. Permission granted only upon the prior written consent of the author. (The University Library will provide addresses where possible).

B. 1962 - 1974. In many cases the author has agreed to permit copying upon completion of a Copyright Declaration.

C. 1975 - 1988. Most theses may be copied upon completion of a Copyright Declaration.

D. 1989 onwards. Most theses may be copied.

This thesis comes within category D.

☐ This copy has been deposited in the Library of UCL

☐ This copy has been deposited in the University of London Library, Senate House, Malet Street, London WC1E 7HU.

A SCREEN FOR GENES REGULATING NEUROBLAST ACTIVITY IN *DROSOPHILA*

Julia Pendred

A thesis submitted to University of London for the degree of Doctor of Philosophy

Division of Developmental Neurobiology
NIMR
London

June 2007

ProQuest LLC
789 East Eisenhower Parkway
P.O. Box 1346
Ann Arbor, MI 48106-1346

PREFACE

The research reported in this thesis was carried out in the Division of Developmental Neurobiology at the MRC National Institute for Medical Research (Mill Hill, London), under the supervision of Dr. Alex Gould. This thesis describes my own original work, except for figure panels 3.1BC, 3.2B, D & F and 3.3B, D & E, provided by C. Maurange and 4.3AB, provided by Justine Oyallon

The genetic screen was initiated in collaboration with the William Chia laboratory at Temasek Lifesciences, National University of Singapore and Cédric Maurange, Louise Cheng and Jennifer Grant in Alex Gould's laboratory at NIMR. I screened 1500 lines from a total of 4200 lines.

ACKNOWLEDGMENTS

I would like to thank several people for their help and support during the course of my PhD. Firstly, my supervisor, Alex Gould, who has been an ongoing source of inspiration and support through both exciting and difficult times. I thank him for the time he has given me, his guidance, advise, enthusiasm, patience and understanding. He has been a great supervisor.

I would also like to thank members of my lab.: Caterina, for her technical support at the beginning of my PhD. Cedric and Louise for their support, advise and enthusiasm both during and after the Screen. Also, Patricia, the "mother" of the lab, Fabrice, Jenny and Irene for creating a good atmosphere in the lab. Most importantly, I would like to thank Keno, who has been a good mentor and very good friend. His smile and ludicrousness carried me through some difficult times.

I would also like to thank the whole "fly community" at NIMR, in particular Iris Salecker for her support and advise, JP Vincent and Eugenia, for their stimulating conversation and finally Justine, PLuc and Xavi for their entertainment. In addition I thank Jose Casals and Peter Lawrence for their advise and assistance with Figure 5.18.

Finally, I must thank my good friends at NIMR; Pete, Katie, Kathrin and Yung, who have given me limitless encouragement, compassion, love and support during my PhD. I must also thank my flat mates; Mel, Ben and Nick for understanding my antisocial behaviour in the last couple of years. I am also thankful for my old friends, who have stood by me through a challenging time and never forgotten me: Tilly, Paul, Omar, Chree, Bob, Matt, Hywel, Kate and Dips. Also, Al, Nial, Dodge, Reena, Phil and my London Buddy. Finally, Finally, the people who made my PhD possible.....My Family. Unarguably, the most supportive, loving and kind family anyone could wish for: My brothers, Jami and Roie, and my parents. They are my best friends.

For My Parents

ABSTRACT

Following embryogenesis, the morphology of the CNS becomes dramatically remodelled to reflect the different locomotive and sensory requirements of the adult relative to the larva. This is largely achieved through the varying spatio-temporal proliferation patterns of the neural stem cell-like precursors (termed postembryonic neuroblasts: pNBs). Although both NB-autonomous and non-cell autonomous mechanisms have been identified, relatively few factors controlling this process are known. My studies focus on using genetic screening to identify new genes involved in this process.

I executed two genetic screens, which were designed to complement each others limitations. The first of these involved screening using Mosaic Analysis with a Repressible Cell Marker (MARCM), to identify embryonic-lethal mutations that act in a cell-autonomous manner to produce under- or over-sized pNB clones. The second screen focused on the rarer class of pupal-lethal mutation, where homozygous mutant larvae were screened for abnormal morphology of the CNS. In total, we screened 4200 mutagenised lines on chromosome III, recovering 82 mutants with interesting phenotypes; 68 from the MARCM screen and 14 from the pupal-lethal screen. These were divided into 69 complementation groups, 9 of which contained multiple alleles. These groups were subdivided into phenotypic classes, with 9 distinct classes recovered from the MARCM screen and 2 from the pupal-lethal screen. These were sub-categorised into CNS-specific or non-CNS specific, according to the absence or presence of a phenotype in the eye disc.

I initially focused my studies on 9 of the pupal-lethal mutations, 5 of which I successfully mapped using chromosomal deficiencies, to 38-329Kb intervals. Two mutations showing undersized brain lobes, *juvenile at mid-third instar (jami)* and *reduced optic and imaginal expansion (roie)* were selected for detailed molecular and genetic analysis and comparison. Both genes are required in differing region- and stage-specific manners throughout the CNS. *jami* positively regulates CNS growth by both non-cell autonomous and cell-autonomous mechanisms, according to the region and stage. In contrast *roie* promotes growth in a strictly cell-autonomous manner with a strong requirement in symmetrically dividing precursors. Using deficiencies, *jami* was fine-mapped to a region containing 5 genes and one strong candidate gene for *roie*, *CG13074*, was identified by *P*-element mediated recombination mapping combined with genetic techniques and available *Drosophila* database resources.

TABLE OF CONTENTS

LIST OF FIGURES

CHAPTER 1

CHAPTER 2

CHAPTER 3

CHAPTER 4

CHAPTER 5

CHAPTER 6

LIST OF TABLES

CHAPTER 2

CHAPTER 3

CHAPTER 4

CHAPTER 5

ABBREVIATIONS

AB	Abdominal
AbdA	Abdominal-A
AD	Antennal Disc
ALH	After Larval Hatching
ana	*anachronism*
AP	Antero-Posterior
AS-C	achaete-scute complex
as/sc	*achaete/scute*
ato	*atonal*
ATP	Adenosine TriPhosphate
β-gal	β-Galactosidase
bHLH	basic Helix-Loop-Helix
BMP	Bone Morphogenetic Protein
boss	*bride of sevenless*
bp	base pairs
brat	*brain tumour*
BrdU	BromodeoxyUridine
cas	*castor*
CB	Central Brain
Cdlc2	Cytoplasmic dynein light chain 2
CNS	Central Nervous System
ctp	*cut up*
da	*daughterless*
Dac	Dachshund
aPKC	*atypical protein kinase C*
dap	*dacapo*
Df	Deficiency
disco	*disconnected*
dpp	*decapentaplegic*
DNA	Deoxyribonucleic Acid
DV	Dorso-Ventral

EC	Endothelial Cell
EcR	Ecdysone Receptor
ED	Eye Disc
EGFR	Epidermal Growth Factor Receptor
EMAP	Echinoderm Microtubule-Associated Protein
EMS	EthylMethaneSulphonate
eNB	embryonic Neuroblast
ey	*eyeless*
eya	*eyes absent*
FGF	Fibroblast Growth Factor
GFP	Green fluorescent protein
GMC	Ganglion Mother Cell
GPC	Glial Precursor Cell
hb	*hunchback*
20HE	20-hydroxyecdysone
hh	*hedgehog*
hid	*head involution defect*
H3P	phosphorylated Histone H3
Hr	Hour
HRP	Horse Radish Peroxidase
Hs	Heat Shock
ind	*intermediate neuroblast defective*
insc	*inscuteable*
IOA	Inner Optic Anlagen
IPC	Inner Proliferation Centre
jami	*juvenile after mid third instar*
JH	Juvenile Hormone
JHBD	Juvenile Hormone Binding Domain
Kb	Kilobases
kr	*kruppel*
L1	First larval instar stage
L2	Second larval instar stage

L3	Third larval instar stage
La	Lamina
l(2)gl	*lethal (2) giant larvae*
Lo	Lobula
LPC	Lamina Precursor Cell
MARCM	Mosaic Analysis with a Repressible Cell Marker
MD	Molecular Distance
Me	Medulla
MF	Morphogenetic Furrow
mira	*miranda*
mRNA	messenger Ribonucleic Acid
msh	*muscle segment homeobox*
NB	Neuroblast
Neo	Neomycin
NSC	Neural Stem Cell
ORF	Open Reading Frame
OL	Optic Lobe
OOA	Outer Optic Anlagen
OP	Overproliferation
OPC	Outer Proliferation Centre
OS	Optic Stalk
p	Probability of null hypothesis
pins	*partner of inscuteable*
PcG	*PolyComb Group*
PL	Pupal Lethal
PMP	Predicted Molecular Position
pNB	postembryonic Neuroblast
PNE	Procephalic Neuroectoderm
PNS	Peripheral Nervous System
pros	*prospero*
R1-R8	Photoreceptor Cells
RNA	Ribonucleic Acid

RNAi	Ribonucleic Acid Interference
robl	*roadblock*
roie	*reduced optic and imaginal expansion*
rpr	*reaper*
RT	Room Temperature
SC	Stem Cell
sens	*senseless*
sev	*sevenless*
SNP	Single Nucleotide Polymorphism
so	*sine oculis*
Su(H)	Suppressor of Hairless
Tb	*Tubby*
TF	Transcription Factor
TGFβ	Transforming Growth Factor-β
trol	*terribly reduced optic lobe*
TrxG	*Trithorax Group*
TX	Thoracic
Ubx	*Ultrabithorax*
UP	Underproliferation
VG	Ventral Ganglion
VNC	Ventral Nerve Cord
vnd	*ventral nervous system defect*
VNE	Ventral Neuroectoderm
wg	*wingless*
wL3	wandering third instar larval stage
Y2H	Yeast 2 Hybrid

CHAPTER 1

INTRODUCTION

1.1 NEURAL PROGENITORS

The development of a complex nervous system involves a large array of different molecular and cellular mechanisms. This thesis focuses on one aspect of neurogenesis, cell number regulation. There are many classes of neural progenitors, however neural stem cells (NSCs) are thought to be the primary progenitor cell in the nervous system. All stem cells (SCs) possess two critical properties; a capacity to self-renew and multipotency, i.e. the ability to generate several different types of daughter cells. Further common attributes include the abilities to undergo asymmetric division, which contributes to the multipotency, to exist in a mitotically quiescent form and to generate clonally all of the different cell types that constitute the tissue from where they derive (Hall and Watt 1989; Potten and Loeffler 1990). Usually, linking the SC to its terminally differentiated progeny, there exists an intermediate population of committed progenitors with limited proliferative capacity and restricted differentiation potential, often known as transit amplifying cells (Watt 2000).

1.1.1 Vertebrate neural stem cells

Early studies led to the isolation of stem-like cells from the embryonic mammalian central nervous system (CNS) (Temple 1989; Cattaneo and McKay 1990; Reynolds et al. 1992; Kilpatrick and Bartlett 1993) and the peripheral nervous system (PNS) (Stemple and Anderson 1992). Since then, NSCs have also been isolated from two neurogenic regions of the adult brain (Reynolds and Weiss 1992; Lois and Alvarez-Buylla 1993), the hippocampus and the subventricular zone, and also from the spinal cord (McKay 1997; Rao 1999; Gage 2000). This raises the possibility that regenerative properties might be awakened even in the adult CNS. However the full extent of plasticity and reprogrammability of adult NSCs is still very much in question (Temple 2001).

Embryonic NSCs originate from the neural plate and appear to be initially specified through a default state, enhanced by inductive mechanisms (Temple 2001). Their widespread distribution in the early embryonic nervous system, combined with their prolific, multipotent nature *in vitro* suggests that NSCs are likely to be the major form of early neural progenitor. The evolving potential and fate of NSCs are subject to spatio-temporal specification (Temple 2001) and as development proceeds the frequency of NSCs declines rapidly, diluted by the production of transit amplifying cells and other progenitors, together with differentiated cells (neurons and glia). NSCs

become restricted to the proliferating ventricular zone, where they generate all differentiated cells in the nervous system, via the production of intermediate precursors such as neuroblasts and glioblasts (producing neurons and glia, respectively), which migrate away from the ventricular zone (Morrison et al. 1997a; Gage 2000; Panicker and Rao 2000).

NSCs can undergo both symmetric and asymmetric divisions (Sommer 2002). Symmetric divisions serve to either expand the progenitor pool (by generating two more SCs) or to reduce it (by generating two differentiated progeny) whereas asymmetric division can maintain the size of the pool while generating differentiated progeny. Thus maintenance of a stable precursor pool requires a fine balance between the two division modes. NSCs have the potential to produce many more progeny when cultured *in vitro* than they would normally make *in vivo*. This raises the question of what mechanisms determine the final number of progeny generated. In principle, this decision could be regulated by cell intrinsic or extrinsic mechanisms. In practice it is likely that there is interplay between intrinsic and extrinsic factors and studies indicate that many different molecules are involved. Several conserved molecules that may be important for this process have been identified including growth factors, asymmetrically distributed molecules, such as Notch and Numb, components that regulate intracellular movement of molecules, and proteolytic enzymes that regulate asymmetric distribution (Gritti 1999; Tropepe 1999; Sommer 2002). Furthermore, a number of different types of interactions, such as with the extracellular matrix and by direct cell-cell contact (Jacques 1998) appear important for this process. The combined action of all these local signals and interactions constitutes a SC niche (Watt 2000; Spradling et al. 2001; Fuchs et al. 2004) with strong evidence for this in the case of NSCs (Fuchs et al. 2004; Wurmser et al. 2004).

Evidence of niche-based regulation arose from the observation that adult NSCs are not randomly distributed throughout the brain, but rather are concentrated around blood vessels (Palmer et al. 2000; Capela and Temple 2002; Louissaint et al. 2002) (Fig. 1.1A). Close proximity of the NSCs to endothelial cells (ECs), that line blood vessels, enables intercellular communication in the form of secreted signals from the ECs, which maintain the proliferative capacity of NSCs and prevent differentiation (Risau 1997; Shen et al. 2004) (Fig. 1.1B). Astrocytes have also been shown to enhance the proliferative capacity and neurogenic properties of NSCs (Song et al. 2002). Conversely, proliferative potential is limited by mechanisms controlling termination of

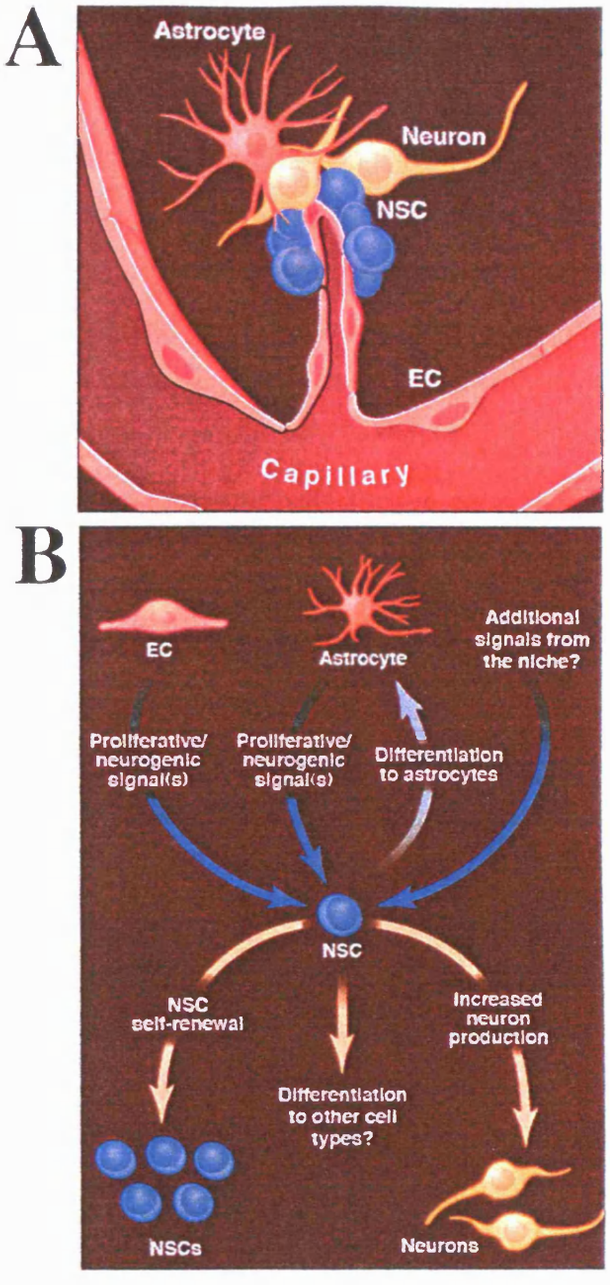

FIGURE 1.1. THE MAMMALIAN ADULT NEURAL STEM CELL NICHE
(**A**) The niche inhabited by mammalian adult NSCs is situated close to blood vessels. NSCs interact with endothelial cells (ECs) and astrocytes. (**B**) Both ECs and astrocytes secrete signalling molecules that influence neighbouring NSCs to proliferate and differentiate into neurons (Adapted from Wurmser et al., 2004).

proliferation, such as cell cycle arrest (reviewed in (Edlund and Jessell 1999; Durand 2000) or programmed cell death (Honarpour et al. 2000; Kuan et al. 2000; Pompeiano et al. 2000). Of note, this role for apoptosis in eliminating progenitors is distinct from its well described function in editing out post-mitotic neurons lacking neurotrophic support (reviewed in (Raff et al. 1993).

In summary, NSC proliferation is regulated by a combination of multiple environmental signals from the niche, together with cell intrinsic factors. The identification of these signalling molecules and an advancement in our understanding of their integration raises many exciting therapeutic possibilities in regenerative medicine and cancer (Ostenfeld and Svendsen 2003; Li and Neaves 2006; Martino and Pluchino 2006).

1.1.2 *Drosophila* neuroblasts

Research on *Drosophila* and vertebrates has revealed that many of the molecular mechanisms used to construct the basic framework of the nervous systems are conserved. This indicates that the fruit fly may provide a good model for gaining insights into vertebrate neurogenesis. Invertebrate neurogenesis was first studied in detail in the grasshopper. Unlike *Drosophila*, the embryo of the grasshopper has large and accessible cells that are easy to visualise and manipulate. These early studies used laser ablation experiments and intracellular dye injections to define the mechanisms of early neural specification and also to identify individual progenitor cells and their lineages (Doe and Goodman 1985a; Doe and Goodman 1985b; Goodman and Doe 1993). In this regard, the early analysis of the grasshopper CNS has been very insightful for the study of the relatively small but highly related fruit fly CNS.

The embryonic CNS of *Drosophila* consists of the developing brain hemispheres and the ventral nerve cord (VNC), the latter comprising segmentally repeated units (neuromeres). Both regions are generated from the neural stem cell-like progenitors called Neuroblasts (NB), which are derived from monolayers of ectodermal cells: the Procephalic Neuroectoderm (PNE) and Ventral Neuroectoderm (VNE), generating brain hemispheres and VNC respectively (Poulson 1950; Hartenstein and Campos-Ortega 1984; Technau and Campos-Ortega 1985; Campos-Ortega 1993a; Younossi-Hartenstein et al. 1996; Skeath and Thor 2003). In contrast to mammals, in which the entire neuroectoderm folds inwards to form the primordium of the nervous system (neural tube), insect NBs primarily segregate from the ectodermal layer as individual scattered

cells. During the early stages of embryogenesis, patterning genes acting along the antero-posterior (AP) and dorso-ventral (DV) axes serve to establish a Cartesian coordinate system by which unique region-specific fates are specified (reviewed in (Skeath and Thor 2003). First, neural equivalence groups containing many neuroectodermal cells are specified, then inhibitory interactions within these groups ultimately select only one cell to acquire a NB as opposed to an epidermal fate. NBs generally divide asymmetrically to regenerate themselves and to produce a smaller ganglion mother cell (GMC). GMCs divide usually only once to produce neurons and glial cells. During the 22hr of *Drosophila* embryogenesis (at 25°C), NB segregation and multiple asymmetric divisions transform a simple neuroectodermal monolayer into a complex three-dimensional functional CNS.

The study of asymmetric division is becoming increasingly important in developing our understanding of vertebrate neurogenesis (Lin and Schagat 1997) as evidence is accumulating for the importance of this division mode in generating the tremendous cellular diversity found in the developing nervous system (Qian et al. 1998; Wakamatsu et al. 1999; Cayouette et al. 2001; Wodarz and Huttner 2003; Betschinger and Knoblich 2004). Furthermore, there is growing evidence for symmetric divisions of *Drosophila* NBs (Hofbauer and Campos-Ortega 1990; Meinertzhagen and Hanson 1993; Ceron et al. 2001; Egger et al. 2007) thus increasing their value in developing our understanding of vertebrate NSC behaviour.

1.2 EMBRYONIC NEUROGENESIS

In the embryonic VNE, the identification of individual NBs is greatly facilitated by their stereotypical position within a neuromere and because the same initial pattern and number of NBs is repeated in every segment. In contrast, little overt metamerism exists in the PNE (Hartenstein and Campos-Ortega 1984), which makes it more difficult to reconstruct the precise pattern of brain NBs. For these reasons, the embryonic development of the VNE has been studied in greater detail than the PNE and, historically, it is experiments on the VNC that have been crucial in elucidating our understanding of the molecular and genetic mechanisms controlling nervous system development. Therefore I will describe VNE development first, followed by a briefer comparative description of brain hemisphere (hereafter referred to as brain) development.

1.2.1 Ventral nerve cord development

During the early stages of embryogenesis, a complex hierarchy of segmentation genes establishes the segmented body plan (Akam 1987) (Fig. 1.2). As the early embryo is a syncytium, localised mRNAs can act as the source for long-range protein gradients. The first AP coordinates are defined by maternally contributed localised mRNAs, such as *bicoid*. These maternal mRNAs encode factors that switch on the expression of the first zygotic genes, the gap genes, which themselves encode transcription factors (TFs) (for example *hunchback*) that are expressed in broad domains. The first sign of molecular segmentation appears with the expression of the pair-rule genes, such as *even-skipped* and *fushi tarazu*. These genes are regulated in two-segment wide stripes by the combined action of the gap gene encoded and other TFs and these in turn initiate the expression of the segment-polarity genes that serve to pattern units of one segment in width. This final class of patterning genes encodes a wide range of proteins important for CNS development, such as TFs, secreted molecules and membrane receptors and includes *engrailed, gooseberry* and *wingless*. (Chu-LaGraff and Doe 1993; Skeath et al. 1995; Bhat 1996; Bhat and Schedl 1997; Bhat 1999). In ventral regions; the stripes of segment polarity gene expression include the neuroectodermal cells that delaminate to form NBs (Fig. 1.3A).

While the segment polarity genes pattern the AP axis, the DV axis is patterned by a gradient of nuclear localisation of the TF Dorsal. This establishes the asymmetric patterns of gene expression along the DV axis by activating regulatory genes, such as *twist* and *snail* (Kosman et al. 1991), which are responsible for the differentiation of the ventral mesoderm. In contrast, *decapentaplegic (dpp)* is repressed by Dorsal protein, confining its activity to the more dorsal regions of the embryo, where there is virtually no Dorsal protein. Subsequently, DV patterning by dpp, in addition to epidermal growth factor receptor (EGFR) signalling pathways determines the DV borders of the neuroectoderm. Furthermore, this gene activity subdivides the neuroectoderm into three longitudinal stripes of columnar genes (Skeath 1998; Von Ohlen and Doe 2000) (Fig. 1.3A). These are *ventral nervous system defective (vnd), intermediate neuroblast defective (ind)* and *muscle segment homeobox (msh)* (Skeath et al. 1994; McDonald et al. 1998; Weiss et al. 1998). The combined expression of AP and DV columnar genes establishes the Cartesian coordinate system which imparts region-specific identity to NBs (Doe 1992; Goodman and Doe 1993; Bhat 1999; Skeath 1999; Skeath and Thor 2003) (Fig. 1.3A).

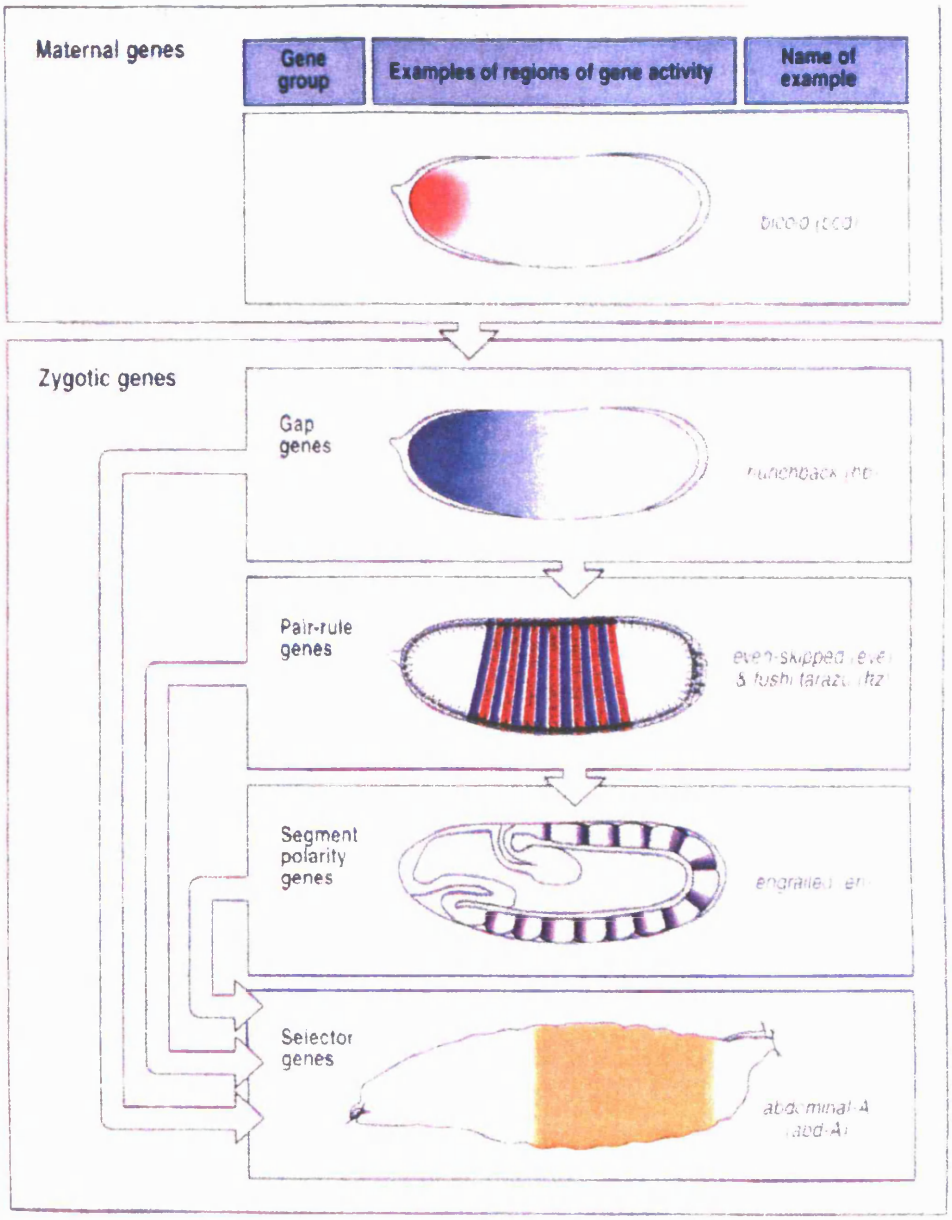

FIGURE 1.2. THE GENETIC HIERARCHY FOR ANTERIOR-POSTERIOR PATTERNING.
Maternally produced products, such as *bicoid*, provide positional information required for the activation of zygotic genes. Three classes of zygotic genes, the gap genes (*hunchback*), the pair-rule genes (*even-skipped* and *fushi tarazu*) and the segment polarity genes (*engrailed*) act along the AP axis. Each of these classes spatially regulates Hox gene expression (*abdA*) along the AP axis. (Adapted from Wolpert *et al.*, 1998)

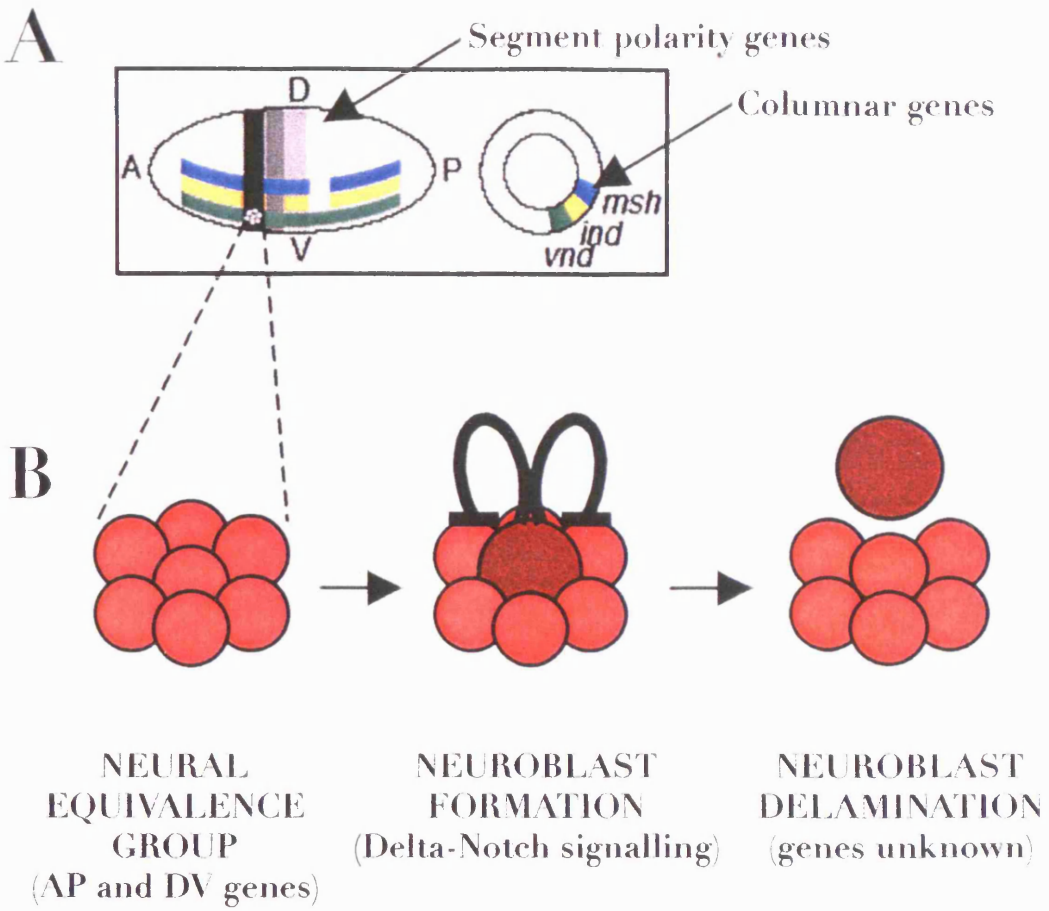

FIGURE 1.3. GENETIC CONTROL OF NEUROBLAST SPECIFICATION AND FORMATION

(**A**) The Segment-polarity (black/grey) and Columnar (green/yellow/blue) genes are expressed in orthogonal stripes. Each neural equivalence group (white dots) expresses a unique combination of these genes (adapted from Skeath and Thor, 2003). (**B**) In each equivalence group the expression of the proneural genes (light red) is initially uniform. Lateral inhibition mediated by the neurogeneic genes *Notch* and *Delta* generates one neuroblast with higher proneural gene expression (dark red) by suppressing the expression of proneural genes in the surrounding cells. The genes involved in neuroblast delamination remain unknown.

A further level of specification, segmental specialisation, is superimposed on this Cartesian system through the highly conserved Hox/homeotic gene network. The expression patterns of the Hox/Homeotic genes impart segment-to-segment differences in neural progenitor and progeny properties, as well as more generally regulating AP patterning (reviewed in (McGinnis and Krumlauf 1992; Carroll et al. 1995; Mann and Morata 2000). Hox genes encode TFs that bind DNA via a 60 amino acid homeodomain. They are located on chromosomal clusters and in *Drosophila,* this cluster is present on the third chromosome and it is split into two complexes: the Antennapedia complex and Bithorax complex (Fig. 1.4A,C). In vertebrates, four Hox clusters are present (Fig. 1.4B,D), these are believed to be the result of genome-wide duplications occurring after evolutionary divergence of arthropods and vertebrates (reviewed in (Carroll 1995).

Hox genes are expressed along the AP axis in an order that is collinear with their arrangement on the chromosome (Fig. 1.4). In this way, each segment is specifically patterned by the activity of a characteristic subset of Hox genes. The different AP domains of Hox expression are often overlapping. In *Drosophila,* negative cross-regulation is observed in these overlaps, whereby the Hox gene located in a more posterior segment tends to repress the expression of the one located more anteriorly (Struhl and White 1985). On the top of this direct transcriptional regulation, phenotypic suppression also occurs; this is a mechanism whereby the more posterior Hox protein suppresses the activity of the more anterior one at the level of the Hox target genes (Gonzalez-Reyes et al. 1992). The "selector gene hypothesis", proposed by Garcia-Bellido predicted that the Hox genes do not act directly to specify the morphological differences between segments but instead they control a battery of numerous subordinate target genes (the "realizator genes") that carry out the diverse cellular functions required for the various patterns of cell differentiation (Garcia-Bellido 1975; Akam 1998). Hox expression is maintained within correct segmental boundaries through expression of two additional groups of genes, the *Trithorax group (trxG)* and *Polycomb group (PcG)*, which are necessary for maintaining Hox activation or silencing Hox expression, respectively (reviewed in (Paro 1990; Paro 1993; Pirrotta 1995; Gould et al. 1997; Orlando 2003).

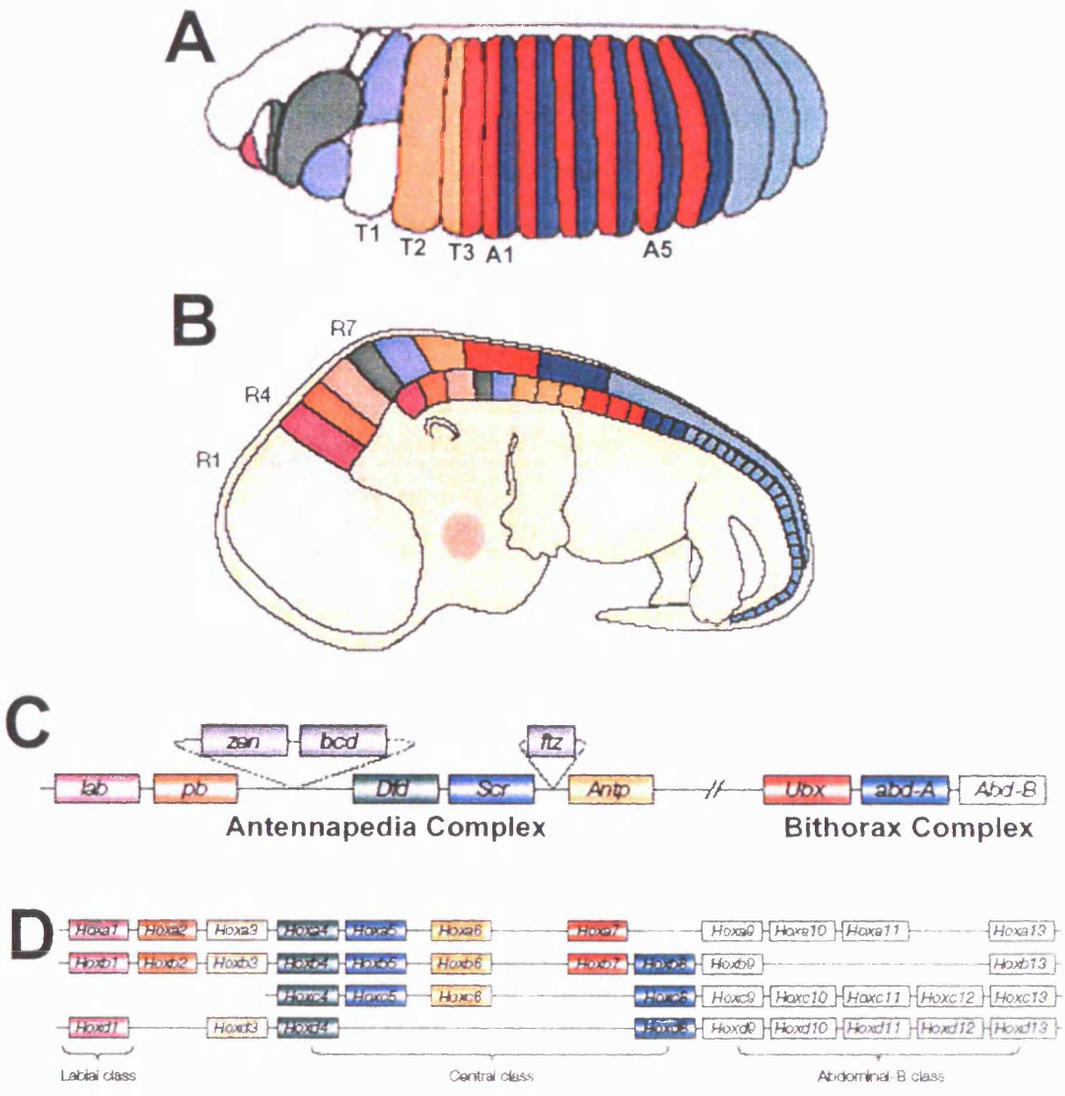

FIGURE 1.4. HOX GENE EXPRESSION IN *DROSOPHILA* AND MOUSE
(**A**) Schematic of a stage 13 *Drosophila* embryo, coloured to indicate domains of Hox gene expression. The segments are labelled (T1-T3, thoracic segments; A1-A9, abdominal segments). (**B**) Schematic of a mouse embryo at embryonic day 12.5, with approximate Hox domains depicted. The positions of hindbrain rhombomeres, r4 and r7 are labelled. (**C & D**) Schematic of Hox gene clusters in the genome of *Drosophila* (**B**) and mouse (**D**). Genes that are orthologous between clusters and species are labelled in the same colour. Three non-Hox homeodomain genes *zen, zerknult; bcd, bicoid* and *ftz, fushi tarazu* are shown in grey. (Adapted from Pearson *et al.*, 2005)

1.2.2 Neuroblast specification

Unique combinations of AP and DV gene expression define what is referred to as a neural equivalence group. For example, *gooseberry* in combination with *vnd* forms a specific equivalence group that confers a unique fate to NB5-2 (Martin-Bermudo et al. 1991; Doe 1992; Buenzow and Holmgren 1995; Skeath 1999). Within neural equivalence groups, a lateral inhibition mechanism is responsible for selecting neural versus epidermal progenitors from the VNE, thus imparting the first level of control over final neuronal number (reviewed in (Campos-Ortega 1993b). The outcome of the neural/epidermal decision is regulated by the antagonistic actions of proneural (Ghysen and Dambly-Chaudiere 1989; Romani et al. 1989; Ghysen and Dambly-Chaudiere 1990) and neurogenic genes (Poulson 1937; Lehmann et al. 1981; Lehmann et al. 1983) (Fig. 1.3B). Proneural genes, named according to their requirement for neural development, include the four transcription units of the *achaete-scute* complex *(AS-C)*: *achaete, scute, lethal of scute and asense* (Stern 1954; Garcia-Bellido and Santamaria 1978; Garcia-Bellido 1979; Ghysen and Dambly-Chaudiere 1988; Campuzano and Modolell 1992; Skeath 1992). These genes encode related basic Helix-loop-Helix (bHLH) transcription factors (TFs) that dimerise with another ubiquitously expressed bHLH factor called Daughterless (Villares and Cabrera 1987; Alonso and Cabrera 1988; Caudy et al. 1988; Cronmiller et al. 1989; Gonzalez et al. 1989; Ghysen et al. 1993; Vaessin et al. 1994). Conversely, Neurogenic genes, named according to their loss-of-function phenotype, such as *Notch* and *Delta*, serve to restrict proneural gene expression and to promote an epithelial fate (Fig. 1.3B).

Notch and Delta are both transmembrane proteins. Upon binding to Delta present in the apposing cell, the intracellular domain of Notch is cleaved and translocates to the nucleus where it interacts with the TF Suppressor of Hairless (Su(H)) and Mastermind (Artavanis-Tsakonas et al. 1999; Kopan 2002). This complex then activates transcription of the genes of the *Enhancer of Split* complex, which encode bHLH-type transcriptional repressors that directly downregulate *as/sc* proneural gene expression (Struhl and Adachi 1998). As the proneural genes are required to activate Delta, this creates a positive feedback loop between the *AS-C* genes and Notch pathway that leads to a bistable switch with respect to cell fates in each equivalence group (Heitzler and Simpson 1991; Heitzler et al. 1996). Thus, although expression of the *Achaete-Scute (Ac/Sc) complex* genes is initially uniform in each cluster, one cell (the presumptive NB) will come to express slightly higher levels than the others and this

small difference will get amplified such that Delta expression increases (Cubas et al. 1991; Martin-Bermudo et al. 1991; Skeath and Carroll 1991). Consequently, lateral inhibition, mediated by Notch and Delta, generates only one NB per cluster (Skeath 1992; Skeath and Thor 2003). The same lateral inhibition mechanism appears to exist in the grasshopper embryo, as targeted NB ablation releases a neighbouring ectodermal cell from inhibitory signalling, allowing it to assume a neural fate (Taghert et al. 1984; Doe and Goodman 1985b).

Once specified, from stage 8 to 11 of embryogenesis (Campos-Ortega 1997), NBs enlarge and start delaminating from the VNE into the interior of the embryo (Cui and Doe 1992) (Fig. 1.3B). Six distinct "waves" of NB segregation (early S1 and S1-S5), lasting approximately 3hr at 25°C, generate an invariant pattern of 30 NBs per neural hemisegment by late stage 11 (Hartenstein and Campos-Ortega 1984; Doe 1992) (Fig. 1.5). A detailed description of each NB and its progeny is now available (http://www.neuro.uoregon.edu/doelab/) (Bossing et al. 1996; Schmidt et al. 1997; Schmid et al. 1999). One interesting finding from these experiments is that clone size at the end of embryogenesis varies from a minimum of 2 interneurons per NB, in the case of MP1, MP2 and MP3, up to a maximum of 37 motorneurons, interneurons and glia generated by NB7-1 (Schmid et al. 1999). Therefore, NBs differ significantly in their mitotic activity depending on AP/DV identity. There is also a tendency for NBs that delaminate early (S1 wave) to generate more cells during embryogenesis than those that are born later (Bossing et al. 1996; Schmidt et al. 1997; Schmid et al. 1999).

1.2.3. Asymmetric division of neuroblasts

Having delaminated, NBs enter an asymmetric division programme, to produce another NB and a smaller GMC which divides asymmetrically, usually only once, to produce two different postmitotic cell types named ganglion cells (Campos-Ortega 1993b). Ultimately 60 glia and approximately 400-500 neurons (motorneurons, interneurons or neurosecretory cells) are produced in each segment (Schmid et al. 1999; Skeath and Thor 2003). Each NB will give rise to a specific progeny lineage (Bossing et al. 1996; Schmidt et al. 1997; Schmid et al. 1999). During divisions, there is a tendency for the NB to retain its proximity to the ventral epidermis, such that progeny cells are pushed more dorsally (Kambadur et al. 1998; Schmid et al. 1999; Udolph et al. 2001). Embryonic glia (midline, longitudinal, nerve root, exit and peripheral) are generated from a variety of different NBs and related precursors, and many come to lie close to

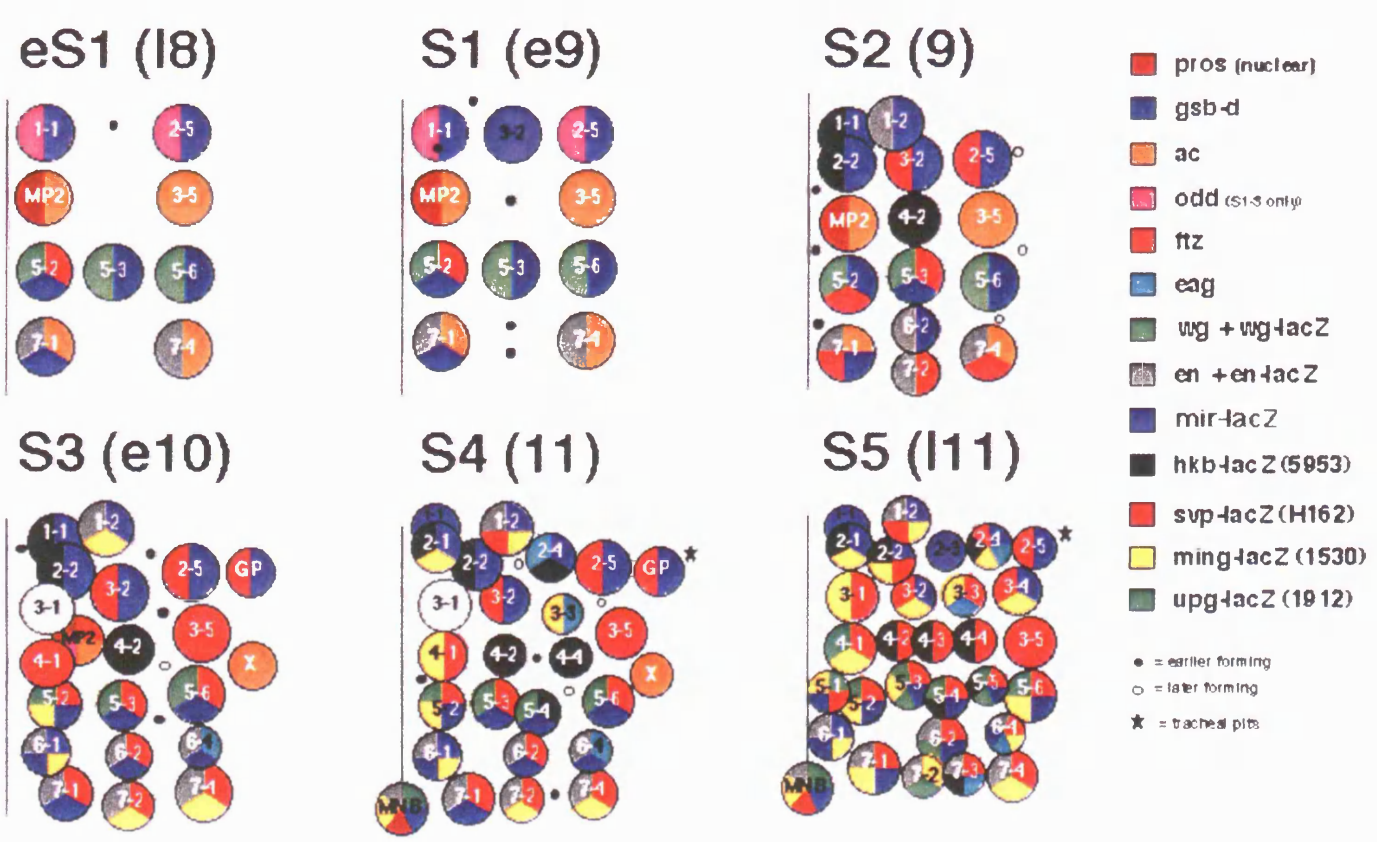

FIGURE. 1.5. DEVELOPMENT OF THE EMBRYONIC NB PATTERN

Each panel shows a hemisegment where the vertical line represents the midline. NB formation is divided into 6 stages (early S1 (eS1) and S1-S5). (A) the early S1 pattern; late stage 8. (B) The S1 pattern; early stage 9 (C) The S2 pattern; stage 9. (D) The S3 pattern; stage 10. (E) the S4 pattern; stage 11. (F) The S5 pattern; late stage 11. Colours represent gene expression profiles of *prospero (pros), gooseberry (gsb-d), achaete (ac), odd-skipped (odd), fushi-tarazu (ftz), eagle (eag), wingless (wg), engrailed (en), mirror (mir), huckebein (hkb), seven-up (svp), ming* and *unplugged (upg)*. NB nomenclature (e.g. NB1-1, 2-5 etc). Adapted from http://www.neuro.uoregon.edu/doelab/nbmap.html.

the neuropil where they are intimately associated with the formation of the initial axon pathways, either through enwrapping or guidance of axons (Ito 1995).

In *Drosophila,* asymmetric division is a common theme during neural development as sensory organ precursors appear to share at least some of the critical molecular components with NBs (Jan and Jan 2000; Jan and Jan 2001; Chia and Yang 2002). Furthermore, there are strong parallels between the asymmetric machinery of *Drosophila* and *C. Elegans* (Doe and Bowerman 2001). Our understanding of the molecular basis of NB asymmetric division has evolved significantly in recent years (for reviews, see (Campos-Ortega 1997; Jan and Jan 2000; Chia and Yang 2002; Wodarz and Huttner 2003). Single embryonic NBs (eNBs) isolated in culture divide asymmetrically, suggesting that extrinsic signals are not required for this process (Broadus and Doe 1997). However, extrinsic cues are necessary for orienting the cell division axis with respect to the embryonic neuroectoderm (Siegrist and Doe 2006). Three important features characterise the early events that establish asymmetric NB division. First, apical and basal crescents form through the segregation of cell fate determinants to the cell poles at metaphase (for reviews, see (Wodarz and Huttner 2003; Betschinger and Knoblich 2004). Second, at metaphase the mitotic spindle undergoes a 90° rotation under the control of Insc (Kraut et al. 1996b), aligning it along the apical-basal axis, which allows the preferential segregation of the cytoplasmic determinants to just one daughter cell. Finally, asymmetry and to a lesser extent displacement of the mitotic spindle are necessary to generate two daughter cells of unequal size (Kaltschmidt et al. 2000; Cai et al. 2003) whereby the GMC inherits the basal components of the NB (Rhyu et al. 1994; Hirata et al. 1995; Knoblich et al. 1995; Spana and Doe 1995; Li et al. 1997; Broadus et al. 1998).

Importantly, the delaminating NB inherits its apical-basal polarity from the neuroectoderm. This is possible because the NB inherits apically-localised components, such as Bazooka/Par3, from its polarised epithelial ancestor (Schober et al. 1999; Wodarz et al. 1999). In the delaminating interphase NB, Bazooka/Par-3 (Kuchinke et al. 1998; Schober et al. 1999; Wodarz et al. 1999), Par-6 (Petronczki and Knoblich 2001) and aPKC (Wodarz et al. 2000), localise to the apical cortex. Via the adaptor protein, Inscuteable (Insc) (Kraut and Campos-Ortega 1996; Kraut et al. 1996b), they recruit Pins and GαI (Parmentier et al. 2000; Schaefer et al. 2000; Yu et al. 2000; Yu et al. 2003a) (Fig. 1.6A). Apical components also control the localisation of basal components, such as the important GMC determinant Prospero (Pros) (Doe et al. 1991;

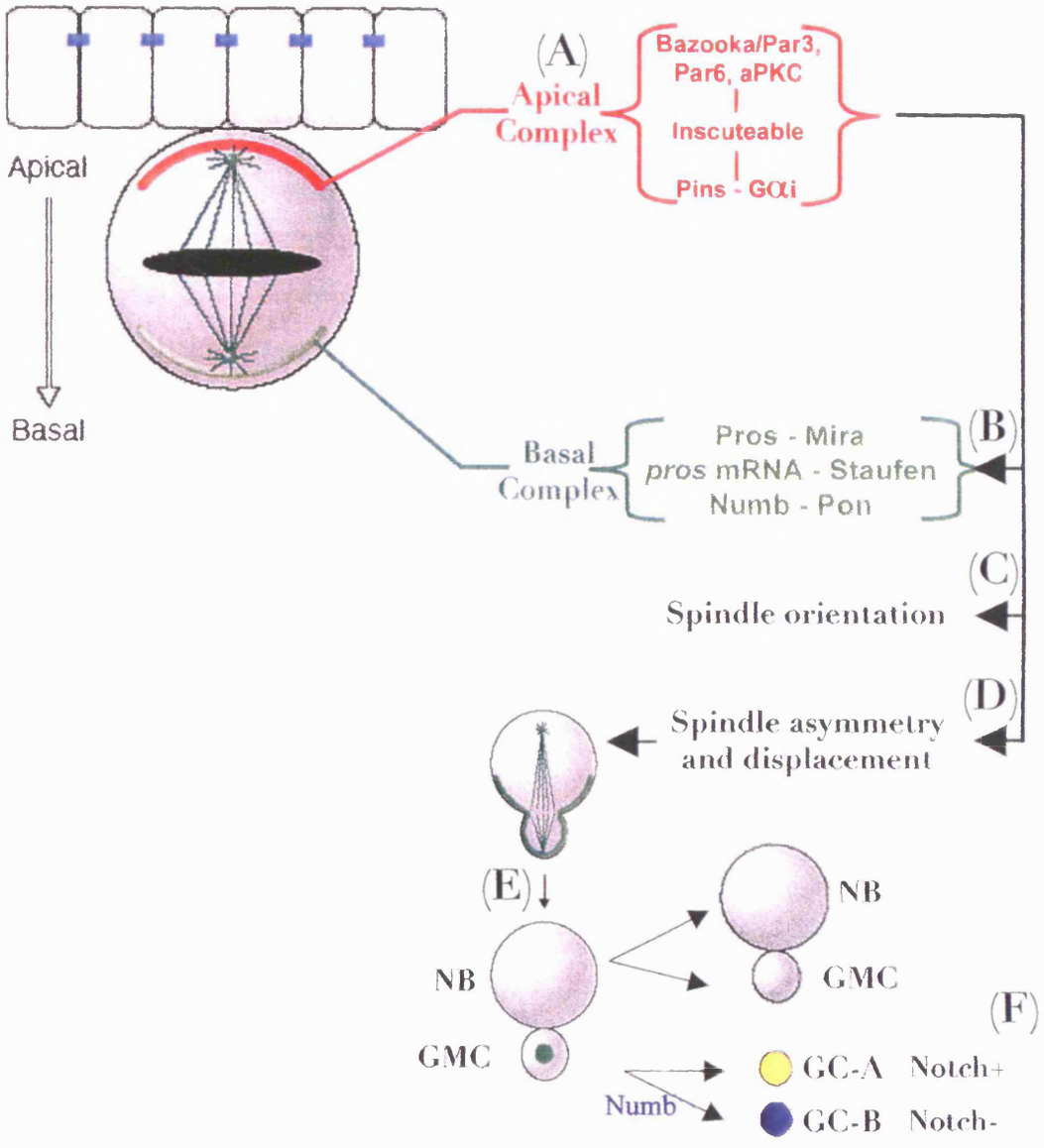

FIGURE 1.6. ASYMMETRIC DIVISION OF NBs
(**A**) In the M-phase neuroblast (NB), the apical Bazooka/Par3, Par6, aPKC complex (red) binds to Inscutable, in turn binding to the Pins-Gαi complex. This apical complex is required for the normal basal localisation of the basal complex (green crescent) (**B**): Prospero-Miranda, *prospero* RNA-Staufen and Numb-Partner of Numb (Pon), as well as for mitotic spindle rotation (**C**). The apical complex also influences the unequal size of daughter cells, through spindle asymmetry and displacement (**D**), producing the NB and ganglion mother cell (GMC) (Adapted from Chia and Yang 2002). (**E**) When the NB divides, cortical Pros (green) is inherited by the GMC and then rapidly translocates into the nucleus, to limit the GMCs mitotic potential. The GMC undergoes only one round of cell division to produce two postmitotic ganglion cells (GC-A and -B) (**F**), made distinct through asymmetric segregation of Numb.

Vaessin et al. 1991; Matsuzaki et al. 1992; Hirata et al. 1995; Spana and Doe 1995). This is achieved indirectly through the asymmetric segregation of Miranda (Mira), which binds Pros protein (Ikeshima-Kataoka et al. 1997) and Staufen, which binds *pros* mRNA (Li et al. 1997; Shen et al. 1997) (Fig. 1.6B). In addition, the apical complex also targets Numb which binds to Partner of Numb (Pon) (Uemura et al. 1989; Knoblich et al. 1995; Broadus et al. 1998) to the basal crescent. Betschinger *et al.* (2003) have demonstrated how the apically-localised Par complex can direct basal proteins like Mira. Apically localised aPKC phosphorylates the cytoskeletal protein Lethal (2) giant larvae (Lgl). As non-phosphorylated Lgl is required for cortical recruitment of Mira, Mira therefore only remains localised to the basal cortex, where aPKC is absent.

Evidence is accumulating that there is an interdependence between the molecules mediating asymmetric division and cell-cycle progression (reviewed in (Chia and Yang 2002; Prokopenko and Chia 2005). For example, the subcellular localisation of both apical and basal NB components shows cell cycle dependence. Indeed perturbing the activity of mitotic regulators, such as cyclin-dependent kinases, results in the mis-segregation of asymmetric determinants (Campos-Ortega 1997; Lu et al. 1999; Tio et al. 2001; Chia and Yang 2002). Conversely, asymmetric determinants are thought to be involved in regulating cell-cycle progression. For example, the segregation of Pros (Doe et al. 1991) into the GMC (Li et al. 1997; Broadus et al. 1998) appears to be one mechanism necessary for termination of proliferation and onset of differentiation in progeny: Pros is transiently localised in the GMC cortex then, quickly translocates to the nucleus (Broadus et al. 1998) (Fig. 1.6E), where it may activate *dacapo (dap),* the cyclin-dependent kinase inhibitor (Ikeshima-Kataoka et al. 1997; Li 2000; Liu 2002), thus limiting the number of divisions the GMC may undergo (Skeath and Thor 2003). Interestingly, this stop mechanism appears to be conserved in vertebrates where *Prox-1*, the mammalian *pros* homolog, has been shown to be required for retinal cells to stop dividing and enter differentiation (Dyer et al. 2003). Recently, a second factor involved in negatively regulating NB proliferation has been identified. The tumor suppressor protein, Brain tumor (Brat), acts as a posttranscriptional inhibitor of the cell cycle regulator dMyc (Betschinger et al. 2006). Brat binds and cosegregates with Mira and is partitioned into GMCs via this interaction. Furthermore, in Brat mutants, Pros is not partitioned into GMCs indicating that Brat may act to stabilise the Pros/Mira interaction (Lee et al. 2006). Moreover, rescue experiments suggest that Pros may act as a key

downstream effector of *brat* in cell fate specification and proliferation control (Bello et al. 2006).

Once generated by the asymmetric division of the NB, each GMC then divides asymmetrically to produce two postmitotic neurons and/or glia that acquire distinct fates. This is achieved through asymmetric partitioning of Numb which inhibits the *Notch* signalling pathway (Spana and Doe 1996; Buescher et al. 1998; Skeath 1998; Skeath and Thor 2003). As in NBs, a protein complex containing Inscuteable coordinates the asymmetric localisation of Numb with respect to the mitotic spindle, such that Numb segregates exclusively into one daughter cell (Spana & Doe, 1996) (Fig. 1.6F). In the B cell, Numb blocks the reception and/or transduction of the Notch signal, thus promoting the B-cell fate. The absence of Numb in the A cell allows active Notch signalling, which results in the activation of Notch target genes and execution of the A fate.

1.2.4. Temporal control of embryonic neuroblast identity

Each eNB also has a temporal identity, allowing it to generate different types of progeny at different times. One mechanism of assigning temporal identity to eNBs involves the sequential expression of a series of different TFs within the eNB (Kambadur et al. 1998; Brody and Odenwald 2000; Isshiki et al. 2001). The zinc-finger protein encoded by the gap gene *hunchback (hb)* begins this cascade, the other TFs that take part in this sublineage-switching are, in order, Kruppel (Kr), Pdm-1 and Castor (Cas) (Fig. 1.7A). *Kr* and Cas both encode zinc-finger proteins while *Pdm-1* belongs to the family of POU-homeodomain TFs. A cross-regulatory network links these factors as each gene activates the transcription of the next factor in the cascade and, in several cases, it represses the next-plus one (Kambadur et al. 1998; Isshiki et al. 2001; Edenfeld et al. 2002) (Fig. 1.7B). Importantly, the GMCs maintain the expression of the TF that was expressed in the parental NB at the moment of birth. This mechanism thus provides a temporal label distinguishing early-born from late-born GMC fates, ultimately influencing post-mitotic neuronal identity (Fig. 1.7C). Most of the embryonic NBs appear to undergo sublineage switching in a similar manner (Isshiki et al. 2001; Pearson and Doe 2003), although there are exceptions to the rules (Cui and Doe 1992; Isshiki et al. 2001). Pearson *et al.* propose a model in which the sequential change in the expression of the determinant factors in the NB progressively restricts the NB competence to generate early-born fate cells (Pearson and Doe 2004). For example, for

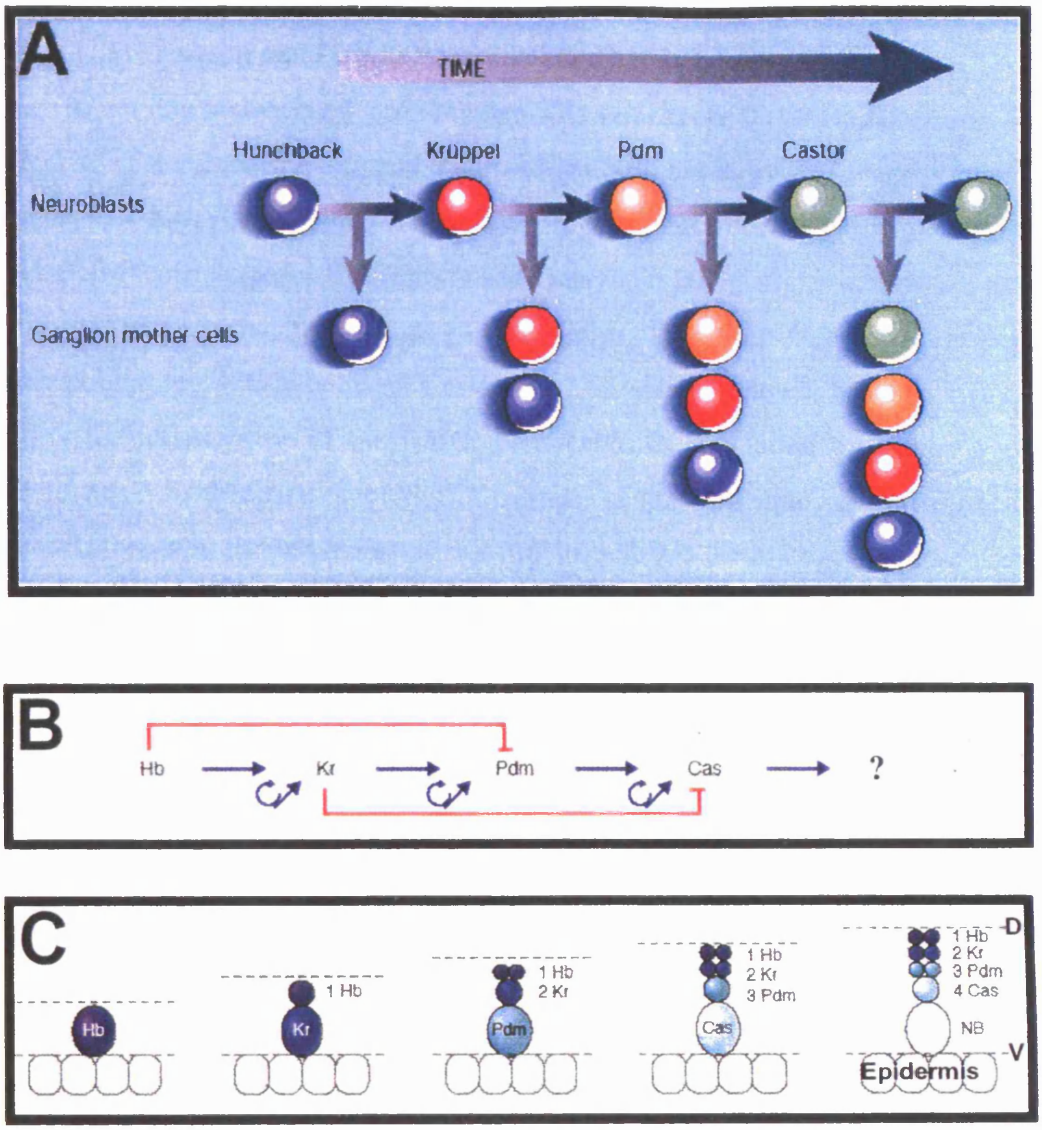

FIGURE 1.7. NB TEMPORAL IDENTITY
(**A**) NBs express four transcription factors: Hunchback (Hb), Kruppel (Kr), Pdm and Castor (Cas), in a temporal sequence that regulates the identity of GMCs and neurons. Each time a NB divides, it gives rise to a new NB and to a GMC, which divides to generate neurons (not shown). GMCs maintain the expression of the factor expressed by the NB when it divided. (Adapted from Livesey and Cepko, 2001). (**B**) Genetic relationships between Hb, Kr, Pdm and Cas. Blue arrows indicate activation, red bars indicate repression. Hb activates Kr but represses Pdm. (**C**) The sequential expression of transcription factors results in a layered organisation of the developing CNS (dashed lines). The first-born Hunchback (Hb) positive neurons are localised dorsally (D) whereas the last-born Castor (Cas) positive neurons are close to the NB, in a more ventral position (V). (Adpated from Edenfeld *et al.*, 2002)

NB7-1, intermediate-born sublineages are competent to make extra "younger" neurons in response to the persistent expression of Hb, however this plasticity is eventually lost in older NBs (Pearson and Doe 2003; Isshiki and Doe 2004).

It has been proposed that another TF, Grainyhead (Grh), takes part in the sequential TF series as the ultimate factor. When NBs are cultured for a few hours they produce Hb-, Kr-, Pdm-1- and Cas-positive progeny, but after an overnight culture the NB and GMC also express Grh (Brody and Odenwald 2000). *In vivo*, Grh is expressed within the NBs starting from stage 14 (Bray et al. 1989) but whether there is direct transcriptional regulation between Cas and Grh is not yet known. Neither is it known whether the identity/fate of the GMCs or neurons is controlled by Grh expression. While there is no evidence that Grh is a member of the TF series influencing neuronal fate, recent work in the lab indicates that it does regulate the number of postembryonic NB divisions (Cenci and Gould 2005) and (see Section 1.3.3A).

Interestingly, switching from *Hb* to *Kr* is dependent upon the progression of the cell cycle. Cells that are unable to undergo the normal cell cycle also fail to exit their Hb-expression status and generate excess "young" neurons, but when the cell cycle block is removed they carry on with the normal series without skipping any factors (Isshiki et al. 2001). This suggests that, in the case of the *Hb* to *Kr* switch, the clock specifying when this transition should occur corresponds to the cell cycle. Interestingly however, this is unique to the *Hb* to *Kr* transition of the TF cascade, suggesting that there is another clock, distinct from the cell cycle that regulates the *Kr* to *Pdm* and *Pdm* to *Cas* transitions. Thus, in summary, progression through the TF cascade acts cell-autonomously to generate cellular diversity within the CNS and this is achieved by assigning a temporal label to the NB, which also acts to restrict its mitotic potential.

In summary, AP and DV patterning genes act to assign a spatial identity to the NB, whereas the TF cascade assigns a temporal identity to it. The combined action of the AP/DV patterning genes and TF cascade has the potential to provide every GMC in the embryonic VNC with a unique identity.

1.2.5 Brain development

The covert segmental organisation of the brain has made our understanding of its development more rudimentary than that of the VNC. The brain originates from the procephalic neuroectoderm (PNE) and gives rise to a bilaterally symmetrical array of about 105 embryonic NBs (eNB). In the adult brain, highly organised neuropil

structures have been described, including the mushroom bodies, central complex, optic lobes (OLs) and antennal lobes, as well as other major fibre tracts required for complex behavioural functions but these appear to have no counterparts in the VNC (Bullock and Horridge 1965; Strausfeld 1976; Hanesch et al. 1989). Given these differences, it is interesting that most genes known to be expressed in the PNE also play a role in VNC development (reviewed in (Urbach and Technau 2004) and that the serial homology observed between NBs of different VNC neuromeres is also found between VNC NBs and some procephalic NBs (Urbach and Technau 2003b).

According to AP and DV patterning gene expression patterns, the brain is derived from four neuromeres (Fig. 1.8A,B) corresponding to the (from posterior to anterior), intercalary, antennal, labral and ocular segments (Urbach and Technau 2003c). These segments give rise to the traditional insect subdivisions of the brain; the tritocerebrum (intercalary), deutocerebrum (antennal) and posterior (labral) and anterior (ocular) protocerebrum (Bullock and Horridge 1965). Like the VNC NBs, procephalic NBs are generated from the neurectoderm between embryonic stages 8 and 11. NBs from one mitotic domain enter mitosis in close synchrony with each other, but out of synchrony with cells in other mitotic domains (Urbach et al. 2003a). Recent research indicates that brain NB formation is achieved through several different modes, related to the mitotic domain of origin (Fig. 1.8C,D). Of note, although most parts of the brain derive from NBs, small 'placode'-like groups of ectodermal cells close to the head midline invaginate during stage 13 long after procephalic NB formation has ceased and contribute subpopulations of cells to the brain (Younossi-Hartenstein et al. 1996; Dumstrei et al. 1998; Noveen et al. 2000) (see Section 1.4.1).

1.3 POSTEMBRYONIC NEUROGENESIS

Drosophila is a holometabolous insect that exists in very different larval and adult forms. Larval stages are divided into three instars, 1st (L1), 2nd (L2) and 3rd (L3), followed by a pupal phase, during which metamorphosis occurs to produce the adult fly (Fig. 1.9). Neurogenesis is split into two distinct phases to accommodate the differing sensory and motor requirements of each bodyform. The embryonic phase of neurogenesis that generates the functional CNS of the larva has been previously described (Hartenstein and Campos-Ortega 1984) (see Section 1.2). During post-embryonic life, a second phase of neurogenesis generates most of the adult neurons

FIGURE. 1.8. NEUROBLAST FORMATION IN THE EMBRYONIC BRAIN. **(A)** Schematic of the segmental topology of a flat-mount embryonic CNS at stage 11. The four neuromeres from anterior to posterior are labral (LR), ocular (OC), antennal (AN) and intercalary (IC) and the classic (inset) brain divisions are protocerebrum (P), deutocerebrum (D) and tritocerebrum (T). **(B)** Neuromeric model of the early embryonic brain, based on the expression of the segment polarity genes *engrailed/invected (en/inv*, red) and *hedgehog* (*hh*, purple) are the DV patterning genes, *muscle segment homeobox (msh*, green) and *ventral nervous system defective (vnd,* yellow). Four neuromeres (divided by red lines) include the labral part of the protocerebrum (Lr-Pc), ocular part of the protocerebrum (Oc-Pc), deutocerebrum (Dc) arising from antennal segment (AN) and tritocerebrum (Tc) arising from the intercalary segment (IC). OLP: optic lobe primordium.. **(C)** Procephalic mitotic domains (1, 2, 5, 9, 20 and B) contributing NBs to the embryonic brain are delimited by different colours. **(D)** NBs from different mitotic domains are formed by different modes: Domain B, basally oriented delamination; Domains 1 and 5, division parallel to ectoderm (forming epidermoblast and NB) then basal delamination; Domain 9, apical movement before reintegration and basal delamination (a1) or division perpendicular to the ectoderm (b), then one daughter moves apically before later reintegrating into the ectoderm to form an epidermoblast, the other delaminates basally as a NB. (Adapted from Urbach and Technau 2003 and 2004).

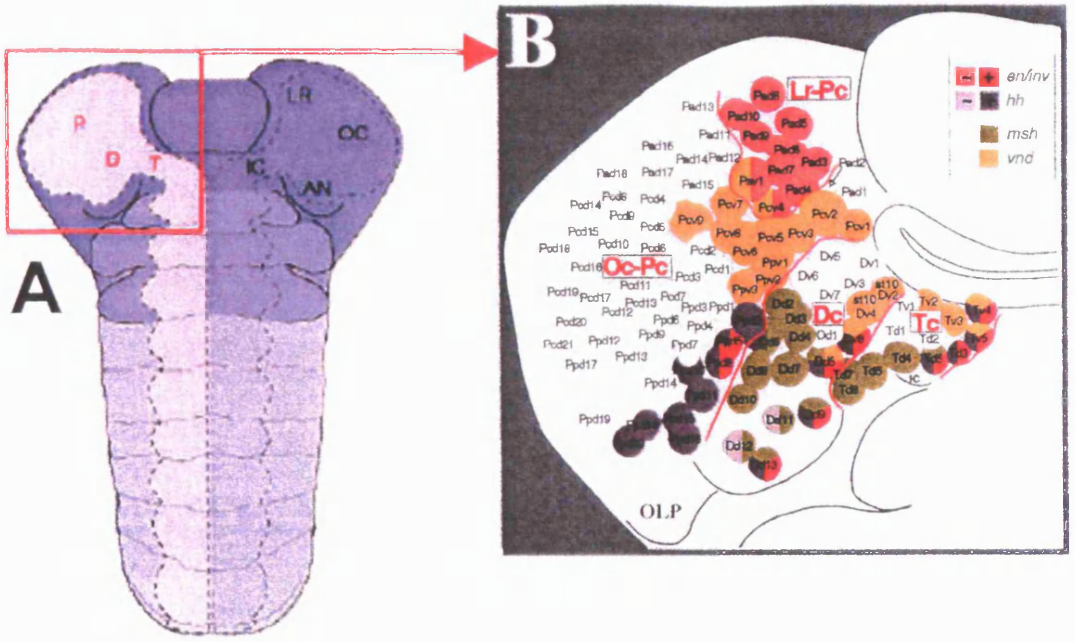
A
P
D
T
LR
OC
IC
AN
B
Lr-Pc
Oc-Pc
Dc
Tc
OLP
en/inv
hh
msh
vnd

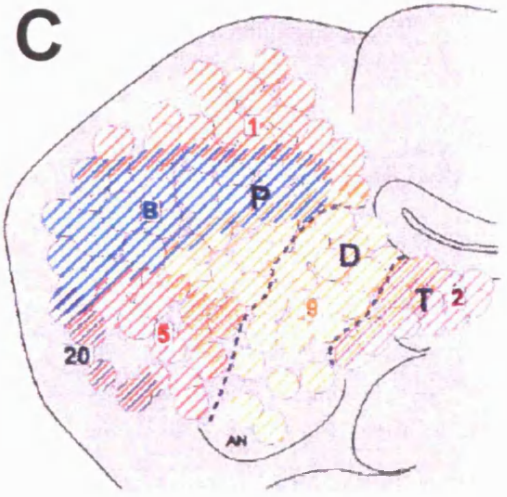
C
1
B
P
D
9
T
2
5
20
AN

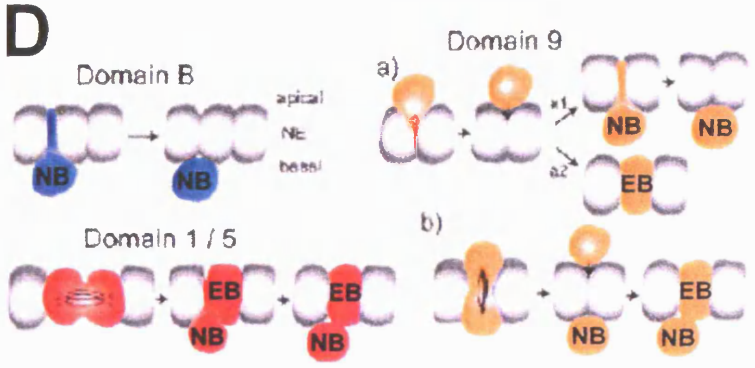
D
Domain B
apical
NB
basal
NB
Domain 9
a)
a1
a2
NB
NB
EB
Domain 1 / 5
EB
NB
EB
NB
b)
EB
NB
NB

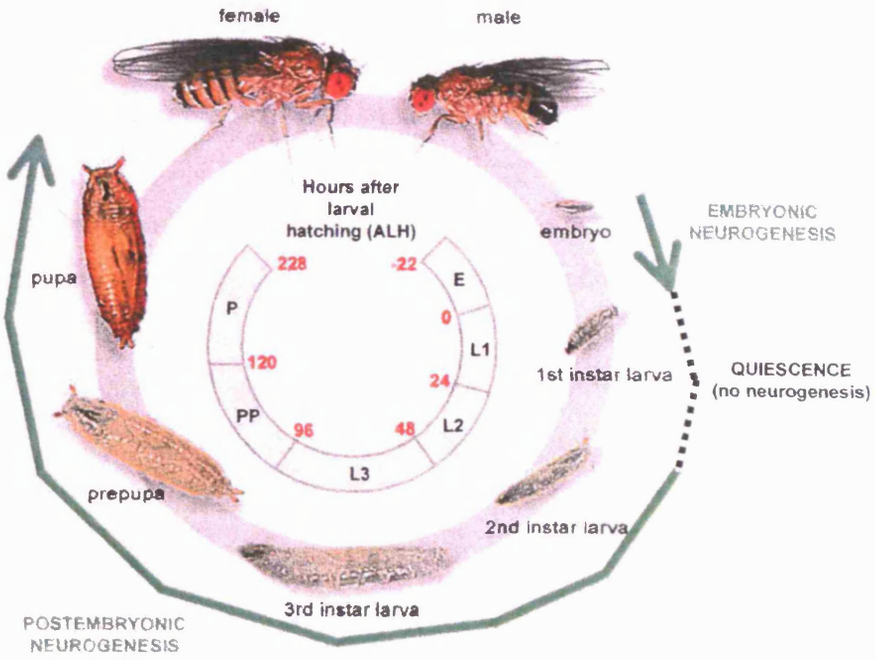

FIGURE 1.9. TWO PHASE OF NEUROGENESIS IN *DROSOPHILA*.
Neurogenesis has two distinct phases; embryonic and postembryonic, separated by a quiescent (mitotically inactive) period. Embryonic neurogenesis lasts ~22hr and serves to generate the functional larval nervous system. The postembryonic neurogenic phase, generating most of the adult nervous system, is divided into; larval (subdivided into first (L1), second (L2) and third (L3) instars), prepupal (PP) and pupal (P) stages. Hours after larval hatching (ALH) marked in red. Adapted from Flyview (http://flyview.uni-muenster.de/).

on top of the larval CNS (White and Kankel 1978; Booker and Truman 1987b; Truman and Bate 1988). This latter phase spans both larval and pupal development.

1.3.1 Embryonic and postembryonic neuroblasts share a common lineage

Since holometabolous insects arose from hemimetabolous ancestors, which exhibit only a single neurogenic period (Malzacher 1968; Bate 1976), the question arises as to whether holometabolous larvae possess an extra set of postembryonic SCs.

Studies of neurogenesis in the tsetse fly, *Glossina pallidipes*, provided visual evidence that postembryonic NBs (pNB) represent a subset of embryonic NBs (reviewed in (Truman 1990). Experimental support for the continuity of the embryonic and postembryonic lineages in *Drosophila* comes from elegant transplantation experiments by Prokop and Technau (Prokop and Technau 1991). In these experiments, *LacZ* transgenic embryos, where all neural cells are labelled by the stable genetic marker, β-galactosidase (β-gal), were injected at very early stages (syncytial blastoderm) with HRP, an enzymatic marker that gets diluted out by cell division. Neuroectodermal cells from these double-labelled donor embryos were then homotopically transplanted into host wild-type embryos and NB clones observed at L3. This technique allows the detection of two kinds of clones in the VNC. The first type of clone is small (<37 cells) and consists of HRP/β-gal double-labelled cells. These correspond to neural cells that were generated only during embryogenesis as they can also be found in specimens fixed at late embryonic stages. The second type of clone contains >100 cells and consists of a small group of double-labelled cells making contact with a larger group of β-gal single-positive cells. Among these latter cells, one large cell that is located ventrally can be identified as the postembryonic NB (pNB) (Truman and Bate 1988; Prokop and Technau 1991). It is thus presumed that this pNB divided during embryogenesis, producing double-labelled progeny, entered a quiescent state and subsequently resumed several additional rounds of division at larval stages, diluting the HRP but not the genetic β-gal label. Importantly, all postembryonic lineages were found associated with a group of double-labelled larval neurons. Although this experiment establishes a clonal relationship between embryonic and postembryonic lineages, it does not formally prove that the two cell types are identical. However, coupled with the *Glossina* observations, this is generally assumed to be the case (Truman et al. 1993).

1.3.2. Spatio-temporal pattern of postembryonic neuroblast divisions

By the end of embryogenesis (stage 17), with the exception of a few late-replicating thoracic NBs (Prokop et al. 1998), 5-bromo-2-deoxyuridine (BrdU) incorporation experiments indicate most NBs have stopped dividing. Around this time, a wave of programmed cell death, dependant upon the proapoptotic gene, *reaper (rpr)* (White 1996; Prokop et al. 1998; Peterson et al. 2002), generates segmental variations in NB number, with 80-85/105 procephalic NBs, 23/30 thoracic NBs but only 3/30 abdominal NBs (called ventro-lateral, vl; ventro-medial, vm and dorso-lateral, dl) surviving (Truman and Bate 1988; Ito and Hotta 1992; Urbach et al. 2003a). The BrdU-labelling studies of Prokop and Technau (1991) suggest that there is not a global stop signal that ends embryonic neurogenesis because the time that eNBs enter their last embryonic S phase varies markedly. Interestingly, isolated eNBs cultured in vitro generate clusters of about 20 neurons (Furst 1985), a number consistent with their embryonic complement, rather than the 100+ neurons they eventually produce during their entire life. These in vitro events may reflect the *in vivo* controls that occur in the late embryo, suggesting that apoptosis or entry into quiescence may be intrinsic to the eNB or determined through a feedback interaction between the NB and its progeny.

Having stopped dividing, surviving eNBs enter a quiescent phase, before resuming proliferation as pNBs during larval and pupal stages. The pattern of pNB proliferation has been studied by tritiated thymidine and BrdU incorporation in the ventral ganglion (White and Kankel 1978; Truman and Bate 1988), central brain (Ito and Hotta 1992) and optic lobe (OL) (Hofbauer and Campos-Ortega 1990). As mentioned above, the L1 CNS already shows clear segment-to-segment differences in pNB number with 3 abdominal and 23 thoracic pNBs per hemisegment and 30-40 pNBs per OL. However, a further level of control over final neuronal number is achieved through segment-specific temporal regulation of the mitotic activity of each pNB. Truman and Bate studied the temporal pattern of pNB divisions throughout larval life by analysing S-phases using BrdU incorporation (Truman and Bate 1988; Truman et al. 1993) (Fig. 1.10). At larval hatching, most pNBs are not dividing and are termed quiescent. However, mushroom body NBs are an exception, continuously dividing to produce prominent structures of the central brain necessary for olfactory learning and memory (Akalal et al. 2006).

The BrdU experiments show that the onset of postembryonic neurogenesis depends upon the position of the pNB along the AP axis. In general, pNBs located in

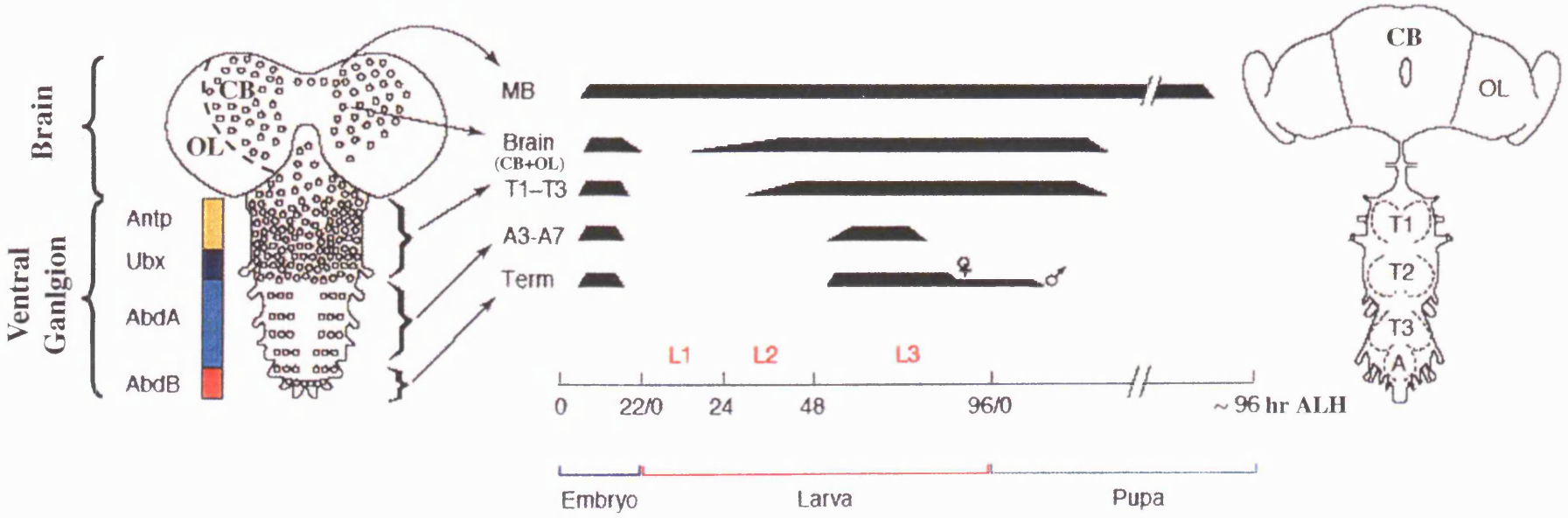

FIGURE 1.10. NEUROGENESIS IN THE LARVAL CNS.
Schematic of L3 larval CNS (left) and adult brain (right), outlining the brain, divided into central brain (CB), mushroom bodies (MB) and optic lobe (OL); and the ventral ganglion, divided into thorax (Tx, T 1-3), abdomen (Ab, A 3-7) and terminal region (Term). Major domains of Hox expression are shown for Antennapedia (Antp, yellow), Ultrabithorax (Ubx, blue), Abdominal-A (AbdA, cyan) and Abdominal-B (AbdB, red). Periods of DNA replication for the pNBs are indicated (black bars). Note that NBs in terminal segments stop dividing at different times in males and females. Timing in hours after larval hatching (ALH). (Adapted from Maurange and Gould, 2005)

more anterior segments start dividing before their more posterior counterparts. DNA replication can be observed in some of the pNBs of the central brain soon after hatching of the L1 larva. At this time, OL precursors are also dividing and it is believed that the increase in OL NB number occurring during L1 and L2 is accounted for by an expansion of neuroepithelial precursors of OL NBs, which undergo symmetric divisions prior to switching to an asymmetric mode to generate OL NBs (see Section 1.4.2B). Replicating pNBs first become detectable in the thoracic neuromeres from 24hr ALH, when the L2 larval stage starts. Finally, the abdominal pNBs commence S-phase at early-L3, with a 24hr delay relative to the thorax.

The time at which pNBs cease replicating DNA also shows dramatic anterior to posterior differences. The pNBs of the brain hemispheres and the thorax continue to divide into the pupal period, whereas abdominal pNBs terminate proliferation at mid-L3, approximately 72hr after larval hatching (ALH). Interestingly, sex-specific differences in pNB division can be observed in the posterior abdomen, where the four terminal pNBs continue dividing for longer in males than in females (Truman et al. 1993).

In summary, segment-specific regulation of pNB number and mitotic activity both contribute to remodelling of the adult CNS from its larval predecessor. The key region-specific control points underlying these pNB division patterns are the timing of re-entry into the cell cycle and the time at which pNB divisions finally cease. The Truman and Bate studies highlight the large number of different pNB division start- and stop-points and consequently the important question arises as to how each of these proliferative windows is regulated. The next section will briefly review our current understanding of how pNB divisions are spatio-temporally controlled (reviewed in (Maurange and Gould 2005) (Fig. 1.11).

1.3.3. Spatio-temporal regulation of postembryonic neuroblast divisions

Following the quiescent period, most pNBs resume dividing asymmetrically, expressing many of the asymmetric cell fate determinants in similar patterns as is seen in the embryo (Ceron et al. 2001; Akong 2002). Numerous genes are required for pNB activity, for example *Drosophila aPKC* (Rolls et al. 2003) and its target *l(2)gl* (Gateff 1978; Betschinger et al. 2003), *brat* (Bello et al. 2006; Betschinger et al. 2006; Lee et al. 2006) (three asymmetric determinants), *Enoki mushroom* (a histone acetyl transferase) (Scott et al. 2001), *Lissencephaly 1* (a coild-coil/ED repeat protein)

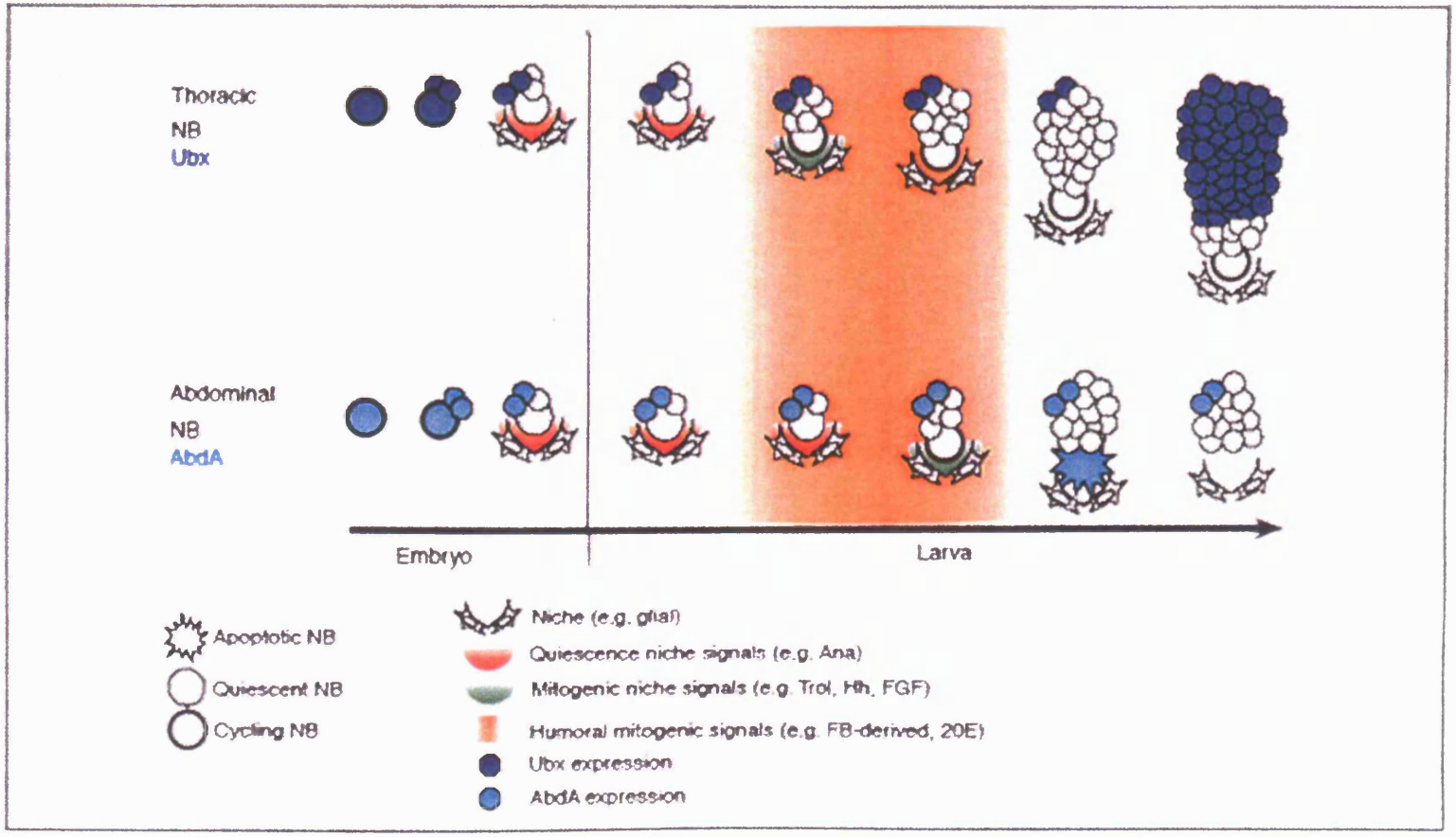

FIGURE 1.11. FACTORS STARTING AND STOPPING NB DIVISIONS
Time lines show the development of a single thoracic (top) and abdominal (bottom) NB lineage during embryonic and larval stages. Both long-range humoral signals and short-range niche signals stimulate the transition from quiescence to mitotic activity. abdominal NB divisions are stopped by a burst of AbdA expression in the NB that induces apoptosis. Absence of Ubx expression in thoracic NBs allows continued larval divisions. (Adapted from Maurange and Gould, 2005)

(Liu et al. 2000) and *RhoA* (a small GTPase) (Lee et al. 2000c), as well as *Dhc64C* and *roadblock (robl)* (which encode Dynein heavy and light chains, respectively) (Reuter et al. 2003). Additionally, although it is not yet known in which neural cell types they are required, the bHLH factors *deadpan* and *asense* have dramatic effects on proliferation in the brain (Wallace et al. 2000). It is not known if these genes play general housekeeping roles or whether they might contribute to the high degree of regional specificity in the proliferation patterns of the developing CNS.

A. Hox Genes

A role for *Hox* genes in generating segment-specific differences in embryonic NB proliferation has already been demonstrated (Prokop and Technau 1994; Prokop et al. 1998). Experiments involving BrdU pulse-labelling of stage 16 embryos has revealed abundant proliferation in the more anterior segments of the VNC compared with rare replicating cells in the abdominal neuromeres (Prokop et al. 1998). Furthermore, it appears that serially homologous NBs often display segment-specific differences in clone size. For example, NB7-1 in the abdominal neuromeres generates fewer progeny than its thoracic counterpart. Similar segment-specific differences in the number of NB divisions have also been described for other NB lineages (Bossing et al. 1996; Schmid et al. 1999).

Loss of function experiments, assessed through BrdU incorporation in late embryogenesis, have demonstrated that, in the central abdomen, AbdA is required to repress divisions in some lateral abdominal NBs, such that *abdA* mutants show abdominal NB division patterns reminiscent of the thorax and consequently the presence of ectopic abdominal pNBs (Prokop et al. 1998). This suggests that AbdA and perhaps Ubx control the 30 to 3 reduction in the number of NBs at the end of embryogenesis. This control appears to be linked to cell death in late abdominal eNBs as embryos lacking the pro-apoptotic gene *reaper* develop into larvae that, similar to *abdA* mutants, carry ectopic abdominal pNBs (White 1996; Peterson et al. 2002).

Initially it was thought that AbdA was no longer expressed in the NBs of the late embryo and larva (Prokop et al. 1998) but a recent study identified a burst of AbdA expression at 60-66hr ALH (Bello et al. 2003) (Fig. 1.11). At this time, during L3, the cells are dividing since they often express phosphorylated Histone H3, marking cells in M-phase. By using TUNEL staining, which positively labels apoptotic cells, Bello *et al* identified a burst of cell-death in the abdominal pNBs that follows the AbdA expression

at 66-78hr ALH. Subsequently, the authors took advantage of the elegant genetic mosaic technique, MARCM (Mosaic Analysis with a Repressible Cell Marker) (Lee and Luo 1999b) (see Section 2.4.2), and demonstrated that the L3 burst of AbdA in the pNBs is required for the induction of cell death. Thoracic pNBs do not express any Hox genes at these stages and thus maintain the ability to divide throughout larval stages. A second factor, *Grh*, has been shown to be involved in this Hox regulated spatio-temporal control of pNB divisions (Cenci and Gould 2005). Interestingly, Grh has opposite effects in the thorax and abdomen, allowing thoracic pNBs to continue dividing into pupal stages, possibly by promoting NB survival, but making abdominal pNBs competent to respond to AbdA-dependent apoptosis.

B. Humoral signals

Long-range hormonal and nutritional cues have been implicated in reinitiating pNB divisions after the quiescent period (Fig. 1.11). Much of this evidence comes from explanted cultures of larval CNS (Truman et al. 1993; Britton and Edgar 1998; Datta 1999). Quiescent pNBs explanted from L1 larvae can initiate cell division when cultured in the presence of fetal calf serum or larval extract. The substitution of either supplement with the steroid hormone that promotes moulting events and metamorphosis, 20-hydroxyecdysone (20HE), is also sufficient to re-activate pNB proliferation (Riddiford 1993; Datta 1999). Since early larval NBs do not express Ecdysone receptor (EcR) (Truman et al. 1994), it is likely that the steroid hormone plays an indirect role in regulating NB re-activation. Ecdysone also appears to play a role in controlling the speed of NB divisions after the NB has been reactivated. When the ecdysone puparial peak required for metamorphosis is suppressed using the temperature-sensitive ecdysone-deficient mutant ecd^1, NBs proliferate at a slower rate than normal but they eventually terminate divisions after producing the appropriate number of progeny (Truman et al. 1993). Thus, ecdysteroids seem to influence the speed of the NB cell cycle rather than affecting the total number of progeny generated.

Nutrition is another important factor in regulating initiation of pNB divisions. pNBs of L3 larvae from over-crowded or nutrient-deprived cultures do not enlarge properly and fail to start dividing, but they can be rescued by providing increased food availability. However, once pNB divisions have commenced they are not halted by starvation suggesting that, once initiated, the mitotic programme becomes independent of nutrition (Truman et al. 1993; Britton and Edgar 1998). It is currently not known how

nutritional status can be translated into signals required for pNB reactivation. However, when CNS isolated from starved larvae are co-cultured in the presence of fat body (an important endocrine tissue involved in lipid storage and metabolism) dissected from well-fed larvae, arrested NBs can be reactivated (Britton and Edgar 1998). This observation has prompted Britton and colleagues to propose the existence of a novel mitogen, derived from fat body.

C. Short-range signals

Although it is unclear whether a SC niche exists for NBs in the early embryo, culture assays do suggest that embryonic divisions can proceed without close proximity to other cell types (Furst 1985; Brody and Odenwald 2000). For pNBs, however, one important component of a larval SC niche is provided by a network of surface glia (Fig. 1.11). The *Drosophila* E-cadherin homologue DE-cadherin is widely expressed by glia, pNBs and their progeny. However, blocking its function specifically in glia, using a dominant-negative approach, reduces the mitotic activity of central-brain NBs (Dumstrei et al. 2003a). A possible role for cadherin-based cell adhesion within the pNB niche is to facilitate local glial-to-NB signalling. For example, it is known that glia secrete the glycoprotein Anachronism (Ana), which regulates the timing of transition from quiescence to proliferation in central brain pNBs (Ebens et al. 1993). A second gene implicated in this process is *terribly reduced optic lobes (trol)* (Datta and Kankel 1992). The distribution of Trol has yet to be characterised in detail but it is known to be expressed by midline glia in the embryo (Friedrich et al. 2000; Voigt et al. 2002). *ana* and *trol* mutants exhibit opposite phenotypes relative to the onset of NB divisions in the central brain; *ana* loss-of-function mutants display premature re-entry into the cell cycle, whereas *trol* mutants show a severe drop in the number of proliferating cells in the brain lobes. *ana* encodes a novel glycoprotein secreted by glial cells whose activity is required for maintaining NBs in a quiescent status (Ebens et al. 1993). However, since Ana expression appears to remain constant once NB division is activated, a second factor, perhaps encoded by *trol*, may be needed to antagonise its activity. As *ana/trol* double mutants manifest the same phenotype as *ana* mutants, *ana* probably acts upstream of *trol* (Datta 1995).

Recently the protein encoded by *trol* has been identified as the fly homologue of vertebrate Perlecan (Voigt et al. 2002; Park et al. 2003a). Perlecan is a multidomain heparan sulphate proteoglycan that can influence intercellular signalling by interacting

with extracellular matrix proteins, growth factors and receptors. The molecular structure of Trol is consistent with a function in releasing the NB from quiescence either by sequestering negative proliferation signals, such as Ana, or by promoting positive proliferation signalling by factors such as Hedgehog (Hh). A combination of genetic interaction data, CNS culture studies and coimmunoprecipitation experiments suggests that Trol could promote progression from G1 to S-phase by facilitating Fibroblast growth factor (FGF) and Hh signalling (Park et al. 2003a). Cell cycle effectors have been identified as the candidate downstream targets of the Ana/Trol pathway, for example ectopic expression of Cyclin E can force pNBs from *trol* mutant larvae into S-phase (Caldwell and Datta 1998). It is however currently unknown how this mechanism can be differentially regulated along the AP axis to produce segment-specific features described for the initiation of pNB divisions.

As with nutrition, the requirement of the *trol/ana* pathway is believed to regulate only the onset, not the maintenance of divisions, as once the cell cycle has been re-initiated NBs can divide without Trol activity (Datta 1995). Interestingly, the nutritional regulation of pNB cell-cycle activation (see Section 1.3.3B) seems to be independent of the *ana/trol* pathway as there is NB arrest in nutrient-deprived *ana* mutants. Furthermore, hormonal regulation lies upstream of *trol* function because cultures of *trol* mutant CNS fail to undergo division following treatment with 20HE (Datta 1999).

In summary, the nutrition and *ana/trol/hh* work suggests that eNBs and pNBs are different such that extrinsic signals are required for pNB but not eNB divisions. However, it can not be ruled out that extrinsic factors provided by other cells in the primary culture or even by growth factors in the medium itself contribute to sustaining eNB divisions *in vitro*. A special case of extrinsic control of proliferation is observed in OL pNBs, which rely on signals provided by the innervating photoreceptor axons for initiation of proliferation (see Section 1.4.2C). This is just one of several ways in which neurogenesis in the visual system differs from that in other CNS regions.

1.4 VISUAL SYSTEM DEVELOPMENT

1.4.1 Embryonic neurogenesis generates the larval visual system

As mentioned in Section 1.2, most CNS regions generate NBs through delamination of individual cells from the neuroectoderm. However, the dorsomedial protocerebral domain and the OL primordium differ in their early developmental programme, in that the precursor cells invaginate *en masse*. The OL primordium

originates from the posterior protocerebral neuroectoderm (reviewed in (Green et al. 1993), called the eye field (Chang et al. 2001), which expresses and requires Dpp, Hh and EGFR signalling for its development (Suzuki and Saigo 2000; Chang et al. 2001; Chang et al. 2003). The OL primordium generates the adult eye disc (ED), the OL that it innervates and the larval eye or Bolwig's organ which projects via Bolwig's nerve, into the OL via the optic stalk (OS) (Pollock and NBenzer 1988; Melzer and Paulus 1989) (Fig. 1.12). Bolwig's organ mediates light avoidance behaviour in larvae and, around Bolwig's nerve both the ED and OL develop.

The cells of the OL primordium remain distinct from those of the more dorsally-derived central brain (Campos-Ortega 1985) and display a different pattern of mitotses during larval and pupal stages (Green et al. 1993). In contrast to the role of *Notch* in VNC NB development, OL progenitors require Notch to stay epithelial and in contact with one another (Green et al. 1993). In early larval stages, OL progenitors initially remain epithelial and are thought to divide equally in the plane of the epithelium, leading to a dramatic growth of the OL during the first half of the larval period (Egger et al. 2007). Subsequently, all OL progenitors convert into non-epithelial NBs, which follow the more common asymmetric division pattern (Younossi-Hartenstein et al. 1996) (see Section 1.2.3). This early symmetrically dividing and later asymmetrically dividing phases have led to much recent interest in using the *Drosophila* OL to model the related switch between these division modes that is thought to accompany mammalian neural progenitor divisions (reviewed in (Temple 2001).

1.4.2. Larval neurogenesis generates the adult visual system

Due to the more sophisticated visual processing of the adult than the larva, it is no surprise that the most dramatic phase of visual system expansion occurs postembryonically. The adult visual system of *Drosophila* consists of the compound eye and the OL (Fig. 1.13). The compound eye is a highly reiterative structure consisting of approximately 800 identical units, called ommatidia. Each unit contains 8 photoreceptor cells (R1-R8, Fig. 1.13B) in addition to 12 accessory cells including bristle, pigment and cone cells. As a consequence of this modular organisation, mutations that produce even subtle defects within a single photoreceptor subtype can disrupt the lattice structure and produce an easily detectable rough-eye phenotype. Photoreceptors extend axons through the OS to innervate the OL, within which there are three main neuropil

FIGURE 1.12. EMBRYONIC DEVELOPMENT OF THE VISUAL SYSTEM. Schematic of lateral views of the embryonic head (anterior left), at stage 9 **(A)**, 12-14 **(B)** and 17 **(C)**. **(A)** The visual system is comprised of the adult eye primordia (ED), the larval eye/Bolwig's organ (BO), and the optic lobe (OL). **(B)** Invagination of the optic lobe primordium (OLP) at three stages (1-3). Cells of the OLP constrict apically and invaginate, forming a V-shaped structure, with anterior lip (ol_a) and posterior lip (ol_p). Concurrently, cells of the head epidermis move together and accompanied by apoptosis (apo), form a closed epidermal cover, separating the optic lobe anlage from the epidermis. Bolwig's organ (BO) develops at the ventral tip of the OLP and invaginates with it, but maintains contact with the head epidermis. At later stages, cells of BO migrate out of the head epidermis and attach to the dorsal pouch. As BO migrates anteriorly, its neurites still retain contact with the OLP and these become Bolwig's nerve (Bn). **(C)** The ED evaginates late in embryogenesis from the posterior-lateral region of the dorsal pouch. (Adapted from Chang et al., 2003 and Dumstrei *et al.,* 2002).

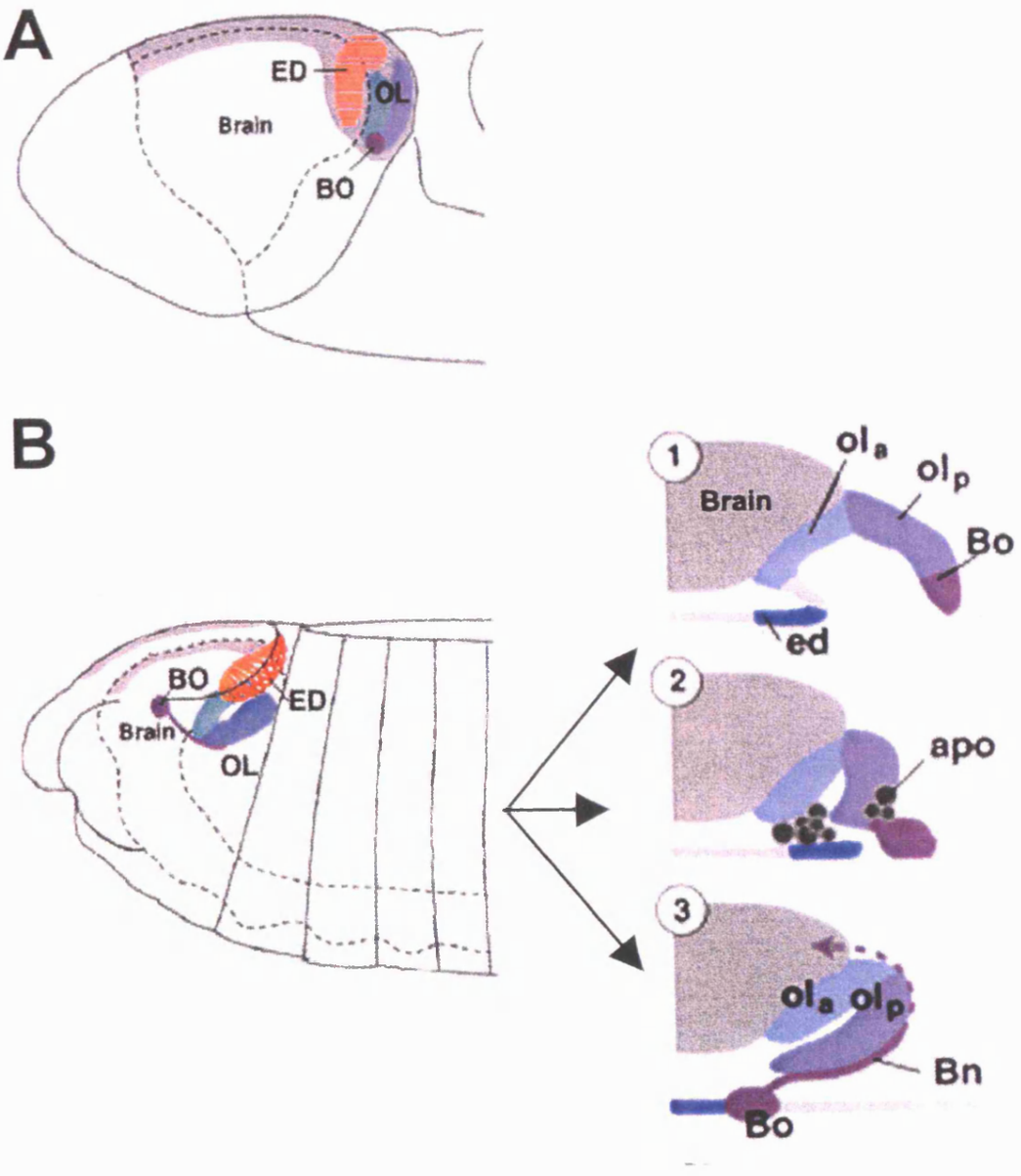
A
ED
OL
Brain
BO
B
BO
ED
Brain
OL
1
Brain
ola
olp
Bo
ed
2
apo
3
ola olp
Bn
Bo
C
dorsal pouch
ED
Brain
BO
BN
OL

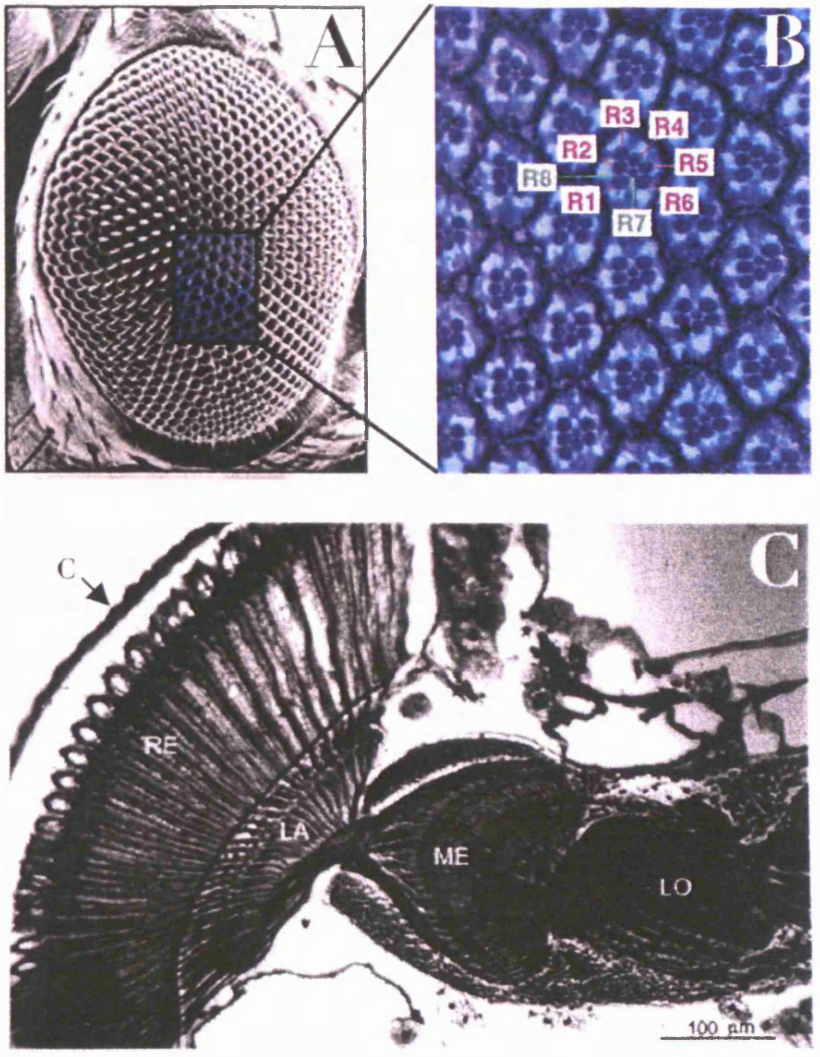

FIGURE 1.13. THE ADULT FLY VISUAL SYSTEM
(**A**) The *Drosophila* compound eye, illustrating the repetitive structure of the ommatidial units. (**B**) Higher magnification of (**A**), demonstrating the outer photoreceptors (R1-R6) forming a trapezoid with the inner photoreceptors (R7 and R8) in the centre. N.B. Since R8 is found below R7, only one of each can be seen in a given transverse section of the eye (provided by I. Salecker) (**C**) Horizontal section of the housefly's optic lobe showing the cornea (C), retina (RE) and three optic neuropils; lamina (LA), medulla (ME) and lobula (LO). Magnification X90, scale bar = 100µm (adapted from Pyza, 2002).

layers. Distally (furthest from the centre of the brain) lies the lamina (La) beneath the compound eye, and proximal to this are the medulla and lobula complexes. Their neuropil reveals a modular composition consisting of an array of columns, which correspond to the ommatidial array of the retina and which are particularly obvious in the lamina and distal medulla. The third neuropil region, the lobula complex, consists of an anterior lobula and a posterior lobula plate. Each neuropil is associated with a cortex of cell bodies lying distal to it in the case of the lamina and medulla and posterior to it, for the lobula.

The stereotypic arrangement of cell types in the ommatidia is generated during L3 and early pupal stages. On the basis of morphology, axon projection pattern and spectral sensitivity, photoreceptor cells are divided into three functional classes; R1-R6 constitute the outer photoreceptors and span the depth of the retina, R7 and R8 are the two inner photoreceptors, spanning the apical and basal half of the retina respectively (Wolff and Ready 1993). Outer photoreceptors (R1-6) terminate in the lamina, whereas the inner photoreceptors (R7 and R8) terminate in two distinct sublayers within the medulla (reviewed in (Meinertzhagen and Hanson 1993) (Fig. 1.13).

A. Eye development

The ED originates during early larval development from a contiguous group of cells that form a single-layer epithelium of dividing unpatterned cells (Ready et al. 1976), termed the eye-antennal imaginal disc (referred to hereafter as ED) (Meinertzhagen and Hanson 1993). Through the combined action of Notch and EGFR, Hh and Wingless (Wg) signalling, these cells commit to either eye or antennal fate (Kumar and Moses 2001b). During late-L2, Notch upregulation in the posterior part of the disc results in the restrictive expression of the eye selector gene *eyeless (ey)* in the eye portion of the disc (Kumar and Moses 2001b). From this stage onward, seven key regulators required for the specification of the compound eye are coexpressed within the presumptive ED (Gehring 1996; Kumar and Moses 2001b).

Neural patterning starts at the posterior margin of the ED (Ready et al. 1976). In L3, Hh expression at the posterior region of the ED induces the expression of Decapentaplegic (Dpp), a member of the transforming growth factor-β/bone morphogenetic protein (TGFβ/BMP) family of secreted proteins in anteriorly adjacent cells and initiates a wave of morphogenesis that traverses the ED from posterior to anterior (Tabata and Kornberg 1994). Consequently the disc provides a visual history of

ommatidial development from early (anterior) to late (posterior) stages. The front of this wave is marked by an apical constriction of the imaginal epithelium, called the morphogenetic furrow (MF) (Heberlein et al. 1993) (Fig. 1.14A). The regular spacing of the ommatidia is established within the furrow where individual cells, spaced by approximately seven cells, assume neural fate and will become the founder photoreceptor cells (R8) (Tomlinson and Ready 1987) (Fig. 1.14B). As cells enter the morphogenetic furrow, they synchronise and arrest in the G1 phase of the cell cycle and either move apically to assemble into preclusters and initiate ommatidial recruitment, or remain undifferentiated at the basal part of the disc. The morphogenetic furrow is propagated across the retinal epithelium, by a continuous supply of Hh and Dpp produced by newly born cells (Heberlein and Moses 1995), until it reaches the anterior end of the disc by early pupal development (Meinertzhagen and Hanson 1993).

Hh and Dpp regulate the expression of a number of molecules associated with neuronal differentiation, such as the proneural bHLH factor, *atonal (ato)* (Jarman et al. 1994). Broad expression of Ato is first observed in a continuous stripe ahead of the morphogenetic furrow in response to diffusing Hh and Dpp proteins and marks the start of neurogenesis (Greenwood and Struhl 1999; Curtiss and Mlodzik 2000). Soon after, its expression becomes restricted to evenly spaced single cells that become R8 founder neurons by a Notch-mediated lateral inhibition process (Baker et al. 1996) similar to that of the NB specification for equivalence groups (see Section 1.2.1). R8 cells are the first photoreceptor neurons to differentiate in each ommatidium and their differentiation is dependent, not only upon the expression of Ato, but also its bHLH heterodimer partner Daughterless (Da) and the downstream zinc-finger TF Senseless (Sens) (Jarman et al. 1995; Nolo et al. 2000). Following R8 selection, Ato-positive R8 cells express the EGFR-like ligand Spitz (Tio and Moses 1997) and via EGFR activation, recruit other photoreceptors and non-neural cells from surrounding undifferentiated cells in a stereotypical sequence to form ommatidial clusters (Freeman 1996) (Fig. 1.14B). This generates a precluster containing R8 and R2-5. EGFR is also activated and is required early on for the spacing between the precluster "intermediate groups" but not for R8 specification itself (Yang and Baker 2001). This is mainly because Sens blocks the activation of EGFR in R8 by repressing the expression of *pointed*, a nuclear effector of EGFR signalling (Frankfort and Mardon 2004). Immediately posterior to the precluster, a second mitotic wave gives rise to the remaining three photoreceptor cells in a sequential order, R1 and R6, and finally R7 (Wolff and Ready 1993) (Fig. 1.14A,B). R7

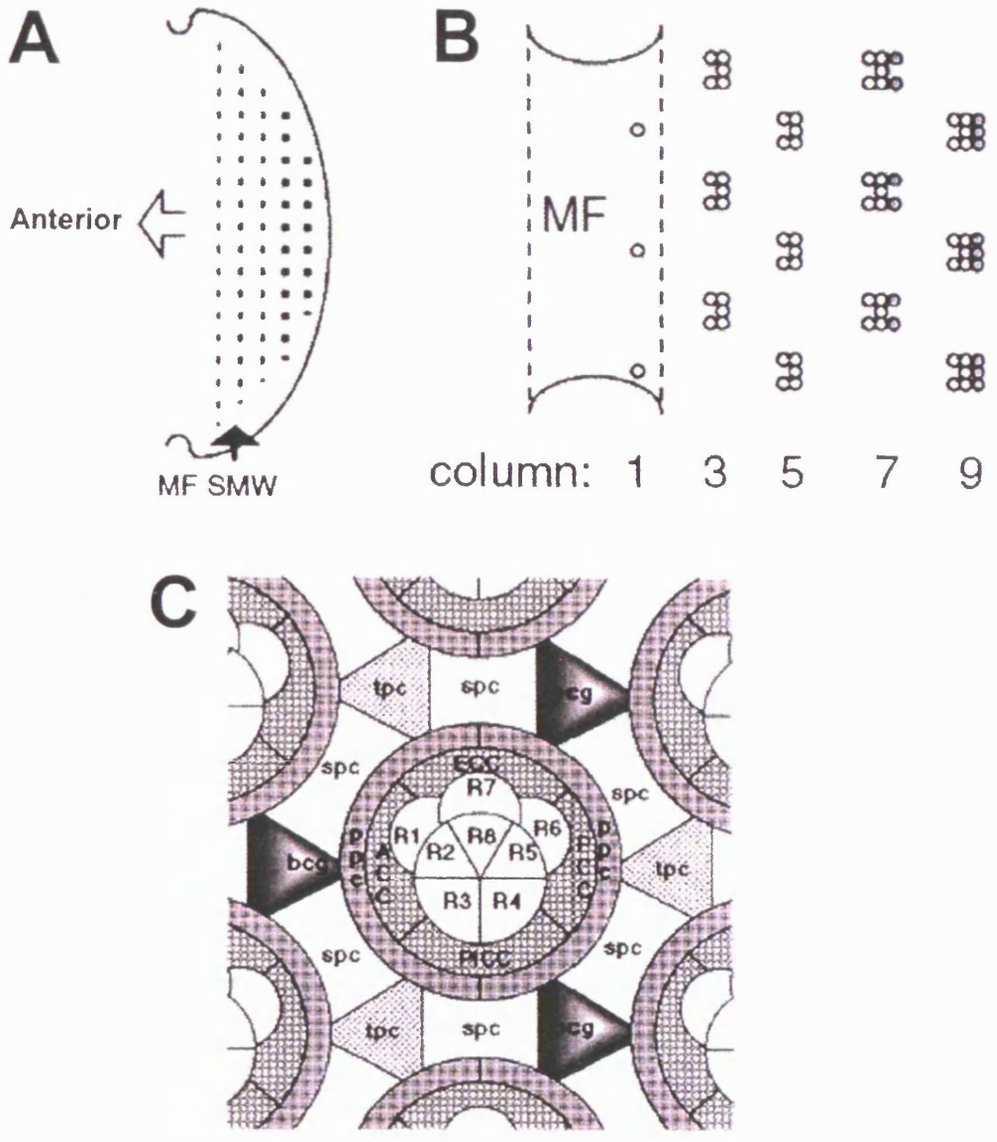

FIGURE 1.14. DEVELOPMENT OF THE *DROSOPHILA* RETINA
(**A**) Eye imaginal discs differentiate progressively, from posterior to anterior. A second mitotic wave (SMW) occurs posterior to the morphogenetic furrow (MF). (**B**) Enlargement of the region near the MF, showing the stepwise recruitment and differentiation of ommatidial cells. R8 are differentiating in column 1, within the MF, the other precluster cells R2, R3, R4 and R5 soon afterwards. All the other cells re-enter the cell cycle in the SMW and are recruited to further ommatidial fates after column 5 (shaded cells). (**C**) Schematic of retinal structure after specification of all 19 precursor cells and death of supernumerary cells. Showing 8 photoreceptor cells (R1-R8), surrounded by accessory cone and pigment cells; anterior cone cell (ACC); Equatorial cone cell (ECC); posterior cone cell (PCC); polar cone cell (PoCC); primary, secondary and tertiary pigment cells (PPC, SPC and TPC, respectively); bristle cell group (bcg). (Adapted from Baker, 2001)

is the last of the R-cells to be recruited in the ommatidial cluster and, in addition to EGFR signalling, requires the activation of the Sevenless (Sev) receptor signalling pathway (Tomlinson et al. 1987b). The Sev ligand, Bride of sevenless (Boss) is expressed in R8 cells and activates the receptor only in R7 (Reinke and Zipursky 1988).

Finally, surplus undifferentiated cells are removed by programmed cell death, tightening the ommatidial pattern (Wolff and Ready 1991) (Fig. 1.14C). Importantly, the different cell types in the eye are specified by cellular interactions (Ready et al. 1976; Tomlinson and Ready 1987) with no fixed lineage relationships between the different cell types within an ommatidium or between the same cell types of adjacent ommatidia (Ready et al. 1976; Lawrence and Green 1979b; Wolff and Ready 1991).

B. Optic lobe development

At larval hatching, each brain hemisphere contains 30-40 precursors of the optic anlage lying superficially in the cell body layer of each hemisphere. Later in L1, these cells then enlarge to become NBs and it is at this stage that they first constitute an epithelium and commence mitoses. Several classic studies have dissected the anatomy of this region (Hertweck 1931; El Shatoury 1956; Satija 1967; White and Kankel 1978; Meinertzhagen and Hanson 1993). Towards the end of L1, two different epithelia can be distinguished, which will develop into the inner and outer optic anlagen (IOA and OOA respectively). Both anlagen remain in contact with each other until the end of L2, when they will be separated by newly generated ganglion cells. During the entire larval period the OOA covers the lateral hemisphere like a dome-shaped shell with a pore at its centre, where the optic stalk (OS) enters the hemisphere (Fig. 1.15A). The IOA is a more ribbon-like structure, wrapped around the optic nerve, which during later development becomes U-shaped, with the opening of the U pointing in the dorso-caudal direction. The IOA and OOA anlagen give rise to the inner and outer proliferation centres (IPC and OPC, respectively), which generate independent cell populations and are separated by a groove called the lamina furrow. Progeny of the OPC give rise to lamina and distal medulla neurons, whereas progeny of the IPC contribute to the proximal medulla, lobula and lobula plate (Meinertzhagen and Hanson 1993).

An analysis of the proliferation pattern of the optic anlagen using [^{3}H]thymidine autoradiography on paraffin sections has been performed by White and Kankel (1978) and Hofbauer and Campos-Ortega (1993). During L1 and L2, the precursors of the OPC and IPC divide, so that by late-L2 the population has increased from 30-40 precursors

FIGURE 1.15. THE DEVELOPING EYE AND OPTIC LOBE AT THIRD INSTAR.

(A) Anatomy of the L3 optic lobe (lateral, left; dorsal up), showing inner and outer optic anlagen (IOA and OOA, respectively). Precursors in the anlagen proliferate in the directions of the arrowheads, contributing cells to the lamina (lamina-forming precursors, lafp), medulla (mfp) and lobula (lofp). Lan, lamina neuropil; mn, medulla neuropil. OS, optic stalk (Adapted from Meinertzhagen & Hanson, 1993) **(B)** Lateral view of visual system. Anterior optic lobe left, eye disc displaced anteriorly for clarity. Photoreceptor cells in the eye disc (ED) project axons through the optic stalk (OS) into the optic lobe. Three photoreceptors are shown terminating in the lamina (LAM, blue). At the lamina furrow (LF, thick black crescent) retinal axons come into close proximity to G1-phase laminar precursor cells (LPCs) (generated by the outer proliferation centre, OPC). They provide Hh which triggers the LPCs to divide, thus giving rise to lamina neurons (See C). Glial precursor cells (GPCs) (pink). (Adapted from Huang & Kunes, 1996, 1998) **(C)** Horizontal view of the visual system. Anterior left. Developmental stages are diagrammed in sequence from left to right. R1-6 (blue) and R7, R8 (green) photoreceptors cells project axons into the brain, where the more posterior cells project before their anterior neighbours. The youngest axons arrive at the edge of the OPC, near the LF, and release Hh (blue arrows). This stimulates LPCs in G1 to enter S phase and complete a final round of cell division. Expression of Hh effector genes (blue circle), such as Dachshund (Dac, blue nucleus), a marker of LPC progeny which are responsive to Spi (open red circle), secreted by photoreceptor axons (red arrows) to induce LPC progeny to express Elav (pink), a neuronal differentiation marker. These lamina neurons form vertical rows, designated lamina columns, each of which contains five lamina neurons (L1-L5). Glial cells migrate from the GPC to the target field. (Adapted from I. Salecker et al., 1998).

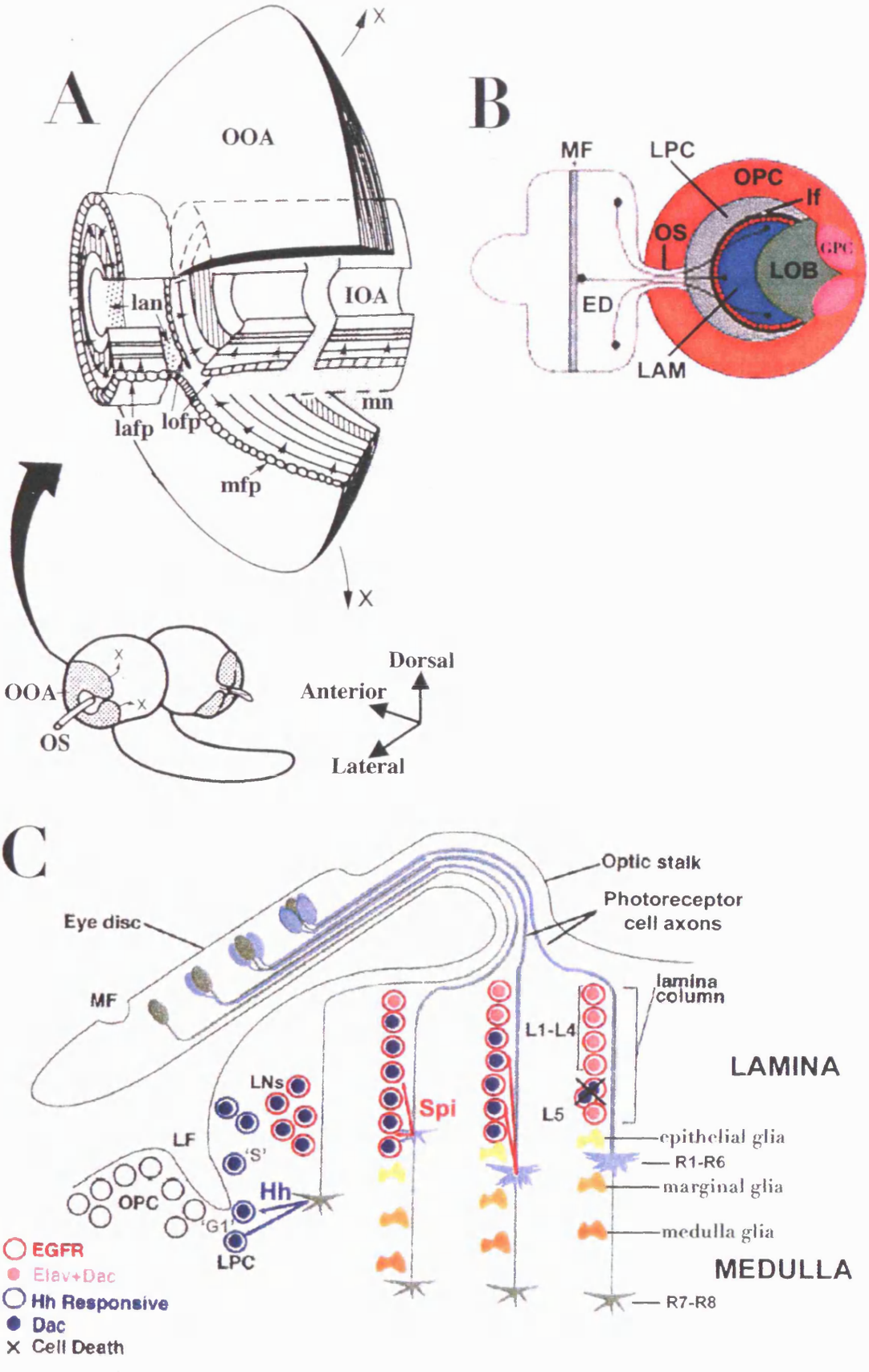
A
X
OOA
IOA
lan
mn
lafp
lofp
mfp
X
OOA
X
X
OS
Dorsal
Anterior
Lateral
B
MF
LPC
OPC
If
OS
GPC
LOB
ED
LAM
C
Optic stalk
Photoreceptor cell axons
Eye disc
MF
lamina column
L1-L4
LAMINA
LNs
Spi
L5
LF
'S'
epithelial glia
R1-R6
OPC
Hh
marginal glia
'G1'
medulla glia
LPC
MEDULLA
R7-R8
EGFR
Elav+Dac
Hh Responsive
Dac
Cell Death

per hemisphere to approximately 700 in the OOA and 400 in the IOA, which implies a doubling of precursor number every 8-9hr on average (Hofbauer and Campos-Ortega 1990). This dramatic increase in NB number is believed to be achieved by an initial round of symmetric precursor divisions occurring before the switch to more typical NB asymmetric divisions in late-L2/early-L3 (Hofbauer and Campos-Ortega 1990; Ceron et al. 2001; Egger et al. 2007) when the NBs begin to generate postmitotic cells of the imaginal OLs. Of note, although these OL precursor cells have been previously referred to as NBs, they do not express the NB marker Mira. True Mira-positive, asymmetrically dividing NBs are believed to be produced from OL precursors by an asymmetric division (Egger et al. 2007). Thus parallels may be drawn between early mammalian NSCs and OL neuroepithelial cells, in that they both undergo a symmetric expansion phase, ultimately to boost the number of transit amplifying cells/NBs. Symmetric divisions are also believed to occur in early pupal stages. Such that, by about 20hr after puparium formation, very few NBs are left, however the absence of detectable cell death at this stage led to the proposal that this is via a final round of symmetric division, producing two GMCs and subsequently four postmitotic progeny (Hofbauer and Campos-Ortega 1990; Meinertzhagen and Hanson 1993).

C. Dependency of optic lobe development on retinal innervation

During early-L3, photoreceptor axons begin to innervate the OL and lamina neurogenesis becomes dependent on incoming signals from the ED. Differentiating photoreceptor cells in the ED extend axons and project through the OS into the OL in a sequential order that follows the posterior to anterior order of their differentiation in the ED (Meinertzhagen and Hanson 1993). In this way, photoreceptor cells in adjacent ommatidia extend axons next to each other forming a topographic map of the ED in the OL. In addition to sequential ordering along the AP axis, photoreceptor cell axons are thought to project into the OL in the order of their recruitment within each ommatidium. The initial direction of photoreceptor cell axonal outgrowth toward the posterior of the ED and into the OS is provided by OS-derived retinal basal glia, whose migration into the posterior region of the ED appears to be regulated by Hh signalling (Hummel et al. 2002). A bidirectional dependency exists, such that migration of retinal basal glia into the ED is temporally and spatially linked to photoreceptor cell development (Choi and Benzer 1994). Studies have demonstrated that the number of glial cells filling the ED increases with the number of photoreceptors (Choi and Benzer 1994) and in mutants

with no photoreceptors, such as *eyes absent (eya)* (Bonini et al. 1993), glial cells do not enter the ED at all but remain in the OS.

Following the R8 axon projections, R1-R6 and finally R7 axons select their target in the OL (Meinertzhagen and Hanson 1993). R1-R6 axons terminate in the lamina, between the rows of epithelial and marginal glia. Whereas R7 and R8 axons project through the lamina and terminate in the medulla (Perez and Steller 1996). The proliferation, differentiation, as well as the migration of neural cells in the OL relies on signals provided by the incoming photoreceptor afferents (Fig. 1.15C). This has been demonstrated experimentally in mutants, such as *sine oculis (so)* (Fischbach 1983), *eya* (Renfranz and Benzer 1989) and *disconnected (disco)* (Steller et al. 1987), where reduced or absent photoreceptor innervation results in hypotrophic OLs and, more specifically, loss of lamina neurogenesis (Power 1943; Selleck and Steller 1991), In addition, for several different mutations affecting both eye and OL, studies of genetically-mosaic flies have shown that the corresponding gene is only required in the ED (Meyerowitz and Kankel 1978; Fischbach and Technau 1984). One important signal provided by the photoreceptors is Hh, transferred along R8 axons and necessary and sufficient for G1-arrested GMC-like cells, called lamina precursor cells (LPCs), to enter S-phase and undergo one cell division at the lamina furrow (Huang and Kunes 1996). Hh also induces the expression of the early neuronal differentiation marker, Dachshund (Dac) (Huang and Kunes 1996). Dac then induces the expression of the EGFR in LPCs (Chotard et al. 2005). The EGFR ligand, Spitz, corresponds to the second signal provided by R-cell axons, activating EGFR in LPCs and triggering the further differentiation of lamina neurons, at least in part, by inducing the expression of the late neuronal differentiation marker Elav (Huang et al. 1998b). In addition to lamina neurons, R-cell axons entering the OL encounter different types of glial cells. Lineage analysis has revealed that lamina glia are derived from different precursors than those of lamina neurons. The former are derived from glial precursor cell (GPC) areas, located at the edges of the R-cell projection field on the surface of the OL (Winberg et al. 1992; Perez and Steller 1996; Chotard et al. 2005) (Fig. 1.15B). Entry of photoreceptor cell axons into the target field induces differentiation and migration of epithelial and marginal glia to their appropriate positions in the lamina (Perez and Steller 1996).

My thesis is concerned with identifying new genes involved in the spatio-temporal regulation of neural proliferation during postembryonic stages.

In Chapter 3, I describe the design and execution of two genetic screens for identifying mutations disrupting neuroblast divisions.

Then in Chapters 4 and 5, I map and characterise two new mutations affecting neural proliferation, within the OL.

CHAPTER 2

MATERIALS AND METHODS

2.1 *DROSOPHILA* STOCKS AND GENETICS

Fly stocks were obtained from the stock centres at Bloomington, Indiana, USA (http://flystocks.bio.indiana.edu/), and Szeged, Hungary (http://expbio.bio.u-szeged.hu/fly/index.php). All stocks are described in detail in Table 2.1. Most genetic elements are described in FlyBase (http:://flybase.bio.Indiana.edu:82/) or (Lindsley 1992; Greenspan 1997; Greenspan 2004).

For the screens, mutant lines were generated from stocks carrying the *FRT2A* site on the left arm of the third chromosome (3L) or *FRT82B* for mutations on the right arm of the third chromosome (3R). The *FRT2A* chromosome was isogenised to ensure that it did not carry any background lethal mutations or other polymorphisms (Greenspan 2004).

Mutant lines were generated, using the chemical mutagen ethylmethanesulfonate (EMS) (see Section 3.2.1), in collaboration with the laboratory of William Chia (MRC Developmental Neurobiology Centre, London and Tamasek laboratory, Singapore). Homozygous *FRT* males were treated with 25mM EMS according to standard methods to generate an average of one lethal hit per chromosome arm (Greenspan 1997; Greenspan 2004). Mutant lines were established by crossing to a double balancer stock (Fig. 2.1). One of the balancers carries a *hs-hid* transgene, in which the proapoptotic gene, *head involution defective (hid)*, is under the control of a heat shock (hs) promoter, and thus acts as a dominant temperature-sensitive lethal. Thus, a larval heat shock allowed elimination of *TM3, hs-hid*, rather than tedious sorting of males and virgins to set up the *TM6B* stock. *TM6B* contains the larval marker Tb and is thus ideal for screening. On the basis of lethal stage, lines were divided into embryonic or late larval/pupal lethal (referred to as pupal lethal hereafter) classes.

2.2 REARING AND STAGING LARVAE

Flies were maintained on standard cornmeal/yeast/agar medium at 25°C. For experiments timed according to a precise developmental stage, embryo collections were taken over a 4hr time window on grape-juice agar plates supplemented with live yeast. Larvae were synchronised at early-L1, by collecting larvae 24hr after the end of the embryo collection and then raising on standard medium at low density. Larval staging is given in hours after larval hatching (ALH) or larval instar; late-L2 refers to 44-48hr ALH, early-L3 to 48-52hr ALH, mid-L3 to 70-74hr ALH and wandering-L3 (wL3) to 92-96hr ALH. Larval instars were confirmed through spiracle morphology

TABLE 2.1. FLY STOCKS.

See Appendix 1 for full list of deficiencies used for mapping.

Name	Full genotype	Source
FRT2A	*w; +; P{w[+], FRT2A} 79D-F*	Bloomington (BL1997)
FRT82B^{neo+}	*+; +; P{ry[+t7.2]=neoFRT}82B ry[506]*	Bloomington (BL2035)
Df H99	*w; +; P{w[+], FRT2A}, Df(3L)H99, Kni[ri-1]/TM6, Tb, Hu*	Recombinant (Lab stock)
MARCM 3L Clone-maker	*P{w[+] elavGAL4[c155]}, P{ry[+] hsFLP}1; P{w[+] UAS-nlacZ}20b, P{w[+] UAS-CD8:GFP}LL5/CyO ; P{w[+] tubP-GAL80} L9, P{w[+] FRT2A}/TM6, Tb, Hu*	Recombinant (Lab stock)
MARCM 3R Clone-maker	*P{w[+]elavGAL4[c155]}, P{ry[+], hsFLP}1 ; P{w[+] UAS-nucZ}20b, P{w[+] UAS-CD8:GFP}LL5/CyO ; P{ry[+], neoFRT82B}, P{w[+], tubP-GAL80}LL3/TM6 Tb, Hu*	Recombinant (Lab stock)
TM3, hs-hid	*w$^-$; +; TM3, Sb, P{w[+], hs-hid}/TM6, Tb, Hu*	Lab stock
Df(3L)Exel7328	*w^{1118}; + ; Df(3R)Exel7328, P+PBac{XP5.WH5}Exel7328/TM6B, Tb*	Bloomington (BL7983)
Df(3L)st-g24	*+ ; + ; Df(3L)st-g24, Ki^1 rn^{roe-1} p^p/TM6B, Tb*	Bloomington (BL3201)
sas^{15}	*sas^{15} pp cu^1 /TM3, Sb*	Bloomington (BL 2098)
lap^{KG06751}	*y^1; P{SUPor-P}lap^{KG06751}ry^{506} /TM3, Sb Ser*	Bloomington (BL 14314)

Gld^{n2}	Dfd^{1} Gld^{n2} p^{p}/TM3, Sb	Bloomington (BL 2439)
n^{roe-2}	Ki^{1} $rn^{roe-2}p^{p}$ /TM3, Sb	Bloomington (BL 2441)
$E(spl)^{rv1}$	$In(3R)E(spl)^{rv1}$, $E(spl)^{rv1}$/TM6B, Tb	Bloomington (BL199)
akt^{6M4}	yw, hs-FLP ; 82B FRT akt^{6M4} / TM6B, y^{+}	Gift from S. Leevers
Akt^{1}	yw ; Sp/CyO ; 82B $dAKT^{1}$ / TM6B, y^{+}	Gift from S. Leevers
Gro^{c105}	Gro^{c105}/TM3, Sb	Bloomington (BL2053)
TM3, act-GFP	TM3, Ser, act-GFP	Lab stock
TM6, Ubi-GFP	TM6b, Tb, Ubi-GFP	Lab stock
$msps^{EY06514}$	y^{1} w^{67c23}; P{w^{+mC} $y^{+mDint2}$=EPgy2}$msps^{EY06514}$/TM3, Sb Ser	Bloomington (BL15825)
$ey^{B.D.}$FLP, FRT80B	yw $eyFLP^{B.D.}$; + ; Pw+70cFRT80B/TM6B	Gift from I. Salecker
Ubi-GFP, FRT2A	+ ; + ; Ubi-GFP FRT2A/TM3	Gift from J. Vincent
FRT2A $M(3)^{i55}$	Y ; + ; FRT2A $M(3)^{i55}$ p[nls-GFP] / TM6B	Gift from F. Schweisguth
$ey^{3.5}$FLP	Yw $ey^{3.5}$-FLP ; + ; TM3 Sb/TM6B	Gift from I. Salecker
srp^{01549}	Ry^{506} ,P{ry[+t7.2]=PZ}srp^{01549}/TM3, ry^{RK}, Sb^{1}, Ser^{1}	Bloomington (BL11538)
pnr^{VX6}	w^{+} ; P{ry[+t7.2]=neoFRT}82B, pnr^{VX6} / TM6B, Tb^{1}	Bloomington (BL6334)
Sb^{1}	TM6 / Sb^{1}	Bloomington (BL2539)
$l(3)72Cde^{11}$	w^{1118}; + ; $l(3)72Cde^{11}$ P{*}71F/TM3, Sb (72C1;72D5)	Bloomington (BL4116)
$l(3)72Db^{8}$	+ ; + ; $l(3)72Db^{8}$/TM6C, cu Sb ca (72D1;72D5)	Bloomington (BL5052)
$l(3)72Df^{3}$	+ ; + ; $l(3)72Df^{3}$/TM2 (72D5-10)	Bloomington (BL5056)
$l(3)72Dg^{2}$	+ ; + ; $l(3)72Dg^{2}$/TM2 (72D5-10)	Bloomington (BL5057)

l(3)72Dh^{1}	*+ ; + ; l(3)72Dh^{1}/TM2 (72D5-10)*	Bloomington (BL5058)
l(3)72Di^{1}	*+ ; + ; l(3)72Di^{1}/TM2 (72D5-10)*	Bloomington (BL5059)
l(3)72Dk^{1}	*+ ; + ; l(3)72Dk^{1}/TM2 (72D5-10)*	Bloomington (BL5061)
l(3)72Dl^{1}	*+ ; + ; l(3)72Dl^{1}/TM6C, cu Sb ca (72D5-10)*	Bloomington (BL5062)
l(3)72Dm^{1}	*+ ; + ; l(3)72Dm^{1}/TM6C, cu Sb ca (72D5-10)*	Bloomington (BL5063)
l(3)72Dq^{01318}	*+ ; + ; P{PZ}kst^{01318} l(3)72Dq^{01318} ry^{506}/TM3, ry^{RK} Sb Ser (72C1;73A4)*	Bloomington (BL11528)
Taf4^{1}	*+ ; + ; Taf4^{1}/TM6C, cu Sb ca*	Bloomington (BL5060)
Pgm^{nGB1}	*+ ; + ; Pgm^{nGB1}/TM3, Sb Ser*	Bloomington (BL4039)
SSRβ^{S1939}	*w^{1118}; + ; P{lacW}SsRβ^{s1939}/TM3, Sb^{1}*	Bloomington (BL12094)
P{Pka-C3}^{KG00222}	*y^{1} w^{67c23} ; + ; P{SUPor-P}Pka-C3^{KG00222} ry^{506} (72B2)*	Bloomington (BL14345)
P{CG6017}^{EY09853}	*y^{1} w^{67c23} ; + ; P{Epgy2}CG6017^{EY09853} (72C1)*	Bloomington (BL17614)
RpL19^{k03704}	*y^{1}w^{67c23}; + ; P{lacW}RpL19^{k03704}/CyO*	Bloomington (BL12209)

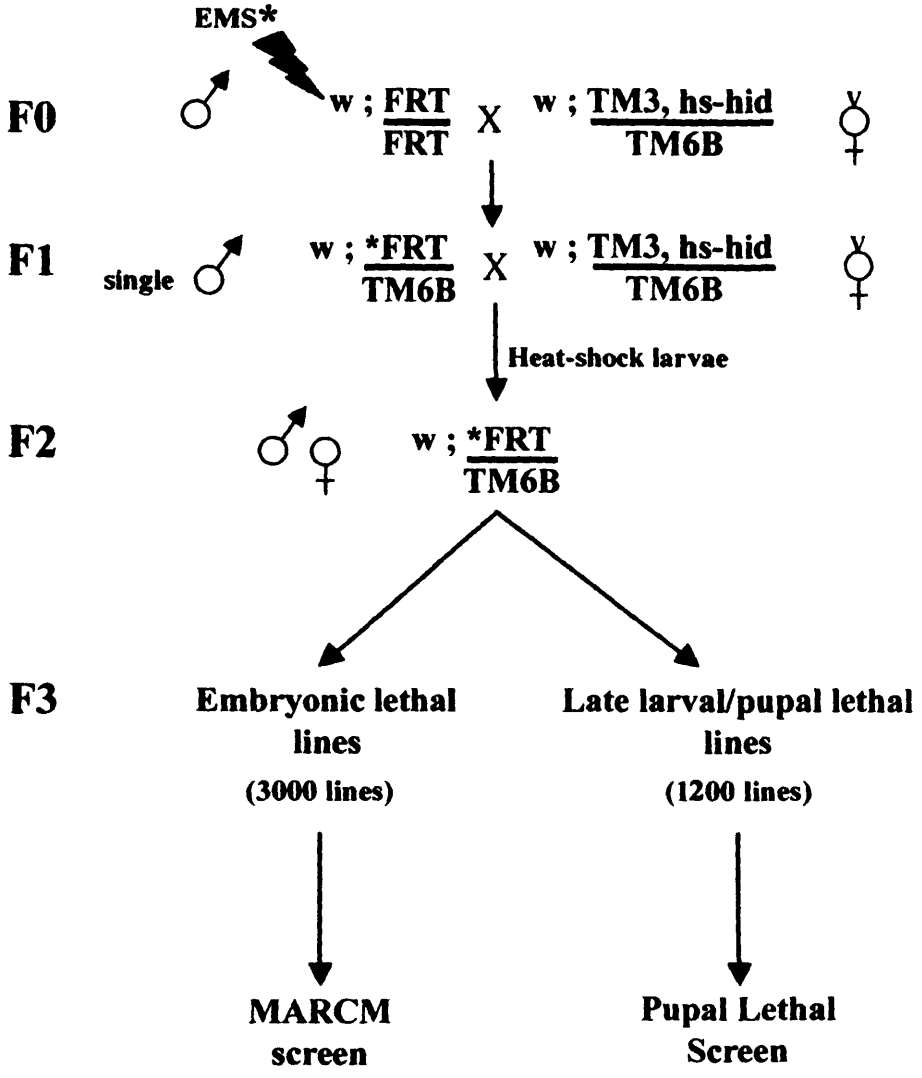

FIGURE 2.1. ESTABLISHMENT OF EMS *FRT* LINES.
Mutagenised males were crossed with a balancer stock (*TM3, hs-hid/TM6B*) to generate multiple mutant lines. A single heat shock at mid-third instar larva was then used to eliminate *TM3, hs-hid* containing genotypes. Surviving flies (all *TM6B* balanced) were used to establish mutant lines, which were subdivided into two classes on the basis of lethal stage. This resulted in approximately 3000 independent embryonic-lethal lines and 1500 pupal lethal lines, which were subsequently screened via the MARCM Screen and Pupal lethal Screen respectively.

(Bodenstein 1994) and wL3 selected by wandering behaviour. Male and female larvae were distinguished by the presence or absence of male gonads. Larvae of the correct genotype were selected by the presence or absence of balancer chromosomes carrying *Tubby (Tb)* or *Green fluorescent protein (GFP)* (Ashburner 1989).

2.3 ANALYSIS OF PUPAL-LETHAL MUTANTS

To be certain that the observed phenotypes mapped to the correct locus, mutants were analysed in the hemizygous state (using a deficiency) or as transheterozygotes (using an independently generated allele at the same genetic locus). Analysis of pupal-lethal mutants was performed using hemizygotes; *jami/Df(3L)Exel7328* and *roie/Df(3L)st-g24*, unless otherwise stated.

To investigate the growth rates of mutants (see Sections 4.2.1 and 5.2.1), 50 washed larvae were weighed per experiment and 3 to 4 replicates were performed, at 36, 60 and 84hr ALH. *roie* hemizygotes and heterozygotes were raised under identical conditions and distinguished for analysis through the absence of *TM6, Tb* and either the presence (heterozygote) or absence (hemizygote) of *TM3, act-GFP*. *jami* hemizygotes were distinguished by absence of the balancer *TM6, Tb* and *TM6, Ubi-GFP* and heterozygotes (*jami/TM3, act-GFP)* were raised in isolation, under the same conditions. Images of whole larvae were recorded from a light microscope (Zeiss Axiophot), using a Leica Firecam.

2.4 CLONAL ANALYSIS

2.4.1 Recombining FRT82B and *jami* using Neomycin selection

To make *jami* clones it was necessary to use recombination to exchange $FRT2A^{w+}$ on the original *jami* chromosome for $FRT82B^{neo+}$ (Fig. 2.2). Neomycin bottles were prepared by adding Geneticin G418 (GIBCO/BRL Invitrogen) to standard fly food (final concentration, 0.5mg/ml) and mixing thoroughly.

2.4.2 MARCM Clones

To generate mosaic animals the MARCM (Mosaic Analysis with a Repressible Cell Marker) System was employed using the pan-neural driver *elavGAL4 (Lin and Goodman 1994)* (Fig. 2.3A) (Lee and Luo 1999; Lee and Luo 2001c). Mosaic analysis involves the generation of homozygous mutant cells from heterozygous precursors via mitotic recombination. All genetic elements required for functional operation of the

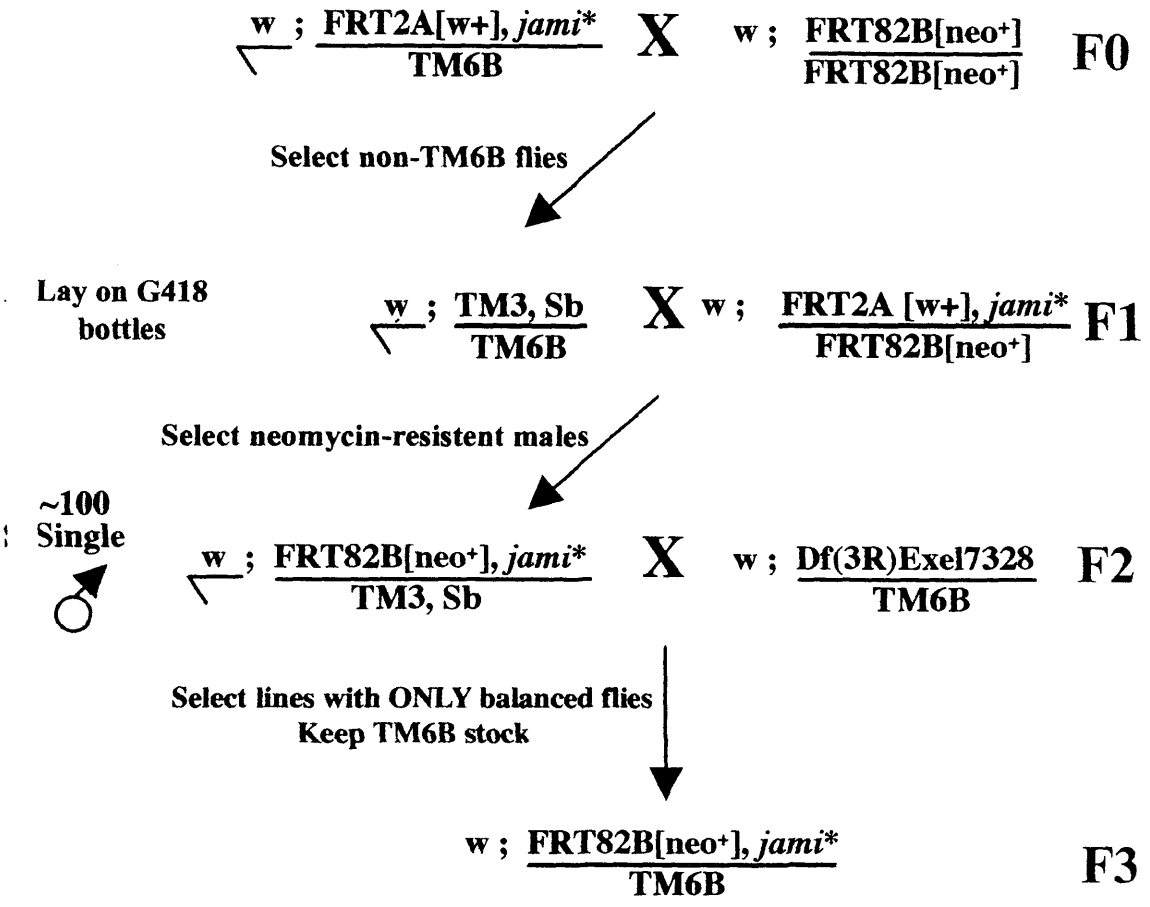

FIGURE 2.2. RECOMBINING FRT82B AND *JAMI*

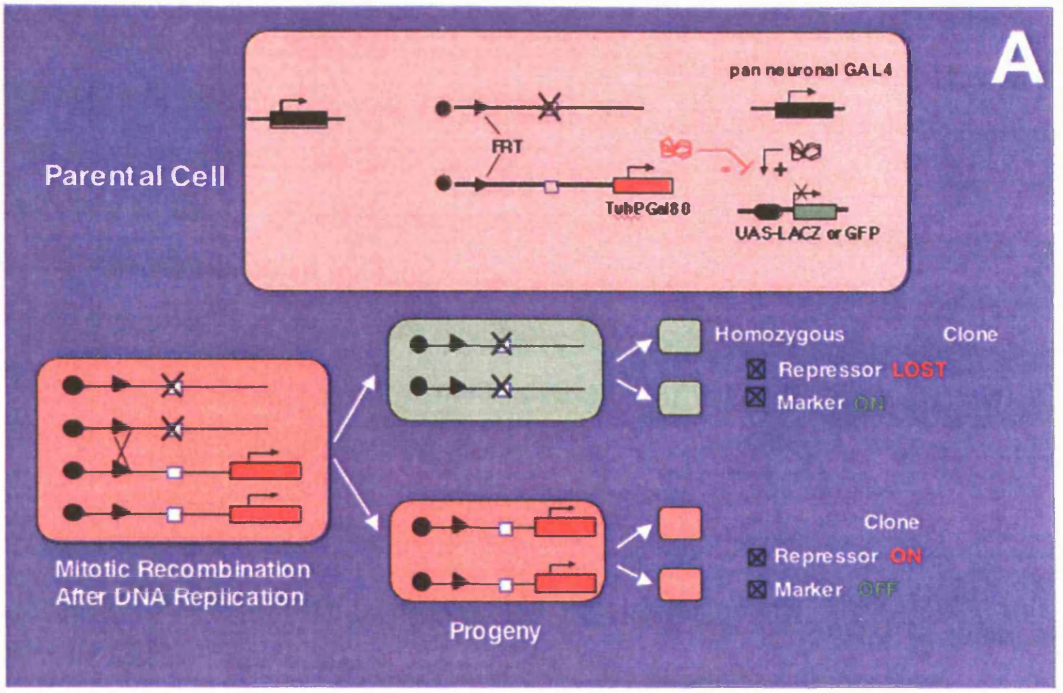

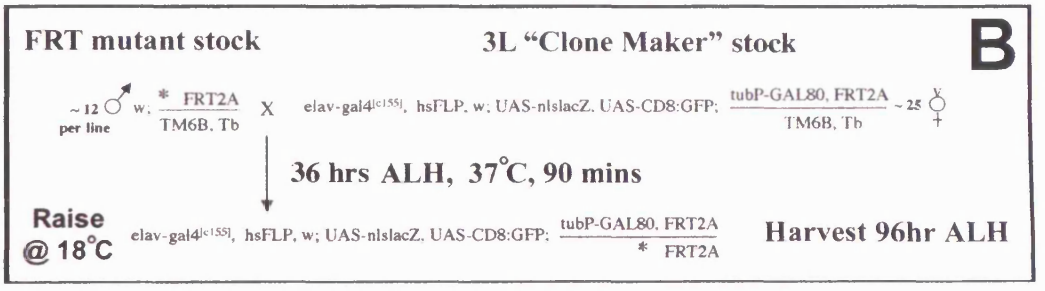

FIGURE 2.3. THE MARCM SYSTEM AND SCREENING PROTOCOL.
(A) Mosaic Analysis with a Repressible Cell Marker (MARCM): In the MARCM System, a transgene unbiquitously encoding a repressor of GAL4 (*tub-GAL80)* is placed distal to a site (FRT) for the Flipase (FLP) recombinase. The homologous chromosome arm contains an identical FRT site proximal to the mutation of interest. Prior to mitotic recombination, GAL80 acts by repressing a pan-neuronal GAL4, thus preventing *UAS-lacZ* and *UAS-GFP* activation. When mitotic recombination is induced in G2 by the use of a heat-inducible FLP, the homozygous mutant progeny cell loses the repressor and therefore expresses *UAS-lacZ* and *UAS-GFP*. The other daughter cell receives two copies of the repressor transgene and therefore does not express the UAS reporters. (Adapted from Lee & Luo, 1999) **(B)** Crossing scheme for the MARCM Screen: Approx. 36hr after larval hatching (ALH) the F1 generation are heat shocked for 90 min at 37°C to induce *FLP/FRT*-mediated mitotic recombination. Larvae are then raised at 18°C before mosaic animals are harvested at wL3.

MARCM system apart from the *FRT* mutant chromosome were built into a single fly strain, termed the "Clone-maker" stock. The MARCM screen protocol (Fig. 2.3B) initially involved crossing 12 male *FRT* mutant flies to 25 virgin female clone-maker flies and allowing them to lay eggs for 24hr. Approximately 36hr later, a heat shock was delivered to the F1 generation in order to induce the FLP-recombinase. The heat shock (hs) was administered by submerging the vial, sealed with parafilm, in a water bath for 90 min at 37°C. Larvae were then harvested at 96hr ALH, before CNS and ED clones were screened using histochemical detection of β-galactosidase (β-gal) with Xgal (see Section 2.6.2) to assess clone size.

2.4.3 *eyFLP* Clones

The $ey^{B.D.}FLP$ system (Newsome et al. 2000) was employed to generate negatively labelled clones in the eye-antennal disc. As the mutant chromosome carried *FRT2A*, it was necessary to replace *FRT80B*, in the original $ey^{B.D.}FLP$ stock, with *FRT2A* in order to generate mutant clones (Fig. 2.4).

2.4.4 *eyFLP/Minute* Clones

This system can be used to generate an ED almost entirely homozygous for a mutation of interest in an otherwise heterozygous animal. The system uses the $ey^{3.5}FLP$ construct (Poeck et al. 2001) to limit clones to the eye-antennal disc while also benefiting from the competitive disadvantage of cells that are heterozygous for *Minute* mutations (Morata and Ripoll 1975; Lambertsson 1998). Homozygous mutant cells out-compete $M(3)^{i55}$ heterozygous cells (Fig. 2.5).

2.5 ANALYSIS OF BRISTLES

Adult flies were anaesthetised then, using a sharp blade, the head, abdomen, appendages and ventral thorax were removed, leaving the dorsal notum and scutelum for bristle examination. Samples were mounted (dorsal up) on a microscope slide, in Hoyer's solution (dissolve 30g gum arabic (acacia powder) in 50ml water, add 200g chloroal hydrate and 20g glycerol). Samples were left at 50°C for 1hr to allow all tissue, except the cuticle and bristles, to dissolve. All images of specimens were taken using an Zeiss Axiophot with a JVC digital camera and a PC running AutoMontage (Synchroscopy).

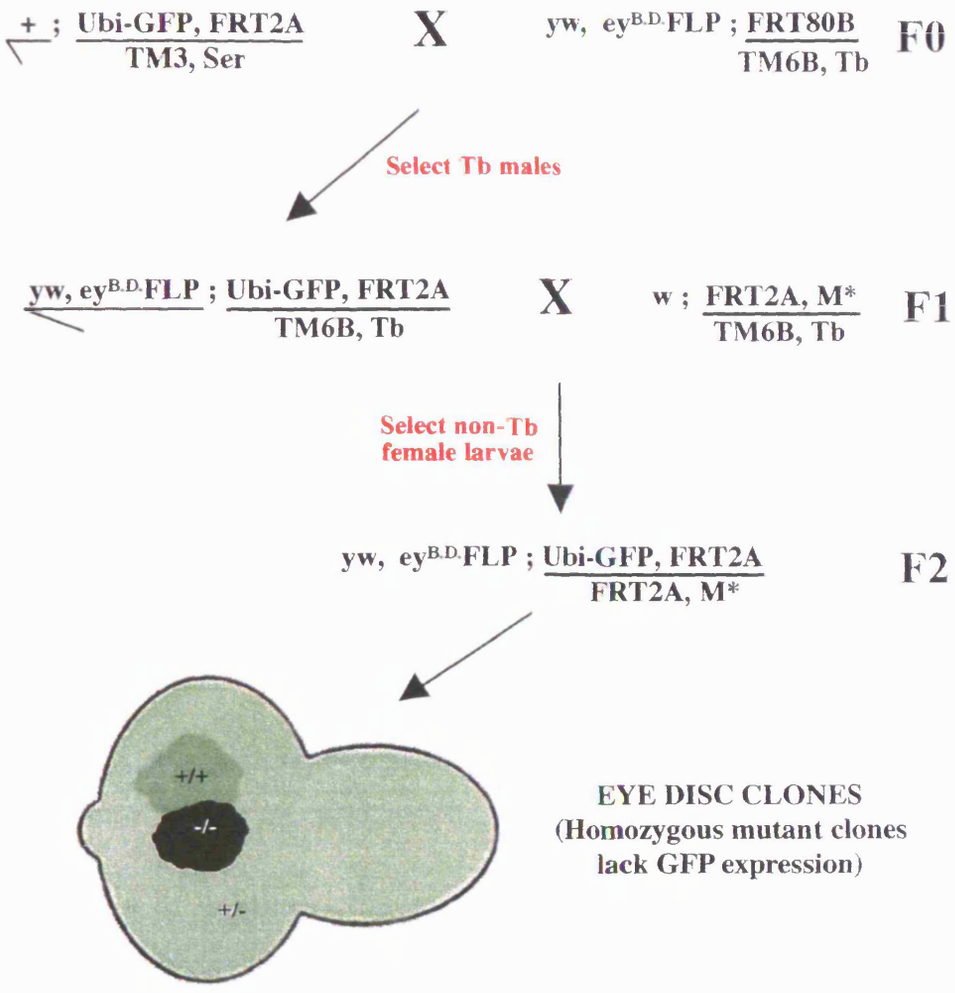

FIGURE 2.4. *eyFLP* CLONES

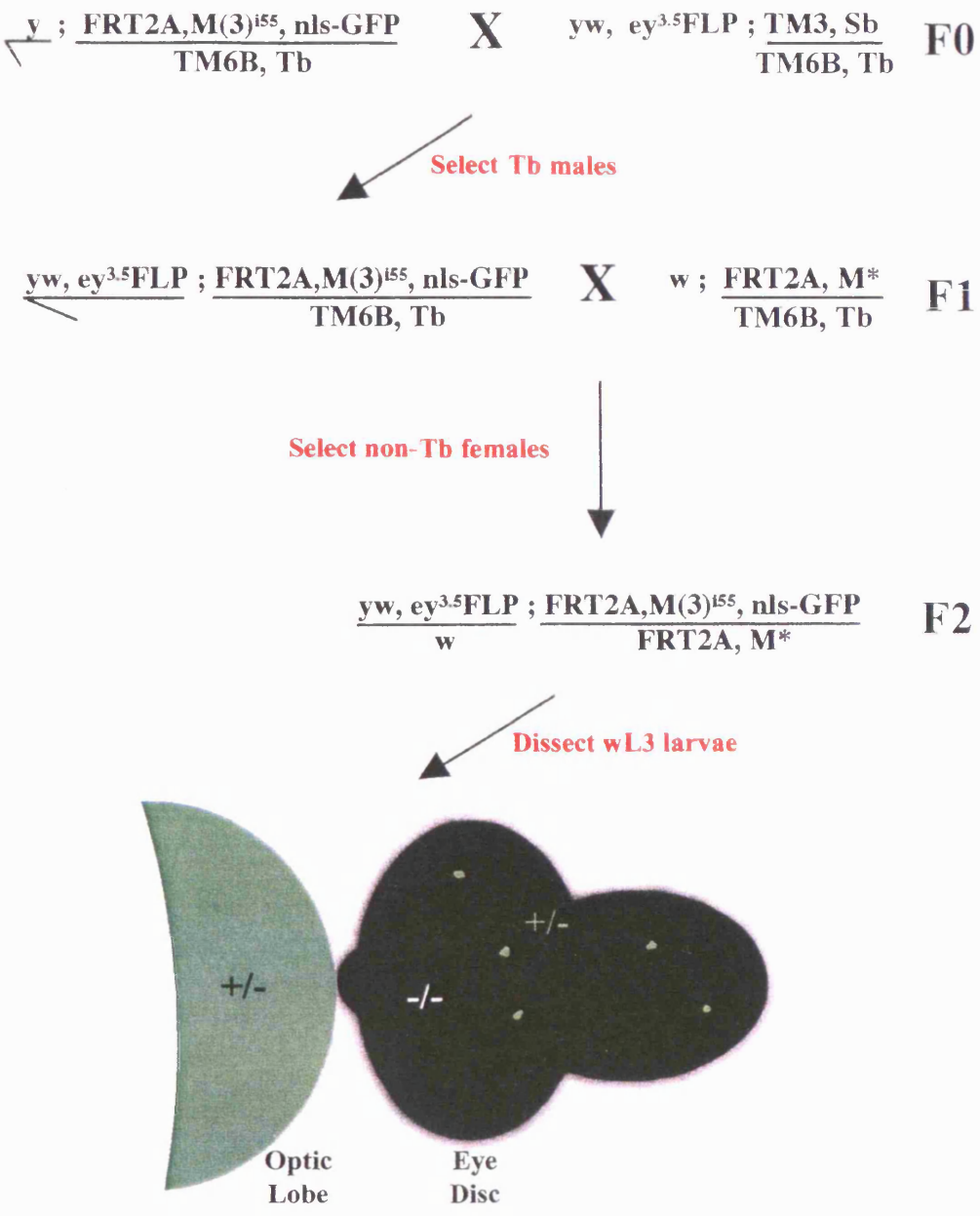

FIGURE 2.5. ***eyFLP/Minute*** **Clones**

2.6 STAINING PROTOCOLS

2.6.1 Immunolabelling

Larvae were partially dissected in 1X PBS to expose the CNS. Fixation was performed in 4% formaldehyde (Sigma) in PBS (Sigma) for 15min at room temperature. After fixation, samples were washed for 15min in PBT (PBS 1X; 0.5% Triton-X-100) (Sigma) and then preincubated for 15min in 90% PBT/10% Normal Goat Serum (Sigma). Specimens were incubated in primary antibody at 4°C overnight on a shaker. Samples were subsequently washed in PBT for 20min, before incubation in secondary antibody at 25°C for 2hr. The tissue was washed in PBS for 30min before the CNS and imaginal discs were completely dissected from the larval body and mounted in Vectashield mounting medium with DAPI (Vector Laboratories) on a microscope slide.

Primary antibodies used were rabbit anti-βgal (1:7000; Cappel) and mouse anti-βgal (1:1000; Promega); rabbit anti-GFP (1:1000; Molecular Probes) and mouse anti-GFP (1:200; Roche); mouse anti-Miranda (Mira, 1:50; gift from F. Matsuzaki); rat anti-Elav (1:5; Developmental Studies Hybridoma Bank, DSHB); mouse anti-Repo (1:15; DSHB), mouse anti-Dachshund (Dac, 1:25; DSHB), mouse mAb24B10 (1:75; DSHB) and mouse anti-Prospero (Pros, 1:10; gift from W. Chia)

Secondary antibodies used were rabbit and mouse Alexa 488 (green) and Alexa 594 (red) fluorescent conjugates (1:200; Molecular Probes). All fluorescent images were taken using scanning confocal microscopy (Leica SP1) with a pinhole of 1. All figures are projections of several sections unless otherwise stated.

2.6.2 MARCM Screening

For the MARCM screen, clone size was initially visualised by Xgal staining. Larval CNS' were dissected in 1X PBS, then fixed for 25min at room temperature in 1% Gluteraldehyde in 1X PBS. Samples were stained in Xgal solution (1mg/ml Xgal (Invitrogen), 5mM $K_3Fe(CN)_6$, 5mM $KFe_4(CN)_63H_2O$, 2mM $MgCl_2$, 0.01% Sodium deoxycholate, 0.02% NP40) at RT overnight and subsequently washed in PBS before mounting in 100% glycerol. All images were recorded from a light microscope (Zeiss Axiophot), using a Leica Firecam.

2.6.3 Screening pupal-lethal mutants

Larvae were dissected, fixed and washed according to Section 2.6.1, then the CNS and EDs were mounted in Vectashield mounting medium with DAPI (Vector Labs) on a microscope slide. All images were recorded from a light microscope (Zeiss Axiophot), using a Leica Firecam.

2.7 MAPPING STRATEGIES

2.7.1 Deficiency mapping

A combination of classic deficiencies from Bloomington and molecularly defined deficiencies generated by Drosdel and Exelixis (see Section 2.1) were used to construct a state-of-the-art deficiency kit for chromosome 3, comprising 95% coverage with 490 stocks (refer to Appendix 1 for complete list). These were used in complementation tests with the mutation to be mapped. (Fig. 2.6A).

2.7.2 P Element-mediated meiotic recombination mapping

This strategy is based on traditional meiotic recombination mapping (Greenspan 2004). Whereby it relies on the fact that the frequency of chromosomal exchange between two loci is related to the distance between them. It involves the use of chromosomes carrying visible genetic markers at known positions. The basic strategy is to generate female's transheterozygous for the chromosome carrying the mutation and the marker chromosome. These recombine during female meiosis and generate various classes of recombinant chromosomes, produced in proportion to the distance between the markers and the mutation. The task is then to measure the proportion of different recombinant chromosomes and determine the position of the mutation relative to the markers.

The overall strategy of *P* element-mediated meiotic recombination mapping is summarised in Figure 2.7 (Zhai et al. 2003). The method requires two independent mutant alleles, or one allele and a deficiency, which fails to complement the mutation, in addition to a minimum of two visibly marked homozygous viable *P* elements, located as close to the mutation as possible. However, if a deficiency is used, the *P* insertions must be outside of the deleted region.

A single heat shock at 37°C for 80mins, 4 days after setting up the cross was used to kill all larvae carrying *TM3, hs-hid.* Because the *P* insertions are molecularly

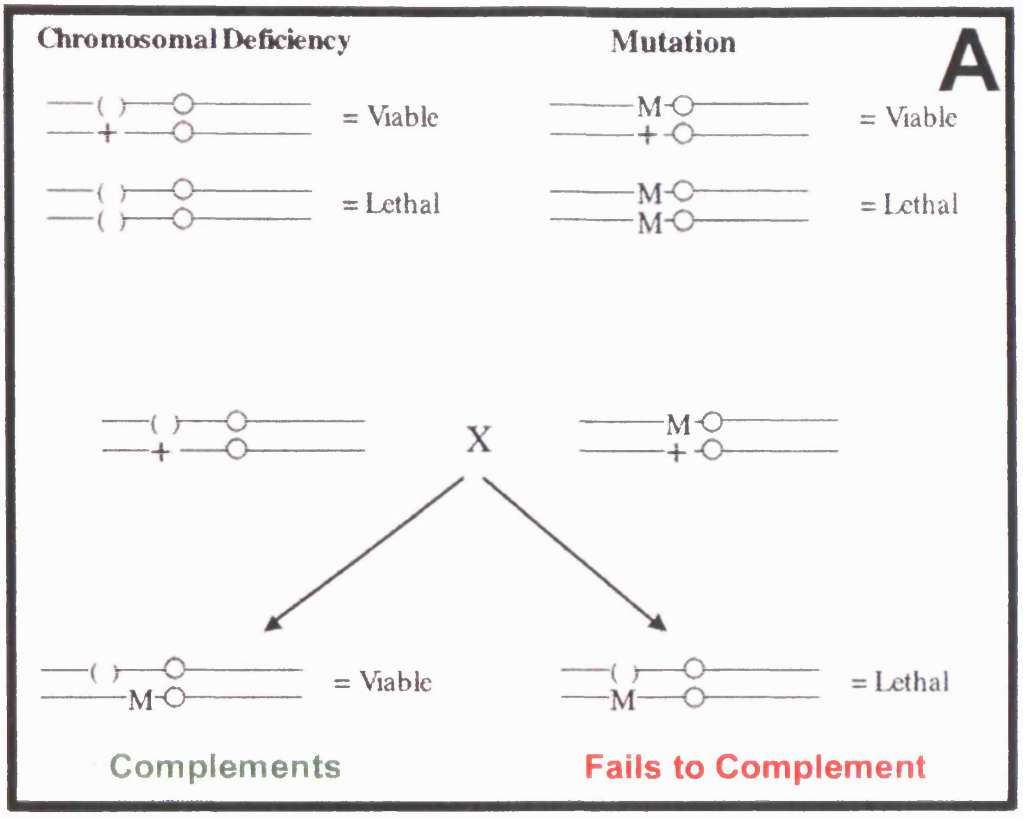

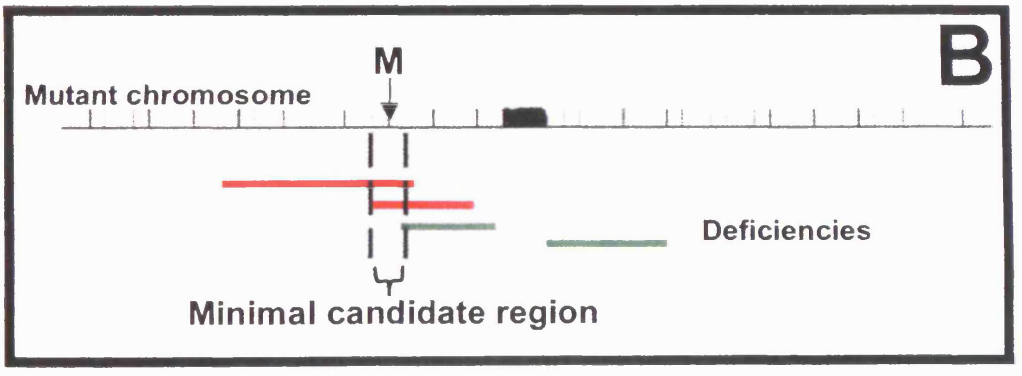

FIGURE 2.6. DEFICIENCY MAPPING STRATEGY.
(**A**) This strategy relies on both mutation and deficiency being homozygous lethal, so that failure to complement can be scored by lethality. (**B**) A combination of overlapping deficiencies can be used to assign the chromosomal region in which the mutation lies.

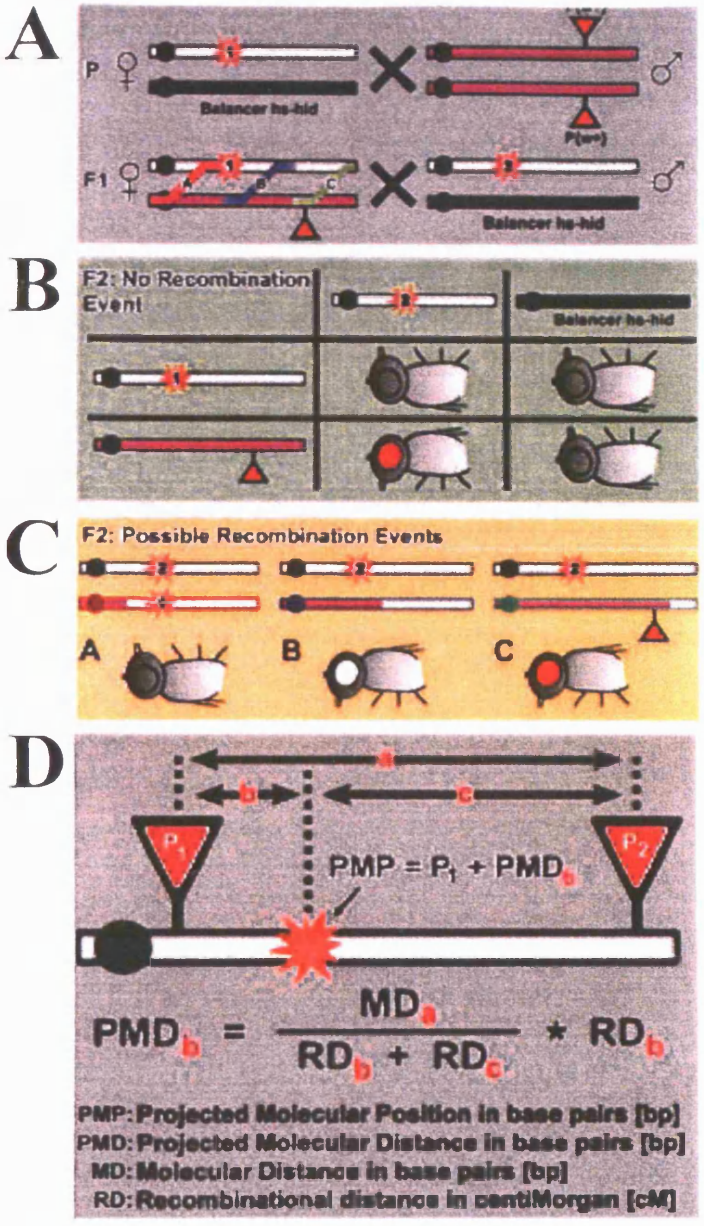

FIGURE 2.7. *P* ELEMENT RECOMBINATION MAPPING STRATEGY.
(**A-C**) Crossing scheme. Mutant chromosomes are indicated by open bars, *P* insertion-containing chromosomes are in pink, and the balancer chromosomes are in black. The mutation sites (red stars) are marked with either 1 or 2 to indicate different alleles. Note that all flies are in a *w*- background, meaning the *P* insertions are the only source of *w*+. (**A**) *P* and F1 crosses. (**B**) Nonrecombinant offspring. (**C**) Three possible recombination events, which are colour-coded and labelled A, B and C. (**D**) Calculation of mapping positions. PMD, projected molecular distance in base pairs; MD, molecular distance in base pairs; RD, recombination distance in cM (from number of *w*- flies/total number of flies scored x 10,000). Adapted from Zhai *et al.*, 2003.

mapped, the molecular distance (MD in base pairs) between any two *P* insertions can easily be calculated from their insertion sites. Hence for a pair of *P* element insertions, a "predicted molecular position" (PMP) of the mutation can be defined. The closer the *P* insertion is to the mutation, the more accurate the calculations become. If more than two *P* insertions are used, it is possible to accrue a number of PMPs and these may be used to define the limits of accuracy of the PMP in which the mutation lies.

Having selected two suitable *P* elements for *roie (P[Pka-C3]* and *P[CG6017])*, it was first necessary to re-balance the mutant and deficiency (which failed to complement *roie*) with *TM3 hs-hid* (Fig. 2.8A). Recombination mapping involved crossing *roie/TM3*, *hs-hid* to each *P* element (Fig. 2.8B). To obtain accurate recombination frequencies for each *P* element, 6000-10,000 flies were scored and at least 15 white-eyed flies were recovered. A modified equation, reformulated for *P* elements on one side of the mutation, was then used to calculate the PMPs (see Section 5.2.11, Fig. 5.16C).

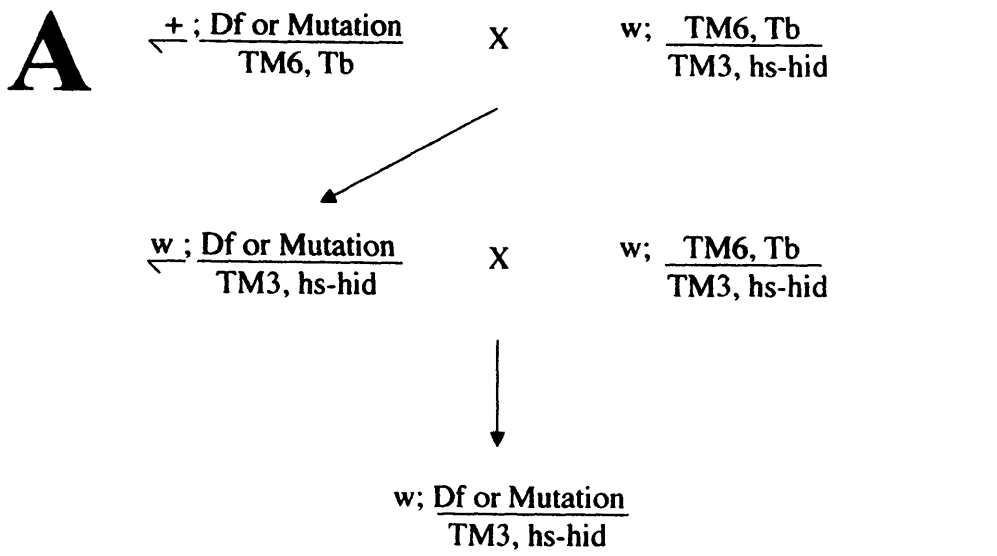

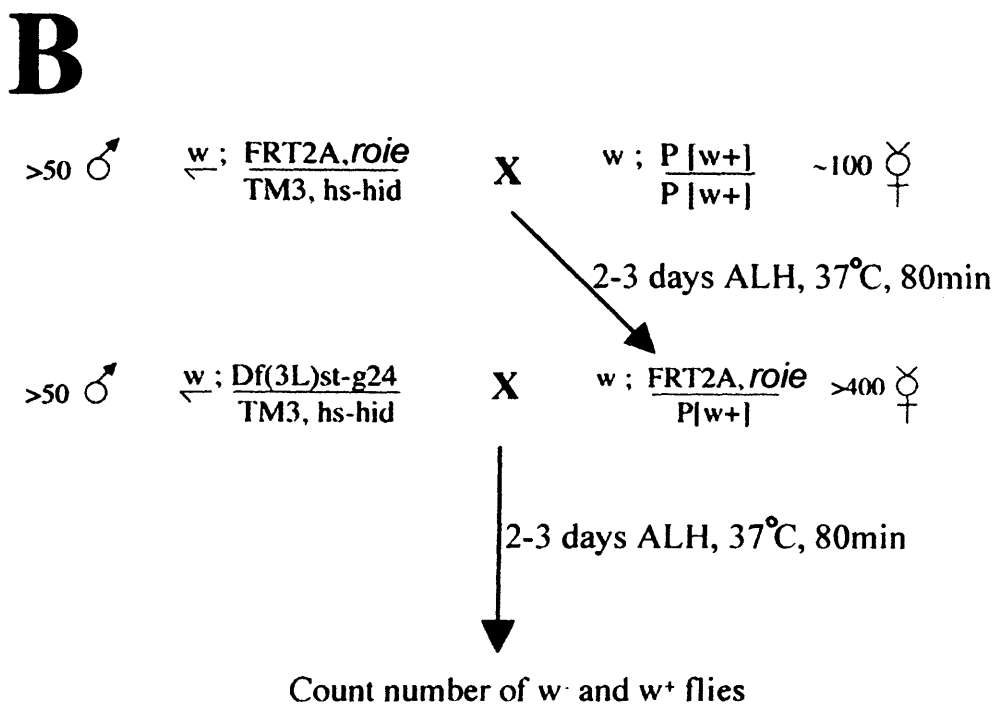

FIGURE 2.8. *P* ELEMENT RECOMBINATION MAPPING *ROIE*
(A) Rebalancing the *roie* mutation and deficiency with *TM3, hs-hid.* **(B)** Crossing scheme for mapping *roie*.

CHAPTER 3

THE GENETIC SCREENS AND MAPPING THE MUTATIONS

3.1 INTRODUCTION

To identify systematically genes important for the normal pattern of postembryonic neuroblast (pNB) divisions, we designed and performed two genetic screens. Many mutations cause embryonic or early larval lethality (referred to as embryonic lethals hereafter) so the effects of such mutations on later developmental events is not possible to study in homozygotes. However, by using genetic mosaics, it is possible to bypass early lethality. Another advantage of using a mosaic-based screening method is that it can be used to identify specifically mutations in genes with an autonomous requirement within the pNB lineage. Furthermore, by screening for altered clone size in the CNS and eye disc (ED), mutations can be grouped into those that are CNS-specific and those with a more widespread requirement in cell proliferation. However, the obvious limitation of a mosaic screen is that it is not possible to uncover genes with a non-cell autonomous requirement for neuroblast divisions.

Consequently, a second screen was designed to uncover genes required either autonomously or non-autonomously in the NB lineages, for correct CNS proliferation patterns. This involved screening for alterations in the size and/or overall morphology of the CNS and ED of the homozygous animal at 96hr ALH (see Fig. 1.9). Obviously, this strategy is only applicable to mutations that are late-larval lethal or pupal lethal (referred to as pupal lethal hereafter).

The first half of this chapter will describe the design and execution of the mosaic and pupal-lethal screens. Subsequently, the mapping of nine of the most interesting pupal-lethal mutations will be described.

3.2 RESULTS

3.2.1 EMS Mutagenesis

EMS is the most commonly used chemical mutagen in *Drosophila* and was selected for our screens. It is an alkylating agent that produces a high proportion of point mutations, although it also produces small deletions and occasionally, other rearrangements as well (Pastink et al. 1991). EMS yields a high frequency of lethal hits per chromosome, with a standard dose of 25mM in 1% sucrose producing an average of one lethal hit per chromosome arm.

3.2A THE GENETIC SCREENS

3.2.2 Optimisation of the Mosaic (MARCM) Screen

To perform the mosaic screen, the MARCM System was selected as it's unique quality of positively labelling clones allows direct visualisation of clone size by a simple histochemical stain (see Sections 2.4.2 & 2.6.2). Prior to screening, it was necessary to optimise the MARCM protocol to maximise the size and frequency of pNB clones. The timing of the heat shock is important for both of these aspects of the clones. Due to perdurance of GAL80 within mutant cells, delivering a heat shock closer than 24hr before the time of analysis does not reveal GAL4/UAS-labelled clones (Lee and Luo 1999; Lee and Luo 2001c). It is also important to ensure that the heat shock is delivered before (or at least close to) 24hr ALH, the beginning of the proliferative window in all regions (see Fig. 1.10). Taking both of these factors into consideration, it was decided that 24hr ALH would be the optimal developmental stage to apply the heat shock.

A second important parameter is the duration of the heat shock, as this also increases the frequency of clones generated. However, there is a trade-off, as prolonged exposure to 37°C results in increased lethality. Therefore a series of experiments were performed to determine the optimum duration of the heat shock (Fig. 3.1A). Although the frequency of thoracic clones increased after 90min, very few larvae were recovered from the heat shock, therefore I decided that 90 minutes was the most suitable duration.

A third parameter affecting clone labelling is related to the temperature at which the larvae are raised. Both the activity of *GAL4* and *GAL80* are sensitive to temperature thus potentially affecting the ability to visualise clones, especially those that are small and weakly labelled, as in the abdomen. In addition, raising larvae at 18°C has a dramatic effect on the developmental rate, which is a half that observed at 25°C (Berrigan and Partridge 1997). I found that although raising larvae at the standard temperature of 25°C rarely gives visible abdominal clones, by switching to 18°C after the heat shock, small clones are more frequently observed (Fig. 3.1B,C).

Finally, the sensitivity of the optimised MARCM screen protocol for measuring variations in abdominal clone size was verified by generating *H99* clones. *H99* is a deficiency which removes the three proapoptotic genes, *grim, head involution defect (hid)* and *reaper (rpr),* and *H99* pNB clones are oversized compared to *wild-type.*

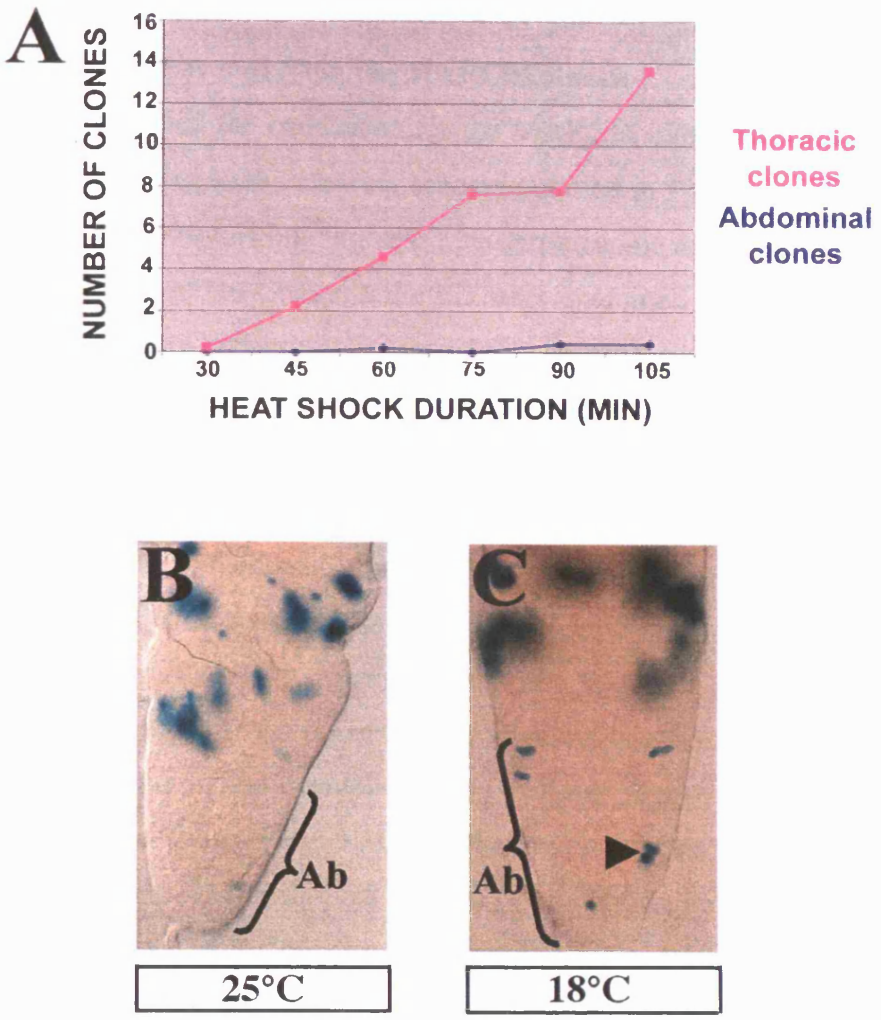

FIGURE 3.1 OPTIMISATION OF MARCM SCREENING PROTOCOL
(**A**) Graph showing the average number of *wild-type* abdominal (blue) and thoracic (pink) larval NB clones per CNS, induced at 12hr ALH and analysed at 96hr ALH, relative to variable heat shock duration. Number of CNS analysed is 10 per time point. (**B-C**) Larval ventral ganglion at 96hr ALH, stained with βgal to label *wild-type* clones. Clones were induced at 12hr ALH, by a 90 min heat shock at 37°C. When larvae are raised at 25°C, abdominal (Ab) clones of >1 cell are very rare (**B**). However, when larvae are raised at 18°C, labelled abdominal clones of ≥2 cells are more frequent (arrowhead, **C**).

(White et al. 1994) Abdominal clones lacking these genes were clearly visible with X-gal staining (see Section 2.6.2) as being larger than wild-type clones (data not shown).

3.2.3 Phenotypes recovered from the MARCM screen

Having optimised the conditions for the MARCM clone induction, the screen was performed according to the crossing scheme outlined in Fig. 2.3 (see Section 2.4.2 for details). In total, 3000 EMS mutagenised 3L chromosome arms were screened using MARCM. All regions of the CNS and the ED were examined for aberrations in clone size. Clones, which were undersized compared to wild-type, were designated as having an "underproliferation" phenotype (UP) and conversely clones, which were oversized compared to wild-type, were designated as having an "overproliferation" phenotype (OP).

68 mutations were recovered from the MARCM screen and these consisted of a number of region- or time-specific phenotypes that can be categorised into 9 classes (Table 3.1A). The numbers of mutants recovered for each phenotypic class are summarised in the graph in Figure 3.2C. The phenotypic classes are schematised in conjunction with the graph and examples of some clonal phenotypes, as revealed with Xgal staining, are also shown (Fig. 3.2D-F). Phenotypic classes were sub-categorised into CNS-specific (Class S) or non-CNS specific (Class N), according to the absence or presence (respectively) of a phenotype in the ED. The classes include Class 1, Abdominal (AB) overproliferation (OP) (Fig. 3.2D), both CNS-specific (1S, n=33) and non-CNS specific (1N, n=3); Class 2(S), CNS-specific, AB OP and thoracic- (TX) underproliferation (UP) (n=2); Class 3(N), AB OP and optic lobe- (OL) UP (n=8); Class 4(N), OL and central-brain (CB) UP (n=4); Class 5, CB and TX UP, both CNS-specific (5S, n=1) and non-CNS specific (5N, n=1); Class 6, OL UP, CNS-specific (6S, n=1) and non-CNS specific (6N, n=2) (Fig. 3.2E); Class 7(N), CB UP (n=1); Class 8, TX UP, CNS-specific (8S, n=3) and non-CNS specific (8N, n=2); Class 9(S), CNS-specific UP (n=7) (Fig. 3.2F). AB OP classes were subsequently divided on the basis of Mira staining (Shen et al. 1997) (see Section 2.6.1) into two categories, according to the presence or absence of the NB in the clone, the former being in sharp contrast to wild-type clones at this time point (C. Maurange and L. Cheng, unpublished).

Finally, complementation testing between all mutations within a phenotypic class was conducted to search for multiple alleles. In total, 56 complementation groups were identified, 9 of which had multiple alleles.

TABLE 3.1. ALLELES RECOVERED FROM THE SCREENS
Columns indicate phenotypic class; CNS phenotype; eye disc phenotype, is absent (wild-type) or present (undersized), which determines CNS-specific and non-specific mutants, respectively; alleles, recovered from the 3L screen, unless otherwise stated (3R). Rows and α, β, γ, δ, χ, ϕ represent complementation groups. **(A)** Phenotypic classes (1-9) recovered from the MARCM screen. **(B)** Phenotypic classes (I-IV) recovered from the pupal-lethal screen. In **Bold**, mutations investigated in this thesis.

A. MARCM SCREEN

CLASS	CNS PHENOTYPE	EYE DISC PHENOTYPE	ALLELES
1	**Abdomen: Oversized clones**		
1S		Wild-type clones	GL57
			222
			261
			324
			404
			L259
			DL97
			144
			212
			A49
			A63
			BL62
			BL64
			CL10
			JL10
			L182
			L189
			L193
			L212
			L217
			L221
			L235
			567, L161
			402, BL56
			BL48, CL53
			$^{\alpha}$*L305*
			$^{\beta}$*L151, L191*
			$^{\gamma}$*171*
			$^{\delta}$*BL52*
1N		Undersized clones	$^{\alpha}$*A18*
			$^{\beta}$L287
			$^{\gamma}$*DL76*
2S	**Abdomen: Oversized clones** **Thorax: Undersized clones**	Wild-type clones	$^{\delta}$*236*
			L133
3N	**Abdomen: Oversized clones**	Undersized clones	$^{\beta}$*469*

	Optic lobe: Undersized clones		*P118*
			332
			318
			369
			LM39
			PL188
			DL67
4N	**Optic lobe: Undersized clones Central brain: Undersized clones**	Undersized clones	*OL77*
			OL32
			JPL87
			[x]JPL126
5	**Central brain: Undersized clones Thorax: Undersized clones**		
5S		Wild-type clones	[♦]DL77
5N		Undersized clones	*L120*
6	**Optic lobe: Undersized clones**		
6S		Wild-type clones	CL45
6N		Undersized clones	*JPL29*
			[x]*JPL30*
7N	**Central brain: Undersized clones**	Undersized clones	*CL62*
8	**Thorax: Undersized clones**		
8S		Wild-type clones	*LC18*
			JL68
			L206
8N		Undersized clones	*L123*
			L145
9S	**CNS: Undersized clones**	Wild-type clones	[♦]*OL92, 509*
			560
			276
			546
			207
			500

B. PUPAL-LETHAL SCREEN

CLASS	CNS PHENOTYPE	EYE DISC PHENOTYPE	ALLELES
I	**CNS: Undersized**	Wild-type	***PV84***
			PL474
			PL106
			PL98
			290
II	**Brain lobes: Undersized**	Wild-type	***PL15***
			PL306 (3R)
III	**CNS: Undersized**	Undersized	***PL340 (3R)***
IV	**Brain lobes: Undersized**	Undersized	***PL26****
			PL93
			[α]PL65
			PL68
			PL77
			L218

FIGURE 3.2. PHENOTYPES RECOVERED FROM THE MARCM SCREEN.
(A) Schematic of a CNS and eye imaginal disc (ED) at 96hr ALH (wL3). The CNS is divided into the brain lobe (BL), consisting of optic lobe (OL) and central brain (CB); and the ventral ganglion (VG) consisting of thorax (Tx), abdomen (Ab) and abdominal tip. **(B)** wL3 CNS and ED stained with βgal to label *wild-type* MARCM clones. **(C)** Graph illustrating the number of alleles, within each phenotypic class, recovered from the MARCM screen (see Table 3.1 for details). Class 1-9 phenotypes are schematised below the graph, where regions generating oversized clones in red and undersized clones are in blue. N.B. abdominal undersized clones cannot be scored, as they are not visible (see text for details, Section 3.3.2). **(D-F)** wL3 CNS and ED (red dotted outline) stained with βgal to label MARCM clones. **(D)** Class 1, abdominal overproliferation (OP), solid red circle indicates over-sized abdominal clone. **(E)** Class 6(N), CNS non-specific OL (yellow dotted outline) underprolferation (UP), where ED also shows UP. **(F)** Class 9, CNS-specific UP, where ED shows *wild-type* size clones. Panels B, D & F provided by Cédric Maurange.

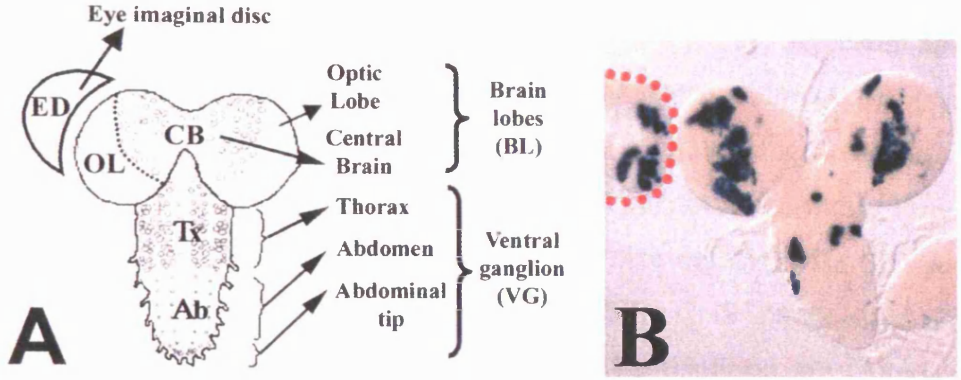
Eye imaginal disc
ED
CB
OL
Tx
Ab
Optic Lobe
Central Brain
Brain lobes (BL)
Thorax
Abdomen
Abdominal tip
Ventral ganglion (VG)
A
B

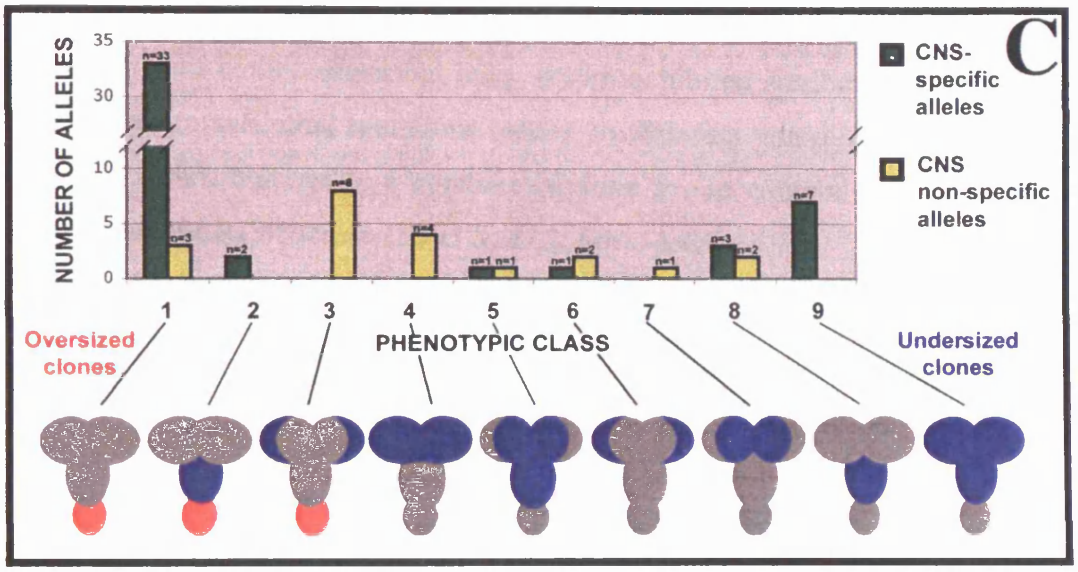
NUMBER OF ALLELES
35
30
10
5
0
CNS-specific alleles
CNS non-specific alleles
C
1
2
3
4
5
6
7
8
9
PHENOTYPIC CLASS
Oversized clones
Undersized clones

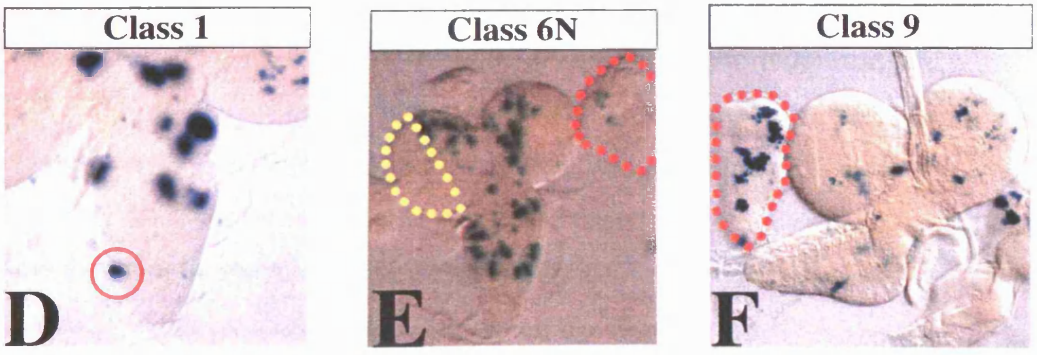
Class 1
Class 6N
Class 9
D
E
F

3.2.4 Phenotypes recovered from the pupal-lethal screen

Approximately 1000 pupal-lethal lines generated for the 3L screen and 200 for the 3R screen were scored for defects in CNS and ED size and morphology (see Section 2.6.3). This led to the identification of 12 mutations from the 3L screen and 2 from the 3R screen which could be assigned to four different phenotypic classes (Table 3.1B & Fig. 3.3C): Class I and II both have CNS-specific size defects, with EDs retaining a normal size. However, in Class I mutants (n=5) the entire CNS is undersized (Fig. 3.3D) whereas in Class II mutants (n=2) only the brain hemispheres are undersized (Fig. 3.3E). Class III and IV mutants have size defects in both CNS and EDs. Class III mutants (n=1) however, show an undersized CNS throughout (Fig. 3.3F), whereas Class IV mutants (n=6) specifically manifest undersized brain hemispheres (Fig. 3.3G).

All pupal-lethal lines were complementation tested with mutants within their class and also with embryonic-lethal lines, which exhibited similar phenotypes. This revealed that all pupal-lethal mutations belong to different complementation groups, except *PL65*, which belongs to a complementation group containing 2 other alleles recovered in the MARCM screen (*L305* & *A18*, Table 3.1A).

For the remainder of my thesis studies I have focused on mapping 9 of the pupal-lethal lines and further characterising two of these in detail.

3.2B MAPPING OF SELECTED MUTATIONS

The pros and cons of two of the most common methods for mapping EMS mutations will now be briefly described.

3.2.5 Mapping Strategies

A. Deficiency Mapping

This is arguably the most rapid method for mapping EMS mutations and utilises an extensive series of defined chromosomal deletions. In general, a recessive mutant phenotype is only uncovered when specific deficiencies that remove the gene of interest are placed transheterozygous to the mutation of interest. After an initial hit has been identified with one deficiency, smaller deletions in a given region can then be used to map the mutation to the smallest interval between the chromosomal breakpoints of the available deficiencies (see Fig. 2.6, Section 2.7.1).

A limiting factor with this technique relates to the accuracy of mapping of the

FIGURE 3.3. PHENOTYPES RECOVERED FROM THE PUPAL-LETHAL SCREEN.

(A) Schematic of a CNS and eye imaginal disc (ED) at 96hr ALH (wL3). The CNS is divided into brain lobes (BL), which consist of optic lobe (OL) and central brain (CB); and the ventral ganglion (VG) consisting of thorax (Tx), abdomen (Ab) and abdominal tip. **(B)** wL3 CNS and ED (green dotted outline) stained with DAPI to label all nuclei, in which the OL region is identifiable as a densely-stained region (red dotted outline). Length *wild-type* CNS, ~500μm; VG, ~350μm; BL diameter, ~150μm. **(C)** Graph illustrating the phenotypic classes (1-4) recovered from the pupal-lethal screen. Class I to IV phenotypes are schematised below the graph, where under-sized regions are in blue. **(D-G)** wL3 CNS and ED stained with DAPI, showing examples of phenotypic classes recovered from the screen: **(D-E)** Class I and II show a CNS-specific "underproliferation" (UP) phenotype, in that the ED (green dotted outline) is wild type in size; **(F-G)** Class III and IV exhibit UP phenotype in CNS, ED and all other imaginal discs. Panels B, D & E provided by Cédric Maurange.

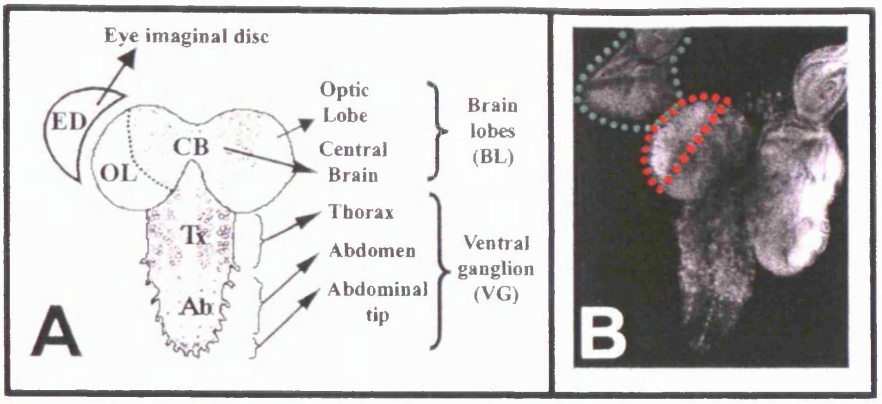
Eye imaginal disc
ED
OL
CB
Optic Lobe
Central Brain
Brain lobes (BL)
Tx
Ab
Thorax
Abdomen
Abdominal tip
Ventral ganglion (VG)
A
B

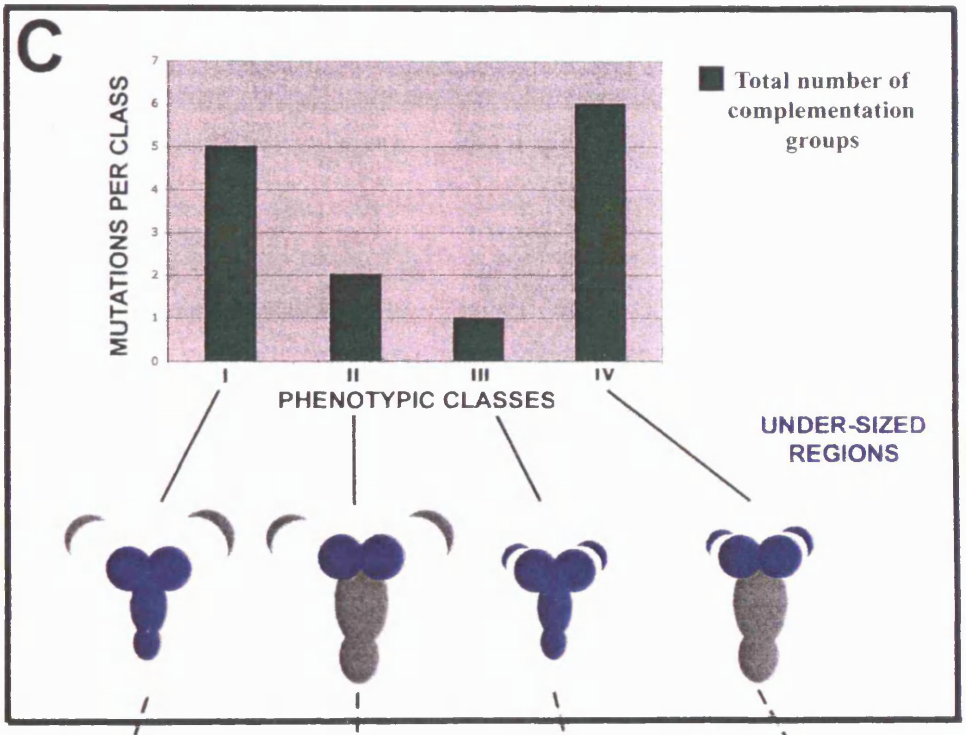
C
MUTATIONS PER CLASS
0
1
2
3
4
5
6
7
I
II
III
IV
PHENOTYPIC CLASSES
Total number of complementation groups
UNDER-SIZED REGIONS

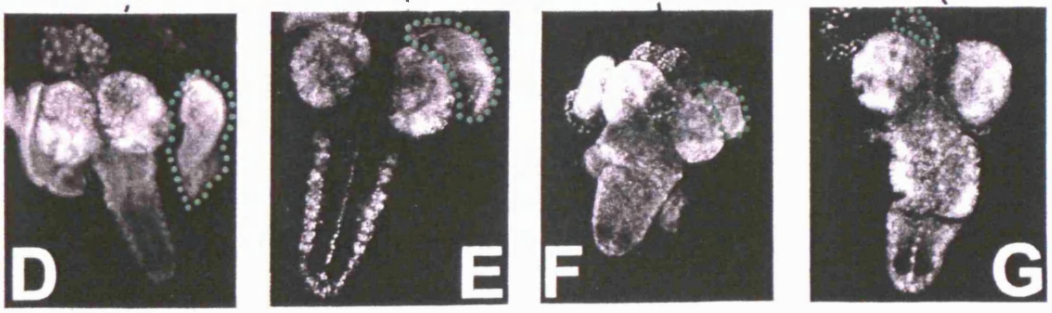
D
E
F
G

breakpoints of the "classical" deficiencies. Older deficiencies from the Bloomington collection (see Section 2.1), used in the standard deficiency kits, have breakpoints defined by polytene analysis which generates only low resolution positioning relative to individual genes in the region. In contrast, more modern deficiencies generated by Exelixis and Drosdel (see Section 2.1) using *FRT* technology, have breakpoints molecularly defined to the single nucleotide level. The latter collections offer a huge advantage in that a complete and accurate list of genes deleted by the deficiency is available. However, due to incomplete coverage by the existing Exelixis and Drosdel collections, employment of some classical deficiencies is inevitable. For those regions of the genome that are not covered by existing molecularly-defined deletions or classical deficiencies, it is possible to generate new deletions, however this takes at least 4 generations (see http://expbio.bio.u-szeged.hu/fly/index.php for details). Fortunately, coverage of the third chromosome by existing deficiencies is relatively high (92%-95%) and this technique was thus adopted as the primary mapping strategy. A second strategy, involving meiotic recombination was selected for those cases where suitable small deficiencies were not available.

B. Meiotic Recombination mapping

Meiotic recombination mapping relies on using the fact that the frequency of chromosomal exchange between two loci is related to the distance between them. The basic strategy is to generate female's transheterozygous for the chromosome carrying the new mutation and a chromosome carrying one or more genetic markers at known positions. These recombine during female meiosis and the proportion of the different recombination products are then measured. The resolution achieved is dependent on the density of markers in the chromosomal region of interest.

The classic version of this mapping strategy uses visible recessive markers, requires two generations and the achievable resolution is rarely <300Kb. More recently a recombination mapping strategy has been developed by the Bellen laboratory which takes advantage of the high density of *P* element insertions now available throughout the *Drosophila* genome (Zhai et al. 2003) (see Fig. 2.7 & Section 2.7.2). As these are marked by *white+* or *rosy+* eye colour they can be used as dominant rather than recessive markers. With a sufficient density of *P* element insertions in the vicinity of a mutation, meiotic mapping can localise its position to < 50Kb. The accuracy of this technique is limited by the degree of colinearity between the physical and

recombinational map, which varies significantly along each chromosome arm (Ashburner 1989).

3.2.6. Deficiency mapping of mutations from the pupal-lethal screen

To obtain maximum coverage of the third chromosome, I designed two customised Deficiency kits for this chromosome, using a combination of stocks from Bloomington and Szeged Stock Centres (Appendix 1). The aim of the first kit (Core Kit) was to incorporate the minimum number of deficiencies necessary to achieve maximum (~95%) coverage. In contrast, the second and larger kit (High Resolution Kit) was designed to provide approximately 95% coverage using the smallest available deficiencies. The first kit was used for mapping mutations to low resolution, with the second kit then employed to give higher resolution mapping.

9 pupal-lethal mutations, representing all 4 phenotypic classes (Table 3.1B), were complementation tested with the Core Kit and the results are summarised in Table 3.2. Four of the mutations *(PV84, PL106, PL15* and *PL306)* complemented all of the deficiencies, suggesting that the mutations lay in chromosomal regions not covered by the kit, that lethality resulted from genetic interactions between more than one viable allele or that some deficiencies were incorrect as has been reported. The remaining 5 mutations were successfully mapped using the Core Kit.

PL474, *PL98* and *PL26* mapped to ~1000Kb, ~326Kb and ~152Kb regions respectively on 3R and *PL93* mapped to a ~366Kb region on 3L. Mapping results for *PL340* were more complex, in that they revealed three lethal mutations on the third chromosome, one mapped to 3L (Hit 1) and two to 3R (Hits 2 and 3). To determine which of the three mutations was responsible for the phenotype, the mutations were put in a transheterozygous condition with the three deficiencies *Df(3L)ri-XT1*, *Df(3R)ED5230* and *Df(3R)Espl3*. Analysis of CNS morphology at wL3 indicates that only *Df(3R)Espl3* uncovers the phenotype. Thus the mutation responsible for the phenotype is Hit 3, mapping to 96F10;97B1.

Using the second deficiency kit, the predicted initial cytological locations were subsequently confirmed by at least one further deficiency (for all mutations except *PL98*) and, in addition to deficiencies which complemented, allowed higher resolution mapping of mutations (see Table 3.3). *PL340* (Hit 3) was mapped to interval of ~214Kb, at 96F10;97A6, containing 22 candidate genes (release 4.3 coordinates 3R:21851963;22076527 base pairs (bp)). This candidate region is defined by lethal

TABLE 3.2. MAPPING PUPAL-LETHAL MUTATIONS USING THE CUSTOMISED CORE DEFICIENCY KIT.
Columns indicate the mutant line number; phenotypic class (see Fig. 3.3 for details); chromosome arm containing the *FRT* site; and mutation; names of deficiencies used in complementation testing with the mutations to delimit the candidate region; cytological breakpoints of deficiencies; results of complementation testing, where 'Fail' is failure to complement and 'Comp' is complementation; predicted cytological location of the mutation, defined by the deficiencies. Grey shading indicates mutations which failed to be mapped using this strategy and Blue shading, the mutations which were successfully mapped. 'N/A' is 'not applicable'. *3 lethal mutations (Hits) were uncovered in PL340, but only Hit 3 generated a CNS phenotype (see text for details, Section 3.2.6).

Mutant line	Phenotypic class	*FRT* site	Mutation location	Deficiency	Cytological breakpoints	Comp. tests	Predicted location
PV84	I	3L	UNKNOWN	NONE	N/A	N/A	N/A
PL106	I	3L	UNKNOWN	NONE	N/A	N/A	N/A
PL15	II	3L	UNKNOWN	NONE	N/A	N/A	N/A
PL306	II	3R	UNKNOWN	NONE	N/A	N/A	N/A
PL340	**III**	**3R**					
Hit 1			3L	Df(3L)ri-79c	77B-C;77F-78A	COMP	77F-78A;78A4
				Df(3L)ri-XT1	77E2-4;78A2-4	FAIL	
Hit 2			3R	*Df(3R)ED7665*	84B4;84E11	COMP	84E11;85A2
				Df(3R)ED5230	84E6;85A5	FAIL	
				Df(3R)Exel6149	85A2;85A5	COMP	
Hit 3*			**3R**	***Df(3R)Espl3***	**96F1;97B1**	**FAIL**	**96F10;97B1**
				Df(3R)ED6232	**96F10;97D2**	**FAIL**	
				Df(3R)ED6235	**97B9;97D12**	**COMP**	
PL474	**I**	**3L**	**3R**	**Df(3R)Antp-X1**	**84A4-5;84C2-3**	**COMP**	**84C2-3;84E6**
				Df(3R)ED7665	**84B4;84E11**	**FAIL**	
				Df(3R)ED5230	**84E6;85A5**	**COMP**	
PL98	**I**	**3L**	**3R**	***Df(3R)Esp13***	**96F1;97B1**	**FAIL**	**96F1;96F10**
				Df(3R)ED6232	**96F10;97D2**	**COMP**	
PL26	**III**	**3L**	**3R**	***Df(3R)Exel7327***	**89A8;89B1**	**COMP**	**89B1;89B5**
				Df(3R)Exel7328	**89A11;89B5**	**FAIL**	
PL93	**IV**	**3L**	**3L**	***Df(3L)st-g24***	**72D1-2;73A9-10**	**FAIL**	**72D1-2;73A1**
				Df(3L)ED223	**73A1;73D5**	**COMP**	

TABLE 3.3. MAPPING PUPAL-LETHAL MUTATIONS USING THE HIGH-RESOLUTION DEFICIENCY KIT.
Columns, from left to right, indicate the mutant line number; predicted cytological location of the mutation and size of the region (Kb), defined by core deficiency kit mapping; names of deficiencies used in complementation testing with mutations; cytological breakpoints of deficiencies, showing the two breakpoints (red) used to define the minimal candidate region; results of complementation testing between each deficiency and the mutations, where 'Fail' is failure to complement and 'Comp' is complementation; minimal candidate region cytology (red), approximate size in Kb (blue) and number of candidate genes (green); candidate genes eliminated by comp. testing with lethal alleles; remaining number of candidate genes. N/A, 'not applicable'.

Mutant line	Location from core kit	Deficiency	Cytological breakpoints	Comp. tests	Minimal region	Eliminated candidate genes	Remaining candidate genes
PL340 (Hit 3)*	96F10;97B1 (368Kb)	Df(3R)Espl3	96F1;97B1	FAIL	3R:21851963; 22076527 (96F10;97A6) 214Kb 22 genes	*E(spl)^{rv1}* *Gro^{c105}*	20
		Df(3R)Exel6204	96F9;97A6	FAIL			
		Df(3R)ED6232	96F10;97D2	FAIL			
		Df(3R)ED6235	97B9;97D12	COMP			
PL474	84C2-3;84E6 (1000Kb)	Df(3R)Antp-X1	84A4-5;84C2-3	COMP	3R:2988384; 3317334 (84C8;84D9) 329Kb 41 genes	*sas^{15}* *lap^{KG06751}* *Gld^{n2}* *rn^{roe-2}*	37
		Df(3R)ED7665	84B4;84E11	FAIL			
		Df(3R)ED5221	84C4;84E11	FAIL			
		Df(3R)EXEL6146	84C8;84D9	FAIL			
		Df(3R)ED5223	84D9;84E11	COMP			
		Df(3R)Exel6263	84E6;84E13	COMP			
		Df(3R)ED5230	84E6;85A5	COMP			
		Df(3R)ED5220	84E6;84E11	COMP			
PL98	96F1;96F10 (326Kb)	*Df(3R)Espl3*	96F1;97B1	FAIL	3R:21565070; 21821129 (96F1;96F9) 306Kb 60 genes	N/A	≤60
		Df(3R)Exel6204	96F9;97A6	COMP			
		Df(3R)ED6232	96F10;97D2	COMP			
PL26	89B1;89B5 (152Kb)	*Df(3R)Exel7327*	89A8;89B1	COMP	3R:11867083; 11923310 (89B3;89B5) 56Kb 7 genes	*msps^{EY06514}*	6
		Df(3R)Exel7328	89A11;89B5	FAIL			
		Df(3R)Sbd104	89B5;89C2-7	COMP			
		Df(3R)Sbd26	89B9-10;89C7-D1	COMP			
PL93	72D1-2;73A1 (366Kb)	*Df(3L)st-f13*	72C1-D1;73A3-4	FAIL	3L:16036363; 16078527 (72D4;72D8) 43Kb 11 genes	*Taf4^{1}* *Pgm^{nGB1}* *SSRβ^{61939}*	8
		Df(3L)Exel6127	72D1;72D8	FAIL			
		Df(3L)st-g24	72D1-2;73A9-10	FAIL			
		Df(3L)ED220	72D4;72F1	FAIL			
		Df(3L)ED4606	72D4;73C4	FAIL			
		Df(3L)st-e4	72D5-10;73A5-8	FAIL			
		Df(3L)Exel6128	72D8;72D10	COMP			
		Df(3L)st4	72D10;73C1	COMP			
		Df(3L)st8p	72E4;73B4	COMP			
		Df(3L)Exel6129	72F1;73A2	COMP			
		Df(3L)ED223	73A1;73D5	COMP			
		Df(3L)81k19	73A3;74F	COMP			

complementation tests with three independent deficiencies *(Df(3R)Esp13, Df(3R)Exel6204* and *Df(3R)ED6232)*, which failed to complement the mutation.

PL474 was mapped to a ~329Kb region at 84C8;84D9, containing 41 candidate genes (release 4.3 coordinates 3R:2988384;3317334 bp). This candidate region was independently confirmed by three deficiencies *(Df(3R)ED7665, Df(3R)ED5221* and *Df(3R)Exel6146), which* failed to complement the mutation.

PL98 mapped to a ~306Kb region, at 96F1;96F9, containing 60 candidate genes (release 4.3 coordinates 3R:21565070;21821129 bp). The minimal candidate region was delimited by one cytologically-defined deficiency which failed to complement *(Df(3R)Esp13)* and one molecularly-defined deficiency, which complemented *(Df(3R)Exel6204).* The results of mapping *PL26* and *PL93* are discussed in Chapters 4 and 5, respectively.

3.2.7. Complementation testing of mutants with lethal alleles

Having employed deficiency mapping to acquire a minimal list of candidate genes, at least some of these could be eliminated by complementation testing. This initially involved searching the *Drosophila* databases (see Section 2.1) for available lethal alleles of candidate genes. Complementation tests with these alleles allowed the elimination of Gro^{c105} and $E(spl)rv^{1}$ for *PL340*, Sas^{15}, $Lap^{KG06751}$, Gld^{n2} and Rn^{roe-2} for *PL474*, $msps^{EY06514}$ for *PL26* and $Taf4^{1}$, Pgm^{nGB9} and $SSR\beta^{S1939}$ for *PL93* (Table 3.3 and Table 2.1). However, no fail-to-complements were obtained, indicating that each of the five pupal-lethal mutations is in a gene previously uncharacterised at the functional level.

3.2.8. Selection of *PL26 (jami)* and *PL93 (roie)* for further analysis

At this point in the analysis, I focused my interests on a subset of the 5 mapped mutants. As all 5 mutants had dramatic CNS phenotypes, the decision was largely based on selecting phenotypes which would be interesting to compare and also on the predicted ease of mapping the mutations to a single gene.

Two mutants, *PL26* and *PL93*, both Class IV mutants (see Fig. 3.3G), were an interesting pair for phenotypic comparison. DAPI staining of both mutants indicated a similar region-specific phenotype in the CNS and ED. In addition, both mutations mapped to regions close to the centre of the chromosome arms, rendering them optimal candidates for *P*-element mapping. Due to the small size of larvae in late-L3, I renamed

PL26 as *juvenile at mid-third instar, (jami)* and, as *PL93* manifests small OLs and EDs at wL3, I renamed this mutant *reduced optic and imaginal expansion, (roie)*. Detailed phenotypic analysis and results of mapping *jami* and *roie* will be discussed in Chapters 4 and 5 respectively.

3.3 DISCUSSION

3.3.1 Phenotypes recovered from the screens

Two genetic screens were performed with the aim of identifying novel genes involved in postembryonic neuroblast divisions. Mosaic analysis using the MARCM system allowed us to identify pleiotropic genes important for this specific biological process but also imposed a limitation. Homozygous mutant clones inherit wild-type protein from their heterozygous precursors and so do not lose gene activity immediately. This perdurance of wild-type protein can prevent identification of genes that function in the earlier stages of larval neurogenesis. Additional inherent limitations of mosaic screens mean that genes will be missed that are located proximal to the *FRT* site, required at stages prior to clone induction, such as entry into the quiescent period, or required non-cell autonomously. These limitations were circumvented by designing a second screen, the pupal-lethal screen which analysed homozygote animals at 96hr ALH. However this protocol has its own limitation in that alleles with a lethal phase before 96hr ALH can not be analysed. As this represents the majority of all lethal EMS alleles, the pupal-lethal screen was restricted to a minority of the alleles that were generated.

We successfully screened 4000 mutagenised lines on chromosome 3L and 200 on chromosome 3R. A total of 82 mutants were recovered; 14 from the pupal-lethal screen and 68 from the MARCM screen. The majority of mutations recovered from the screens are single allele hits (see Table 3.1), indicating that the screens did not achieve saturation. This was expected as an insufficient number of lines were screened to achieve saturation (3000 embryonic lethal and 1200 pupal-lethal). In spite of the lack of saturation, our screen did identify multiple alleles for 9 out of 69 complementation groups, suggesting that we have nevertheless sampled a significant proportion of the genes located on chromosome arm 3L.

We recovered 9 phenotypic classes from the MARCM screen (see Fig. 3.2) and 4 from the pupal-lethal screen (see Fig. 3.3). The most frequently observed phenotype in the MARCM screen was CNS and ED UP (Approx. 1 in 10 mutant lines). This

phenotype could be due to homozygous loss of housekeeping genes that are required for cell division, cell survival or basic metabolic functions in neural cells. We discarded mutants in this class as the screens were targeted at identifying genes required in a region-specific manner.

The proportion of pupal-lethal mutants recovered from the screen (0.6%) was significantly lower than the proportion of embryonic lethal mutants recovered from the MARCM screen (2.4%). This 1.8% difference suggests that there are a larger number of neural proliferation genes with embryonic-lethal, than pupal-lethal classes of alleles or that the primary mechanisms for controlling pNB proliferation are cell-autonomous. However, this difference may also highlight the degree of subjectivity in scoring phenotypes in both screens. An UP phenotype, observed in clones, may be more obvious than a more subtle change in overall CNS size or morphology in the homozygous animal. Of note, pupal-lethal classes of mutations do not necessarily reflect a genuine zygotic late requirement for the gene, as maternally-contributed gene products can perdure into late-larval stages. One method to resolve this uncertainty is to generate germline clones (Greenspan 2004).

A consistent feature of both screens is the greater number and variety of UP phenotypes recovered compared to OP phenotypes. This suggests that many more genes are involved in positively-regulating neural cell divisions than negatively. However, the probability of recovering mutations also depends on the severity of their phenotypes. For example, the complete lack of OP mutants from the pupal-lethal screen may reflect the fact that OP phenotypes tend to be lethal in the whole animal prior to wL3. Likewise, X-gal staining MARCM clones is most sensitive in detecting dramatic UP phenotypes, such that OP phenotypes in the already large thoracic and brain lobe clones may have been missed. In addition, abdominal UP phenotypes were not detected as the clones would never reach a sufficient size to dilute the GAL80 and be visualised. Conversely, AB OP phenotypes were recovered in large numbers as they were easy to score due to the rarity and small size of wild-type abdominal clones. The biasing of the MARCM screen to detect this class of mutants was deliberately encouraged by careful optimisation of the MARCM protocol. This was because, after the previous work on *H99*, *grh* and *abdA* in the lab, AB OP mutants were of particular interest.

In summary, we designed and executed two genetic screens, which allowed detection of 69 genes involved in control of pNB proliferation and for 9 genes, we recovered multiple alleles. The majority of these genes act region-specifically within the

CNS and are potentially required in a temporally-controlled manner, indicating that we have discovered a significant number of genes involved in regional control of pNB proliferation.

3.3.2. The resolution of deficiency mapping

Although deficiency mapping does not always guarantee a positive result, it is a rapid way to define a predicted cytological or molecular region for the mutant locus. It is surprising that 4 out of the 9 pupal-lethal mutations could not be mapped with deficiencies, considering the deficiency kit afforded approximately 95% coverage of the third chromosome. However, 5 mutations were mapped from the entire third chromosome to relatively small regions. Results demonstrated the variability in the achievable resolution of this strategy, where mutations were mapped to between 38 and 329Kb, where the average interval was 186Kb. However, results of mapping *PL26* (*jami*) and *PL93* (*roie*) highlight the more successful extreme of this strategy. Whereby the mutations were mapped from the entirety of chromosome III to 7 and 11 candidate genes, respectively, in just two generations.

In conclusion, deficiency mapping was successfully employed to map 5 out of 9 mutations to high resolution demonstrating that deficiencies, particularly those that have molecularly defined breakpoints, are a fantastic resource for mapping EMS-generated mutations. Furthermore, all 5 of these mutations are likely to be in genes previously uncharacterised at the functional level and are therefore novel genes involved in the control of pNB proliferation.

CHAPTER 4

JAMI, A GENE REGULATING GROWTH OF THE LATE-LARVAL CNS

4.1 INTRODUCTION

PL26 was assigned to Class IV of the pupal-lethal phenotypes indicating that there is a growth deficit in the brain hemispheres and imaginal discs (Fig. 3.3C,G). In this chapter, the phenotype and mapping of this mutant, named *juvenile at mid-third instar (jami)* (see Section 3.2.8), are investigated in more detail. This analysis focuses on addressing four questions: First, is there an effect on the growth of polyploid larval tissues in *jami* mutants? Second, does removing *jami* activity from the whole organism affect progenitor or post-mitotic imaginal cells in the CNS and ED? Third, are the requirements for *jami* cell or non-cell autonomous? And finally, what is the molecular identity of *jami*?

4.2 RESULTS

4.2A PHENOTYPIC CHARACTERISATION OF *JAMI*

4.2.1 The *jami* phenotype first appears during the third instar

Preliminary examination of larval size and spiracle morphology in *jami* homozygotes, suggested that they never reached the wL3 larval stage. In wild-type larvae, there is a 200-fold increase in mass from the newly hatched L1 to the mature wL3 stage (Church 1965) and this is achieved largely through an increase in polyploid cell size rather than cell number. To quantify the apparent growth deficit of *jami* mutants, the overall growth rate was assessed during larval stages (see Section 2.3). Larvae were weighed at three time points; mid-L2 (36hr ALH), early-L3 (60hr ALH) and late-L3 (84hr ALH). The average larval weights of *jami* hemizygous larvae (*jami/Df(3R)Exel7328*) were compared to that of *jami* heterozygotes (*jami/TM3*). Up to 60hr ALH, *jami* larvae gain weight normally, however by 84hr ALH, larvae fail to increase in weight (Fig. 4.1A) and by 96hr ALH, larvae are very markedly undersized (Fig. 4.1B,C). Developmental arrest of *jami* mutant larvae was also observed, with larvae remaining in the L3 state for up to 13 days. No larvae reach the mature-L3 weight and most die before beginning wandering and pupariation. The few larvae that did pupariate were undersized and never reached the pharate adult stage of pupation (Bainbridge and Bownes 1981).

To determine if there was a corresponding size deficit in imaginal tissues, the CNS and imaginal discs of hemizygous *jami* mutants (hereafter referred to as *jami* mutants) were examined at 96hr ALH. The OL in *wild-type* specimens stains intensely with DAPI, reflecting the high density of nuclei associated with proliferation during

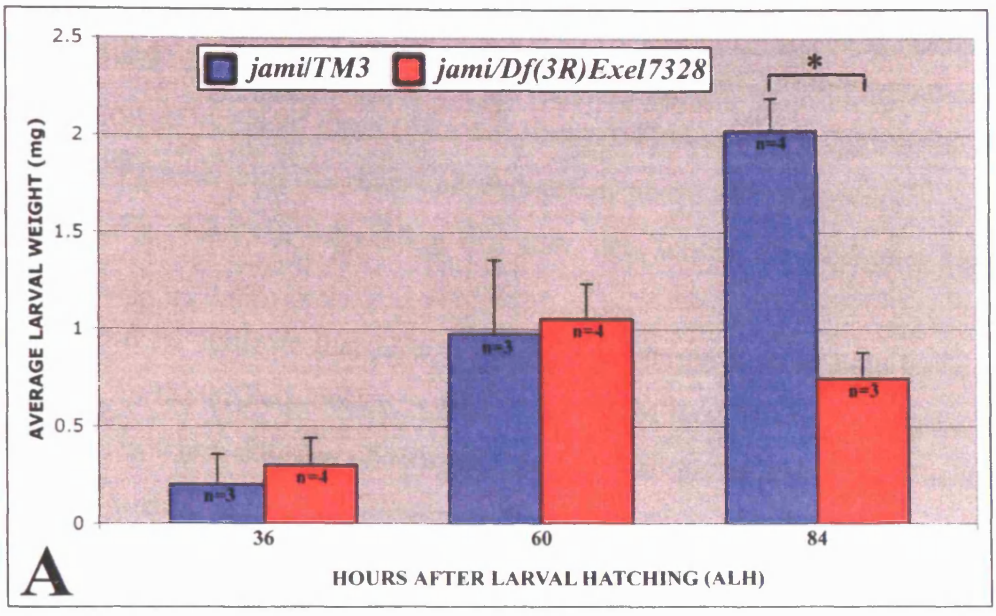

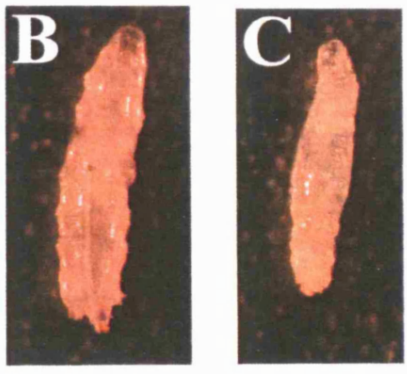

FIGURE 4.1. HEMIZYGOUS *JAMI* LARVAE FAIL TO GROW DURING THIRD INSTAR.

(**A**) Graph showing the weights of *jami/TM3* (blue) and *jami/Df(3R)Exel7328* (red) larvae, at mid-L2 (36hr ALH, blue, m=0.20, S.D=0.16; red, m=0.30, S.D.=0.14), early-L3 (60hr ALH, blue, m=0.98, S.D.=0.38; red, m=1.05, S.D.=0.18,) and late-L3 (84hr ALH, blue, m=2.02, S.D.=0.17; red, m=0.75, S.D.=0.13,). Where n is number of replicate weighings and error bars represent 1 S.D. *jami* hemizygotes gain weight at the normal developmental rate until early-L3, after which they do not gain any weight. * indicates $p<0.01$. (**B-C**) Larvae at 96 hr ALH, that are *jami/TM3* (**B**) or *jami* hemizygous (**C**). Magnification **B=C**.

larval stages (Fig. 4.2A). However, no corresponding DAPI-intense region is identifiable in *jami* mutants (Fig. 4.2C). *jami* mutants also display a significant reduction in the size of the eye-antennal imaginal disc (Fig. 4.2B,D), leg imaginal disc (Fig. 4.2C) and other imaginal discs (data not shown). However, the ventral ganglion (VG) of the CNS (containing thoracic and abdominal neuromeres) appears relatively normal in size (Fig. 4.2A,C), suggesting that *jami* acts within the CNS in a region-specific manner.

The data so far indicate that *jami* is required for the growth of both larval and imaginal tissue. As the growth deficit is first observed in larval tissue during L3, the question arises as to when the *jami* phenotype first appears in imaginal tissue. Therefore analysis was performed at an earlier stage of development, in late-L2. DAPI staining revealed no obvious gross morphological defects at late-L2 in either CNS or imaginal tissues (data not shown). However, to look more specifically at the development of neural populations, expression of Elav, a marker of all postmitotic neurons (Robinow and White 1988) and Repo, a marker of most glial cells (Halter et al. 1995), were examined (Halter et al. 1995). Preliminary analysis of the distribution and density of neurons and glia shows no obvious aberrations in the OL or in any other region of the CNS (Fig. 4.3).

In summary, the data indicates that *jami* is required, during L3, for growth of both polyploid larval and diploid imaginal tissue. Furthermore, within the CNS, the phenotype is most dramatic in the brain lobes, suggesting a region-specific requirement for *jami*.

4.2.2 *jami* is required in CNS and imaginal discs in a cell- and region-specific manner

To investigate further the underlying nature of the imaginal growth deficit in *jami* mutants, the number and distribution of specific precursor and post-mitotic cell populations were assessed in the CNS and ED at 96hr ALH.

Neuroblasts

Mira immunostaining was used to label all neuroblasts (NBs) in the CNS (Shen et al. 1997). The density of both the thoracic (Tx) and abdominal (Ab) NB populations in *jami* mutants appears normal at 96hr ALH (Fig. 4.4A,C).

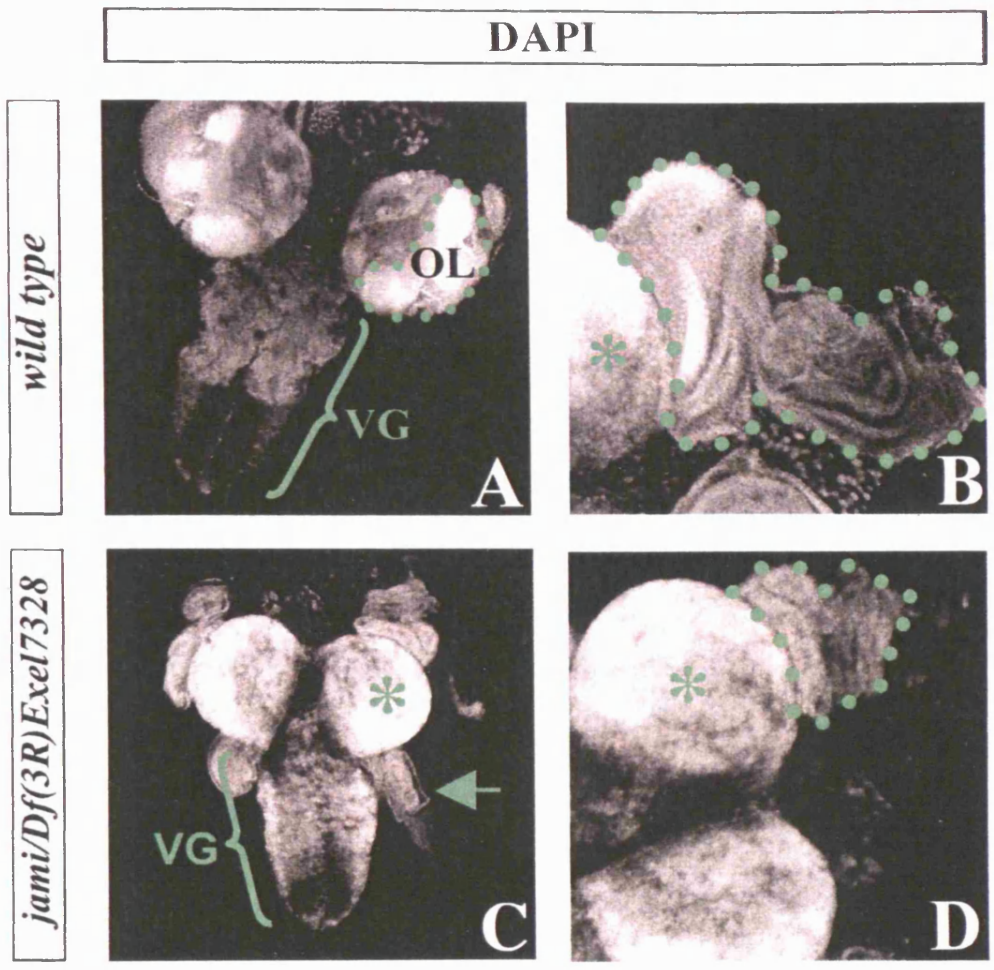

FIGURE 4.2. *JAMI* MUTANTS HAVE UNDERSIZED BRAIN LOBES AND IMAGINAL DISCS.
Larval CNS (A & C, anterior up) and eye-antennal discs (B & D, posterior left) at 96hr ALH, stained with the nuclear dye, DAPI. (**A-B**) *wild-type* CNS showing (**A**) optic lobe (OL, dotted outline) and ventral ganglion (VG) and (**B**) eye disc (ED, dotted outline) and brain lobe (asterisk). (**C-D**) *jami* mutant CNS showing (**C**) VG, undersized brain hemisphere (asterisk) and leg imaginal disc (arrow) and (**D**) reduced-size ED (dotted outline) and brain hemisphere (asterisk). Magnifications; **A=C** and **B=D**.

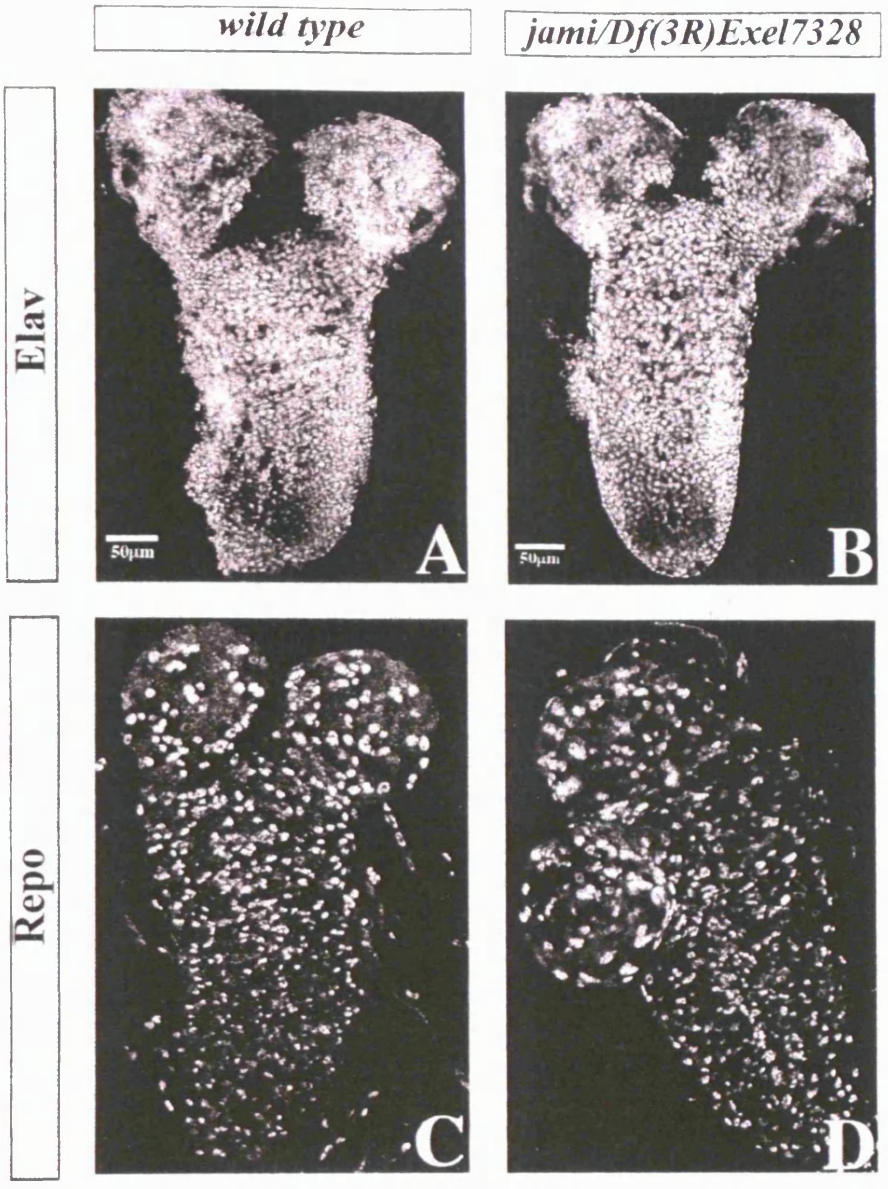

FIGURE 4.3. NEURONS AND GLIA APPEAR NORMAL IN *JAMI* MUTANTS AT LATE-SECOND INSTAR.
Confocal projections of larval CNS (anterior up) at 46hr ALH. Stained for (**A-B**) anti-Elav, to label all neurons and (**C-D**) anti-Repo, to label most glial cells. (**A-B**) Elav expression pattern in (**A**) *wild-type* CNS and (**B**) *jami* mutant CNS shows similar densities of neurons. Approx. diameter of neuron, 2-3μm (**C-D**) Repo expression pattern in *wild-type* CNS (**C**) and *jami* mutant CNS (**D**) also shows no obvious differences.

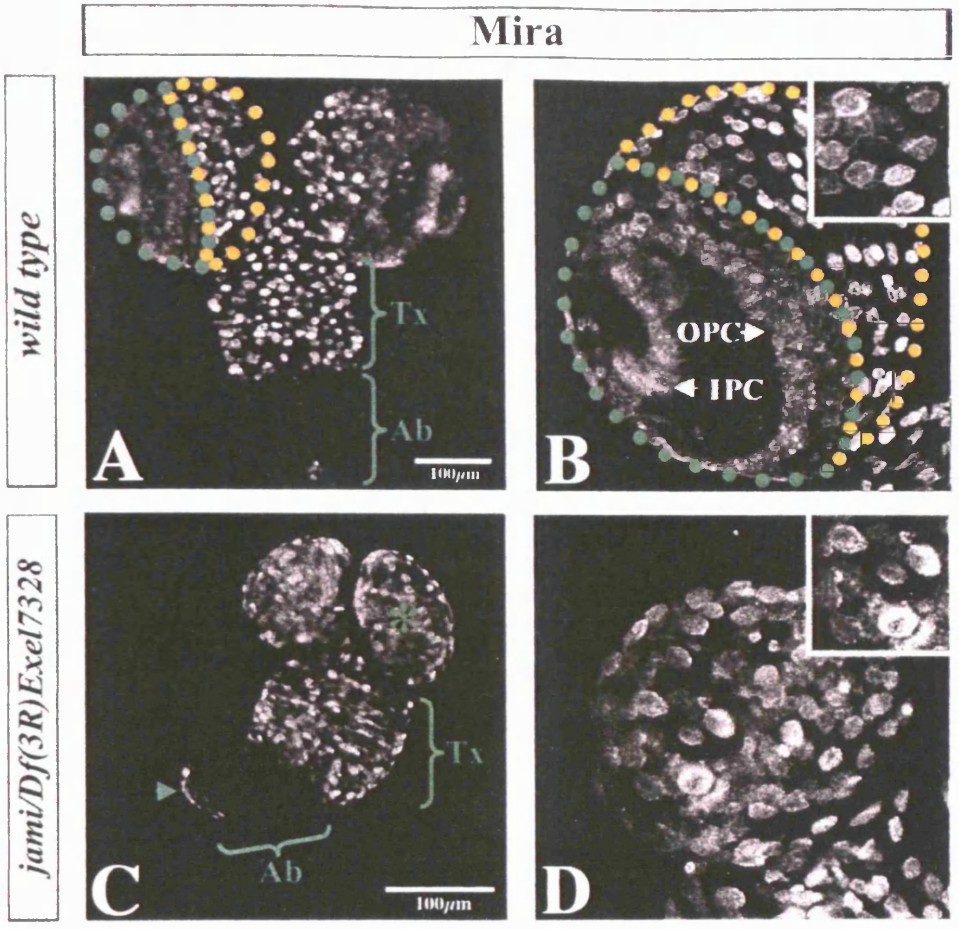

FIGURE 4.4. OPTIC-LOBE NEUROBLASTS ARE MISSING IN *JAMI* MUTANTS.
Confocal projections of entire larval CNS (**A & C**) or brain lobes (**B & D**) at 96hr ALH, stained for anti-Mira to label neuroblasts (NB) (anterior up). (**A-B**) Mira expression pattern in *wild-type* CNS illustrating optic lobe (OL, green dotted outline) and central brain (CB, yellow dotted outline). Also showing (**A**) thorax (Tx) and abdomen (Ab) and (**B**) CB NBs (inset) and Inner and Outer Proliferation Centres (IPC and OPC, respectively) of the OL. (**C-D**) Mira expression in *jami* mutant CNS (**C**) showing a reduced NB number in brain hemispheres (asterisk) but no obvious difference in Tx and Ab NBs. N.B. Mira-positive cells in Ab (arrowhead) correspond to the expected wild-type pattern in male larvae. (**D**) Brain hemisphere shows absence of small OL NBs. Inset **D** shows NBs from lateral brain region at same magnification as CB NBs in inset **B**. Approx. diameter of CB NB, 10-12μm.

In *wild-type* OLs, two rings of NBs, associated with the inner and outer proliferation centres (IPC and OPC, respectively) (Meinertzhagen and Hanson 1993) are Mira-positive (Fig. 4.4B & see Section 1.4.2B). These OL NBs, which are characteristically smaller than those in the central brain, thorax and abdomen are lacking in *jami* mutants, indicating that both OL proliferation centres are greatly reduced or absent at 96hr ALH (Fig. 4.4D). Instead, the lateral part of the brain hemisphere is occupied by large scattered Mira-positive NBs. These probably correspond to central-brain NBs that have expanded laterally from their normal medial (central brain) territory (insets, Fig. 4.4B,D).

Thus in summary, the Mira expression pattern indicates that *jami* is required for OL NBs but apparently not for central-brain and thoracic NBs.

Neurons

In the central brain, thorax and abdomen, Dac labels neurons born during embryonic neurogenesis (Mardon et al. 1994). Analysis of Dac expression indicates that embryonic neuronal populations are not affected in *jami* mutants (Fig. 4.5A,B). Expression of Elav, a marker of all postmitotic neurons, is consistent with this result and with the observed Mira pattern, thus demonstrating that neuronal populations, born postembryonically in these regions, also appear unaffected (Fig. 4.7A,B).

The absence of OL NBs in *jami* mutants at 96hr ALH raises the question as to whether there might also be a deficit in the generation of post-mitotic neural progeny in this region. To address this issue Dac was again used, this time to label early postmitotic neurons born in the postembryonic OL. The wild-type OL consists of a ring of Dac-positive lamina (la) and lobula (lo) neurons, apposed medially by a ring of Dac-negative cells (Fig. 4.5C). In *jami* mutants, although Dac-positive lamina and lobula neurons and Dac-negative cell populations all remain discernable, they are dramatically reduced in number (Fig. 4.5D).

Therefore, the loss of Mira-positive NBs in the *jami* mutant OL, at 96hr ALH, is associated with a strong reduction in the number of postembryonic neuronal progeny generated in this region. Importantly, however, the remaining OL NB progeny are capable of undergoing differentiation to a Dac-positive state. In addition, neuronal differentiation in CNS regions outside the OL does not appear to be affected.

FIGURE 4.5. *JAMI* MUTANTS HAVE REDUCED NUMBERS OF OPTIC-LOBE NEURONS AND GLIA.

Confocal projections (anterior up) of entire larval CNS (**A, B, E & F**) or brain lobes (**C & D**), at 96hr ALH. Stained for anti-Dac (**A-D**), to label all differentiated neurons born during embryogenesis and optic lobe (OL) neurons born postembryonically and anti-Repo (**E-F**). Dotted outlines indicate OL region. (**A-D**) Dac expression in *wild-type* CNS (**A & C**) showing (**A**) OL, thorax (Tx) and abdomen (Ab) and in (**C**) brain lobe showing OL, comprising a Dac-positive region of lobular (lo) and laminar (la) neurons apposed medially by a Dac-negative region (asterisk). (**B & D**) *jami* mutant CNS showing (**B**) reduced numbers of OL neurons, but no obvious defect in Tx or Ab Dac-positive neurons and (**D**) brain lobe showing OL with reduced numbers of Dac-positive cells (lo & la) and smaller Dac-negative territory (asterisk). (**E-F**) Repo expression pattern in (**E**) *wild-type* CNS showing OL region, containing concentrically arranged glial strata (arrow), Tx and Ab and in (**F**) *jami* mutant CNS showing a reduced number of glial cells in brain hemispheres (asterisk) and no organisation into strata. Tx glial cell number may also be reduced whereas there is no obvious reduction in the Ab.

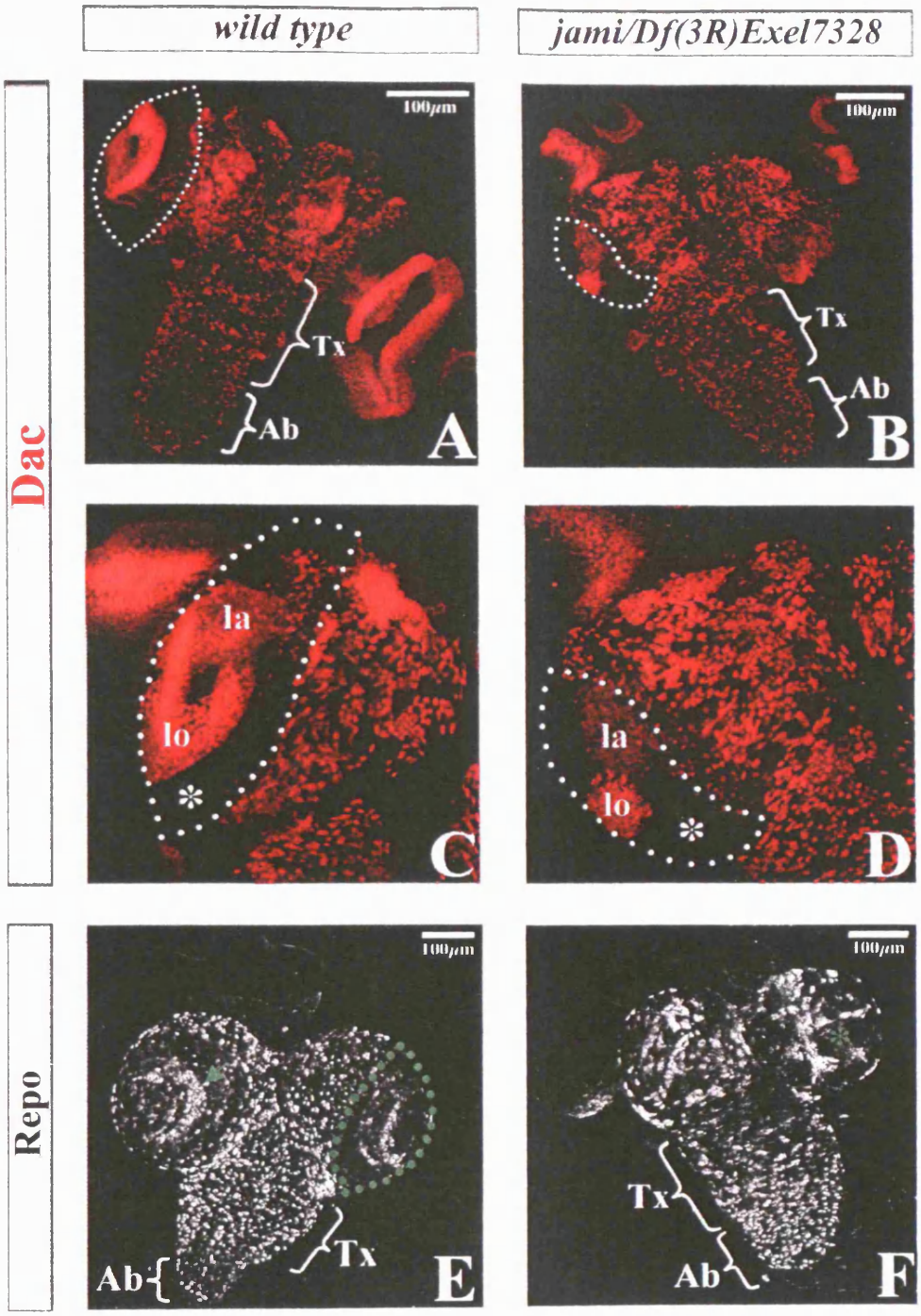
wild type
jami/Df(3R)Exel7328
Dac
Repo
100µm
Tx
Ab
A
B
la
lo
C
D
E
F

Glia

To investigate the distribution and density of glial cells, Repo expression was examined. I find that the density of abdominal glia is not obviously affected in *jami* mutants (Fig. 4.5E,F). In contrast, the brain hemispheres show a dramatic reduction in both central-brain and OL glial number and the density of thoracic glia may be slightly reduced (Fig. 4.5E,F).

In *wild-type* OLs, glial subsets are organised into multiple horseshoe-shaped strata (Fig. 4.5E & Fig. 4.6A), including the lamina glia (epithelial glia and marginal glia), medulla glia and medulla neuropil glia. Analysis of serial confocal sections through *jami* brain hemispheres indicates that these strata are missing. In addition, the reduced-glia phenotype generally appears more prominent in the deeper subpopulations of glia (cortex and neuropil glia), (Pereanu et al. 2005)). Such that the majority of remaining Repo-positive cells are large and lie superficially (Fig. 4.6B) and are thus most likely to correspond to surface glia (Pereanu et al. 2005). This lack of deep OL glia, together with the observed reduction in OL neurons and NBs, indicates the absence of the majority of OL cell types in *jami* mutants. Interestingly, although the *jami* NB phenotype appears restricted to the OL, glia in the central brain and thorax are also affected.

Photoreceptors

As *jami* mutants display a reduced-size ED, the post-mitotic neural populations in this region were assessed by Elav-expression, which labels all differentiated photoreceptors(Campos et al. 1987; Robinow and White 1988). Consistent with smaller EDs, *jami* mutants display a reduction in the number of photoreceptors and their normal regular arrangement is also disrupted (Fig. 4.7C,D). However, as the density of photoreceptors appears similar between *jami* and *wild type*, it is unlikely that *jami* is required directly for photoreceptor differentiation.

I also examined the population of retinal basal glia using Repo expression. Even in undersized *jami* EDs, this population of glia are able to migrate into the disc and the proportion of glia relative to the overall size of the disc appears similar in *jami* and *wild type* (Fig. 4.7E,F). Other studies have demonstrated that this migration is tightly linked to photoreceptor differentiation (see section 1.4.2C), therefore the presence of a similar density of glial cells and photoreceptors in *jami* EDs, compared to *wild-type*, suggests that the interdependency of glial migration and photoreceptor differentiation is largely

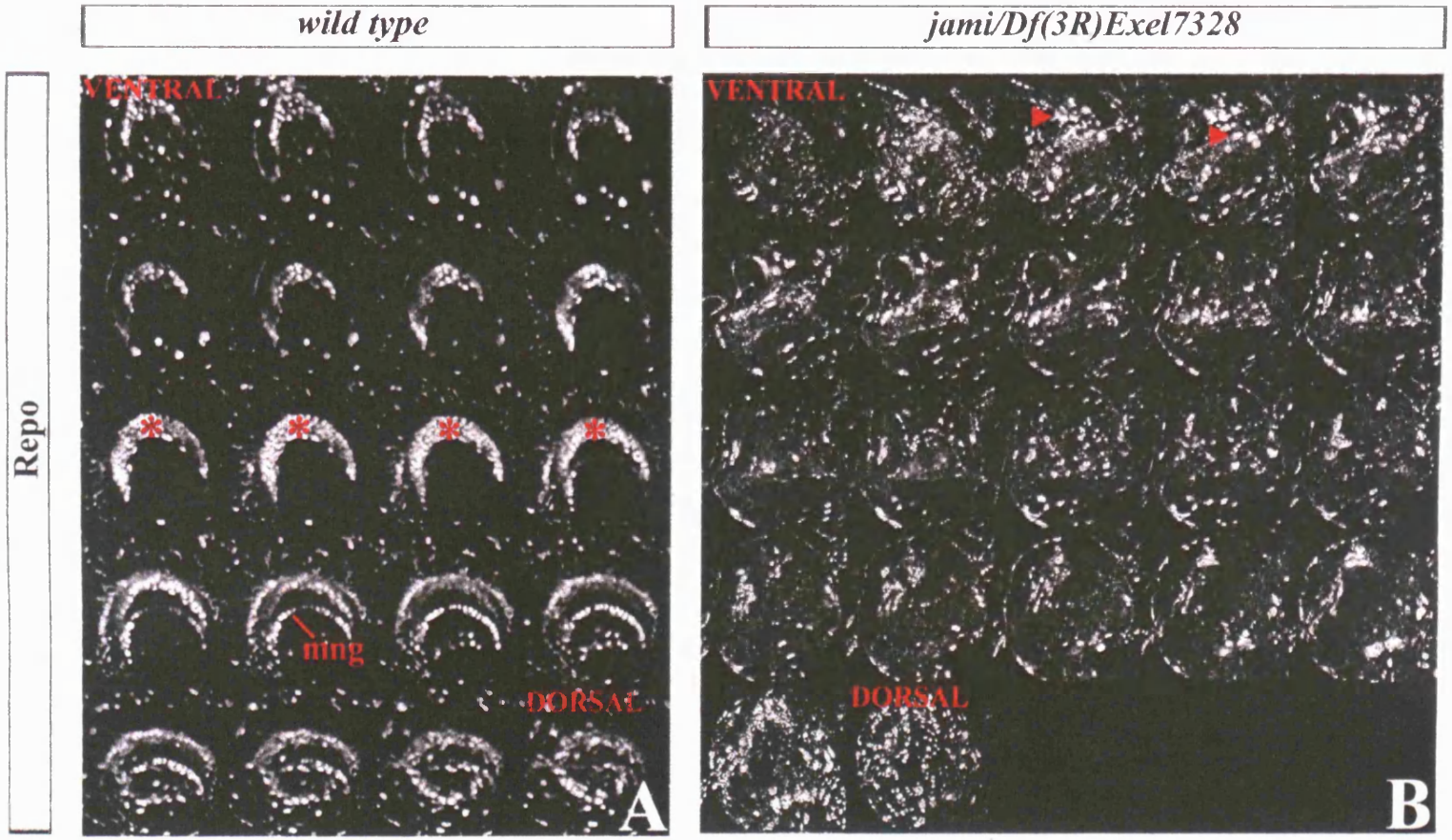

FIGURE 4.6. *JAMI* MUTANTS HAVE REDUCED NUMBERS OF BRAIN GLIA.
Serial 1μm confocal sections (ventral to dorsal) through larval brain hemispheres at 96hr ALH, stained for anti-Repo. **(A)** *wild-type* expression pattern highlights organisation of glia into specific horse-shoe shaped strata. Two strata are labelled; medulla neuropil glia (mng) and laminar glia (asterisk, consisting of epithelial glia and marginal glia). **(B)** *jami* mutant brain hemispheres have reduced numbers of glial cells and lack any organisation into regular strata. The majority of remaining glia are large and lie superficially (arrowheads).

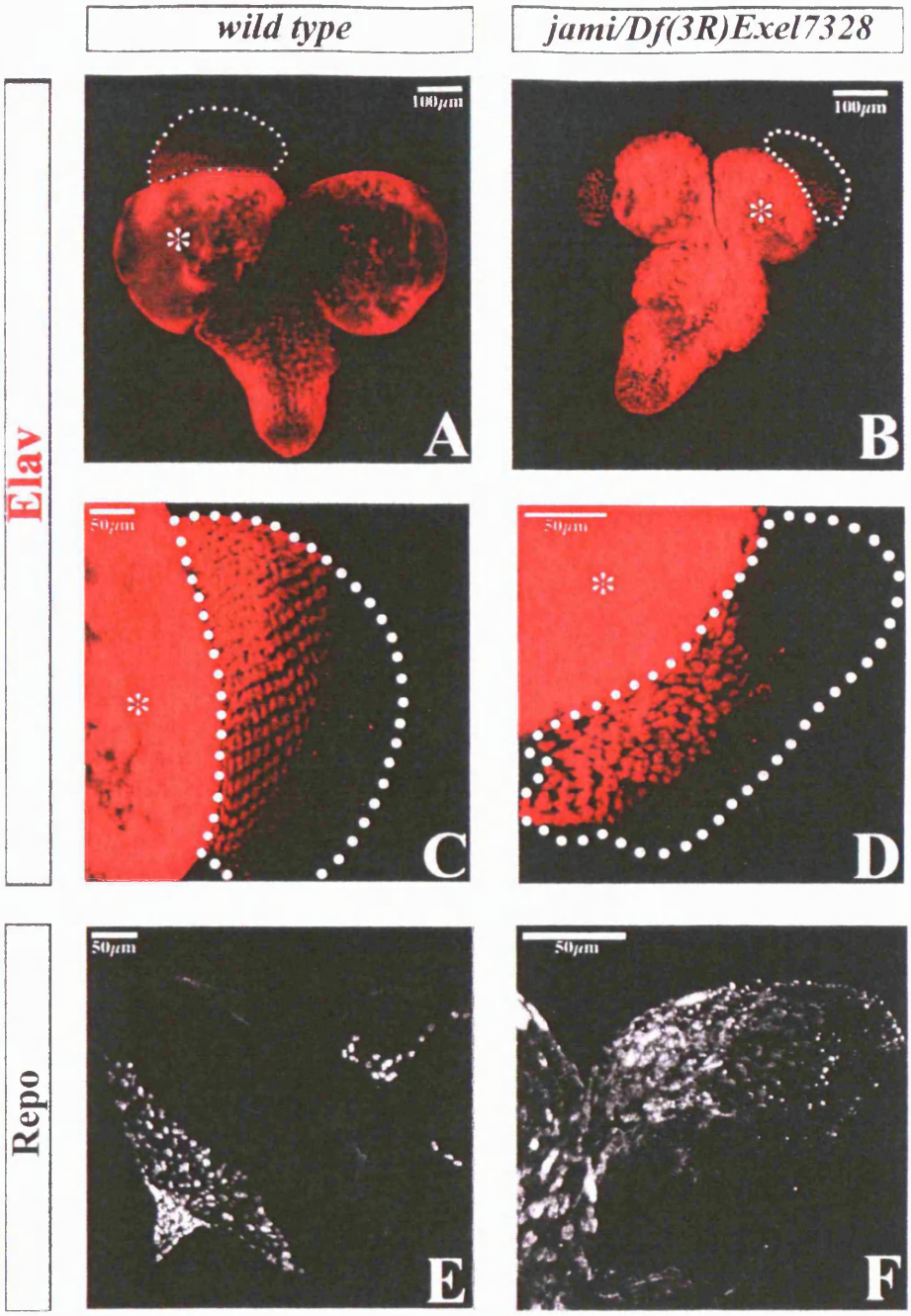

FIGURE 4.7. *JAMI* MUTANT EYE DISCS CONTAIN DIFFERENTIATED PHOTORECEPTORS AND GLIA.
Confocal projections of larval CNS and eye-antennal disc (ED) at 96hr ALH, stained for (**A-D**) anti-Elav to label neurons and photoreceptors and (**E-F**) anti-Repo. (A & B, anterior up). (**A-D**) Elav expression in (**A & C**) *wild-type* CNS (asterisk) and ED (dotted outline), illustrating regular arrangement of photoreceptors and (**B & D**) *jami* mutant CNS (asterisk) and ED (dotted outline), showing a reduced number of disorganised photoreceptors. (**E-F**) Repo expression pattern showing glial cells populating the posterior portion of the *wild-type* (**E**) and *jami* mutant (**F**) ED.

unaffected in *jami* mutants.

In summary, the analysis so far indicates that *jami* acts in a region-specific manner during CNS and imaginal disc proliferation such that, in *jami* mutants by 96hr ALH, the OL and ED show a dramatically reduced number of cells (NBs, neurons and glia) whereas other CNS regions appear much less affected.

4.2.3. *jami* photoreceptors can innervate the optic lobe

In the wild type visual system, the regular array of photoreceptors project axons through the optic stalk (OS), via the optic nerve and into the OL (Fig. 4.8A-A", B), before defasciculating to terminate in two discrete layers; the lamina (L) and medulla (M) (Fig. 4.8C). This projection is dependent on retinal basal glia whereby, in the absence of glia, photoreceptor axons are unable to enter the OS (Rangarajan et al. 1999). Considering the reduced number of glia and photoreceptors in *jami* EDs, the question arises as to whether the photoreceptor axons innervate the OL appropriately. To test this, all photoreceptor axons were labelled with 24B10 (Zipursky et al. 1984) and their projection patterns were examined in the OL. In *jami* hemizygotes, 24B10 expression confirms the Elav results showing reduced numbers of differentiated photoreceptors in the ED (Fig. 4.8D,E). The depleted population of 24B10-positive photoreceptors are, however, capable of projecting axons through the optic nerve and into the OL. Furthermore, having reached the OL they even manage to enter the dramatically reduced and disorganised lamina and medulla (Fig. 4.8D,F).

Therefore, in summary, although *jami* EDs contain a reduced number of photoreceptors, these can still differentiate and project into the OL. Together with the previous analyses, this suggests that the *jami* phenotype specifically affects the proliferation of ED precursors rather than the differentiation of postmitotic photoreceptors.

4.2.4 *jami* is required non-cell autonomously for proliferation in the eye disc and optic lobe

Previous studies have demonstrated a dependence of OL development on ED input (see Section 1.4.2C). A reduced number of photoreceptors or a failure of photoreceptors to innervate adequately the OL in early-L3, results in an absence of lamina neurogenesis (Selleck and Steller 1991), the initiation of OL cell death

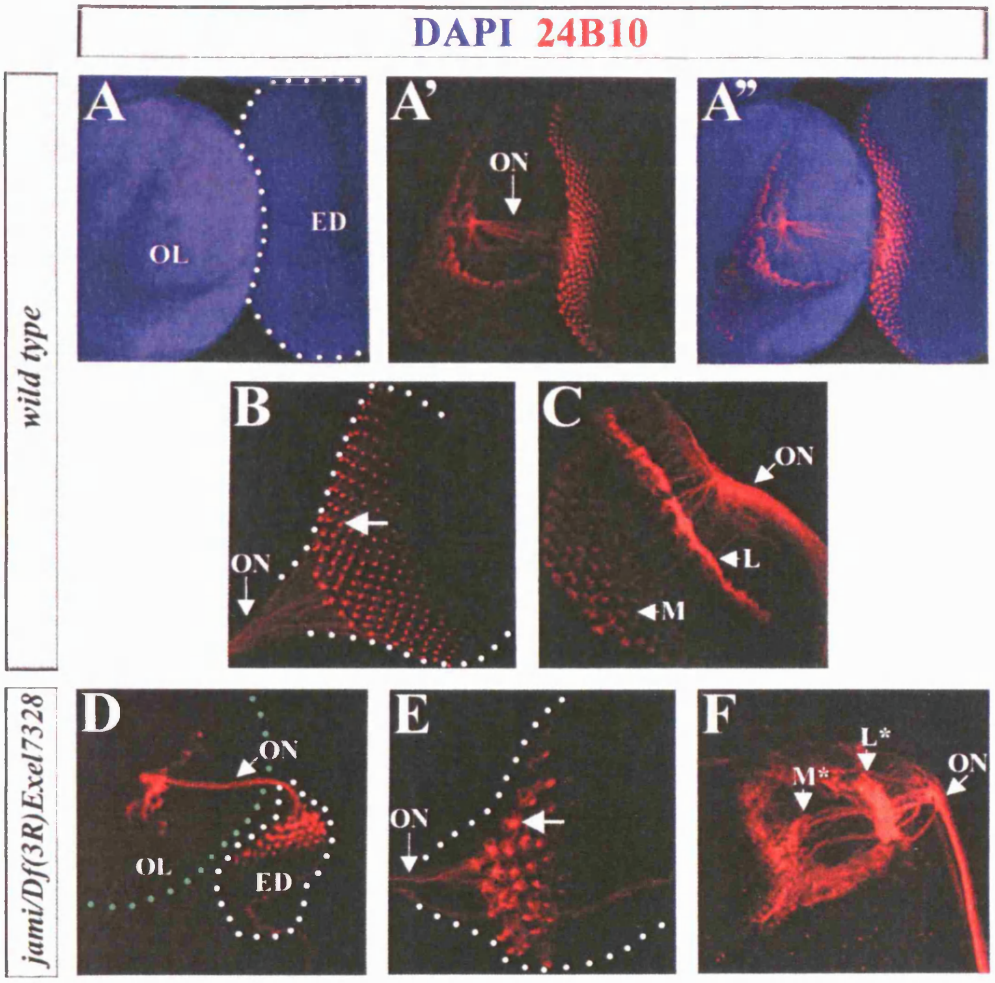

FIGURE 4.8. *JAMI* PHOTORECEPTOR AXONS PROJECT TO THE OPTIC LOBE.

Confocal projections of larval CNS and eye disc (ED, white dotted line) at 96hr ALH, stained for anti-24B10 (red), to label all differentiated photoreceptors and DAPI (blue). (**A-C**) *wild-type* (**A-A"**) optic lobe (OL, anterior up) and ED showing photoreceptor axons projecting from ED to OL, via the optic nerve (ON) (**B**) ED (posterior left) showing photoreceptors arranged in a regular array (arrow), with axons bundling for exit into ON. (**C**) High power view of photoreceptor axon projections into the OL through the ON, where they defasciculate and terminate in the lamina (L) and medulla (M). (**D-F**) *jami* mutant (**D**) OL (green dotted line, anterior up) and ED, showing photoreceptor axons projecting from ED to OL, via the ON. (**E**) ED (posterior left) where photoreceptor number is reduced (arrow) and they lack organisation. Photoreceptor axons belonging to a single ommatidial cluster do not appear to fasciculate correctly into punctate units (compare arrowheads in **B** and **E**), although they do loosely bundle to enter the ON. (**F**) High power view illustrating that photoreceptors project axons through the ON into the OL, where they defasciculate and terminate aberrantly in lamina- (L*) and medulla- (M*) like regions.

(Fischbach and Technau 1984) and disrupted differentiation and migration of glial cells (Perez and Stellar 1996). Therefore, the reduction in photoreceptor number in the *jami* ED could, in principle lead to compromised OL development and thus account for reduced neural and glial populations. To uncouple the potential requirements for *jami* in the OL and ED, in addition to investigating whether *jami* is required cell-autonomously in the CNS and imaginal discs, clonal analysis was performed using the MARCM system (see Section 2.4.2). Clones were induced at 48hr ALH and analysed at 96hr ALH. Consistent with the *jami* hemizygous analysis, coexpression of Dac with βgal in the OL demonstrates that *jami* is not required cell-autonomously for the differentiation of OL neurons (Fig. 4.9). Furthermore, expression of 24B10 and Pros in ED clones also indicates no cell-autonomous requirement for *jami* in photoreceptor differentiation and R7 cell specification, respectively (Fig. 4.10).

MARCM was also employed to test whether there might be a cell-autonomous requirement for *jami* in OL or ED clone size. Dac-expression was used to delimit the OL from the central brain and ßgal to label clones. No dramatic differences between *jami* and *wild-type* clones were observed in either the ED or OL (Fig. 4.11A,B). As statistically significant differences in average OL clone sizes are difficult to obtain due to large variations in the *wild type* sizes (I. Salecker, personal communication), quantification was not performed in this region. However, quantification was performed in the ED, where average clone sizes in *jami* and *wild type* were found to be similar (Fig. 4.12). These results suggest that there is not a cell-autonomous requirement for *jami* in promoting ED or OL growth. Together with the hemizygous analyses, they strongly suggest that there is a non-cell autonomous or extrinsic requirement for *jami* in positively regulating OL and ED growth.

4.2.5. *jami* is required cell-autonomously for persistence of thoracic neuroblasts to late-third instar

MARCM analysis was also performed in the thorax, by inducing clones at 24hr ALH and analysing clone size at 96hr ALH. Initial observations suggested that a subset of thoracic NB clones are undersized (Fig. 4.11A',B'). Consistent with this, quantitative analysis revealed that a difference existed in the minimum clone size observed between *jami* (n=13) and *wild-type* (n=33) clones (Fig. 4.13A). However, the spread of *wild-type* thoracic clone sizes largely overlaps with the *jami* distribution such that the mean thoracic clone sizes show no statistically significant difference (*wild type*, m=57 and

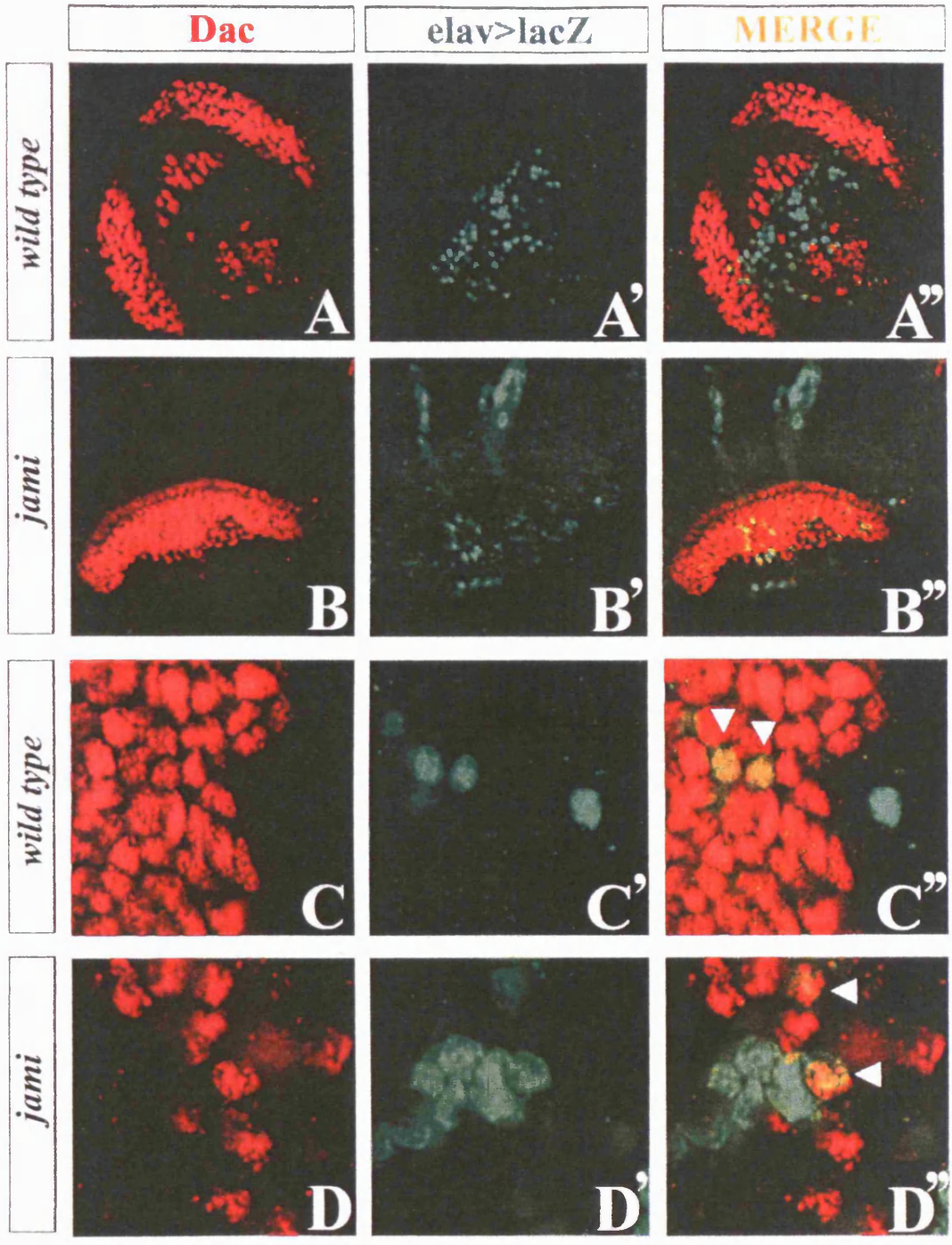

FIGURE 4.9. *JAMI* OPTIC-LOBE CLONES DIFFERENTIATE DAC-POSITIVE NEURONS.
Confocal projections (**A & B**) and single sections (**C & D**) of laterally-viewed optic lobes (OL) at 96hr ALH, stained for anti-Dac (red) to delimit the OL region and for anti-ß-gal (green) to label MARCM clones. Clones were induced at 48hr ALH. (**A & C**) *wild-type* OL clones express Dac and differentiate into lamina neurons (arrowheads, **C"**). (**B & D**) *jami* clones express Dac and differentiate into lamina neurons (arrowheads, **D"**).

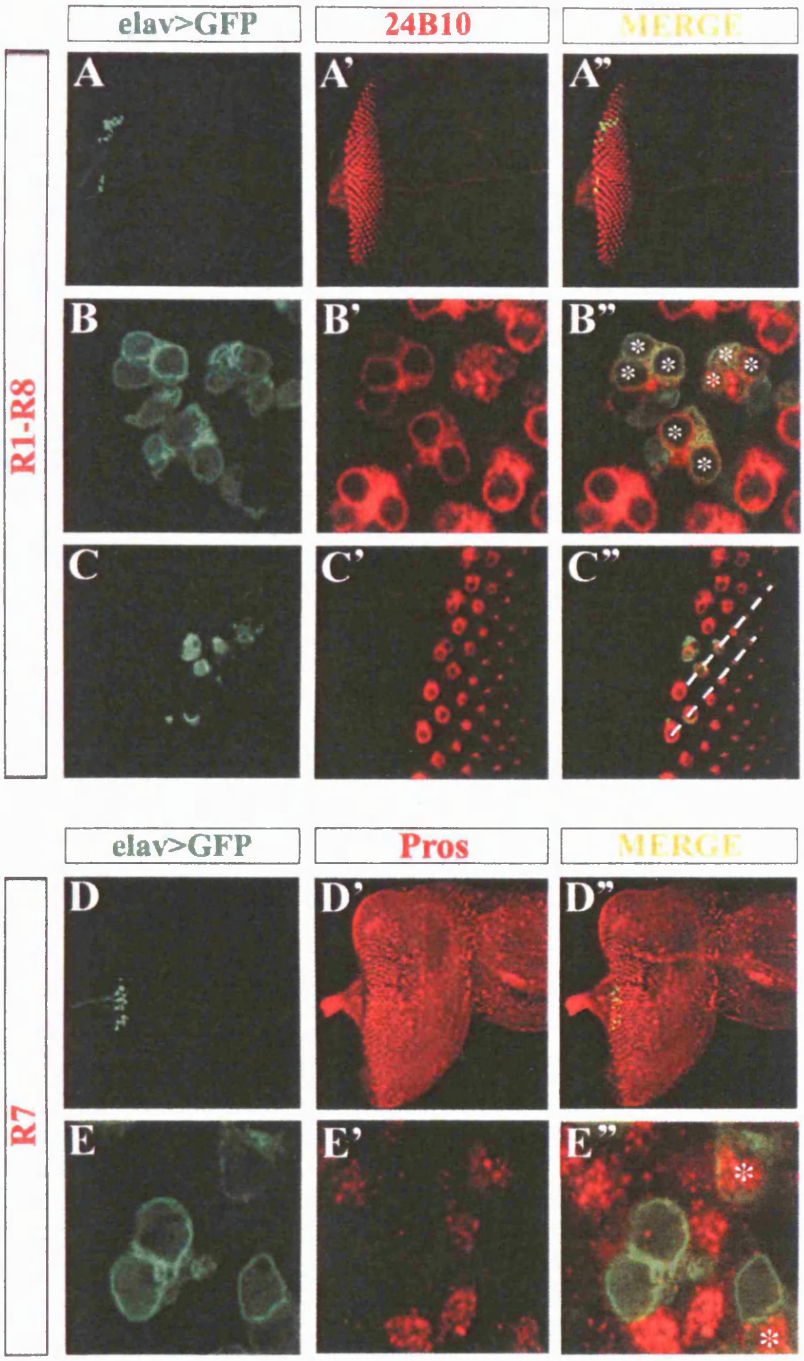

FIGURE 4.10. *JAMI* EYE-DISC CLONES DIFFERENTIATE NORMALLY. Confocal projections (**A, C & D**) and single sections (**B & E**) of the eye disc (ED, posterior left) at 96hr ALH, stained for anti-GFP to label MARCM clones (green) induced at 48hr ALH. (**A-C**) Co-stained for anti-24B10 (red) to label differentiated photoreceptors, showing (**A**) ED at low power, (**B**) *jami* clones express 24B10 (asterisks, **B"**) and (**C**) photoreceptors are arranged into a regular array and this organisation is not disrupted through *jami* clones (dashed lines, **C"**). (**D-E**) Co-stained for anti-Prospero (Pros, red) to label R7 photoreceptor cells, showing (**D**) ED at low power and (**E**) *jami* clones express Pros (asterisks, **E"**).

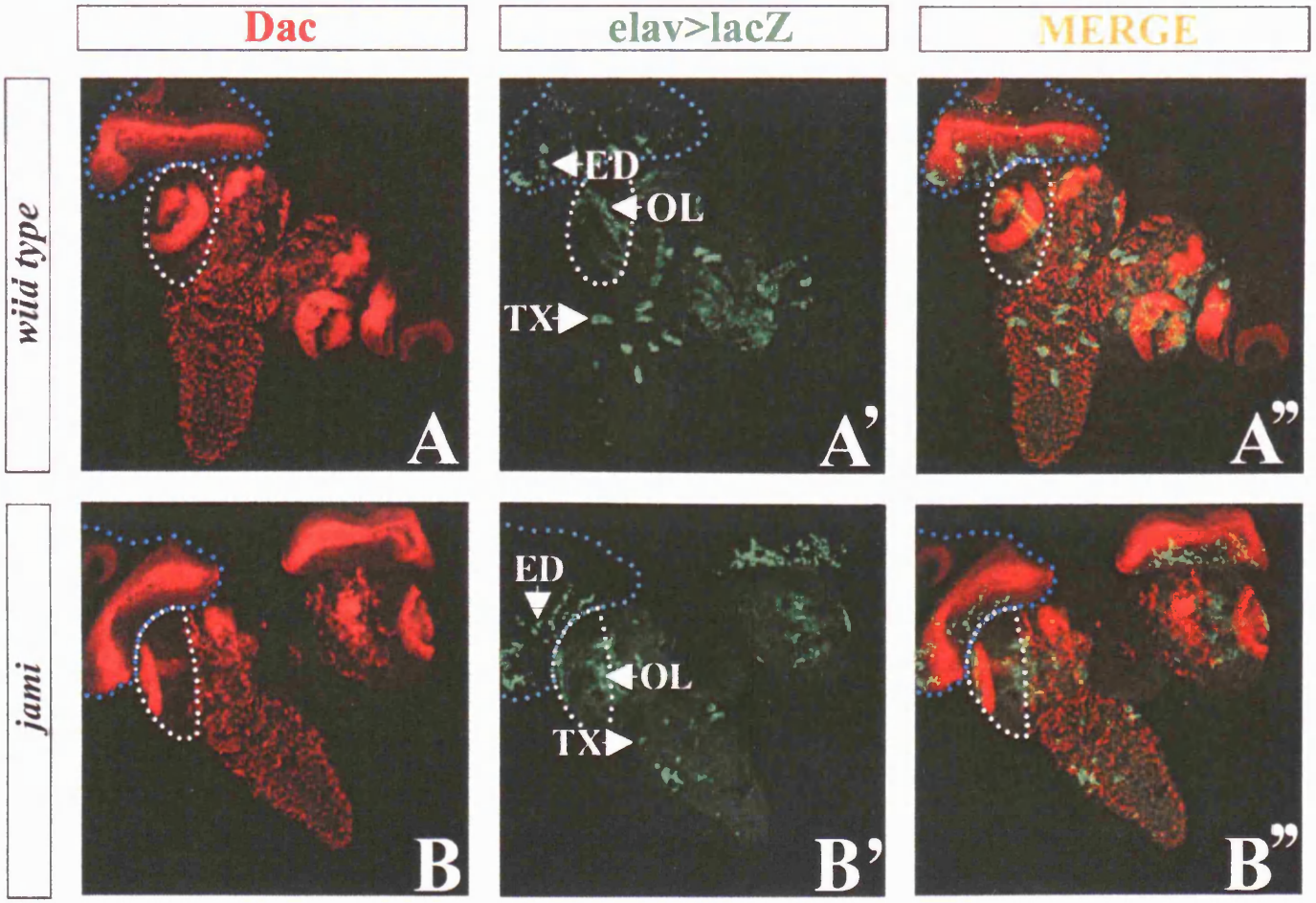

FIGURE 4.11. *JAMI* EYE-DISC AND OPTIC-LOBE CLONE SIZES APPEAR NORMAL.
Confocal projections of larval CNS (anterior up) and eye disc (ED, blue dotted outline) at 96hr ALH. Stained for anti-Dac (red), to delimit the optic lobe (OL, white dotted outline) and central brain regions, and anti-ß-gal (green) to label MARCM clones induced at 48hr ALH. Size and distribution of *wild-type* (**A'-A"**) and *jami* (**B'-B"**) ED and OL clones show no obvious differences. However, some *jami* thoracic clones appear smaller than *wild-type* (compare Tx, **A'** & **B'**).

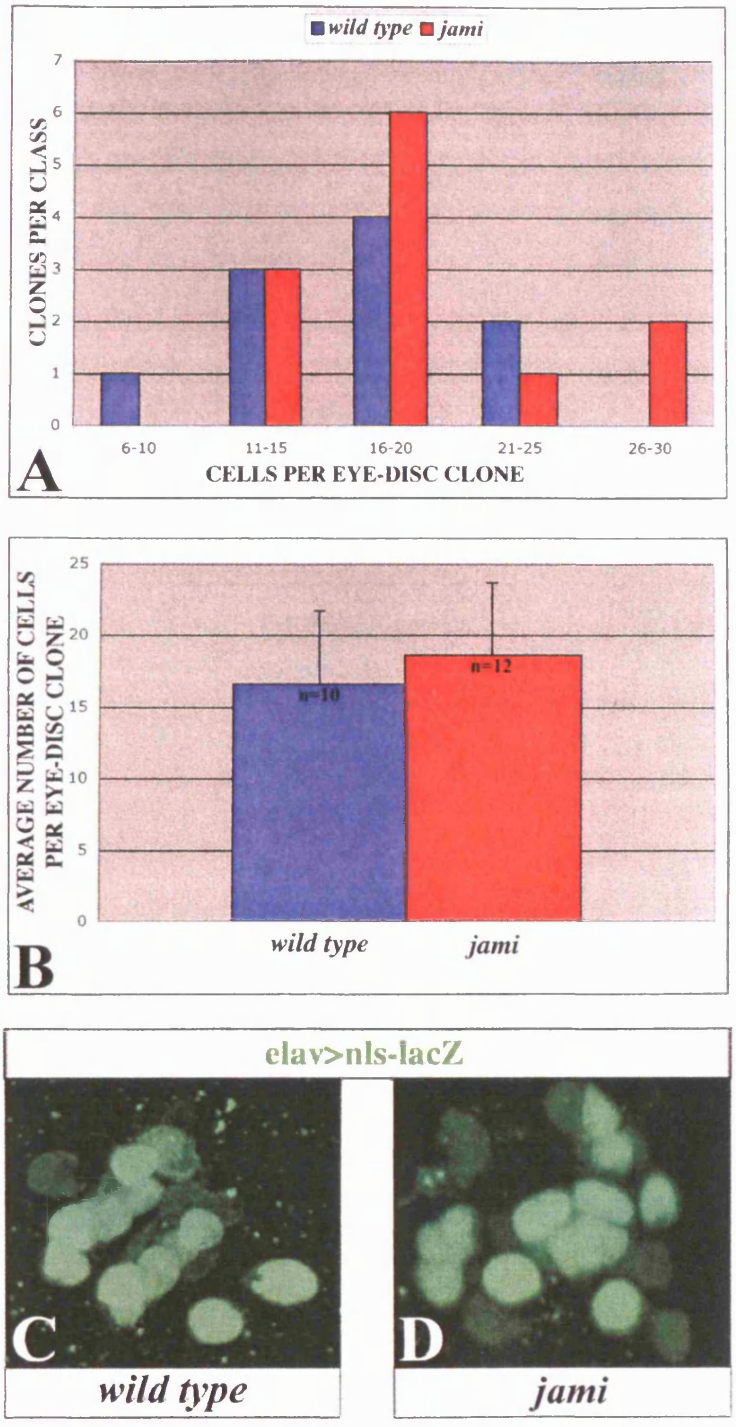

FIGURE 4.12. *JAMI* EYE-DISC CLONES ARE NORMAL SIZE.
MARCM was used to induce clones at 48hr ALH and clone size was assessed at 96hr ALH. (**A**) Graph showing the similar size distributions of *wild-type* (blue) and *jami* mutant (red) eye-disc clones. (**B**) Graph demonstrating that there is no statistically significant difference in the average *wild-type* (blue, m=17, S.D.=5) and *jami* mutant (red, m=19, S.D.=5) eye-disc clone size (p=0.41). n= number of clones analysed and error bars represent 1 S.D. (**C-D**) βgal labelling of typical *wild type* (**C**) and *jami* mutant (**D**) clones.

FIGURE 4.13. *JAMI* THORACIC CLONES ARE ROUGHLY NORMAL IN SIZE BUT LACK A NEUROBLAST AT LATE-THIRD INSTAR.
MARCM was used to induce clones at 24hr ALH and clone size was assessed at 96hr ALH. **(A)** Graph showing the size distribution of *wild-type* (blue) and *jami* mutant (red) thoracic clones. **(B)** Graph demonstrating that there is no statistically-significant difference in the average *wild-type* (blue, m=57, S.D.=24) and *jami* mutant (red, m=42, S.D.=22) thoracic clone sizes (p=0.159). Error bars represent 1 S.D. **(C-D)** βgal labels examples of average clone sizes in *wild type* **(C)** and *jami* mutants **(D)**. The neuroblast (NB) is present in *wild-type* clones (dotted outline, **C**) but absent in *jami* clones **(D)**. **(E)** Graph showing percentage of clones containing a NB, where 80% of *wild-type* clones (blue) are NB-positive but 0% of *jami* clones contain a NB. n= number of clones analysed.

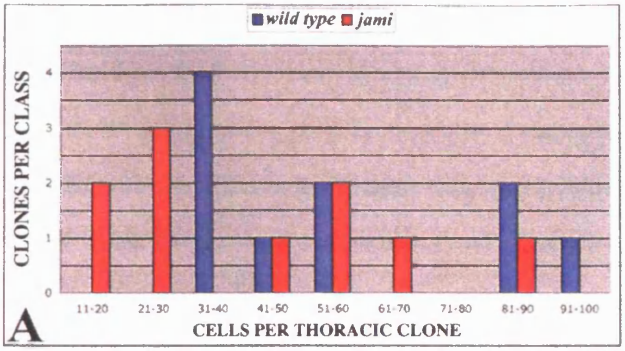
wild type
jami
CLONES PER CLASS
0
1
2
3
4
11-20
21-30
31-40
41-50
51-60
61-70
71-80
81-90
91-100
CELLS PER THORACIC CLONE
A

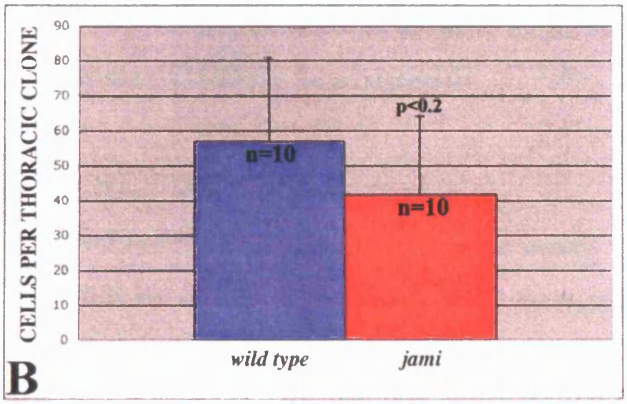
CELLS PER THORACIC CLONE
0
10
20
30
40
50
60
70
80
90
p<0.2
n=10
n=10
wild type
jami
B

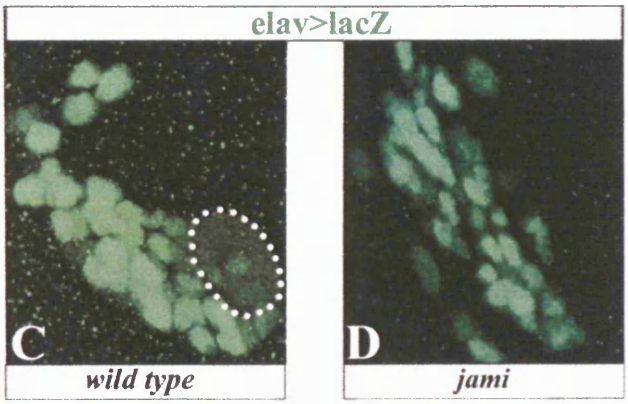
elav>lacZ
C
wild type
D
jami

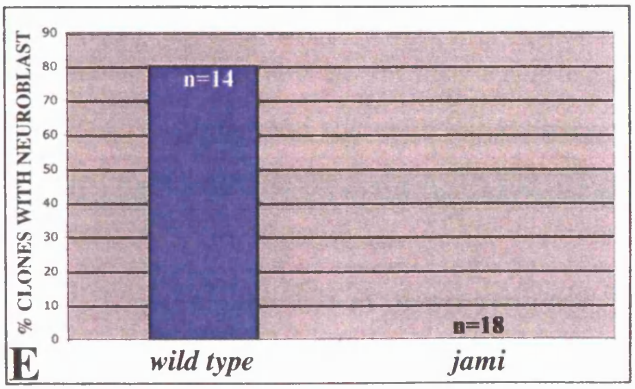
% CLONES WITH NEUROBLAST
0
10
20
30
40
50
60
70
80
90
n=14
n=18
wild type
jami
E

jami, m=42). As individual thoracic NB lineages in the wild type vary greatly in size (Bello et al. 2003), statistical significance is difficult to detect. Obtaining statistical significance would require a method for focusing quantification on only the specifically affected thoracic lineages, which is not currently feasible. I nevertheless strongly favour the idea that there is a cell-autonomous requirement for *jami* in thoracic clone size. This is based on the striking observation that the number of thoracic clones containing a large distinguishable NB falls from 80% in the *wild-type* to 0% in *jami* mutants (Fig. 4.13C-E). While this observation clearly indicates a cell-autonomous requirement fort *jami* for thoracic NB persistence, because average thoracic clone size is not significantly affected, NB loss in *jami* mutants is likely be a late effect.

4.2B IDENTIFYING THE *JAMI* LOCUS

Having characterised *jami* phenotypically, it was necessary to map the mutation to a specific gene. This enables further investigation into the nature of the *jami* gene product and the molecular mechanism by which it acts.

4.2.6. High-resolution deficiency mapping of *jami*

As discussed in Section 3.2.6, the *jami/PL26* mutation was initially cytologically mapped to a 152Kb interval, between the cytological locations 89B1;89B5. This interval was delimited by two molecularly-defined deficiencies, one that complemented *jami (Df(3R)Exel7327)* and one that failed to complement the mutation *(Df(3R)Exel7328)*. To verify independently the candidate interval, I obtained one additional large deficiency *(Df(3R)sbd105)* and three smaller deficiencies (*Df(3R)Sbd104*, *Df(3R)Sbd26* and *Df(3R)Sbd45*). However, all four deficiencies complemented the mutation, contradicting the initial results (Table 4.1). To resolve this inconsistency, all six deficiencies involved in this experiment were tested by complementation testing with each other and also with lethal alleles for known genes in the region. This revealed that the Df(3R)Sbd45 and Df(3R)Sbd105 chromosomes do not carry the deletions described in Flybase (Table 4.1).

In conclusion, complementation testing revealed that *jami* fails to complement *Df(3R)Exel7328* and complements *Df(3R)Exel7327*, *Df(3R)Sbd104* and *Df(3R)Sbd26*. These results place the *jami* mutation in a ~56Kb interval, between 3R:11867083;11923310bp (Release 4.3 coordinates), containing 7 candidate genes (Fig. 4.14).

	jami	*DF(3R) Exel7328*	*Df(3R) Exel7327*	*Df(3R) sbd105*	*Df(3R) sbd45*	*Df(3R) sbd104*	*Df(3R) sbd26*	*srp*^{01549}	*pnr*^{VX6}	*msps*^{EY06514}	*Akt1*^{04226}	*Sb*^{1}
jami		FAIL	COMP	COMP	COMP	COMP	COMP	N/D	N/D	COMP	COMP	COMP
DF(3R)Exel7328			FAIL	COMP	COMP	FAIL	FAIL	COMP	FAIL	N/D	N/D	N/D
Df(3R)Exel7327				COMP	COMP	COMP	COMP	FAIL	FAIL	N/A	N/D	N/D
Df(3R)sbd105					COMP	COMP	COMP	COMP	COMP	N/D	N/D	COMP
Df(3R)sbd45						FAIL	FAIL	N/D	N/D	N/D	N/D	N/D
Df(3R)sbd104							FAIL	COMP	COMP	N/D	N/D	FAIL
Df(3R)sbd26								COMP	COMP	N/D	N/D	FAIL
srp^{01549}									N/D	N/D	N/D	N/D
pnr^{VX6}										N/D	N/D	N/D
msps^{EY06514}											N/D	N/D
Akt1^{04226}												N/D
Sb^{1}												

TABLE 4.1. COMPLEMENTATION TESTING IN THE *JAMI* CANDIDATE REGION.
Showing results of complementation testing which agree (black) or conflict (red) with published deficiency data. 'FAIL', failure to complement and 'COMP', complementation. ND indicates 'Not Done'. All crosses were repeated twice. For details of deficiencies, see Appendix 1 and for alleles, see Table 2.1).

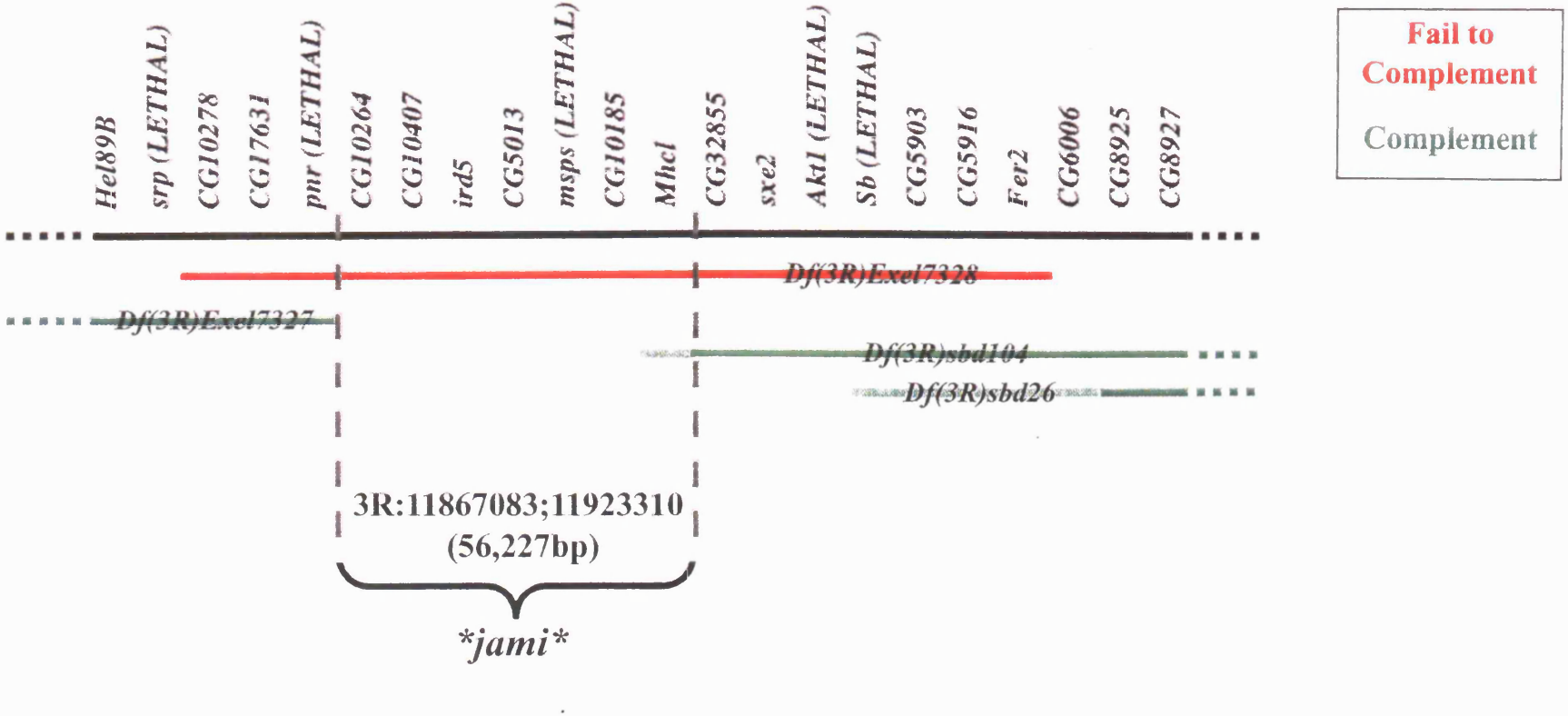

FIGURE 4.14. HIGH RESOLUTION DEFICIENCY MAPPING OF *JAMI* TO THE 89B3;89B5 INTERVAL.
Solid Black line represents a section of the right arm of chromosome three (approximate cytological region 89A11;89B7). Gene names/CG numbers are listed above. 'LETHAL' refers to the availability of lethal alleles for complementation testing. Coloured lines show named deficiencies used for complementation testing with *jami:* In red are deficiencies which fail to complement *jami* and in green are deficiencies which complement *jami*. Dotted coloured lines indicate the cytological breakpoint of the deficiency lies outside the schematic map. Pale green lines indicates region of uncertainty (as cytologically mapped deficiencies do not have molecularly-defined breakpoints). Dashed grey lines indicate the predicted cytological region in which the *jami* locus lies (3R: release 4.3 coordinates from 11867083 to 11923310 base pairs, bp).

4.2.7. A candidate approach to identifying the *jami* locus

Using all available databases (see Section 2.1) a search was performed for each of the 7 candidate genes (Table 4.2). The first search undertaken was for available lethal alleles of the candidate genes. One lethal allele was available for *msps*, allowing this gene to be eliminated from the candidate list, as it complemented *jami* (Grey, Table 4.2). Investigation into previous work on *ird5* revealed that existing null alleles of the gene are adult viable (Lu et al. 2001), thus allowing elimination of this candidate gene as *jami* is late larval/pupal lethal.

Of the remaining five candidate genes, little information is available. PSI-BLAST searches reveal that *CG10264* contains a DUF233 domain (pfam 03027). This family includes the Juvenile Hormone Binding Protein (JHBP) of the tobacco hawkmoth, as well as a number of *Drosophila* proteins of unknown function. *CG10407* also contains a DUF233 domain and also a related JHBP domain (pfam 06585). Juvenile hormone (JH) has many functions in insects; it regulates embryogenesis, maintains the status quo of larvae during moults and stimulates reproductive maturation in the adult. JH is transported from the sites of its synthesis to target tissues by the haemolymph carrier, JHBP. This protects JH molecules from hydrolysis by non-specific esterases present in the insect haemolymph. Very little is known about *CG5013* and *CG10185* except that PSI-BLAST searches reveal that the former is a predicted methyl transferase (COG3897) and the latter contains a WD40 domain (cd00200).

The most information regarding candidates for *jami* relates to *Mhcl*. It encodes a product containing a PDZ domain and a myosin head motor domain (Tzolovsky et al. 2002). It is known from yeast-2-hybrid (Y2H) interactions (Giot et al. 2003) that *Mhcl* interacts, at a high confidence level (>0.5, where 1 is maximum) with *CG5355* (confidence level, 0.6857), *CanB* (confidence level, 0.5952), *Crk* (confidence level, 0.6330) and *yellow-e3* (confidence level, 0.5203). Little is known about the functions of these three genes. *CG5355* encodes esterase/lipase/thioesterase domains, and *Crk* codes for an SH2 domain protein involved in G-protein coupled receptor signalling. Finally *yellow-e3* codes for a MRJP (major royal jelly protein) domain and is involved in pigmentation, adult cuticle and larval mouthpart development.

In conclusion, I successfully mapped the *jami* mutation to an interval containing five candidate genes. Unfortunately there is not yet enough information available to convincingly implicate any one of these candidates as *jami*. However, it is interesting that one candidate, *Mhcl*, was recently identified in an RNAi screen for genes affecting

Gene	Name	Annotated Functions/ PSI-BLAST searched	Size (bp)	Lethal Allele available?	Curagen Y2H (Confidence >0.5)
CG5000	*mini spindles (msps)*	Mitosis and microtubules	N/A	$msps^{EY06514}$ (Complements)	N/A
CG4201	*immune response deficient 5 (ird5)*	Protein kinase	N/A	Null viable^{+} ($ird5^{1}$, $ird5^{2}$)	N/A
CG10264	N/A	DUF233 domain	813	NO	NO
CG10407	N/A	DUF233 & JHBP domains	912	NO	NO
CG5013	N/A	Methyl transferase domain	974	NO	NO
CG10185	N/A	WD40 domain	5199	NO	NO
CG31045	*Myosin heavy chain-like (Mhcl)*	Myosin motor & PDZ domain	6706	NO	*CG5335* (0.6857) *CanB* (0.5292) *Crk* (0.6330) *yellow-e3* (0.5203)

TABLE 4.2. *JAMI* CANDIDATE GENES.
Summary of available information regarding candidate genes for *jami,* including CG number; gene name; annotated function and PSI-BLAST search results; size of coding region (base pairs, bp); availability of lethal alleles (from Bloomington, http://flystocks.bio.indiana.edu/ and GETDB, http://flymap.lab.nig.ac.jp/~dclust/getdb.html); and protein-protein interaction data (Yeast-2-hybrid Screen, Y2H, http://portal.curagen.com/cgi-bin/interaction/flyHome.pl, Giot et al., 2003), indicating the confidence level (maximum=1, see text for details). In Grey are genes eliminated by complementation testing (CG5000) or on the basis of a published viable null allele (CG4201) $^{+}$(Lu, Wu et al. 2001). In blue are the remaining 5 *jami* candidate genes (see text for details). N/A indicates 'Not applicable'.

the embryonic development of the nervous system (Ivanov et al. 2004). These authors demonstrated that RNA interference of *Mhcl* gene function resulted in loss of PNS and CNS neurons and disorganisation of the ventral nerve cord. To pursue identification of the *jami* gene, I would have to focus on all five candidates, using two approaches. One approach involves sequencing the open-reading frames of all five genes (which amounts to 15Kb of exonic DNA in total) to search for the base pair change responsible for the mutant phenotype. However, it is possible that the mutation may lie in a regulatory region (e.g. an enhancer) outside the exonic DNA. I could also generate lethal alleles of the five genes, using customised micro-deficiencies (http://www.drosdel.org.uk/ and http://expbio.bio.u-szeged.hu/fly/index.php) or imprecise excision of viable *P* element or *piggyBac* insertions, followed by complementation testing with *jami*. Subsequently, the entire candidate gene could be sequenced to identify the *jami* mutation at the DNA level.

4.3 DISCUSSION

4.3.1 *jami* is required for imaginal tissue growth but not cell differentiation

A requirement for *jami* in neural differentiation is unlikely based on two lines of evidence. Firstly, analysis of the hemizygote demonstrates that cells in the CNS and ED are capable of differentiating, albeit in reduced numbers. Secondly, analysis of *jami* mutant clones has confirmed that there is no cell-autonomous requirement for differentiation in OL and thoracic neurons or in ED photoreceptors.

In contrast to analysis of imaginal tissue during L3 (96hr ALH), preliminary phenotypic analysis of late-L2 *jami* hemizygote CNS and ED suggest that neuronal and glial populations are normal at this time. This data is consistent with analysis of overall larval growth rate which indicates a deficit specifically during L3. The fact that *jami* mutants reach and exceed the critical mass (Beadle et al. 1938) yet fail to pupariate is interesting and suggests that larval developmental arrest can not solely be explained by a nutritional deficit such as reduced food intake.

My data suggest a specific temporal zygotic requirement for *jami* activity in both diploid imaginal and polyploid larval tissue growth, during L3. However, an alternative explanation for the late manifestation of the *jami* phenotype is that *jami* is required throughout development, but perdurance of the maternal contribution of Jami masks any earlier phenotype.

4.3.2 *jami* is required cell-autonomously in thoracic NBs

Clonal analysis has demonstrated a clear cell-autonomous requirement for *jami* in thoracic CNS development. Strikingly, the absence of the NB in all thoracic MARCM clones at 96hr ALH is in contrast to observations of an apparently normal size thoracic population of Mira-positive NBs in the 96 hr ALH hemizygous animal. There are two possible hypotheses to resolve these apparently conflicting observations. First, it could be that a second site lethal mutation present on the third chromosome is responsible for the absence of the NB, as this mutation would only be homozygous in clones and not observed in the hemizygous analysis. However, I have ruled this out as the thoracic Mira pattern in the homozygous larva is similar to that in the hemizygous larva and is normal (data not shown). The second possibility is that the requirement for *jami* in the thoracic NB is very late, at a developmental stage not reached by the hemizygous animal. As the entire *jami* hemizygous larva is undersized at 96 hr ALH, this possibility is very likely. A test of this reconciling hypothesis, namely that the hemizygote at 96 hr ALH is developmentally retarded relative to the MARCM 96 hr ALH specimens, would be to score for NBs in MARCM clones at a younger stage when the overall CNS is at a similar size to hemizygous specimens. In any case, the loss of the NB must be a late event, as analysis of thoracic clone size shows only a moderate, non-statistically significant difference in *wild-type* and *jami* clone sizes.

4.3.3 *jami* is required non-cell autonomously for optic-lobe and eye-disc growth

Both hemizygous and clonal analysis in the central brain and abdomen, indicate no requirement for *jami* in the growth of these regions. Moreover, the presence of large Mira-positive NBs throughout the larval CNS, indicates that *jami* is not required for NBs to exit quiescence, as Mira is progressively downregulated in quiescent NBs, such that by mid-L1 they are not Mira-positive. In contrast, a clear requirement for *jami* in promoting OL and ED growth has been demonstrated through analysis of *jami* hemizygotes. The reciprocal interdependence of the OL and ED makes it difficult to determine where *jami* is required by simply looking at hemizygotes at 96 hr ALH. To address this issue, clonal analysis was performed and the results indicate that, in fact, there is no cell-autonomous growth requirement for *jami* in either tissue. This strongly suggests that *jami* regulates ED and OL neural growth by being required for the production of a signal manufactured outside of these neural lineages or even outside of both tissues.

The undersized imaginal discs and OL in the hemizygote, combined with no apparent clonal phenotype, suggests the involvement of an extrinsic mechanism for regulating growth. A number of different global growth signals have been found, including fat-body derived growth factor(s) (Britton and Edgar 1998), the insulin receptor/TOR signalling pathway (Leevers 2001) and the ecdysone signalling pathway (Sliter et al. 1989; Song and Gilbert 1994). A role for *jami* in insulin/TOR signalling could be tested genetically by rescuing the phenotype by overexpressing components of this pathway. In addition a role for *jami* in ecdysone signal production could be investigated by trying to rescue the phenotype with exogenous applications of ecdysone (Li et al. 2001).

Thus the data strongly suggest a non-cell autonomous requirement for *jami* in growth of OL and ED neural populations. The question of whether *jami* is required in cell proliferation or survival has not been directly addressed in this study. To test if *jami* is required specifically for cell survival, the number of cells expressing activated caspase could be quantified using immunocytochemistry. This analysis could be coupled with a measurement of cell-cycle speed, through BrdU pulse labelling, to give a measure for cell proliferation. Genetic approaches could also be used to test if *jami* is required for cell survival by testing if, in the absence of cell death, the *jami* phenotype could be rescued. One rescue approach would use two overlapping deficiencies to remove the proapoptotic genes, *grim, head involution defect (hid), reaper (rpr)* and *sickle* (Peterson et al. 2002). A second rescue approach would be through ectopic expression of the baculovirus P35 protein, which has been shown to act as an inhibitor of activated caspases and thus apoptosis (Hay et al. 1994; Bump et al. 1995).

CHAPTER 5

ROIE, A CELL-AUTONOMOUS REGULATOR OF NEURAL GROWTH

5.1 INTRODUCTION

PL93 was assigned to class IV of the pupal-lethal mutants, the same category containing *jami,* on the basis of a region-specific reduction in the size of the brain hemispheres and imaginal discs (see Fig. 3.3C,G). In this chapter, the phenotype and mapping of this mutant, renamed *reduced optic and imaginal expansion (roie)* are investigated in detail. First, I address the degree to which the *roie* phenotype is region or tissue specific. Second, I assess whether the requirement for *roie* within the CNS and imaginal discs is cell-autonomous. Third, I identify a strong candidate gene for *roie*.

5.2 RESULTS

5.2A PHENOTYPIC CHARACTERISATION OF *ROIE*

5.2.1 The *roie* mutation reduces growth of imaginal, but not larval, tissues

To assess whether *roie* affects overall larval growth, larvae were weighed at three time points. A comparison of average larval mass at 36hr, 60hr and 84hr ALH for *roie* hemizygous larvae (*roie/Df(3L)st-g24*) and *roie* heterozygous controls (*roie/TM3)* indicates that both genotypes exhibit a similar rate of growth (Fig. 5.1A). Therefore, unlike *jami*, *roie* does not significantly affect overall growth of the larval body.

In contrast to the larval body, and similar to *jami* hemizygotes, CNS growth is dramatically affected in hemizygous *roie* mutants (*roie/Df(3L)st-g24,* referred to as *roie* hemizygotes hereafter). The size reduction of the brain hemispheres at 96hr ALH appears to correlate with the loss of intense DAPI-stained tissue, characteristic of the OL (Fig. 5.1B,D). EDs are also dramatically reduced in size (Fig. 5.1C,E) along with other imaginal discs (data not shown). However, the ventral ganglion (thorax and abdomen) appears relatively normal in size (Fig. 5.1B,D). Therefore, in summary, the *roie* mutation specifically affects imaginal rather than larval tissue growth but, like *jami*, *roie* may act within the CNS in a region-specific manner.

5.2.2 Thoracic neural cell populations are largely normal in *roie* hemizygotes

To investigate further the regional specificity of *roie* during CNS growth, thoracic development was assessed at 96hr ALH, using Mira immunostaining to label all NBs. This demonstrated that the number of NBs in the thorax is not noticeably altered in *roie* hemizygotes (Fig. 5.2A,B). I next addressed whether the glial population was affected in *roie* mutants using Repo staining. This revealed no obvious affect on glial number in the thorax (Fig. 5.2C,D).

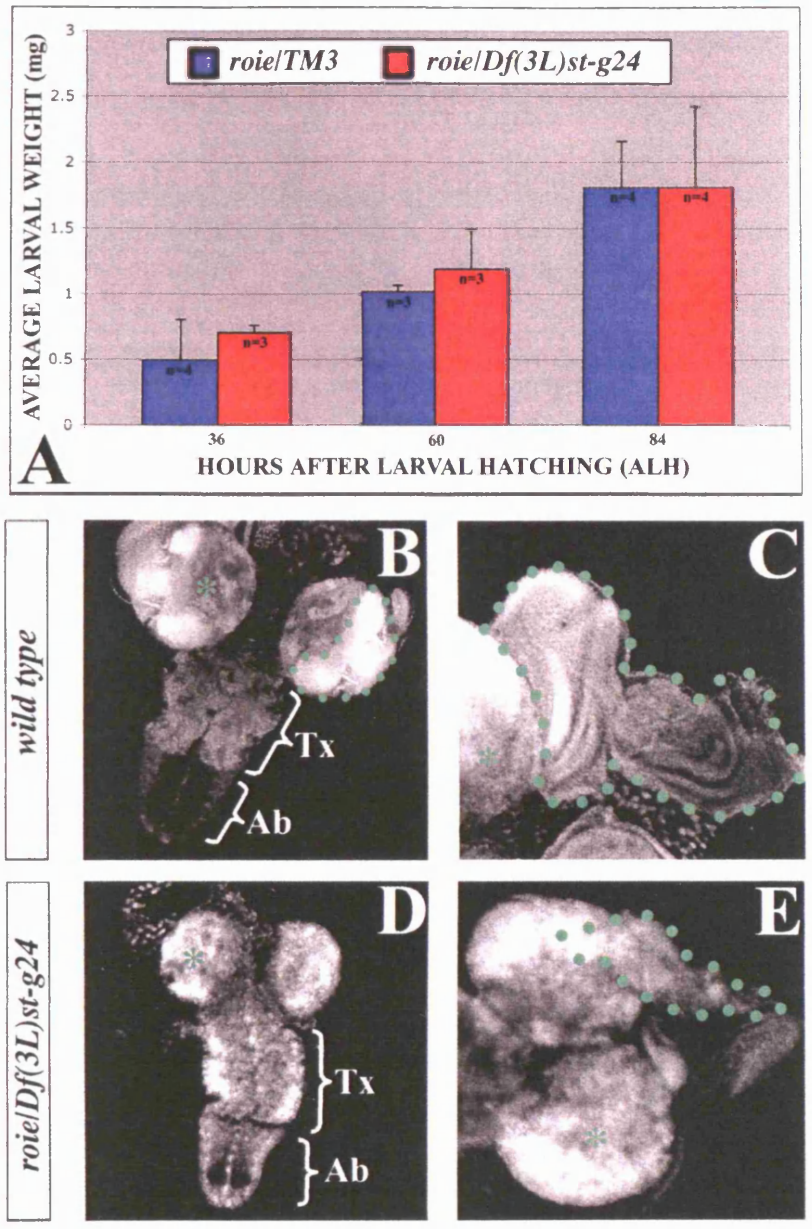

FIGURE 5.1. *ROIE* HEMIZYGOTES GROW NORMALLY BUT DISPLAY UNDERSIZED BRAIN LOBES AND IMAGINAL DISCS.
(**A**) Graph showing the weights of *roie/TM3* (blue) and *roie/Df(3L)st-g24* (red) larvae at mid-L2 (36hr ALH, blue, m=0.50, S.D.=0.31; red, m=0.70, S.D.=0.06), early-L3 (60hr ALH, blue, m=1.02, S.D.=0.05; red, m=1.19, S.D.=0.30) and late-L3 (84hr ALH, blue, m=1.81, S.D.=0.35; red m=1.81, S.D.=0.61). Where n = number of replicative weighings and error bars represent 1 S.D. (**B-E**) L3 larval CNS (**B & D,** anterior up) and eye-antennal imaginal discs (**C & E,** posterior left) at 96hr ALH, stained with the nuclear dye DAPI. (**B-C**) *wild-type* CNS showing (**B**) brain lobe (asterisk), optic lobe (OL, dotted outline), Thorax (Tx) and Abdomen (Ab) and (**C**) eye disc (ED, dotted outline) and brain lobe (asterisk). (**D-E**) *roie* hemizygous CNS showing (**D**) undersized brain hemispheres (asterisk), but a near normal-sized thorax (Tx) and abdomen (Ab) and (**E**) undersized ED (dotted outline) and brain lobe (asterisk). Magnifications; **B=D** and **C=E.**

FIGURE 5.2. OPTIC-LOBE, BUT NOT THORACIC NEURAL POPULATIONS ARE DEPLETED IN *ROIE* HEMIZYGOTES.
Confocal projections of L3 larval CNS (anterior up) at 96hr ALH, showing optic lobe (OL, dotted outline) and thorax (Tx). Stained for **(A-B)** anti-Miranda (Mira) to label neuroblasts (NB), **(C-D)** anti-Repo to label most differentiated glial cells and **(E-F)** anti-Dacschund (Dac) to label all differentiated neurons born during embryogenesis and OL neurons born post-embyonically. **(A-B)** Mira expression pattern in **(A)** *wild-type* and **(B)** *roie* hemizygotes, illustrating that the majority of OL NBs are absent, although Tx NBs appear normal in number. **(C-D)** Repo expression pattern in **(C)** *wild-type*, illustrating the glial precursor centre (GPC, arrow) and **(D)** *roie* hemizygotes, demonstrating that in the undersized brain hemispheres (asterisk) no clear GPC or even OL (dotted outline, **C**) is present. No obvious reduction is observed in Tx glial number. **(E-F)** Dac expression pattern in **(E)** *wild-type* and **(F)** *roie* hemizygotes, demonstrating that the majority of lobular and laminar neurons of the OL are absent.

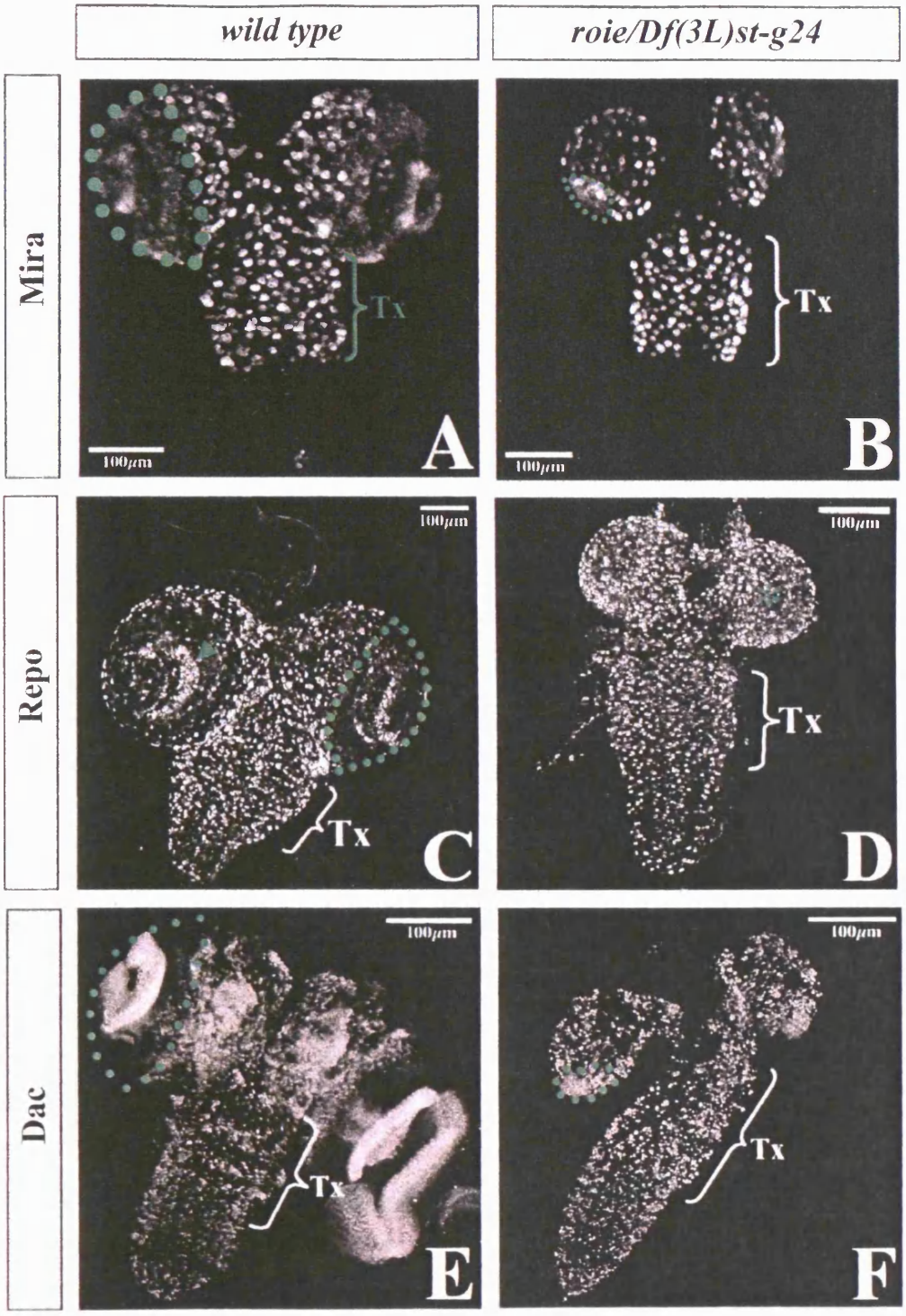
wild type
roie/Df(3L)st-g24
Mira
Repo
Dac
Tx
100μm
A
B
C
D
E
F

Although, *roie* hemizygotes have a relatively normal thoracic CNS size and Mira pattern, in order to rule out a subtle cell-autonomous requirement in thoracic NB divisions, clonal analysis was performed using MARCM (see Section 2.4.2). When clones were induced at 24hr ALH and clone size was analysed at 96hr ALH, the distribution of *roie* thoracic clone sizes was similar to *wild-type* (Fig. 5.3A), although the maximum *roie* clone size was only 73, compared to 89 in *wild type.* The average clone size for *roie* (m=45) is somewhat less than that for *wild-type* clones (m=57), although standard deviations are large and this is only statistically significant with 90% confidence (Fig. 5.3B). The large standard deviations are consistent with previous studies which have demonstrated large lineage-to-lineage differences in thoracic clone size (Fig. 1g & Fig. 3b; (Bello et al. 2003). In addition, consistent with the *roie* hemizygous analysis, no difference was observed in the number of clones containing a large Mira-positive NB at 96hr ALH (Fig. 5.3C,D and data not shown). In addition, the observation of ß-gal-positive neurons within the NB clone, demonstrates that these cells are capable of expressing Elav, a marker of neuronal differentiation.

Together, the hemizygous and MARCM analyses indicates no strong requirement for *roie* in thoracic pNB division, although I cannot rule out a minor effect on thoracic NB clone size. Furthermore, thoracic neurons and glia do not appear to require *roie* for their differentiation.

5.2.3 Optic lobe neural progenitors are severely depleted in *roie* hemizygotes

Next OL development was assessed in *roie* hemizygotes at 96hr ALH. Small Mira-positive NBs, characteristic of the wild-type OL, appear absent in *roie* hemizygotes such that a discernable IPC and OPC are missing (Fig. 5.2A,B & Fig. 5.4A). As with *jami*, large Mira-positive NBs, typical of the wild-type central brain, appear to occupy the lateral regions of *roie* brain hemispheres. In addition, some giant NBs are observed in this OL-like region, which are ~20µm in diameter, approximately twice the normal size (Fig. 5.4B).

I next addressed whether the Mira-positive NBs in the prospective OL region of *roie* hemizygotes are capable of generating their wild-type complement of neurons. Immunostaining for Dac demonstrates that, in the lateral OL, there is a clear and severe reduction in the number of Dac-positive lamina and lobula neurons (Fig. 5.2E,F & Fig. 5.4C,D). Furthermore, the data suggest that the medial Dac-negative region of the OL is also reduced or absent.

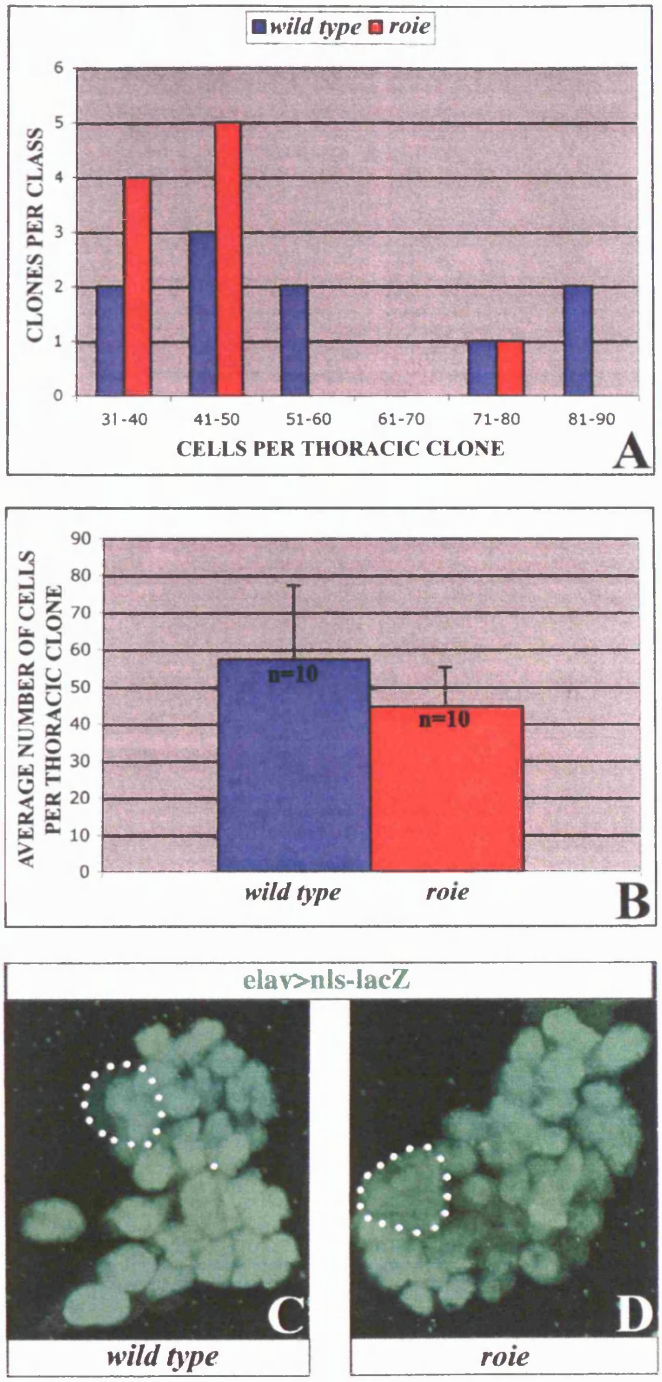

FIGURE 5.3. *ROIE* CLONE SIZE APPEARS NORMAL IN THORACIC CNS. MARCM clones were induced at 24hr ALH and analysed at 96hr ALH. (**A**) Graph showing that the size distribution of thoracic clones in *wild-type* (blue) and *roie* mutant (red) are similar. (**B**) Graph showing statistically significant difference in average thoracic clone sizes between *wild-type* (blue, m=57, 1 S.D.=20) and *roie* mutant (red, m=45, S.D.=11) (p=0.0954). n= number of clones analysed and error bars represent 1 S.D. (**C-D**) Nuclear βgal labelling of (**C**) *wild-type* and (**D**) *roie* NB clones. Dotted outlines indicate NBs.

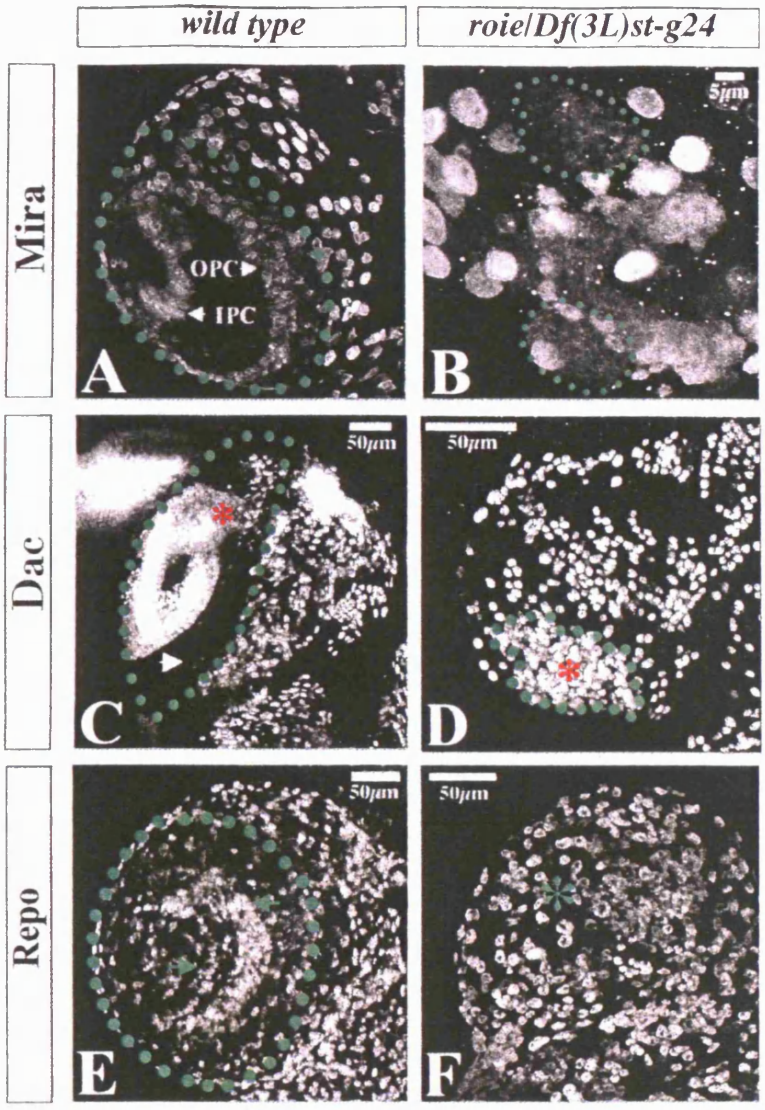

FIGURE 5.4. OPTIC-LOBE NEUROBLASTS, NEURONS AND GLIA ARE DEPLETED IN *ROIE* HEMIZYGOTES.
Confocal projections of L3 larval brain lobes (anterior up) at 96hr ALH, stained for (**A-B**) anti-Mira to label neuroblasts (NB), (**C-D**) anti-Dac to label differentiated neurons and (**E-F**) anti-Repo to label most glial cells. (**A-B**) Mira expression pattern in (**A**) *wild-type*, illustrating optic lobe (OL, dotted outline), containing Inner and Outer Proliferation Centres (IPC & OPC). (**B**) The residual OL-like region in *roie* hemizygotes shows a mix of abnormally large (dotted outline) and normal-sized Mira-positive NBs, approximately equal in size to central brain NBs. (**C-D**) Dac expression pattern in (**C**) *wild-type* OL (dotted outline), consisting of a lateral Dac-positive region (asterisk) apposed medially by a Dac-negative (arrow) region and (**D**) in *roie* hemizygotes, showing OL-like region (dotted outline), containing a high density of Dac-expressing cells. Note the dramatic reduction in Dac-positive cells (asterisk) and the absence of the Dac-negative region (arrow, **C**). (**E-F**) Repo expression pattern in (**E**) *wild-type* OL (dotted outline), containing concentrically arranged glial strata, highlighting the glialproliferation centres (arrow) and (**F**) in *roie* hemizygotes, the glial population is reduced in brain hemispheres (asterisk) and clear glial proliferation centres are missing.

Finally, I addressed whether the OL glial population was affected in *roie* hemizygotes. Repo staining revealed a dramatic difference between the OL of *wild-type* and *roie* hemizygote larvae (Fig. 5.2C,D). In *roie* hemizygotes, glial cells show no obvious organisation into horseshoe-shaped strata as seen in the wild type (Fig. 5.4E,F). This is confirmed by serial confocal sections through the OL showing a reduced number of Repo-positive glial cells in *roie* brain hemispheres and the lack of any coherent organisation into strata (Fig. 5.5A,B).

In summary, the strong requirement for *roie* in OL growth is in sharp contrast to the thorax. As with *jami,* NBs, neurons and glia are all dramatically reduced in number in the *roie* hemizygous OL. However, the remaining neurons and glia express differentiation markers, suggesting that *roie* may primarily affect numbers of neural progenitors rather than neural cell differentiation.

5.2.4 *roie* is not required for neuronal differentiation in the optic lobe or eye disc

To investigate further if *roie* is required cell-autonomously for the differentiation of OL neurons, expression of Dac was assessed in MARCM clones. Clone induction at 24hr or 48hr ALH indicates that OL neurons mutant for *roie* can still express Dac at 96hr ALH (Fig. 5.6). Thus, together with the hemizygous analysis, these experiments strongly suggest that *roie* is not required for the differentiation of the lamina and lobula neurons of the OL. Rather, *roie* seems specific for the proliferation, maintenance or survival of OL progenitors.

The hemizygous *roie* phenotype includes a dramatic reduction in ED size (Fig. 5.1C,E). To investigate if *roie* is cell-autonomously required for ED precursor proliferation or photoreceptor differentiation, the *eyFLP* system was employed, which limits clones to primarily the eye-antennal disc (see Section 2.4.3). Analysis of *eyFLP* clones, using the expression of the ubiquitous photoreceptor marker 24B10 (Newsome et al. 2000);(Zipursky et al. 1984), demonstrated that all photoreceptors within a *roie* ED clone become 24B10-positive (Fig. 5.7A,C). Furthermore, an absence of 24B10 expression anterior to the morphogenetic furrow indicates no ectopic photoreceptor specification (Fig. 5.7B). Labelling with Elav and Pros which mark R8 and R7 photoreceptors respectively (Robinow and White 1988);(Kauffmann et al. 1996), indicates that photoreceptor subtype specification is unaffected (Fig. 5.7D,E & F,G, respectively). In addition, the regular organisation of Elav-expressing R8 cells through the clone indicates that the stereotyped spatial recruitment of photoreceptors is not

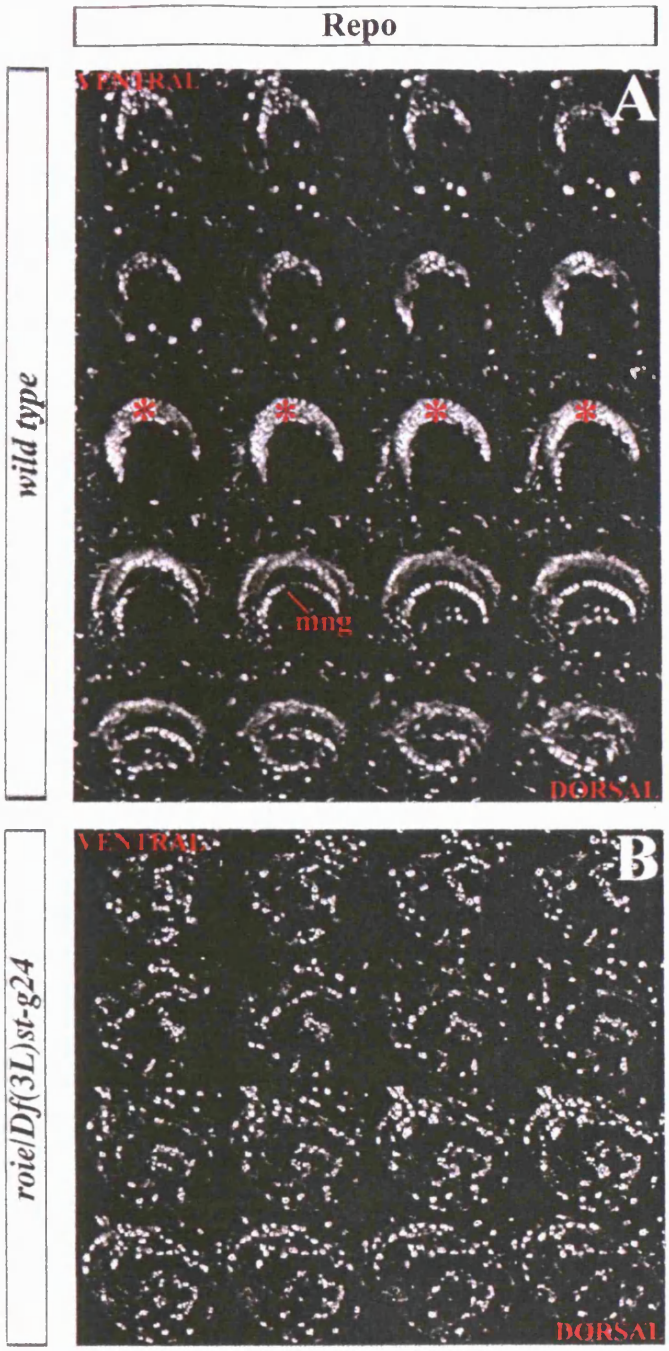

FIGURE 5.5. GLIAL ORGANISATION IS DISRUPTED IN *ROIE* HEMIZYGOUS BRAIN LOBES.
Ventral to dorsal series of 1μm confocal sections through L3 larval brain lobes, at 96hr ALH, stained for anti-Repo. (**A**) wild-type optic lobe expression pattern highlights organisation of glia into specific horse shoe-shaped strata. Two strata are labelled; medulla neuropil glia (mng) and laminar glia (asterisk, consisting of epithelial glia and marginal glia). (**B**) *roie* hemizygotes have a severe glial depletion and lack regular organisation into strata.

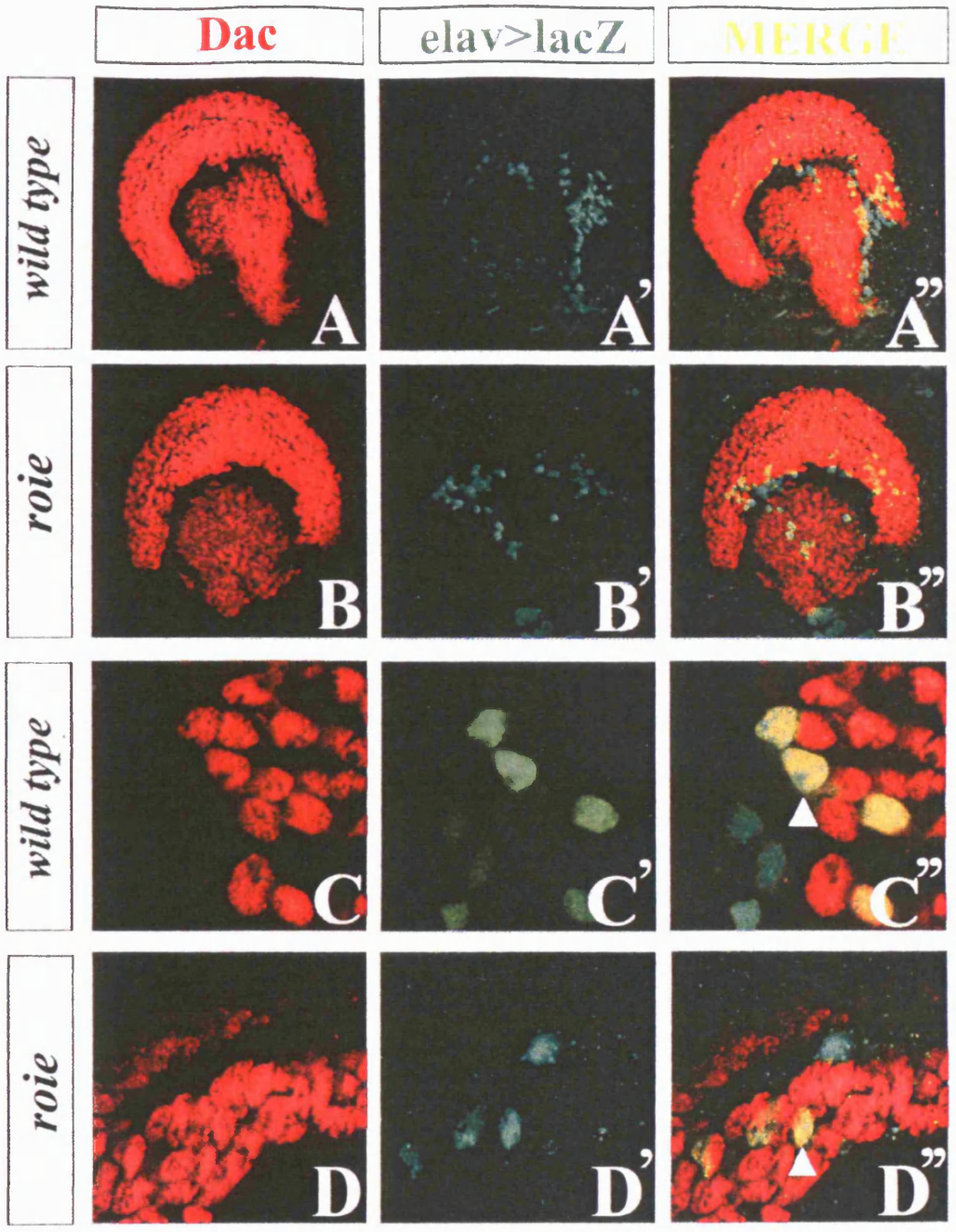

FIGURE 5.6. OPTIC- LOBE NEURONS DIFFERENTIATE IN *ROIE* CLONES. Laterally viewed optic lobes (OL) at 96 hr ALH, stained for anti-Dac (red) to delimit the OL region, and anti-ß-gal (green), to label MARCM clones. Clones were induced at 48hr ALH. **(A-B)** Confocal projections of **(A)** *wild-type* and **(B)** *roie* mutant clones. **(C-D)** Single confocal sections of OL clones where expression of Dac is observed within the clone in *wild-type* cells (arrowhead, **C"**) and in *roie* mutant cells (arrowhead, **D"**).

FIGURE 5.7. *ROIE* CLONES DIFFERENTIATE PHOTORECEPTORS.
Low power confocal projections (**A, D & F**) and high power single sections (**B, C, E & G**) of the eye disc (posterior left) at 96hr ALH. Stained for anti-GFP (green) to negatively label *eyFLP* clones. (**A-C**) Co-stained for anti-24B10 (red) to label all differentiated photoreceptos, showing (**B**) *roie* clones posterior to the morphogenetic furrow (MF) do not ectopically express 24B10 and (**C**) three *roie* cells anterior to the MF express 24B10 (dotted outline and asterisks, **C"**). Note *roie* mutant cell size appears normal (compare * and +, **C"**); (**D-E**) Anti-Elav (red) labels (**D**) all photoreceptors and (**E**) only R8 photoreceptors, in this plane of view. *roie* R8 cells express Elav (arrowheads, **E"**) and organisation into a regular array is not disrupted (dashed lines, **E"**); (**F-G**) Anti-Prospero (Pros, red) labels R7 photoreceptor cells. (**G**) *roie* R7 cells express Pros (dotted outline and asterisks, **G"**).

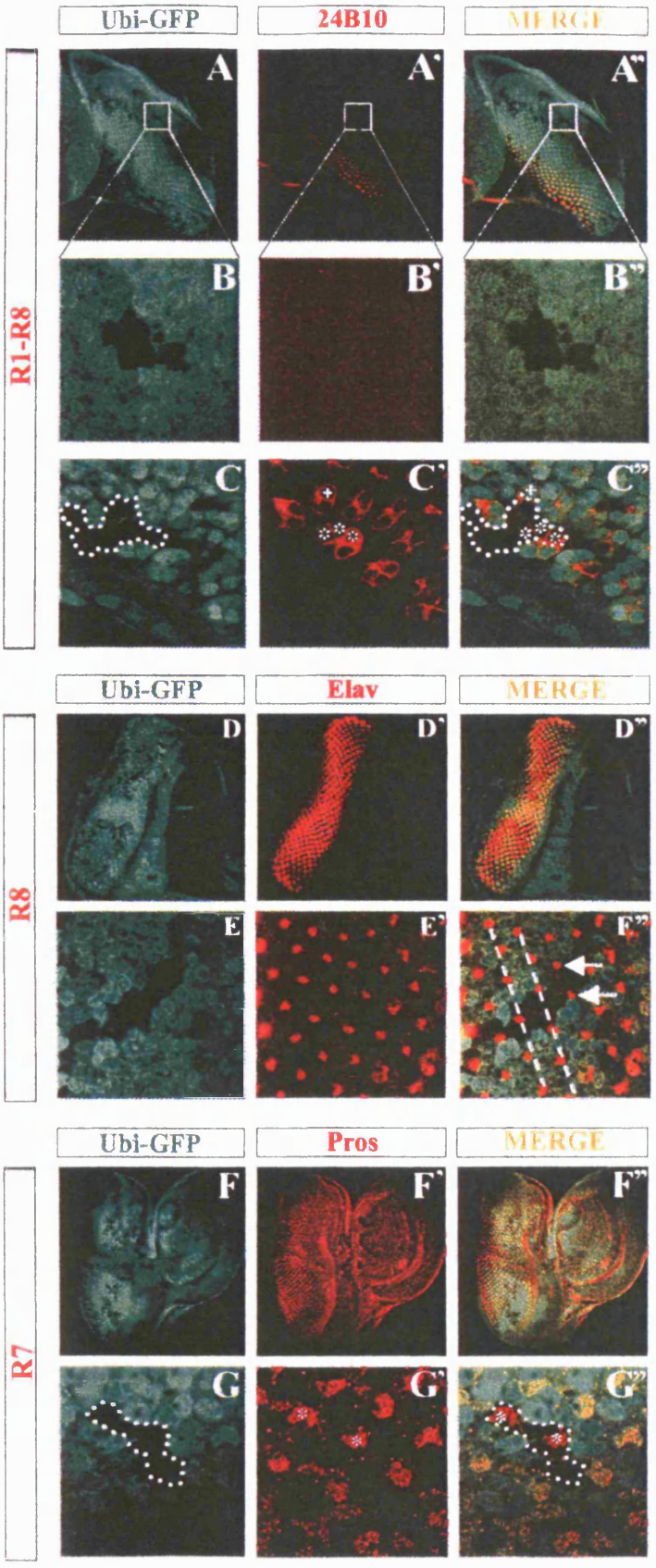
Ubi-GFP
24B10
MERGE
A
A'
A"
B
B'
B"
C
C'
C"
R1-R8
Ubi-GFP
Elav
MERGE
D
D'
D"
E
E'
E"
R8
Ubi-GFP
Pros
MERGE
F
F'
F"
G
G'
G"
R7

disrupted (Fig. 5.7E). Of note, 24B10 expression only demonstrated a maximum of three mutant cells in any one ommatidial cluster. Therefore although correct R7 and R8 cell specification occurs in the absence of *roie* activity, it remains formally possible that the three labelled cells only represent cells from the first (R8) and last (R1, R6, R7) stage of EGFR-recruitment and therefore that the middle step (i.e. the induction of R2-R5) could be aberrant in some way.

Consistent with clonal analysis, hemizygous roie mutant EDs contain Elav-positive cells (Fig. 5.8E). However, consistent with the very small ED size, a dramatically reduced number of labelled photoreceptors is observed compared to *wild type* and there is a complete lack of organisation into a regular array (Fig. 5.8A-C, E). I also examined the populations of glial cells in the ED, as previous studies have demonstrated a proportional relationship between the number of glial cells and photoreceptors in the disc (see Section 1.4.2C). Consistent with this, a dramatic reduction in the number of Repo-positive cells in *roie* hemizygote EDs is observed compared to *wild type* (Fig. 5.8D,F).

Thus, the combined results of hemizygous and clonal analyses demonstrate that *roie* is not required for OL or ED neural differentiation, but somehow it plays a growth role in both tissues.

5.2.5. A cell-autonomous requirement for *roie* in eye disc growth

To explore, in detail, the functions of *roie* in ED growth, clonal analysis was again performed. The *eyFLP* system was employed, as clone induction depends upon developmental activation of the *eyeless* gene, as opposed to a heat shock, and thus generates greater consistency in clone size between individuals than does MARCM. Comparing negatively marked *wild-type* and *roie* mutant clones indicates a dramatic reduction in ED clone size and also the apparent absence of *roie* clones in the antennal disc (AD) (Fig. 5.9A,B). The absence of *roie* AD clones does not necessarily indicate a stronger requirement for *roie* in the cells of this region, as *wild-type* AD clones tend to be much smaller than ED clones. Of note, the frequency of *roie* ED clones appears relatively normal and, as with *wild type, roie* clone size does appear to increase in more anterior regions of the ED.

To quantify the deficit in clone size accurately, in terms of numbers of cells, is difficult using *eyFLP* as, in contrast to MARCM, clones are negatively labelled. In addition, using MARCM it is possible to control the time of clone induction so that the

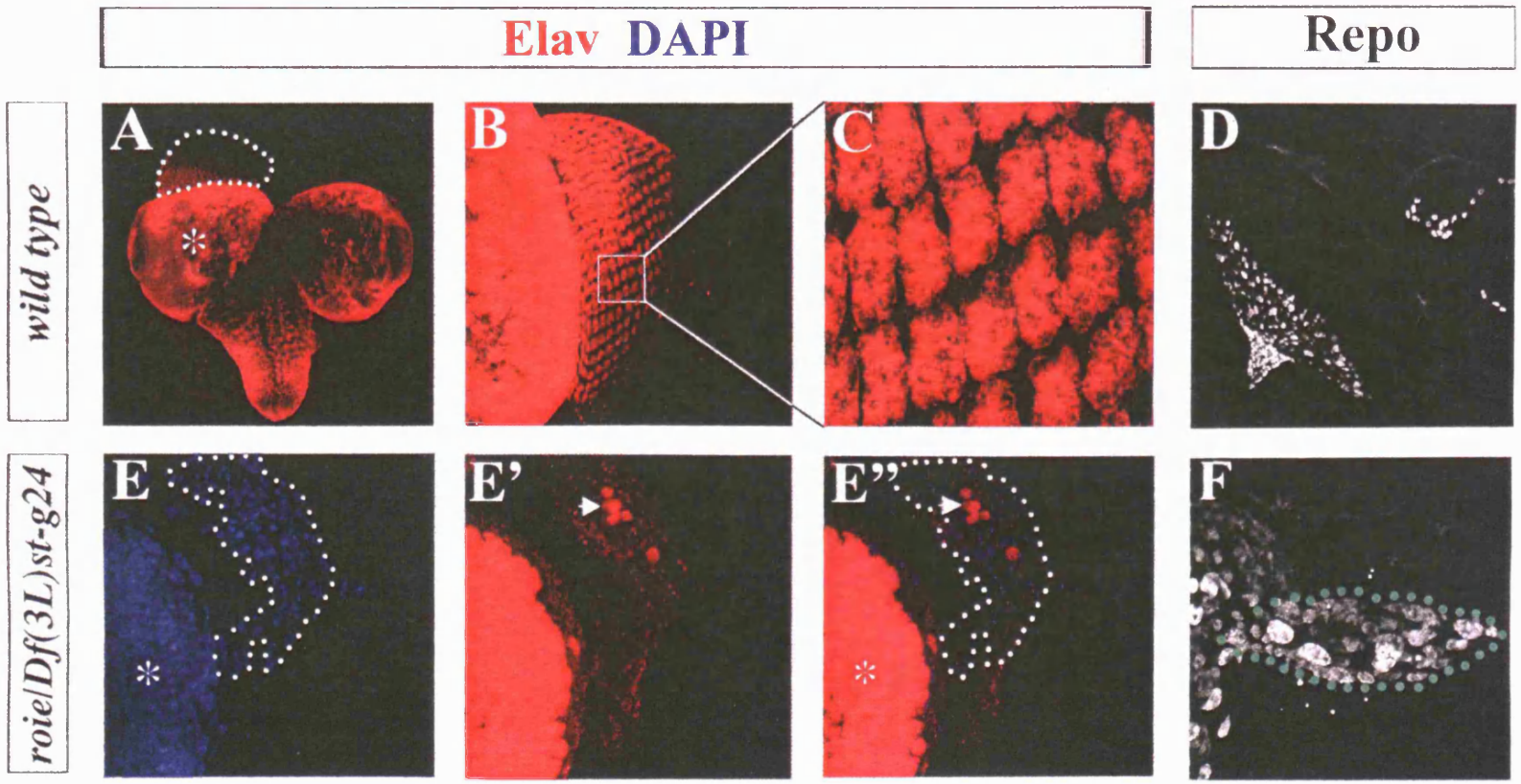

FIGURE 5.8. REDUCED NUMBERS OF PHOTORECEPTORS AND GLIA IN HEMIZYGOUS *ROIE* EYE DISCS.
Confocal projections of L3 larval CNS (**A**) and eye discs (ED, **B-F**) at 96hr ALH. Stained for (**A-C & E**) anti-Elav (red) to label all differentiated neurons and photoreceptors and (**D & F**) anti-Repo. Elav expression in *wild-type* (**A**) CNS, showing brain lobe (asterisks) and ED (dotted outline), (**B**) ED and (**C**) photoreceptors. (**D**) Repo expression in *wild-type* ED showing (**D**) glial cells populating the posterior portion of the ED. (**E-F**) *roie* hemizygous ED (dotted outline) and partial brain lobe (asterisk) stained for (**E**) anti-Elav (red) and DAPI (blue), showing a small number of differentiated photoreceptors are present (compare **B** and arrowhead **E'**) and stained for (**F**) anti-Repo, demonstrating a reduced number of glial cells (compare **D** and **F**).

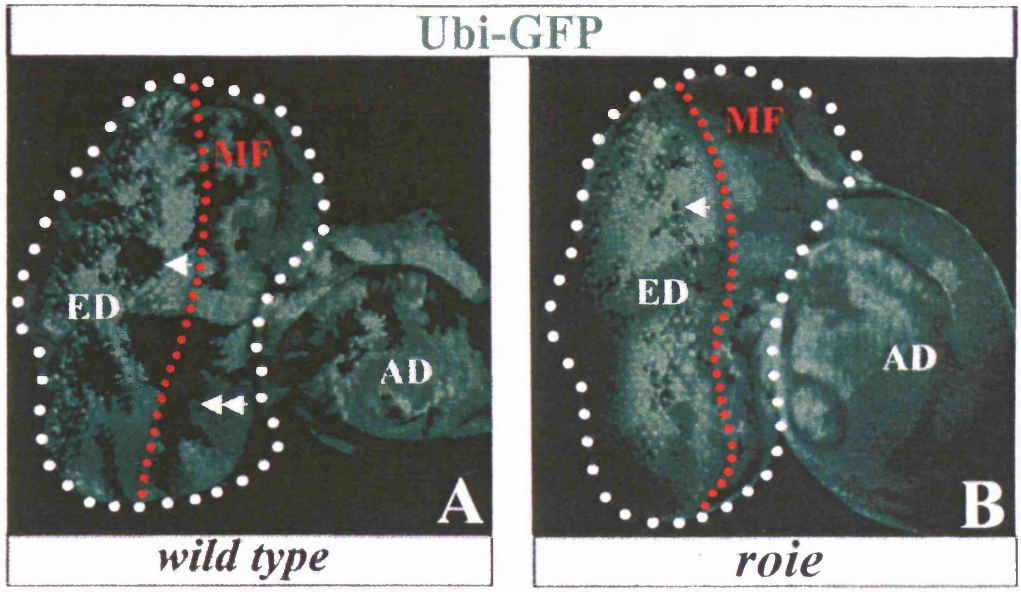

FIGURE 5.9. *ROIE eyFLP* CLONES ARE DRAMATICALLY REDUCED IN SIZE.
Single confocal sections of eye-antennal discs at 96hr ALH, illustrating the eye disc (ED, white dotted outline), antennal disc (AD) and the approximate location of the morphogenetic furrow (MF, red dotted line). Anti-GFP (green) negatively labels (**A**) *wild-type* and (**B**) undersized *roie* clones (compare arrowheads, **A** and **B**). Double arrowhead illustrates example of larger clone located in anterior eye disc.

temporal requirement for *roie* can be investigated. MARCM clones were visualised using the *elav-GAL4*^{c155} driver, limiting clonal analysis to differentiated cells posterior to the morphogenetic furrow. The size of MARCM ED clones, induced at early-L2 (24hr ALH) was dramatically reduced by the *roie* mutation. At 96hr ALH, the minimum *roie* clone size was 2 cells, (compared to 15 cells in *wild type*) and the maximum *roie* clone size was 10 cells, (compared to 35 cells in *wild type*) (Fig. 5.10A). Average clone sizes reflect this, with a mean *roie* clone size of 5 cells, compared to 29 cells in *wild-type* clones (Fig. 5.10B). This difference is statistically significant at the $p<0.001$ level.

To investigate whether the cell-autonomous requirement for *roie* in ED clone size is restricted to L2, or is also observed later, clones were induced at early-L3 (48hr ALH) and again clone size analysed at 96hr ALH. Although *roie* clone size was less dramatically affected under these conditions, there was still a statistically significant reduction in size ($p<0.01$) compared to *wild type* (Fig. 5.10C,D). Average clone size was reduced from 13 cells in wild type to 9 cells in *roie*. For *wild-type* clones analysed at 96hr ALH, not surprisingly, the average size of early-L3 induced clones (13 cells) is less than that of early-L2 induced clones (29 cells). However for *roie* clones the early-L3 induced average size (9 cells) is greater than that of early-L2 induced clones (5 cells). This strongly suggests that *roie* has a more dramatic effect on clone size in the ED during L2 than during L3.

In summary, MARCM clonal analysis is consistent with, and quantifies, the observations made with *eyFLP* clonal analysis, clearly demonstrating that *roie* is cell-autonomously required for normal ED growth, playing a role in growth (cell proliferation and/or survival), but not in neural differentiation. This contrasts with the minor or zero requirement for *roie* in thoracic NB clone size and demonstrates a clear region-specific difference in the neural growth requirement for *roie* activity. The L2 versus L3 clone induction data also indicate that the *roie* neural growth requirement is stage-specific, and is stronger in L2 than in L3 (see Section 5.3.2).

5.2.6. The interdependency of optic lobe and eye disc growth

Due to the interdependency of OL and ED development (see Section 1.4.2C), as with *jami*, the observation of reduced OL size in *roie* hemizygotes could be the result of inadequate photoreceptor innervation of this region in early-L3. Very few Elav-positive photoreceptors differentiate in the *roie* hemizygous ED (Fig. 5.8E) and consistent with

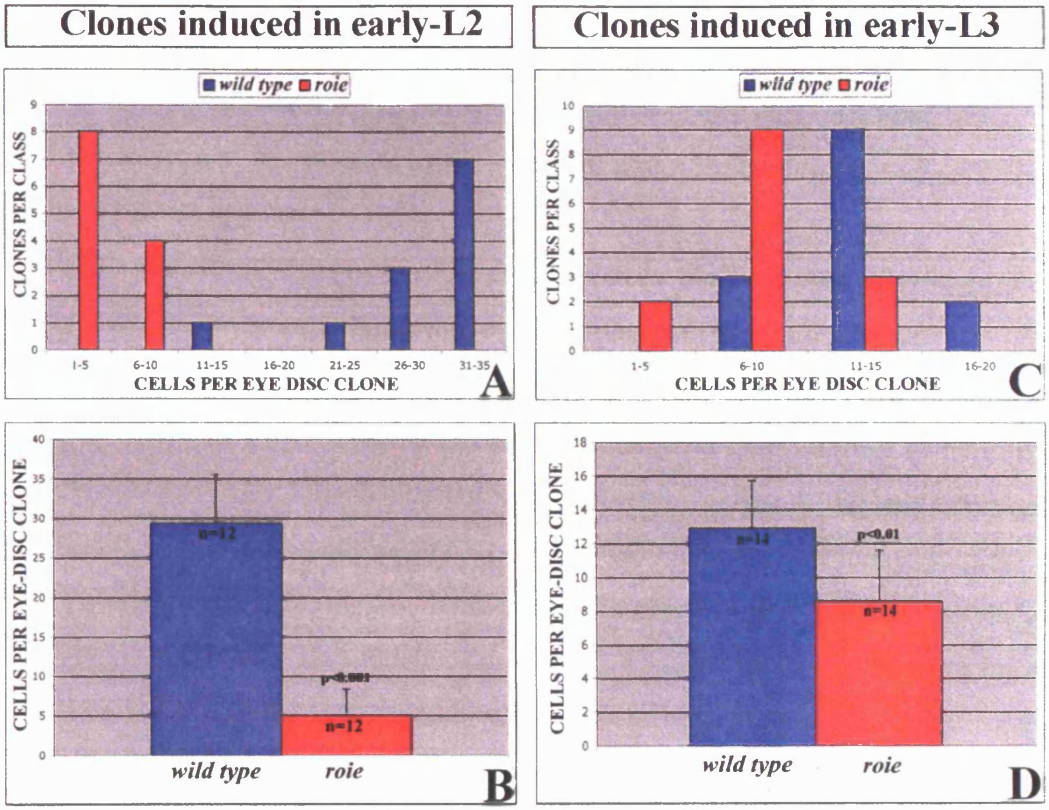

FIGURE 5.10. *ROIE* EYE-DISC CLONES ARE STRONGLY REDUCED IN SIZE.

MARCM was used to induce clones at 24hr ALH (**A & C**) and 48hr ALH (**B & D**) and eye-disc (ED) clone size was assessed at 96hr ALH. (**A-B**) Graphs showing the size distribution of *wild-type* (blue) and *roie* mutant (red) ED clones, demonstrating a strong reduction in the distribution of *roie* clone sizes with early-clone induction (**A**) than with late-clone induction (**B**). (**C-D**) Graphs showing the average clone size, demonstrating a (**C**) large and statistically significant reduction in *roie* (red, m=5, S.D.=3) compared to *wild type* (blue, m=29, S.D.=6) with early-clone induction ($p<0.001$) and (**D**) a smaller reduction in *roie* (red, m=9, S.D.=3) compared to *wild type* (blue, m= 13, S.D.=3) with late-clone induction ($p<0.01$). n= number of clones analysed and error bars represent 1 S.D.

this, there is a correspondingly dramatic reduction in 24B10-positive photoreceptor axon projections from the ED to OL (Fig. 5.11). The majority of the remaining projections are likely to result from the larval pioneer axons of Bolwig' nerve, identifiable through the characteristic termination pattern in the larval optic neuropil (Fig. 5.11C,D), rather than from ED photoreceptor axons (Fig. 5.11B). Thus, it is possible that a lack of ED photoreceptor innervation contributes to the reduced size of the OL in *roie* hemizygotes.

If the deficit in OL growth, observed in *roie* hemizygotes, is accounted for solely by reduced/missing photoreceptor innervation, then OL clones would be predicted to be of normal size. To explore the cell-autonomous requirement for *roie* in OL NBs, MARCM analysis was used in combination with Dac staining to delimit the OL (Fig. 5.12). *wild-type* OL clones, induced at early-L2 (24hr ALH) and analysed at 96hr ALH, are large and can spread across most of the Dac-negative territory of the OL (Fig. 5.12A). However, *roie* mutant clones in the OL are rare and, if present at all, very small in size (Fig. 5.12B). This indicates a strong cell-autonomous requirement for *roie* in controlling OL NB clone size. In addition, NB clone size may be somewhat reduced in the CB, but much less dramatically than in the OL.

Interestingly, when clones were induced later, at early-L3 (48hr ALH), no obvious reduction in OL or central brain clone size was apparent at 96hr ALH (Fig. 5.12C,D). Without cell-counting, a small difference cannot be ruled out, but statistical analysis of OL clone size is difficult due to very large variations.

Thus, similar to the stage-specific requirement in ED growth, *roie* has a strong cell-autonomous role during L2 in OL growth. Importantly, the overall deficit in OL growth observed in *roie* hemizygotes is likely to be accounted for by a combination of reduced photoreceptor innervation and a strong OL NB lineage-autonomous requirement.

5.2.7 *Minute* ($M(3)^{i55}$) heterozygous cells out-compete *roie* homozygous cells

To attempt to uncouple the non-autonomous (ED) and cell-autonomous requirements for *roie* in OL growth, the *eyFLP/Minute* System was used (see Section 2.4.4). In this analysis, homozygous mutant clones are generated in a background heterozygous for a *Minute* allele, which disrupts ribosome function (Garcia-Bellido and Merriam 1969; Morata and Ripoll 1975; Lambertsson 1998). This gives the homozygous mutant cells a growth advantage such that they outcompete their *Minute*

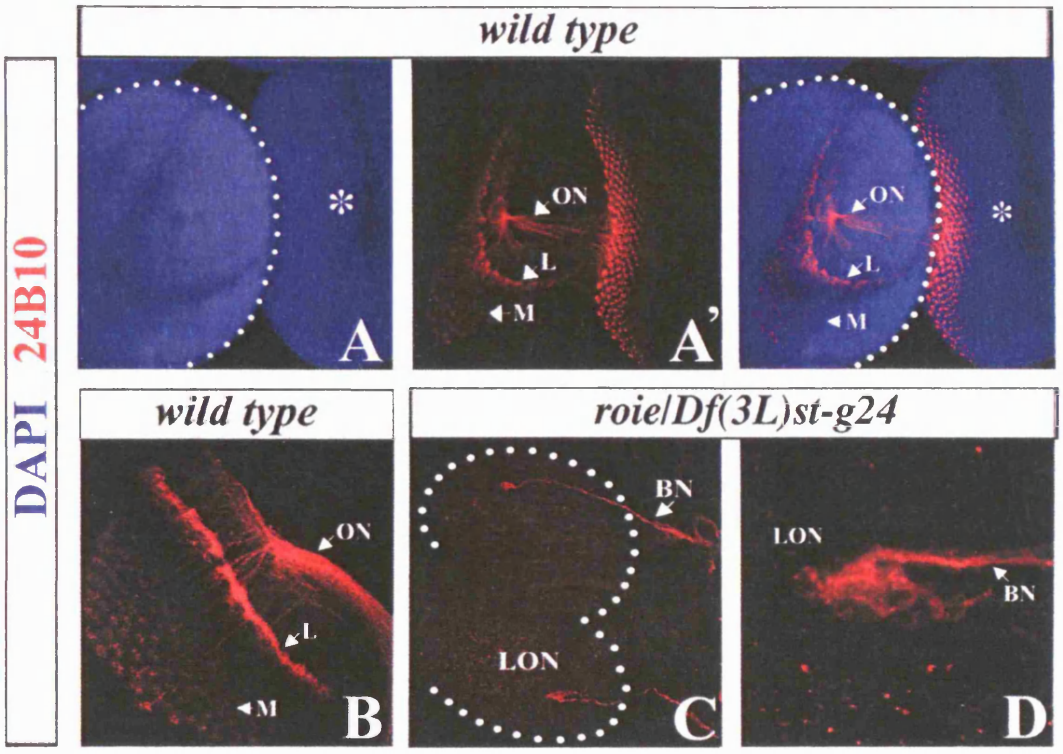

FIGURE 5.11. EYE-DISC PHOTORECEPTOR PROJECTIONS ARE MISSING IN *ROIE* HEMIZYGOTES.
Confocal projections of L3 larval CNS and eye discs (ED) at 96 hr ALH, stained with anti-24B10 (red), to label photoreceptor axons and DAPI (blue). (**A-B**) *wild-type* (**A**) brain lobe (dotted outline) and ED (asterisk), showing photoreceptors project axons from ED, through the optic nerve (ON) and into optic lobe (OL) to terminate in two discrete layers, the laminar (L) and medulla (M) and (**B**) high power view of photoreceptor axon projections into the OL, through the ON, where they de-fasciculate and terminate in the L and M. (**C-D**) *roie* hemizygote (**C**) brain lobes (dotted outline), showing projection of Bolwig's nerve (BN) into the OL region to terminate in the larval optic neuropil (LON) and (**D**) high power view of OL demonstrating the characteristic termination pattern of BN in the LON.

FIGURE 5.12. *ROIE* OPTIC-LOBE CLONES INDUCED IN EARLY-L2 ARE STRONGLY REDUCED IN SIZE.
Confocal projections of larval brain lobes (anterior up) at 96 hr ALH, stained for anti-Dac (red) to de-limit the optic lobe (OL) region (dotted outline) and anti-ß-gal (green) to label MARCM clones, illustrating OL clone size and distribution. **(A-B)** When clones are induced in early-L2 (24hr ALH), *roie* clones **(B)** are dramatically reduced in size compared to *wild-type* **(A)**. **(C-D)** When clones are induced in early-L3 (48hr ALH) *wild-type* **(C)** and *roie* clones **(D)** are more similar in size and distribution.

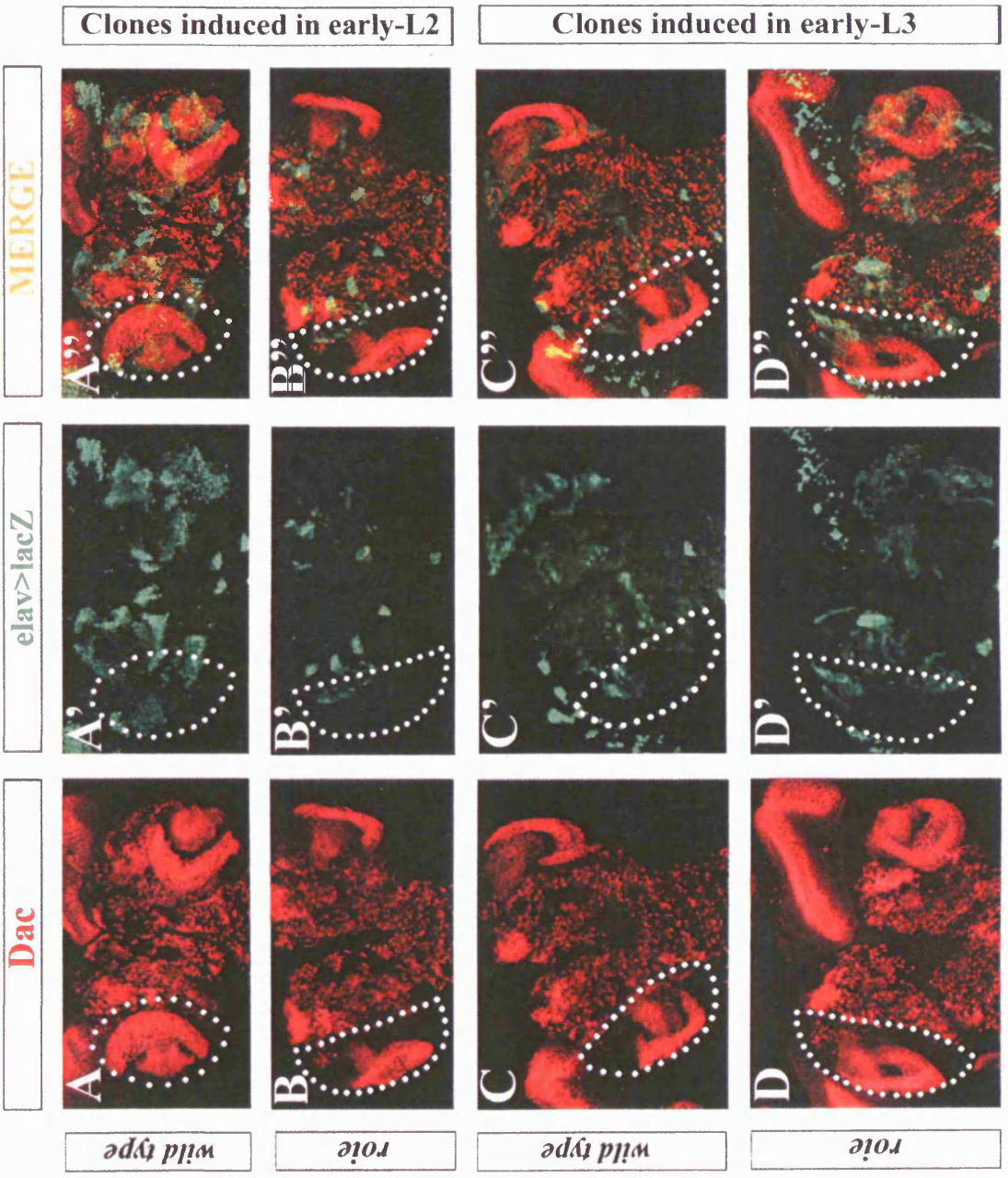
Clones induced in early-L2
Clones induced in early-L3
MERGE
elav>lacZ
Dac
A''
B''
C''
D''
A'
B'
C'
D'
A
B
C
D
wild type
roie
wild type
roie

heterozygous neighbours (Gallant 2005). In this way, it is possible to generate an almost completely homozygous mutant ED, leaving the OL effectively wild type.

As expected, when *wild-type* homozygous clones are generated with this system, the *wild-type* cells outcompete the *Minute* heterozygous cells in the ED, resulting in an almost entirely *wild-type* ED (data not shown). However, when GFP-negative *roie* mutant clones were generated with this technique, they remained very small in a background of GFP-positive *Minute* ($M(3)^{i55}$) heterozygous cells (Fig. 5.13). This surprising result prevents making a *roie* mutant ED but, importantly, it does indicate that *roie* cells are so growth-disadvantaged that they are unable to outcompete *Minute* heterozygous neighbours.

In summary, *roie* appears to be required in a region-specific, stage-specific and cell-autonomous manner for neural growth but not for neuronal or glial differentiation. In addition, the observed clonal growth deficit of *roie* mutant cells versus *Minute* heterozygous cells suggests a function for *roie* activity in mediating cell competition.

5.2B IDENTIFYING THE *ROIE* LOCUS

Having assessed the phenotypic nature of the *roie* mutation, I turned my attention towards identifying the specific gene mutated, as characterisation of the gene product allows a more detailed analysis of *roie* function and activity.

5.2.8. Identification of three additional alleles of *roie*

As mentioned in Section 3.2.4, our EMS-Screen only generated one allele of *roie*. Having a series of alleles can be useful for providing information on null and hypomorphic phenotypes. Furthermore, it increases the chance of finding relevant base-pair changes within the open-reading frame of the gene during sequencing, rather than in some remote piece of non-coding DNA.

To identify additional *roie* alleles, I searched FlyBase (see Section 2.1) and found 12 lethal complementation groups, which had been mapped to the same cytological region as *roie* (72D1-2;73A1). None of these had yet been assigned to a particular CG number. Crossing representative alleles of these 12 complementation groups with *roie* revealed that one group, *l(3)72Di*, failed to complement *roie* (Fig. 5.14A). Fortunately *l(3)72Di* is represented by three alleles (all provided by J. Kennison) bringing the total number of available *roie* alleles to four. To independently verify that *l(3)72Di* maps to the same interval as *roie*, complementation testing was also

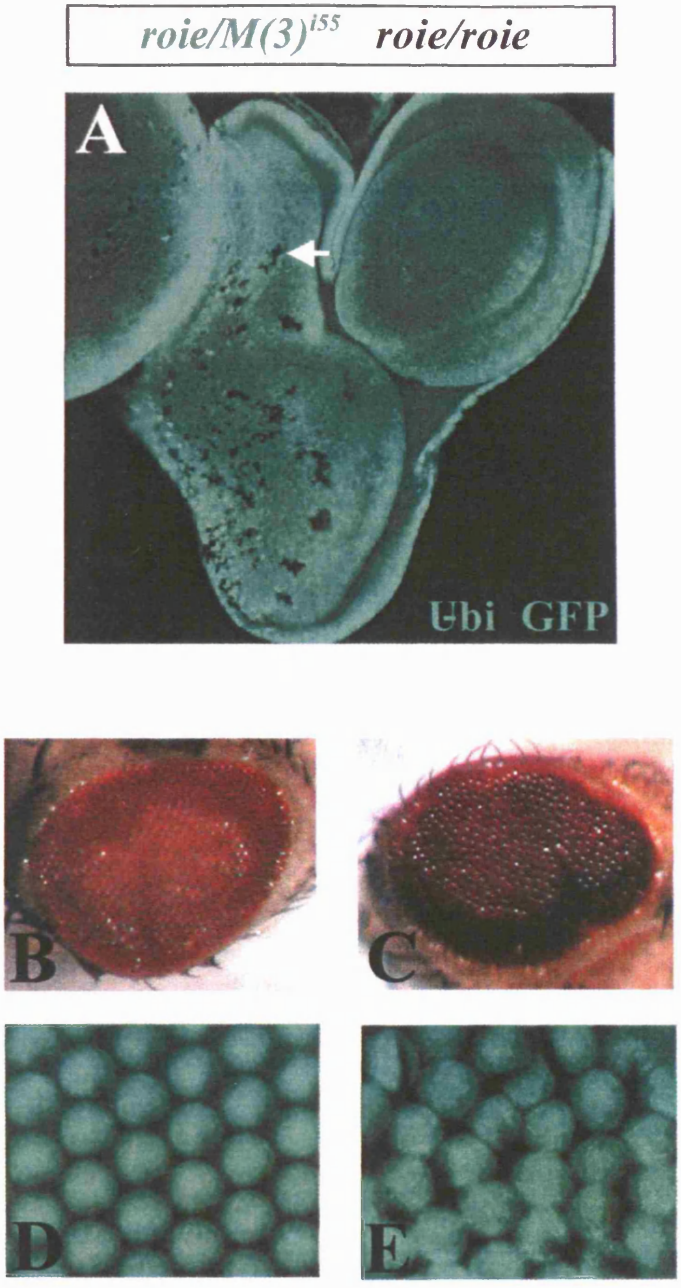

FIGURE 5.13. *ROIE* HOMOZYGOUS CELLS ARE OUT-COMPETED BY *MINUTE* HETEROZYGOUS CELLS.
(A) Single confocal section of eye disc at 96 hr ALH, stained with anti-GFP (green) to negatively label *roie eyFLP* clones. The *eyeless-FLP/Minute* technique was employed to generate *roie* mutant clones in a *Minute* ($M(3)^{i55}$) heterozygous background. In theory, homozygous mutant cells should out-compete the *Minute* heterozygous cells, which have a growth disadvantage. However, the small size of *roie* mutant clones demonstrates that $roie^{-/-}$ cells (arrow) are not able to out-compete $Minute^{+/-}$ cells. **(B-C)** Adult eyes of **(B)** wild type and **(C)** *eyeless-FLP/Minute/roie* mutants which show a rough eye phenotype. **(D-E)** GFP-expressing ommatidia of adult eyes in **(D)** wild type and **(E)** *eyeless-FLP/Minute/roie* mutants which have a disrupted ommatidial lattice.

A

Lethal Line	Cytological location	Comp testing with *roie*
l(3)72Cde^{11}	72C1;72D5	COMP
l(3)72Db^{8}	72D1;72D5	COMP
l(3)72Df^{3}	72D5-10	COMP
l(3)72Dg^{2}	72D5-10	COMP
l(3)72Dh^{1}	72D5-10	COMP
l(3)72Di^{1}	72D5-10	FAIL
l(3)72Dk^{1}	72D5-10	COMP
l(3)72Dl^{1}	72D5-10	COMP
l(3)72Dm^{1}	72D5-10	COMP
l(3)72Dq^{01318}	72C1;73A4	COMP

B

	roie	*l(3)72Di*^{1}
l(3)72Di^{1}	FAIL	N/A
l(3)72Di^{2}	FAIL	FAIL
l(3)72Di^{3}	FAIL	FAIL
Df(3L)ED4606	FAIL	FAIL
Df(3L)Exel6128	COMP	COMP
Df(3L)st-g24	FAIL	FAIL

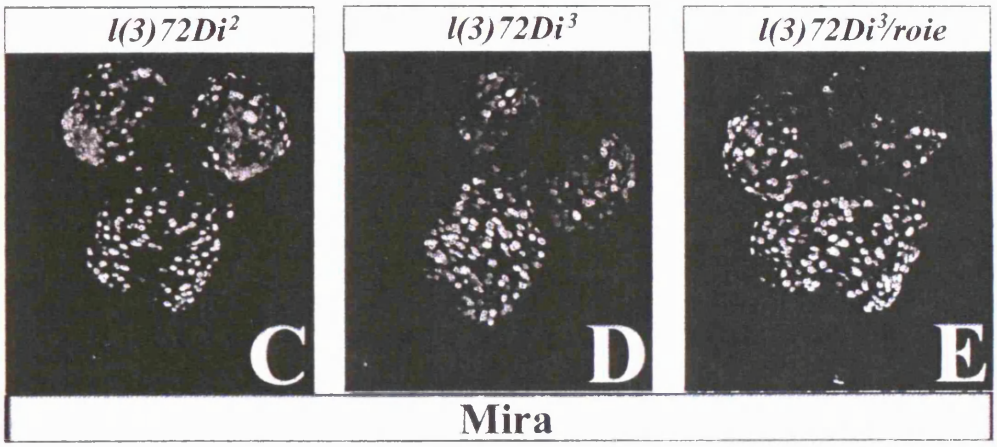

FIGURE 5.14. *ROIE* IS ALLELIC TO *l(3)72Di*.
(**A**) Table summarising the 11 cytologically mapped candidate alleles used in complementation testing with *roie*. 'Comp' = Complementation and 'Fail' = fail to complement. (**B**) Table summarising complementation tests between *roie*, three alleles of the complementation group, *l(3)72Di* and three deficiencies used to define the candidate region for *roie*. *roie* belongs to the complementation group *l(3)72Di*. (**C-E**) L3 CNS (anterior up) at 96hr ALH showing the expression pattern of Mira in (**C**) homozygous *l(3)72Di*^{2}, (**D**) homozygous *l(3)72Di*^{3} and (**E**) transheterozygous *l(3)72Di*^{3}*/roie*. All three genotypes recapitulate the Mira phenotype seen in *roie* hemizygous larvae, showing a reduced number of optic lobe neuroblasts, with no obvious effect on the thoracic neuroblast population.

done with all *l(3)72Di* alleles and two deficiencies that fail to complement *roie,* and one deficiency that complements *roie* (Fig. 5.14B).

To confirm that the lethal locus mutated in *l(3)72Di* is responsible for the *roie* CNS phenotype, DAPI staining of *l(3)72Di/roie* and *l(3)72Di* homozygotes was assessed. This revealed the same small brain hemisphere and imaginal disc phenotype as is seen in *roie* hemizygotes (data not shown). Mira staining also demonstrated that the NB pattern seen in *roie* hemizygotes, where most OL NBs appear absent, (but the central-brain and thoracic populations appear largely unaffected) is mimicked with *l(3)72Di* alleles and *roie/l(3)72Di* transheterozygotes (Fig. 5.2B, Fig. 5.14C-E & data not shown). Of note, it appears that $l(3)72Di^{3}$ is a stronger allele than *roie* and $l(3)72Di^{2}$ as it reduces the number of OL NBs more dramatically.

5.2.9 High-resolution deficiency mapping of *roie*

As discussed in Section 3.2.6, the *roie* mutation was initially cytologically mapped with deficiencies to a 366Kb interval, between the cytological locations 72D1-2;73A1 (see Table 3.2). Subsequently 12 smaller deficiencies, spanning this region, were used for complementation testing to map the locus with higher resolution (Fig. 5.15 & see Table 3.3). From the 12 deficiencies, six failed to complement *roie,* thus independently confirming the predicted candidate region (red bars, Fig. 5.15). Based on failure to complement with *Df(3L)ED220* and *Df(3L)ED4606,* and complementation with *Df(3L)Exel6128*, this high resolution deficiency mapping placed the *roie* mutation in a 42Kb region, containing 11 genes (3L: release 4.3 coordinates, 16,036,363;16,078,527 base pairs).

5.2.10. A candidate approach to identifying the *roie* locus

Using the available databases (see Section 2.1) a search was performed for each of the 11 candidate genes (Table 5.1). The first search undertaken was for available lethal alleles of the genes. Lethal alleles were available for *CG5215*, *CG5444*, *CG5165* and *CG5474*, allowing all four genes to be eliminated from the candidate list, as they complemented *roie.*

Of the remaining 7 candidates, there is little information potentially associating them with the *roie* phenotype. However, two candidate genes appeared linked, at least in some tenuous way, with *roie*. CG12272 is a conserved component of the TRF2 chromatin remodelling complex (Hochheimer et al. 2002). It has strong homology to a

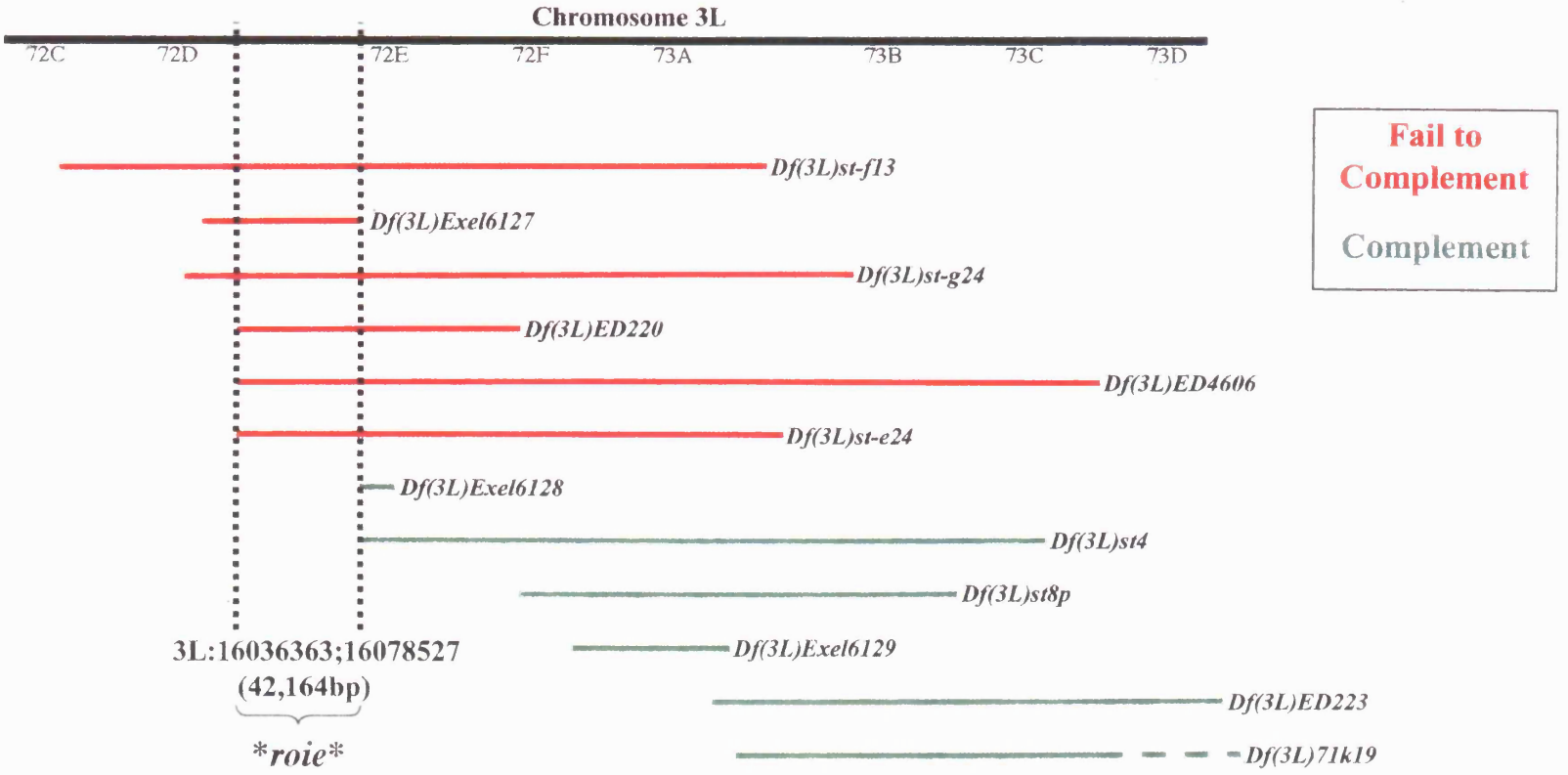

FIGURE 5.15. HIGH-RESOLUTION DEFICIENCY MAPPING OF *ROIE* TO THE 72D4;72D8 INTERVAL.
Solid black line represents the left arm of the third chromosome (cytological region approx.72C;73D, not drawn to scale). Coloured lines show deficiencies used for complementation testing with *roie:* In red are deficiencies which failed to complement *roie* and in green are deficiencies which complement *roie*. Dashed coloured lines indicate the cytological breakpoint of the deficiency lies outside this schematic map. Dashed black lines indicate the predicted cytological region in which the *roie* locus lies (3L: release 4.3 coordinates from 16,036,363 to 16,078,527 base pairs, approx. 42Kb). (For explanation of deficiency mapping, see Section 2.6.1). Results of comp testing with *Df(ED220, Df(3L)ED4604* and *Df(3L)Exel6128* define the minimal candidate region precisely, as these deficiencies have been molecularly mapped.

TABLE 5.1. *ROIE* CANDIDATE GENES.
Summary of available information regarding candidate genes for *roie,* including functional information and gene size (base pairs (bp), coding region only); availability of lethal alleles (from Bloomington, http://flystocks.bio.indiana.edu/ and GETDB, http://flymap.lab.nig.ac.jp/~dclust/getdb.html); *in situ* hybridisation data (BDGP, http://www.fruitfly.org/DGC/index.html)) and protein-protein interaction data (Yeast-2-hybrid Screen, Y2H, http://portal.curagen.com/cgi-bin/interaction/flyHome.pl, Giot *et al.*, 2003), indicating the confidence level (maximum = 1): In Grey are genes eliminated by complementation testing; in Blue are the remaining seven *roie* candidate genes. N/A indicates 'Not applicable'.

Gene	Name	Annotated Function	Size (bp)	Lethal Allele	BDGP *in situ*?	Curagen Y2H (Confidence >0.5)
CG5215	*Zn72D*	Zn72D transcription factor (*Brumby et al., 2004)	N/A	*l(3)72Dk** COMP	N/A	N/A
CG5444	*TBP-associated factor (Taf4)*	Taf4 transcription factor	N/A	$Taf4^{1}$ COMP	N/A	N/A
CG5165	*Phosphogluconate mutase (Pgm)*	Phosphoglucomutase activity	N/A	Pgm^{nGB1} COMP	N/A	N/A
CG5474	*Signal sequence receptor β (SSRβ)*	Signal sequence receptor beta	N/A	$SSR\beta^{S1939}$ COMP	N/A	N/A
CG5414	N/A	Isoleucine-tRNA ligase	2673	$CG5414^{[KP5930]}$ (GETDB)	NO	NO
CG5389	N/A	"F1" proton-transporting ATP synthase	2038	NO	NO	NO
CG5235	N/A	Dopamine monoxygenase	2704	NO	YES, Embryonic CNS	NO
CG5284	N/A	Voltage-gated chloride channel	3641	NO	NO	NO
CG5222	N/A	Non-canonical mRNA cleavage/polyadenylation (Related to human RC-74 (G_1 progression and S phase entry) (Dominski et al., 2005)	2063	NO	NO	*eyeless* (0.5417)
CG12272	*P118*	Component of TRF2 chromatin remodelling complex (Hochheimer et al., 2002) Homology with human KIAA0196 (Porkka et al., 2004, Van Duin et al., 2005)	3576	NO	NO	NO
CG13074	*N/A*	WD40 domain	1356	NO	NO	*Rpl19* (0.6882) *ctp* (0.7104) *robl* (0.5931)

family of vertebrate proteins including human KIAA0196 involved in prostate cancer (Porkka et al. 2004; Van Duin et al. 2005). The link with chromatin remodelling is interesting as several neural growth mutations recovered from our MARCM screen were found to correspond to other components of chromatin remodelling complexes (C. Maurange, L. Cheng & A. Gould, personal communication). *CG13074* contains a WD40 domain predicted to mediate protein-protein interactions and is not detected at significant levels in adults, which is consistent with a developmental role (http://flyatlas.org/). More interestingly, it is known from a Y2H interaction database (Giot et al. 2003) that CG13074 protein physically interacts, at a high-confidence level (0.6882, maximum score is 1.0), with Ribosomal protein L19 (RpL19). Mutations in *RpL19*, also called *Minute(2)60E,* exhibit a *Minute* phenotype (Schmidt 1996) and this is particularly exciting given my previous results showing that *roie* homozygous mutant cells are unable to out-compete *Minute(3)*^{i55} *(M(3)*^{i55}*)* heterozygous cells (see Section 5.2.7). This result might make sense if *M(3)*^{i55} heterozygous cells were in competition with cells homozygous for another mutation that interacts with a *Minute*-encoded protein.

Despite the tenuous links between *roie* and the genes *CG12272* and *CG13074,* the other five genes in the critical region remain, in essence, equally likely candidates. Consequently, rather than undertaking the sequencing of all seven candidates (18Kb of exons), I decided to employ *P* element-mediated recombination mapping to map *roie* to even higher resolution.

5.2.11 *P* Element-mediated recombination mapping

A detailed explanation of this technique has been given in Section 2.7.2. In brief, it uses *P* element insertions as molecular markers for meiotic recombination mapping. The recombination rate between a *P* element and the mutation is scored and, due to the colinearity of the physical and recombinational map, it is then possible to convert the recombination rate into a physical distance between the *P* element and mutation (Zhai et al. 2003).

I adapted the *P*-element mapping method for the purposes of our screen as the *w+ FRT* site on the mutant chromosome contributes to eye colour and therefore disrupts the usual recombinant scoring scheme. For example, if the *P* element is proximal to the mutation and distal to the *FRT* site, it is not possible to recover white-eyed flies from a single recombination event (events 1-3, Fig. 5.16A). The only white-eyed flies

FIGURE 5.16. *P* ELEMENT RECOMBINATION MAPPING WITH *FRT*, *w+* CHROMOSOMES.

(A-B) Potential recombinants generated if the *P* element is **(A)** proximal to and **(B)** distal to the mutation. **(A)** A recombination event distal to all three elements produces orange-eyed flies due to the presence of the *P* element (1); recombination between the mutation and *P* element produces orange eyes due to the *FRT* element (2); recombination proximal to the *P* element and mutation, but distal to the *FRT* site, produces red eyes due to the *P* and *FRT* elements (3). **(B)** A recombination event distal to all three elements produces orange eyes due to the *P* element (1); recombination between the *P* element and mutation produces white eyes (2); and recombination between the mutation and *FRT* site produces red eyes due to both *P* element and *FRT* site (3). Chromosomes carrying M* are not shown in **A** and **B** as these are not recovered in viable adults (see Section 2.6.2, Fig. 2.7). **(C)** Adapted formula used to transpose the recombination rate (i.e. percentage of white-eyed flies) into a predicted molecular position (PMP) for the mutation: P_1 & P_2 represent molecular insertion sites for *P* elements 1 and 2; MD, Molecular Distance between P_1 & P_2; RD, Recombination distance (number white-eyed flies/total number flies scored x 10,000); PMD_{P2}, Predicted Molecular Distance between P_2 and PMP.

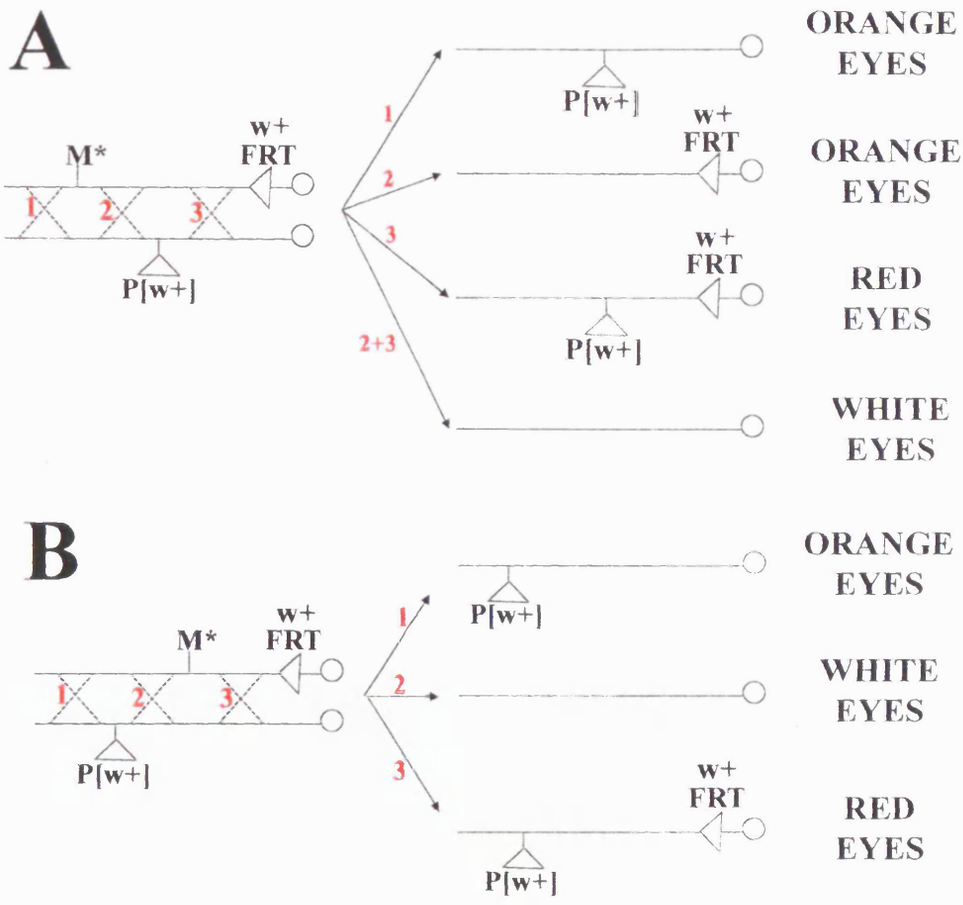
A
M*
w+
FRT
1
2
3
P[w+]
1
2
3
2+3
P[w+]
w+
FRT
w+
FRT
P[w+]
ORANGE
EYES
ORANGE
EYES
RED
EYES
WHITE
EYES
B
M*
w+
FRT
1
2
3
P[w+]
1
2
3
P[w+]
w+
FRT
P[w+]
ORANGE
EYES
WHITE
EYES
RED
EYES

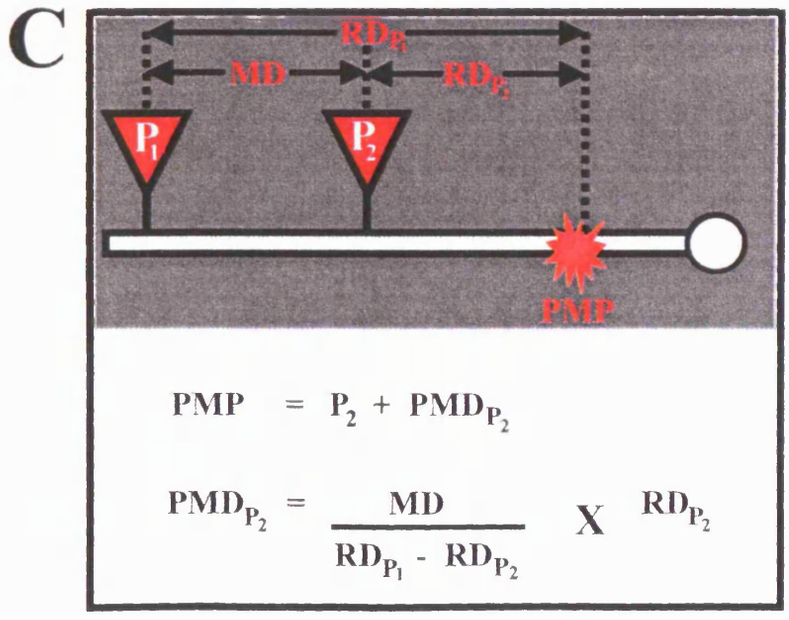
C
RD$_{P_1}$
MD
RD$_{P_2}$
P$_1$
P$_2$
PMP
PMP = P$_2$ + PMD$_{P_2}$
PMD$_{P_2}$ = MD / (RD$_{P_1}$ - RD$_{P_2}$) X RD$_{P_2}$

recovered would be extremely rare, as a result of a double recombination event (event 2+3, Fig. 5.16A). Fortunately, if the *P* element used for mapping is selected distal to the mutation and *FRT* site, recombinants can still be distinguished (Fig. 5.16B). The three possible eye colours recovered in this case are orange, white and red, where recombination between the *P* element and mutation produces white-eyed flies due to the absence of any elements (event 2, Fig. 5.16B). Therefore the percentage of white-eyed flies can be used to score single recombination events between the mutation and *P* element. A final amendment to the original strategy (Zhai et al. 2003) was to rearrange the traditional equation (see Fig. 2.7D) used to calculate the Predicted Molecular Position (PMP) of the mutation (Fig. 5.16C).

Two *P* elements were selected, which lay close but distal to the cytologically defined region to which *roie* had been mapped with deficiencies. The experiment was conducted according to the crossing scheme in Fig. 2.8 and 7,000-10,000 potential recombinant flies were scored (Fig. 5.17A). The recombination rates between *P[Pka-C3]* and *roie,* and *P[CG6017]* and *roie* were then used in the equation to generate the PMP for *roie* at 16,061,523 base pairs (3L: Release 4.3 coordinate, Fig. 5.17B). This lies within the critical region defined by deficiency mapping, providing an independent verification of the location of *roie*. Coordinate 16,061,523bp lies within *CG13074* (Fig. 5.17C), however, as the resolution of this strategy is limited by deviations from the regular colinearity of the physical and recombinational maps, the limits of the *roie* gene could include a few Kb either side of the PMP. Nevertheless, it is interesting that this recombination mapping result places the *roie* mutation within *CG13074*, a candidate gene from deficiency mapping that is linked to a *Minute* mutation.

5.2.12 *roie* genetically interacts with *RpL19*

As mentioned earlier, CG13074, a good candidate for Roie, binds to RpL19 with high confidence and mutations in *RpL19* belong to the class of *Minute* mutants. In addition, *roie* homozygous cells cannot outcompete *Minute* heterozygous cells. Therefore, to explore further the *RpL19-roie* link, I decided to look for *in vivo* genetic evidence that *roie* and *RpL19* interact.

Adult flies of *roie* heterozygotes were crossed with *RpL19* heterozygotes and all classes of progeny were examined for the short and slender bristle phenotype associated with *Minute* mutations (Fig. 5.18). Using the double balancer flies as a control (Fig. 5.18B), results indicate that *RpL19* heterozygotes have short bristles, as expected with a

FIGURE 5.17. *P* ELEMENT RECOMBINATION MAPPING OF *ROIE* TO *CG13074*.

(A) Figure shows a schematic of the central region of chromosome arm 3L (not drawn to scale), dotted lines indicate proximal and distal regions of chromosome arm, circle indicates the centromere. Brackets indicate the predicted cytological region of *roie* as indicated by deficiency mapping. Red triangles represent the two *P* elements *(P[Pka-C3]* and *P[CG6017],* see Table 2.1 for details) with the precise insertion sites indicated below. The number of flies counted is indicated above each *P* insertion (white-eyed flies/total). The red cross marks the predicted molecular position (PMP) of *roie*. **(B)** Calculations to determine the PMP of *roie*. See Fig. 5.16 for details. **(C)** Schema shows an enlargement of the bracketed section in **A** (cytology 72D4;D9), including the 11 candidate genes for *roie*, as defined by deficiency mapping. Green 'X' indicates candidate genes eliminated by complementation testing with lethal alleles. Red 'X' marks the predicted molecular position (PMP) of the *roie* mutation (3L: release 4.3 coordinate16.061,426bp). This PMP places the *roie* mutation within the gene *CG13074* (arrow).

A

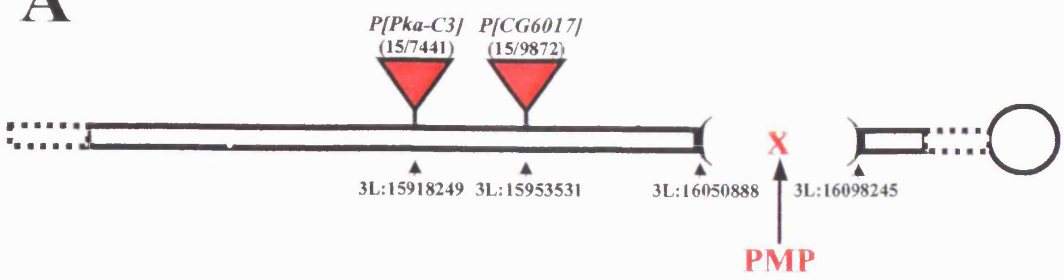

B

$$MD = P_{[CG6017]} - P_{[Pka\text{-}C3]} = 15{,}953{,}531 - 15{,}918{,}249 = 35{,}282$$

$$RD_{[Pka\text{-}C3]} = (15 / 7441) \times 10{,}000 = 20.158$$

$$RD_{[CG6017]} = (15 / 9872) \times 10{,}000 = 15.194$$

$$PMD_{[CG6017]} = \frac{35{,}282}{20.158 - 15.194} \times 15.194 = 107{,}992$$

$$PMP = P_{[CG6017]} + PMD_{[CG6017]} = 15{,}953{,}531 + 107{,}992 = 16{,}061{,}523$$

C

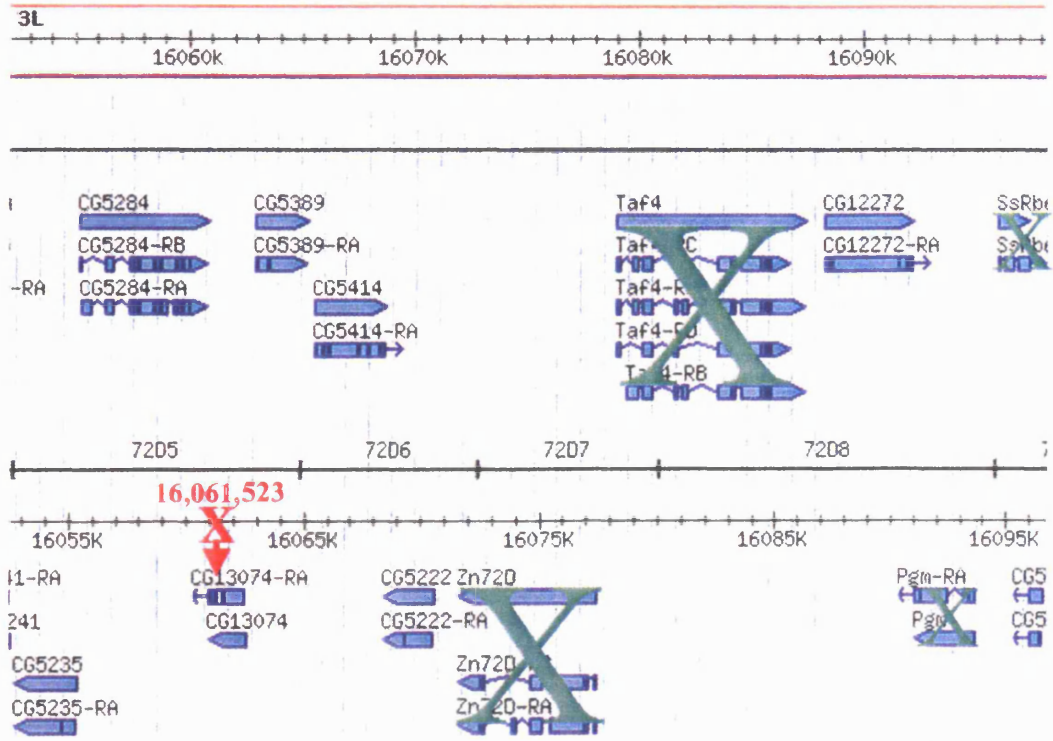

FIGURE 5.18. *ROIE/RPL19* TRANSHETEROZYGOTES DISPLAY A MINUTE BRISTLE PHENOTYPE.

To test for a genetic interaction between *roie* and *RpL19*, *RpL19* heterozygotes were crossed with *roie* heterozygotes **(A)** and progeny were examined for a bristle phenotype. **(B-E)** The four classes of progeny, showing genotype, dorsal thorax (low magnification) and posterior scutellar bristle (high magnification). All low power panels and all high power panels at same magnification. n= number of flies analysed. **(B)** *Cyo;TM6* display wild-type bristles. **(C)** *roie* heterozygotes do not display a bristle phenotype. **(D)** *RpL19* heterozygotes display short bristles and **(E)** *roie/RpL19* transheterozygotes display short and slender bristles. Bristle lengths, **B ≈ C > D ≈ E**; Bristle diameters, **B ≈ C ≈ D > E.**

A
yw / Y ; RpL19 K03/04 / CyO ; + / +
X
w / w ; + / + ; FRT2A, roie / TM6B
B
CyO / + ; TM6B / +
n=12
C
CyO / + ; roie / +
n=17
D
RpL19 / + ; TM6B / +
n=10
E
RpL19 / + ; roie / +
n=17

Minute phenotype, although they appear to lack the characteristic *Minute* slenderness (Fig. 5.18D). In contrast, *roie* heterozygotes do not display any noticeable bristle phenotype (Fig. 5.18C). Interestingly however, 100% of transheterozygotes (*roie;RpL19)* do have short and slender bristles (Fig. 5.18E). This indicates that *roie* genetically interacts with *RpL19* and is consistent with the hypothesis that *roie* is *CG13074.*

5.3 DISCUSSION

5.3.1 *roie* has a tissue- and region-specific role in neural growth but not in cell differentiation

Immunohistochemical analysis of *roie* hemizygotes at 96hr ALH indicated a region-specific growth deficit within the CNS, where neural populations in the brain hemispheres were reduced in size but appeared roughly normal in the ventral ganglion. This growth deficit was also observed in other imaginal (adult) tissues, such as the imaginal discs, however no effect was observed on the growth of the larval body. Therefore the *roie* phenotype appears to be specific for imaginal not larval tissues and, as larval cells are polyploid but imaginal cells are diploid, one may speculate that *roie* is only required in tissues that grow by increasing cell number rather than cell size. Analysis of salivary gland cell size would allow direct confirmation that polyploid cell growth does not require *roie* activity.

Analysis of the *roie* hemizygous CNS and ED, combined with clonal analysis, indicates that *roie* is not required for the differentiation of OL lamina and lobula neurons, thoracic neurons or ED photoreceptors and glia. Therefore, in combination, the data indicate that *roie* is not required for neural cell differentiation.

Analysis of 24B10 expression in *eyFLP* clones demonstrated that cell size is normal in *roie* mutant photoreceptors. In addition in MARCM clones, thoracic NB size appears normal. Interestingly however, some giant Mira-positive cells were observed in the prospective OL region (see Fig. 5.4B). It is possible that these are transformed mushroom body or central brain NBs, although their origin has not yet been investigated. Resolving this issue is difficult as few markers are available to distinguish individual postembryonic NBs, however one could examine neurite projection patterns, which have been characterised for many individual NB lineages. In addition, it would be interesting to examine apical and basal markers in these giant NBs to examine if

localisation of these components, and consequently asymmetric cell division, is disrupted.

In summary, my results indicate that *roie* is required for growth of imaginal tissue in a region- and cell-specific manner. The absence of a requirement for *roie* in neural differentiation and the tissue-specific nature of the growth phenotype suggest that *roie* does not correspond to a typical house-keeping or cell-lethal gene.

5.3.2 Zygotic *roie* activity is required cell-autonomously in rapidly dividing adult neural cells

The most striking cell-autonomous growth deficit is observed in the OL and ED, when clones are induced at early-L2 and analysed at 96hr ALH. Weaker growth phenotypes, if present at all, are observed in the central brain and thoracic CNS. The severity of the CNS phenotype appears to correlate with positioning along the AP axis and thus NB clone size. Clone size depends, at least in part, on when the NB disappears. Of note, hemizygous and MARCM analyses together suggest that *roie* is required for the presence of the NB at 96hr ALH in the OL but not in the thorax. It is therefore possible that perdurance of maternally-contributed Roie protein accounts for the regional variations in clone size within the CNS. Such that dilution of the gene product occurs at a faster rate in more rapidly dividing regions, such as the OL. However, it may equally reflect region-specific differences in levels of gene product. In any case, the data suggest that *roie* is required throughout the CNS but that rapidly growing regions, like the ED and OL, are most sensitive to loss of zygotic *roie* activity. Whether *roie* is required for proliferation and/or cell survival has not been directly addressed in this study. This could be tested through examining anti-active caspase staining and BrdU pulse labelling, combined with a complementary approach employing genetic techniques (see Section 4.3.3).

Analysis of MARCM clone sizes in the ED revealed an additional interesting finding. As mentioned previously, clone induction in both regions three days before analysis (early-L2) revealed a strong requirement for *roie* in clonal growth. However, inducing clones later, two days before analysis (early-L3), produced little or no effect. This result might be interpreted as typical of a *wild-type* gene product that perdures. However, comparing the ED data from the two induction time-points reveals that the average *roie* mutant clone size at 96hr ALH with late-induction is greater than with early-induction. Consequently, perdurance cannot solely explain the stage-specific

differences and therefore it is likely that *roie* is more strongly required in the ED during L2 than during L3. Results from OL MARCM analysis have not been quantified, however they appear consistent with this stage-specific hypothesis. In this regard, it is interesting to note that it is believed that the OL neuroepithelium, which generates NBs during L3, undergoes expansion via symmetric divisions in L2 (see Section 1.4.2B). Therefore, there may be a stronger requirement for *roie* during symmetric divisions than during the asymmetric divisions typical of many parts of the postembryonic CNS.

Although a clear cell-autonomous requirement for *roie* in OL clones has been demonstrated, it should be noted that the overall OL phenotype could also be influenced by a cell-extrinsic contribution due to innervative failure of photoreceptors. Two lines of evidence support this hypothesis; First, the significantly reduced number of Retinal Basal Glia in the *roie* hemizygous ED would clearly disrupt photoreceptor axon guidance into the OL. Second, as ED growth is severely compromised in hemizygotes, there are very few photoreceptors available to innervate the OL.

In summary, *roie* appears to be required cell-autonomously for growth in most, if not all, imaginal cell types but not in larval polyploid tissue. However, there is a spatially- and temporally-graded effect of the mutation within the CNS, which appears to correlate with the most active periods of symmetric cell division.

5.3.3 Does *roie* correspond to *CG13074*?

Six independent deficiencies confirmed that *CG13074* is one of 11 candidates for *roie* and *P* element-mediated recombination mapping directly implicated *CG13074* to be the *roie* gene. *CG13074* encodes a WD40 protein and interacts with high confidence (0.6882) at the protein-protein level with RpL19. RpL19 is a structural constituent of the cytosolic large ribosomal subunit (60S) and is conserved in vertebrates (Chan et al. 1987). Mutations in *RpL19* (also called *Minute(2)60E)* belong to the *Minute* class of mutants, which generally affect ribosomal components. *Minute* mutations are haploinsufficient (dominant), such that heterozygous adults exhibit the classic *Minute* phenotype of short slender bristles and delayed development, and heterozygous cells are defective in cell competition. The described genetic interaction between RpL19 and CG13074 is intriguingly in light of results from the *eyFLP/Minute* experiment (see Section 5.2.7). This experiment was designed to use cell competition to uncouple the ED and OL interdependency. However, it did not produce the expected result but did yield a more interesting finding. In the ED, loss of *roie* activity gave a

stronger proliferation defect than reducing *Minute* $(M(3)^{i55})$ gene dosage by half. Thus raising the possibility that *roie* is a *Minute* mutation itself, or that Roie interacts with a Minute-encoded protein. Therefore it is interesting that CG13074, a good candidate for *roie*, interacts directly with the ribosomal protein, RpL19 and that *roie* interacts genetically with RpL19.

In summary, the *eyFLP/Minute* experiment demonstrated that *roie* homozygous cells have a stronger proliferation defect than *Minute* heterozygous cells. Bristle analysis of *roie* heterozygotes suggest that *roie* is not a typical *Minute* mutant but, importantly, it genetically interacts with a well characterised *Minute* mutant, *RpL19*. The genetic and protein-protein interaction data, together with results from *P*-mediated mapping, implicate *CG13074* to be the *roie* gene. While the data do not prove the hypothesis that *roie* corresponds to *CG13074*, they do present a strong case for sequencing *CG13074*, in all four *roie* alleles, to look for the base pair changes responsible for the *roie* mutant phenotype.

CHAPTER 6

DISCUSSION

Neurogenesis requires a delicate balance between cell proliferation and differentiation to generate the appropriate final number of cells in the brain. Maintenance of this equilibrium is largely achieved by controlling the division mode of precursor cells. Symmetric divisions can serve to either expand the progenitor population or to limit it (by generating two differentiated progeny), whereas asymmetric divisions serve to maintain the size of the progenitor pool while also generating differentiated progeny. In *Drosophila*, neural precursor activity varies markedly along the AP axis via segment-specific regulation of the division mode, and the timing of the initiation and termination of divisions. However, our knowledge of the factors controlling these spatio-temporal patterns of neural proliferation is limited. Consequently, during the course of my PhD, I executed two genetic screens to identify novel genes involved in this process.

6.1 Evaluation of the screening strategies

Using two independent protocols, we cumulatively screened 4,200 mutagenised chromosomes. The two screens were designed to complement each others limitations. For example, the MARCM, but not the pupal-lethal screen, allowed us to identify pleiotropic genes required during larval stages. However, using a mosaic system does prevent identification of certain genes, such as those required non-cell autonomously or at early larval stages and those located near centromeres.

We recovered a total of 82 mutants with interesting phenotypes, which were subdivided into 69 complementation groups, 9 of which contained multiple alleles (see Table 3.1). This indicates a good degree of chromosome coverage but also shows that the screen, as expected, was well below saturation levels. The 9 primary phenotypic classes recovered from the MARCM screen include Abdominal (AB) overproliferation (OP), AB OP and thoracic- (TX) underproliferation (UP), AB OP and optic lobe- (OL) UP, OL and central-brain (CB) UP, CB and TX UP, OL UP, CB UP, TX UP and CNS-specific UP. Of note, the term proliferation was used somewhat loosely at this stage of the analysis, as we had not distinguished whether cell proliferation or cell survival is involved. The pupal-lethal screen recovered only 2 primary classes; undersized brain hemispheres and undersized CNS. Phenotypic classes recovered from both screens were sub-categorised into CNS-specific or non-CNS specific, according to the absence or presence (respectively) of a phenotype in the eye disc (ED).

The absence of any complex immunocytochemistry or quantification in both sceening protocols proved effective in providing a high throughout and efficient approach. However, comparing the results from our screen to those of our collaborators, who screened the same set of mutagenised chromosomes for Mira mislocalisation by confocal immunocytochemistry (Slack et al. 2006), reveals some surprising differences. For example, the Chia laboratory recovered 3 pupal-lethal mutants with reduced size brain hemispheres (LVC73, PL13 and PL17), which we failed to recover and, conversely, we recovered 13 pupal-lethal alleles that they did not. In addition, as we did not score for specific markers of pNB division, the growth/clone size mutants that we recovered could affect several aspects of neurogenesis, such as neural proliferation and/or survival. This is important as we know that abdominal pNB clone size for example, is not only regulated by cell division, but also by programmed cell death. The Chia laboratory screen was more specific than ours, and they recovered only 4 Mira mislocalisation mutants. This is in contrast to the 69 complementation groups affecting clone size or overall CNS growth that we identified. However, by broadening their selection criteria, the Chia laboratory did also recover a number of additional classes of mutants with cell division defects, including proliferation defects, which provided an additional 47 complementation groups. One very surprising issue is why only 2 mutants were recovered by both laboratories (PL26 and OL77). A likely explanation is that a large number of proliferation mutants recovered from the Chia screen were discarded by us as they severely affected growth or clone size in eye discs or other non-CNS tissues, indicating that the mutations affected general house-keeping genes, which we were not interested in studying.

In summary, our screening protocols allowed the recovery of a large number of neural mutations. Clearly, much future analysis with molecular markers is required to subdivide all of these into those affecting the cell cycle, asymmetric cell division and cell death/survival. For example, Mira could be used to detect the presence/absence of the NB, H3P to look at mitotic activity and anti-activated caspase to investigate cell death within the CNS.

6.2 Comparison of how *jami* and *roie* regulate neuroblast divisions

jami and *roie* were selected for comparative analysis due to their similar overall CNS undergrowth phenotypes which severely affect the optic lobe region. Interestingly, however, my phenotypic analysis indicates that these mutations reduce growth via quite

different mechanisms. Firstly, *roie*, but not *jami*, acts tissue-specifically, such that comparing the growth rates of the larval body and the CNS clearly demonstrated that *jami* is required for both polyploid larval and diploid imaginal tissue growth, whereas *roie* is specific for imaginal tissues. Previous work in the wing disc has demonstrated that the growth of this organ is regulated both at the level of cell number and cell size (Neufeld et al. 1998). For the CNS, it is unclear whether growth is regulated by one or both of these factors. While my results have identified a role for *roie* in restricting the size of some NBs in the brain, postmitotic neural cell size appears normal. For *jami*, cell growth of NBs and neurons appears normal throughout the CNS. Therefore, I suggest that the growth deficit observed in both mutants is a result of an effect on cell number rather than cell size. In addition, hemizygous and clonal analyses of the CNS from both mutants strongly suggest that neither *jami* nor *roie* play a role in cell differentiation, but that both are involved in NB proliferation or survival.

Even within the CNS, both *jami* and *roie* appear to act region-specifically and in both mutants the OL and ED display the greatest growth deficit. Within these regions, I have provided clear evidence, from MARCM analysis, that *roie* is required cell-autonomously for precursor divisions. In contrast however, *jami* clones are not significantly smaller than *wild type* in any CNS regions. This lack of a phenotype does not necessarily reflect a non-cell autonomous function of the *jami* product on NBs, as it may be that it is required within the NB, but at a stage prior to clone induction.

The size of the hemizygous thoracic CNS suggests no strong requirement during NB divisions for either *roie* or *jami* in this region, at least during larval life. However, interestingly, MARCM analysis has demonstrated that *jami* is required cell-autonomously for the persistence of the NB until 96hr ALH, which is consistent with a minor reduction in thoracic clone size if *jami* is required shortly prior to 96hr ALH. *roie* hemizygous and MARCM analyses together also support the idea that *roie* is required for the presence of the optic lobe NBs at 96hr ALH. Furthermore, throughout the CNS, hemizygous and MARCM analyses suggest that *jami* is required in the latter half of L3, although this might reflect perdurance of maternal gene product. In contrast, *roie* has a strong requirement during L2 in the OL and ED and this may reflect a critical role in symmetrically-dividing precursor cells. Thus in addition to region-specific requirements, genetic analyses of *roie* and *jami* indicate that their activities vary in a stage-specific manner.

In summary, *jami* appears to be required during late-L3 and *roie* during L2. The requirement for both genes varies throughout the CNS according to AP positioning. *jami* serves two functions: a non-cell autonomous requirement in OL, ED and larval body growth and a cell-autonomous requirement in thoracic NB persistence at late-larval stages. In contrast, the requirement for *roie* is cell-autonomous throughout the CNS and ED, however this requirement is graded according to AP positioning, such that it is stronger in more anterior CNS regions (Fig. 6.1).

The tissue-, region- and stage-specific nature of the *jami* and *roie* phenotypes strongly suggests that neither gene is a general house-keeping gene. Furthermore, the fact that very few *jami* mutants pupariate, even though they exceed the critical mass required for wild-type larvae to enter metamorphosis (Beadle et al. 1938), indicates that the *jami* growth phenotype is not solely due to a nutritional deficit but it may nevertheless be involved in a growth signalling pathway. Interestingly, the *jami (PL26)* chromosome was also recovered from the Chia laboratory screen, as having a spindle misalignment phenotype in the homozygote (Slack et al. 2006). The *PL26* chromosome has at least 2 lethal hits, but it was not clear to Slack *et al.* which of the mutations is responsible for the spindle phenotype. As I have successfully mapped the *jami* lethal hit to the interval 89B3;89B5, it will be interesting to see if the transheterozygote, *jami/Df(3R)Exel7328*, not only gives my undergrowth phenotype but also the spindle phenotype.

Thus far, I have not been able to map *jami* to a single gene, although 5 strong candidate genes have been identified by deficiency mapping and complementation testing with lethal alleles. The ~14.5Kb of total ORF from these candidates could be sequenced to try and uncover the base pair change(s) responsible for the mutant phenotype. However, this is a significant undertaking and consequently, one could argue for the use for a fine-mapping strategy, such as *P*-mediated recombination mapping, to be employed prior to sequencing, to reduce the number of candidate genes (see Section 6.1).

6.3 A speculative model for CG13074 as a ribosome-microtubule motor adaptor.

Although sequencing is required to confirm the identity of *roie*, there are three lines of evidence from *P*-mapping and complementation testing that *CG13074* is a strong candidate for this gene. First, three alleles, $l(3)72Di^{1}$, $l(3)72Di^{2}$ and $l(3)72Di^{3}$ all fail to complement *roie* and all map to 72D5-D10, a region of the third chromosome

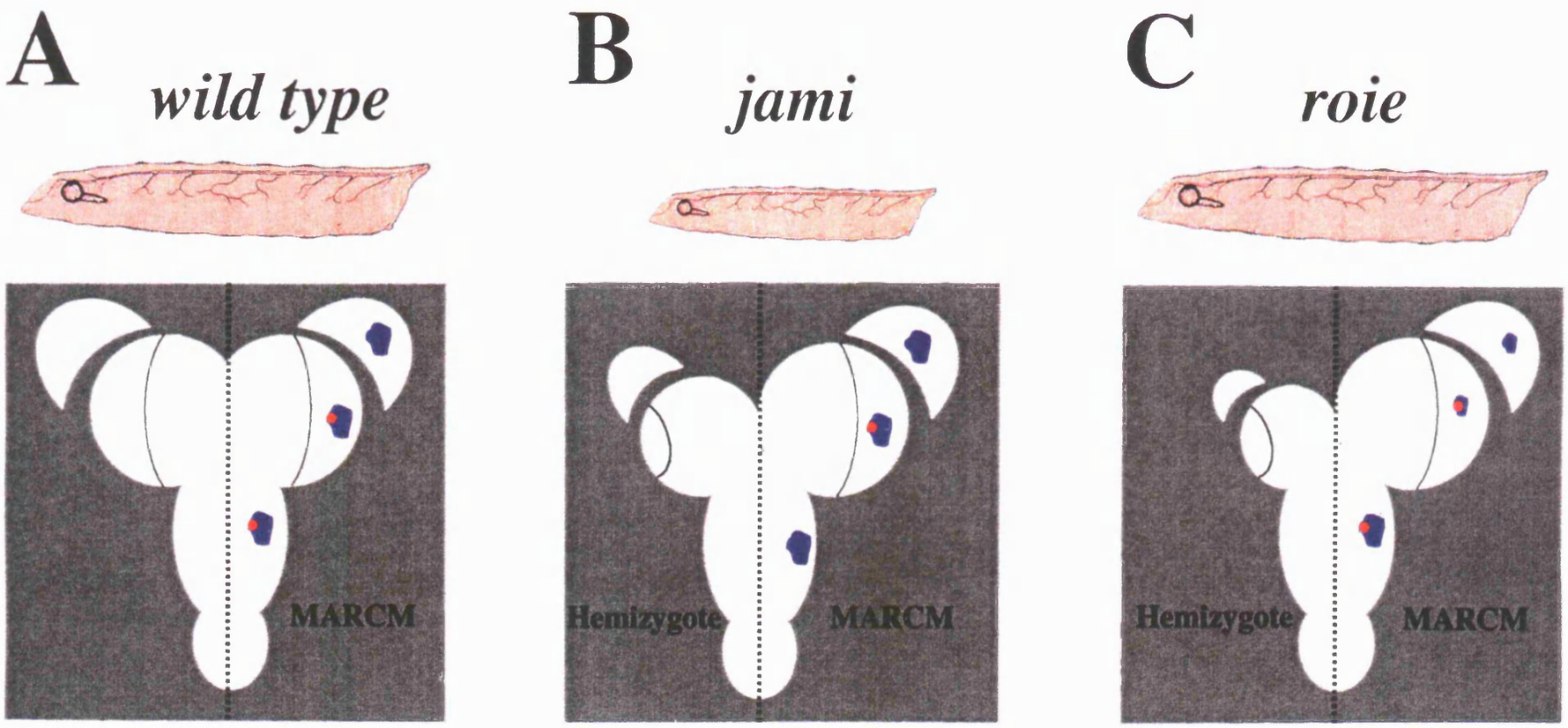

FIGURE 6.1. SUMMARY OF *JAMI* AND *ROIE* PHENOTYPES.
(**A**) *wild type*; larval size (top), CNS size (bottom left) and MARCM clone size (bottom right). (**B**) *jami*; hemizygous larval optic lobe (OL) and eye discs (ED) are all undersized. Clone size is similar to *wild type* throughout the CNS but the thoracic (TX) neuroblast (NB) is absent at 96 hr ALH. (**C**) *roie;* hemizygous larval size is normal but hemizygous OL and ED are undersized. TX clone size is similar to *wild type*, but OL and ED clones are undersized. N.B. Left half of schemas: Neuroblast (red), neurons (blue).

containing *CG13074*. Second, deficiency mapping of the *roie* mutation implicated *CG13074* to be one of seven candidate genes for *roie* and this was confirmed by 8 independent deficiencies and 4 lethal alleles. And third, *P*-mediated mapping directly indicated that the *roie* mutant locus lies within *CG13074*.

Three additional lines of evidence from the cell competition experiments and Y2H protein-protein interaction data are consistent with *CG13074* being equivalent to *roie*. First, the *eyFLP/Minute* experiment demonstrated that *roie* homozygous cells have a stronger cell competition deficit than cells heterozygous for a characterised *Minute* mutation. Second, although *roie* heterozygous adults do not show the characteristic *Minute* bristle phenotype, indicating that *roie* is not a classic *Minute* mutant itself, *roie* does genetically interact with *RpL19*, a known *Minute* gene. Third, this result is particularly interesting in light of the reported high-confidence Y2H protein-protein interaction between CG13074 and RpL19 (Fig. 6.2). My data present a particularly strong case for sequencing *CG13074* to identify the *roie* mutation, which will be greatly facilitated by the prior isogenisation of the 3L starting chromosome. Furthermore, with four alleles for *roie*, there is a good chance that DNA sequencing will locate a base pair change in a coding region.

Little is known about CG13074 other than it contains a WD40 domain of 248 amino acids (Fig. 6.3A), in which I identified one good match to the 38 amino acid WD40-repeat consensus sequence between residues 229-265, using a motif scanning database (http://myhits.isb.sib.ch/cgi-bin/motif_scan) (Fig. 6.3B). Generally WD40 domains contain between 4 and 16 WD40-repeat units, each containing a conserved core which is typically bracketed by two characteristic dipeptide sequences; GH (gly-his) towards its N-terminus and WD (trp-asp) at the C-terminus. Given that the WD40 domain in CG13074 is 248 amino acids, I would predict the presence of 6-7 repeats, although as only one of these matches strongly the consensus, they are likely to only be partial repeats. Although WD40 proteins all share a common sequence motif and probably three-dimensional structure, and most assume a regulatory role, they exhibit a high degree of functional diversity. For example, regulation of signal transduction, transcription, pre-mRNA splicing, cytoskeletal organisation, vesicular fusion and various aspects of cell cycle regulation and programmed cell death (Neer et al. 1994). Therefore it is difficult to predict the function of CG13074 based on the presence of a WD40 domain.

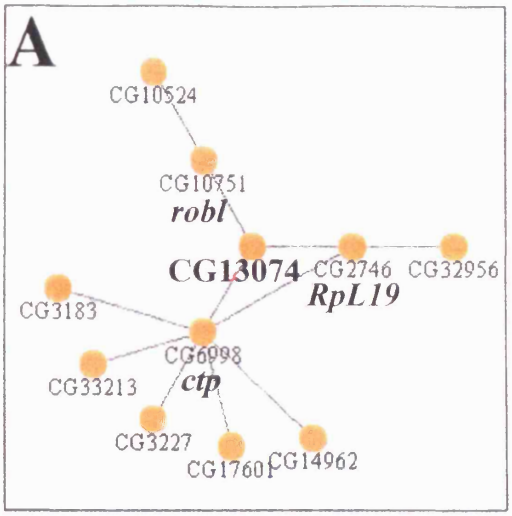

B

Gene Name	Protein	Possible functions	Curagen interaction with CG13074 (Max. = 1)
cut up (ctp)	Dynein ATPase activity	Microtubule-based movement	0.7104
Ribosomal protein L19 (RpL19)	L19 ribosomal protein	Protein biosynthesis	0.6882
Roadblock (robl)	Dynein ATPase activity	Microtubule-based movement	0.5931
PDFG- and VEGF-related factor 1 (Pvf1)	Growth factor activity	Cell projection biogenesis	0.4515
Glyceraldehyde 3 phosphate dehydrogenase 1 (Gapdh1)	Glyceraldehyde-3-phosphate dehydrogenase	Glycolysis	0.3569
Cytoplasmic dynein light chain 2 (cdlc2)	Dynein ATPase activity	Microtubule-based movement	0.2643
Ribosomal protein L41 (RpL41)	L41 ribosomal protein	Protein biosynthesis	0.1625
Ribosomal protein L15 (RpL15)	L15 ribosomal protein	Protein biosynthesis	0.1126

FIGURE 6.2. CG13074 INTERACTING PROTEINS.
(**A**) Schematic of high confidence Yeast2Hybrid interactions between *ctp, rbl, RpL19* and *CG13074*. (**B**) Table summarising all Yeast2Hybrid interactions with CG13074, with high (blue, ≥0.5) and low (grey, <0.5) confidence levels.

FIGURE 6.3. CG13074 PROTEIN SEQUENCE AND PREDICTED FUNCTION
A) Schematic of CG13074 protein structure. Showing N- and C-terminus; amino acid residue number; In red is the WD40 domain, in yellow the best match WD40-repeat and in blue, residues outside the WD40 domain. **B)** Amino acid sequence of CG13074. For colour coding, see **A. C)** Model for function of CG13074: acting as an adaptor protein between RpL19 and Robl and Ctp, for microtubule-mediated transport of RpL19. Arrows indicate possible minus-end directed movement.

A

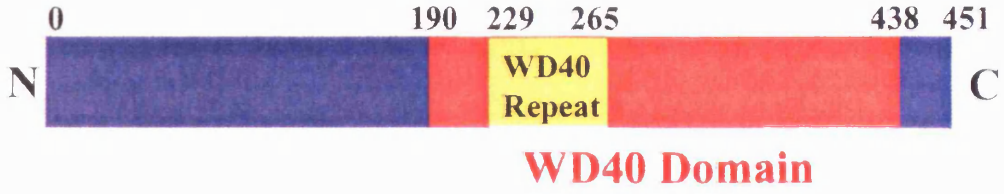

B

MDVLSHYSSPIVEFPATQPLEKQHALVDNCTGTDPPPPSQDAATGTQEKL
HVATQTEQRVVSSKDVEYDERALAKWLRQICPMVERELMNPTPLMEDLTM
SQCRLEEKLQVYTYQKLIMGGAENSQGLAIWLCVHTNNAPVLVATTVAPH
DDWCEHVDQQLKLFVPQRMSVGNLVIYTEAKTLPLKSCLRSLCTNPFNKT
MFAGSTMDGELFIWLYEQARGSDSSVDIKQLYSVSSTQGAAVALDWPREH
LLLACFANGSVRQWDLSRQMALDWEYTLPATVSSEPTAMVTLGLDDFVVG
TNDGGVYRCWNTGRQTAAIKQIKLLALRRHRFMVSTLLRTEMEGNLFVLS
CDLSGQAFYHDMRLVDEDMAQLIVQIPLPFKNVIACSRDGNIIFCPANDG
SLEYYRVSDGAHAHVKGGLRGKGSLIRSSDNGRWLIAGLYGDEFQIFYVE
H

C

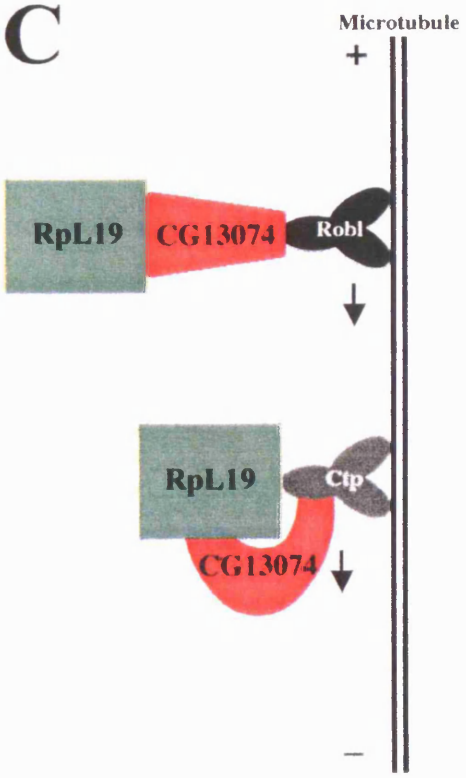

In order to investigate the evolutionary conservation of CG13074, I performed a PSI-BLAST search (http://www.ncbi.nlm.nih.gov/BLAST/) of the protein sequence, which revealed 4 insect proteins with high sequence similarity. The *Drosophila pseudobscura* protein, GA1202, has extremely high similarity to CG13074 (E value = 0.0), even though these two species diverged 36-46 million years ago. Two mosquito proteins, also showing strong sequence similarity with CG13074 are EAT43332, from *Aedes aegypti* (E value = 4e-71) and EAA06043 from *Anopheles gambiae* (E-value = 7e-59). As mosquitoes and *Drosophila* diverged ~250 million years, it is likely that there is some evolutionary pressure to maintain a CG13074-like protein, at least among Diptera.

Intriguingly, a full search for high-confidence level Y2H protein-protein interactions with CG13074 not only revealed RpL19, but also two cytoplasmic dynein light chains, Cut up (Ctp) and Roadblock (Robl), which are subunits of minus end-directed cytoplasmic dynein motors (Fig. 6.2). Interestingly, Ctp also binds directly to RpL19 (confidence level 0.5240), raising the possibility that CG13074 forms a trimeric complex with RpL19 and Ctp. Comparison of *robl* and *ctp* mutant phenotypes with the characterised *roie* phenotype reveals a number of parallels. Both *robl* and *roie* mutants are late larval/pupal lethal and show reduced size CNS and imaginal tissue, and clonal analysis has demonstrated that both genes are required cell-autonomously for normal pNB clone size. As with *roie*, *robl* mutants have a strong mitotic defect within the CNS, such that late-larval brains lack precursors capable of division (Bowman et al. 1999; Reuter et al. 2003). In addition to mitotic defects, *robl* mutants display defective axonal transport, a phenotype also observed in *ctp* mutants (Phillis et al. 1996). Therefore it would be interesting to examine if axonal transport is also disrupted in *roie* mutant larvae. *ctp* mutants also display bristle loss and a reduction in bristle length and thickness reminiscent of *Minute* mutations. This phenotype is consistent with results from the Y2H screen indicating an interaction between Ctp and RpL19 proteins (Fig. 6.2).

The Y2H interaction database identifies five further gene products that are predicted to bind CG13074, albeit at low confidence levels (<0.5, grey, Fig. 6.2B). These include Cytoplasmic dynein light chain 2 (Cdlc2) (Betran et al. 2002) and two more Ribosomal proteins L15 (RpL15) (Schulze et al. 2005) and L41 (RpL41) (Kulkarni et al. 2002). Thus CG13074 may directly bind to a total of three dynein light

chains and three components of the large ribosomal subunit. This raises the question as to whether there are any CG13074-binding sequences in common between the three dyneins and also perhaps between the three ribosomal proteins. It would also be interesting to test *in vivo*, for genetic interactions between *roie* and all of these dyneins *(ctp, robl* and *cdlc2)* and the additional ribosomal components *(RpL15* and *RpL41).*

The interaction of CG13074 with three dyneins also raises the question as to whether CG13074 is a component of the dynein complex (Holzbaur and Vallee 1994). The cytoplasmic dynein complex consists of a homodimer of heavy chains that form the stems and globular head of the complex and provide the sites of ATP hydrolysis and microtubule motor activity. These heavy chains are tightly associated with four light intermediate chains and several light chains that may directly regulate motor function. The base of the dynein complex consists of an additional subcomplex comprised of two closely related intermediate chains that, intriguingly like CG13074, contain WD40 repeats.

Largely based on the Y2H interaction data, I would like to propose a speculative model that CG13074 acts as an adaptor protein, involved in the attachment of cargo (ribosomes) to the dynein complex for intracellular transport along microtubules (Fig. 6.2C). Many studies have demonstrated that protein synthesis is targeted to specific subcellular sites by attachment of mRNA to the cytoskeleton for transport (Suprenant 1993; Lopez de Heredia and Jansen 2004). However, I only found one published study suggesting that ribosomes may themselves attach to the microtubule, via an adaptor protein (Suprenant et al. 1989). The authors purified microtubules from sea urchin eggs and demonstrated that they are associated with ribosomes via a long tapered stalk of unknown composition. In a later study, these authors postulated that the protein Echinoderm Microtubule-Associated Protein (EMAP) may form part or all of the stalk that binds these two organelles, in addition to being involved in the formation and function of the mitotic apparatus (Suprenant et al. 1993). As EMAP contains a WD40 domain, it is interesting to speculate that CG13074 may play a similar role to that proposed for EMAP. That is, CG13074 may mediate the ribosome-microtubule interaction by acting as an adaptor protein necessary to attach RpL19/RpL15/RpL41 to dynein motors (Ctp/Robl/Cdlc2) (Fig. 6.2C). Alternatively, CG13074 could serve a static function, by anchoring the ribosomal complex in the correct subcellular location after translocation (for example (Kamiya et al. 2005)). Targeted protein synthesis at specific subcellular sites could facilitate the cell division process, perhaps by locally

synthesising proteins required close to the mitotic apparatus (for example Fig. 1 (Suprenant 1993).

This thesis has reported an investigation into just 2 of the 80 mutants recovered from our screens. To advance our understanding of *roie* and *jami* it is necessary to sequence the mutant candidate genes to identify the base pair change responsible for the mutant phenotype. Further work into the phenotypes of *jami* and *roie* and the other mutants recovered from the screens is sure to enhance our understanding of neural proliferation and ultimately may help develop our understanding of how and why proliferation persists abnormally in cancer cells.

APPENDIX 1. CUSTOMISED DEFICIENCY KT

Columns indicate, from left to right, Line number; Bloomington stock number (if applicable); Deficiency name; Cytological breakpoints; Molecular breakpoints; and whether the deficiency is part of the core kit (also listed in bold text) (see Section 3.2.6). N.B. Df(3R).14, 139, 151, 177 and 221 are not listed as after designing the kit, which included these deficiencies, it was found that stocks were not available.

3L DEFICIENCY KIT

NO.	BL. STOCK NO.	DEFICIENCY	CYT. BREAKPOINTS	MOLECULAR BREAKPOINT		HIGH RES. KIT
				START	STOP	
Df(3L).1	**5838**	**Df(3L)B71**	**3LT;61B**	**n/a**	**n/a**	**Y**
Df(3L).2	**2577**	**Df(3L)emc-E12**	**61A;61D3**	**n/a**	**n/a**	**Y**
Df(3L).3	1452	Df(3L)P47	61A1-2;61A1-2	n/a	n/a	N
Df(3L).4	n/a	ED4079	61A5;61B1	20950	112410	N
Df(3L).5	7562	Df(3L)Exel6083	61A6;61B2	84918	160729	N
Df(3L).6	n/a	ED201	61B1;61C1	104554	328571	N
Df(3L).7	7563	Df(3L)Exel6084	61B2;61C1	160729	327487	N
Df(3L).8	7920	Df(3L)Exel9057	61C1;61C1	286693	300135	N
Df(3L).9	n/a	ED4177	61C1;61E1	300476	1015811	N
Df(3L).10	1478	Df(3L)Ar12-1	61C;61F	n/a	n/a	N
Df(3L).11	n/a	ED4191	61C3;62A2	524902	1459566	N
Df(3L).12	7564	Df(3L)Exel6085	61C3;61C9	528975	729839	N
Df(3L).13	n/a	ED4196	61C7;62A2	620212	1459566	N
Df(3L).14	7565	Df(3L)Exel6086	61C9;61E1	730438	940280	N
Df(3L).15	n/a	ED202	61C9;61F7	719368	1317010	N
Df(3L).16	n/a	ED4238	61C9;62A5	719368	1527560	N
Df(3L).17	**n/a**	**ED207**	**61C9;62A6**	**719368**	**1548737**	**Y**
Df(3L).18	197	Df(3L)st-b11	61E4-5;61E4-5	n/a	n/a	N
Df(3L).19	7566	Df(3L)Exel6087	62A2;62A7	1459297	1567450	N
Df(3L).20	n/a	ED4256	62A5;62A7	1526733	1567292	N
Df(3L).21	**n/a**	**ED4283**	**62A5;62B12**	**1526733**	**1944181**	**Y**
Df(3L).22	7567	Df(3L)Exel6088	62B4;62B7	1774835	1856713	N
Df(3L).23	n/a	ED4284	62B4;62B12	1776071	2532390	N
Df(3L).24	**n/a**	**ED4287**	**62B4;62E6**	**1776071**	**2532390**	**Y**
Df(3L).25	57	Df(3L)R	62B7;62B12	n/a	n/a	N
Df(3L).26	**2400**	**Df(3L)R-G7**	**62B8-9;62F2-5**	**n/a**	**n/a**	**Y**
Df(3L).27	7568	Df(3L)Exel6089	62D1;62D4	2132355	2236721	N

Df(3L).28	7569	Df(3L)Exel6090	62E2;62E4	2398068	2470786	N
Df(3L).29	**7570**	**Df(3L)Exel6091**	**62E8;62F5**	**2636710**	**2801700**	**Y**
Df(3L).30	3650	Df(3L)M21	62F;63D	n/a	n/a	N
Df(3L).31	**7571**	**Df(3L)Exel6092**	**62F5;63A3**	**2801700**	**3027783**	**Y**
Df(3L).32	**3647**	**Df(3L)HR370**	**63A1;63D1**	**n/a**	**n/a**	**Y**
Df(3L).33	11	Df(3L)HR218	63A2-7;63B9-10	n/a	n/a	N
Df(3L).34	n/a	ED4288	63A6;63B7	3051456	3129720	N
Df(3L).35	n/a	ED4293	63C1;63C1	3207030	3231193	N
Df(3L).36	7572	Df(3L)Exel6093	63C1;63D3	3231085	3398715	N
Df(3L).37	3648	Df(3L)HR232	63C1;63D2	n/a	n/a	N
Df(3L).38	**n/a**	**ED208**	**63C1;63F5**	**3229777**	**3873777**	**Y**
Df(3L).39	7573	Df(3L)Exel6094	63D2;63E1	3339746	3441195	N
Df(3L).40	7574	Df(3L)Exel6095	63E1;63E3	3441195	3525554	N
Df(3L).41	7575	Df(3L)Exel6096	63E3;63E4	3522849	3574487	N
Df(3L).42	7576	Df(3L)Exel6097	63E3;63F2	3525554	3805762	N
Df(3L).43	**7577**	**Df(3L)Exel6098**	**63F2;63F7**	**3805762**	**3906112**	**Y**
Df(3L).44	**n/a**	**ED4341**	**63F6;64B11**	**3885720**	**4520177**	**Y**
Df(3L).45	7578	Df(3L)Exel6099	63F7;64A5	3906112	4054549	N
Df(3L).46	7579	Df(3L)Exel6100	64A5;64A10	4054549	4208063	N
Df(3L).47	7921	Df(3L)Exel9000	64A10;64B1	4207870	4264889	N
Df(3L).48	7922	Df(3L)Exel8098	64A12;64B6	4239946	4386723	N
Df(3L).49	8062	ED4342	64B1;64B13	4258613	4603313	N
Df(3L).50	7924	Df(3L)Exel9001	64B2;64B6	4321820	4386723	N
Df(3L).51	7580	Df(3L)Exel6101	64B5;64B11	4364109	4519621	N
Df(3L).52	7925	Df(3L)Exel9028	64B9;64B11	4488223	4506042	N
Df(3L).53	**7926**	**Df(3L)Exel7208**	**64B9;64B15**	**4487454**	**4670052**	**Y**
Df(3L).54	7923	Df(3L)Exel9058	64B11;64B11	?	?	N
Df(3L).55	**n/a**	**ED210**	**64B11;64D1**	**4522175**	**5314650**	**Y**
Df(3L).56	7581	Df(3L)Exel6102	64B15;64C5	4670346	4954095	N
Df(3L).57	3096	Df(3L)ZN47	64C;65C	n/a	n/a	N
Df(3L).58	7582	Df(3L)Exel6103	64C5;64C10	4954344	5144105	N
Df(3L).59	**7583**	**Df(3L)Exel6104**	**64C10;64D1**	**5144105**	**5325370**	**Y**

Df(3L).60	6464	Df(3L)CH20	64D1-2;65C3	n/a	n/a	N
Df(3L).61	**7584**	**Df(3L)Exel6105**	**64D1;64D6**	**5325370**	**5567299**	**Y**
Df(3L).62	**7585**	**Df(3L)Exel6106**	**64D6;64E2**	**5567299**	**5650237**	**Y**
Df(3L).63	**6940**	**Df(3L)XAS96**	**64E;65C1-2**	**n/a**	**n/a**	**Y**
Df(3L).64	7586	Df(3L)Exel6107	64E5;64F5	5712191	5861823	N
Df(3L).65	Df(3L).66	Df(3L).67	Df(3L).68	Df(3L).69	Df(3L).70	N
Df(3L).66	4503	Df(3L)v65c	64F2-5;65D1-3	n/a	n/a	N
Df(3L).67	4551	Df(3L)W5.4	65A;65E1	n/a	n/a	N
Df(3L).68	7927	Df(3L)Exel7210	65A1;65A5	5885881	6024728	N
Df(3L).69	4393	Df(3L)XD198	65A2;65E1	n/a	n/a	N
Df(3L).70	7928	Df(3L)Exel8101	65A3;65A9	6002148	6177575	N
Df(3L).71	6461	Df(3L)CH12	65A7-11;65C1-3	n/a	n/a	N
Df(3L).72	7587	Df(3L)Exel6108	65A9;65A11	6177612	6223459	N
Df(3L).73	8063	ED211	65A9;65B4	6177664	6512288	N
Df(3L).74	**n/a**	**ED212**	**65A9;65D5**	**6178182**	**6924270**	**Y**
Df(3L).75	7588	Df(3L)Exel6109	65C3;65D3	6702563	6903076	N
Df(3L).76	**6867**	**Df(3L)BSC27**	**65D4-5;65E4-6**	**n/a**	**n/a**	**Y**
Df(3L).77	4501	Df(3L)RM5-1	65E;65E	n/a	n/a	N
Df(3L).78	**4502**	**Df(3L)RM5-2**	**65E1-12;66B1-2**	**n/a**	**n/a**	**Y**
Df(3L).79	7589	Df(3L)Exel6110	65E4;65E8	7054323	7115714	N
Df(3L).80	7590	Df(3L)Exel6111	65E7;65F4	7093965	7288267	N
Df(3L).81	6964	Df(3L)BSC33	65E10-F1;65F2-6	n/a	n/a	N
Df(3L).82	1420	Df(3L)pbl-X1	65F3;66B10	n/a	n/a	N
Df(3L).83	7929	Df(3L)Exel8104	65F7;66A4	7319524	7488461	N
Df(3L).84	7745	Df(3L)Exel6279	66A17;66B5	7828494	8055119	N
Df(3L).85	7930	Df(3L)Exel9034	66A22;66B3	7940663	8014087	N
Df(3L).86	**8065**	**ED4408**	**66A22;66C5**	**7938638**	**8258284**	**Y**
Df(3L).87	7591	Df(3L)Exel6112	66B5;66C8	8055119	8317312	N
Df(3L).88	**1541**	**Df(3L)N[spl-1]**	**66B8-9;66C9-10**	**n/a**	**n/a**	**Y**
Df(3L).89	**3024**	**Df(3L)h-i22**	**66D10-11;66E1-2**	**n/a**	**n/a**	**Y**
Df(3L).90	n/a	ED4414	66D14;66E6	8704036	8937697	N
Df(3L).91	**n/a**	**ED4421**	**66D14;67B1**	**8704036**	**9342785**	**Y**

Df(3L).92	n/a	ED4415	66D15;66E6	8724681	8937697	N
Df(3L).93	n/a	ED4416	66E1;67A8	8786189	9308334	N
Df(3L).94	7592	Df(3L)Exel6113	66E3;66F5	8871536	9086548	N
Df(3L).95	209	Df(3L)66C-165	66C7-10;66C7-10	n/a	n/a	N
Df(3L).96	7079	Df(3L)BSC35	66F1-2;67B2-3	n/a	n/a	N
Df(3L).97	1688	Df(3L)Rdl-2	66F5;66F5	n/a	n/a	N
Df(3L).98	2479	Df(3L)29A6	66F5;;67B1	n/a	n/a	N
Df(3L).99	**997**	**Df(3L)AC1**	**67A2;67D11-13**	**n/a**	**n/a**	**Y**
Df(3L).100	7593	Df(3L)Exel6114	67B10;67C5	9466146	9652180	N
Df(3L).101	7442	Df(3L)BSC46	67C2-4;67C8-10	n/a	n/a	N
Df(3L).102	7933	Df(3L)Exel9048	67D1;67D2	9860432	9921347	N
Df(3L).103	**n/a**	**ED4457**	**67E2;68A7**	**10321480**	**11083341**	**Y**
Df(3L).104	6471	Df(3L)BSC14	67E3-7;68A2-6	n/a	n/a	N
Df(3L).105	89	Df(3L)lxd6	67E5-7;68C2-4	n/a	n/a	N
Df(3L).106	**n/a**	**ED4470**	**68A6;68E1**	**11054521**	**11790716**	**Y**
Df(3L).107	**8070**	**ED4475**	**68C13;69B4**	**11544572**	**12366148**	**Y**
Df(3L).108	7594	Df(3L)Exel6115	68E1;68F2	11779401	12039402	N
Df(3L).109	7595	Df(3L)Exel6116	68F2;69A2	12039402	12161522	N
Df(3L).110	5913	Df(3L)F10	69A2;69D1	n/a	n/a	N
Df(3L).111	**n/a**	**ED4483**	**69A4;69D3**	**12234767**	**12650761**	**Y**
Df(3L).112	5492	Df(3L)eyg[C1]	69A4-5;69D4-6	n/a	n/a	N
Df(3L).113	4507	Df(3L)iro-2	69B1-5;69D1-6	n/a	n/a	N
Df(3L).114	n/a	ED215	69B5;69C4	12375100	12461845	N
Df(3L).115	**n/a**	**ED4486**	**69C4;69F6**	**12471966**	**12990032**	**Y**
Df(3L).116	7596	Df(3L)Exel6117	69D1;69E2	12585375	12747632	N
Df(3L).117	6456	Df(3L)BSC10	69D4-5;69F5-7	n/a	n/a	N
Df(3L).118	**6457**	**Df(3L)BSC12**	**69F6-70A1;70A1-2**	**n/a**	**n/a**	**Y**
Df(3L).119	**7728**	**Df(3L)Exel6261**	**69F6;70A3**	**12990045**	**13186051**	**Y**
Df(3L).120	**7597**	**Df(3L)Exel6118**	**70A3;70A5**	**13186051**	**13304190**	**Y**
Df(3L).121	**n/a**	**ED4502**	**70A3;70C10**	**13185312**	**13942431**	**Y**
Df(3L).122	7934	Df(3L)Exel9017	70B1;70B2	13415647	13434811	N
Df(3L).123	7598	Df(3L)Exel6119	70B2;70C2	13434569	13624373	N

Df(3L).124	n/a	ED4543	70C6;70F4	13884105	14706920	N
Df(3L).125	n/a	ED4515	70C6;70C15	13888052	13985912	N
Df(3L).126	n/a	ED4529	70C6;70D2	13888052	14025903	N
Df(3L).127	n/a	ED4536	70C11;70D3	13951641	14154204	N
Df(3L).128	n/a	ED4528	70C15;70D2	13985944	14025903	N
Df(3L).129	n/a	ED4534	70C15;70D3	13985944	14142574	N
Df(3L).130	7599	Df(3L)Exel6120	70D1;70D3	14008425	14139737	N
Df(3L).131	7600	Df(3L)Exel6121	70D3;70D4	14139737	14222043	N
Df(3L).132	7601	Df(3L)Exel6122	70D4;70D7	14222043	14358644	N
Df(3L).133	7602	Df(3L)Exel6123	70D7;70E4	14358644	14563262	N
Df(3L).134	5357	Df(3L)Brd12	70E;71A1-2	n/a	n/a	N
Df(3L).135	5356	Df(3L)Brd6	70E;71F1	n/a	n/a	N
Df(3L).136	**6549**	**Df(3L)XG3**	**70E3-4;71C2-D4**	**n/a**	**n/a**	**Y**
Df(3L).137	7603	Df(3L)Exel6124	70E4;70F4	14563262	14704217	N
Df(3L).138	n/a	ED217	70F4;71E1	14706950	15537975	N
Df(3L).139	7604	Df(3L)Exel6125	71A3;71B3	14917208	15028466	N
Df(3L).140	7605	Df(3L)Exel6126	71A3;71B3	14917172	15028466	N
Df(3L).141	**n/a**	**ED218**	**71B1;71E1**	**14962947**	**15537975**	**Y**
Df(3L).142	7729	Df(3L)Exel6262	71B3;71C1	15028321	15183338	N
Df(3L).143	**n/a**	**ED219**	**71E1;72F1**	**15481449**	**16360556**	**Y**
Df(3L).144	2993	Df(3L)st-f13	72C1-D1;73A3-4	n/a	n/a	N
Df(3L).145	7606	Df(3L)Exel6127	72D1;72D8	15995819	16078527	N
Df(3L).146	**3201**	**Df(3L)st-g24**	**72D1-2;73A9-10**	**n/a**	**n/a**	**Y**
Df(3L).147	n/a	ED220	72D4;72F1	16036363	16360556	N
Df(3L).148	n/a	ED4606	72D4;73C4	16036363	16729003	N
Df(3L).149	1317	Df(3L)st-e4	72D5-10;73A5-8	n/a	n/a	N
Df(3L).150	7607	Df(3L)Exel6128	72D8;72D10	16078527	16166201	N
Df(3L).151	3642	Df(3L)st4	72D10;73C1	n/a	n/a	N
Df(3L).152	2424	Df(3L)st-gl8	72E1-2;74F4-75A1	n/a	n/a	N
Df(3L).153	2995	Df(3L)st8P	72E4;73B4	n/a	n/a	N
Df(3L).154	7608	Df(3L)Exel6129	72F1;73A2	16360572	16432436	N
Df(3L).155	**n/a**	**ED223**	**73A1;73D5**	**16400704**	**16839757**	**Y**

Df(3L).156	2998	Df(3L)81k19	73A3;74F	n/a	n/a	N
Df(3L).157	2996	Df(3L)st7	73A3-4;74A3	n/a	n/a	N
Df(3L).158	7609	Df(3L)Exel6130	73B5;73D1	16610165	16755473	N
Df(3L).159	**n/a**	**ED4674**	**73B5;73E5**	**16610164**	**16998298**	**Y**
Df(3L).160	7935	Df(3L)Exel9002	73D1;73D1	16755454	16793729	N
Df(3L).161	7936	Df(3L)Exel9003	73D1;73D4	16755454	16820438	N
Df(3L).162	7937	Df(3L)Exel9004	73D1;73D5	16775106	16844220	N
Df(3L).163	7938	Df(3L)Exel7253	73D5;73E4	16842815	16981180	N
Df(3L).164	**n/a**	**ED4685**	**73D5;74E4**	**16839956**	**17561049**	**Y**
Df(3L).165	7610	Df(3L)Exel6131	74A1;74B2	17187056	17370461	N
Df(3L).166	7611	Df(3L)Exel6132	74B2;74D2	17370461	17481906	N
Df(3L).167	**n/a**	**ED4710**	**74D1;75B11**	**17436342**	**18088178**	**Y**
Df(3L).168	7939	Df(3L)Exel9005	74D1;75A6	17435988	17791446	N
Df(3L).169	7940	Df(3L)Exel9006	75A4;75A6	17772531	17790321	N
Df(3L).170	2608	Df(3L)W10	75A6-7;75C1-2	n/a	n/a	N
Df(3L).171	n/a	ED224	75B2;75C6	17918082	18347398	N
Df(3L).172	7612	Df(3L)Exel6133	75B4;75B11	17965576	18088200	N
Df(3L).173	**2990**	**Df(3L)Cat**	**75B8;75F1**	**n/a**	**n/a**	**Y**
Df(3L).174	2607	Df(3L)W4	75B10;75C1-2	n/a	n/a	N
Df(3L).175	1576	Df(3L)H99	75C1-2;75C1-2	n/a	n/a	N
Df(3L).176	n/a	ED225	75C1;75D4	18135024	18570216	N
Df(3L).177	**7613**	**Df(3L)Exel6134**	**75C7;75D4**	**18412069**	**18571329**	**Y**
Df(3L).178	**n/a**	**ED4782**	**75F2;76A1**	**18944773**	**19119581**	**Y**
Df(3L).179	**n/a**	**ED4786**	**75F7;76A5**	**19049830**	**19244541**	**Y**
Df(3L).180	n/a	ED4789	76A1;76A5	19119585	19244541	N
Df(3L).181	n/a	ED4799	76A1;76B3	19119585	19431051	N
Df(3L).182	n/a	ED228	76A1;76D2	19119585	19790347	N
Df(3L).183	**n/a**	**ED229**	**76A1;76E1**	**19119585**	**19921249**	**Y**
Df(3L).184	7941	Df(3L)Exel9046	76A5;76A6	19240112	19279450	N
Df(3L).185	7942	Df(3L)Exel9007	76B3;76B11	19373590	19585746	N
Df(3L).186	7943	Df(3L)Exel9008	76B3;76B11	19415120	19585746	N
Df(3L).187	7944	Df(3L)Exel9009	76B5;76B11	19459604	19585746	N

Df(3L).188	7945	Df(3L)Exel9011	76B8;76B11	19532809	19585746	N
Df(3L).189	7614	Df(3L)Exel6135	76B11;76C4	19585782	19709572	N
Df(3L).190	7946	Df(3L)Exel9061	76C3;76C3	19669619	19679501	N
Df(3L).191	7947	Df(3L)Exel9045	76D1;76D2	19764159	19782458	N
Df(3L).192	**n/a**	**ED4858**	**76D3;77C1**	**19813911**	**20320358**	**Y**
Df(3L).193	n/a	ED4861	76F1;77E6	20023363	20703531	N
Df(3L).194	2052	Df(3L)rdgC-co2	77A1;77D1	n/a	n/a	N
Df(3L).195	**7615**	**Df(3L)Exel6136**	**77B2;77C6**	**20228752**	**20411597**	**Y**
Df(3L).196	**3127**	**Df(3L)ri-79c**	**77B7-9;77F1-5**	**n/a**	**n/a**	**Y**
Df(3L).197	**5878**	**Df(3L)ri-XT1**	**77E2-4;78A2-4**	**n/a**	**n/a**	**Y**
Df(3L).198	**4429**	**Df(3L)ME107**	**77F3;78C8-9**	**n/a**	**n/a**	**Y**
Df(3L).199	3627	Df(3L)31A	78A-78E	n/a	n/a	N
Df(3L).200	3068	Df(3L)Pc-MK	78A2;78C9	n/a	n/a	N
Df(3L).201	3002	Df(3L)Pc	78C4-5;78C9-D1	n/a	n/a	N
Df(3L).202	**4430**	**Df(3L)Pc-sq**	**78C5-6;78E3-79A1**	**n/a**	**n/a**	**Y**
Df(3L).203	7949	Df(3L)Exel9065	78D5;78D5	?	?	N
Df(3L).204	7950	Df(3L)Exel9066	78D5;78D6	?	?	N
Df(3L).205	**n/a**	**ED4978**	**78D5;79A2**	**21451085**	**21797963**	**Y**
Df(3L).206	**7616**	**Df(3L)Exel6137**	**78F4;79A4**	**21760691**	**21872248**	**Y**
Df(3L).207	**4506**	**Df(3L)Ten-m-AL29**	**79C1-3;79E3-8**	**n/a**	**n/a**	**Y**
Df(3L).208	**n/a**	**ED230**	**79C2;80A4**	**22051929**	**22751649**	**Y**
Df(3L).209	7617	Df(3L)Exel6138	79D3;79E3	22185015	22325065	N
Df(3L).210	5951	Df(3L)HD1	79D3-E1;79F3-6	n/a	n/a	N
Df(3L).211	4504	Df(3L)Ten-m-AL1	79E1-4;79E3-8	n/a	n/a	N
Df(3L).212	4370	Df(3L)Delta1AK	79E5-F1;79F2-6	n/a	n/a	N
Df(3L).213	6649	Df(3L)BSC21	79E5-F1;80A2-3	n/a	n/a	N
Df(3L).214	**7618**	**Df(3L)Exel6139**	**80B1;80C2**	**22752317**	**22877429**	**Y**
Df(3L).215	**n/a**	**ED5017**	**80B1;80C3**	**22752775**	**22915579**	**Y**
Df(3L).216	n/a	ED231	80B2;80C1	22789094	22862798	N
Df(3L).217	**7002**	**Df(3L)1-16**	**80F;80F**	**n/a**	**n/a**	**Y**
Df(3L).218	**2593**	**Df(3L)3-52**	**80Fb;80Fg**	**n/a**	**n/a**	**Y**
Df(3L).219	2592	Df(3L)6-61	80Fd;80Fe	n/a	n/a	N

Df(3L).220	**2590**	**Df(3L)1-166**	**80Fg;80Fj**	**n/a**	**n/a**	**Y**
Df(3L).221	**2591**	**Df(3L)8A-80**	**8oFf;80Fg**	**n/a**	**n/a**	**Y**
Df(3L).222	**2595**	**Df(3L)10-26+Df(3R) 10-26**	**80Ffg;80Fg**	**n/a**	**n/a**	**Y**
Df(3L).223	**2588**	**Df(3L)9-56**	**80Fi;80Fj**	**n/a**	**n/a**	**Y**
Df(3L).224	**2589**	**Df(3L)2-66**	**80Fh;80Fj**	**n/a**	**n/a**	**Y**
Df(3L).225	**2587**	**Df(3L)2-30**	**80Fj;80Fj**	**n/a**	**n/a**	**Y**
Df(3L).226	**2596**	**Df(3L)6B-29+ Df(3R)6B-29**	**81Fa;81Fa**	**n/a**	**n/a**	**Y**

3R DEFICIENCY KIT

NO.	BL. STOCK NO.	DEFICIENCY	CYT. BREAKPOINTS	MOLECULAR BREAKPOINT		CORE KIT
				START	STOP	
Df(3R).1	n/a	Df(3R)ED5100	82A1;82E8	22994	912804	N
Df(3R).2	**n/a**	**Df(3R)ED5071**	**82A1;82E4**	**22994**	**778401**	**Y**
Df(3R).3	n/a	Df(3R)ED5046	82A1;82D3	22994	564852	N
Df(3R).4	n/a	Df(3R)ED5021	82A1;82B1	22994	216112	N
Df(3R).5	7619	Df(3R)Exel6140	82A3;82A5	107285	186686	N
Df(3R).6	n/a	Df(3R)ED5092	82A3;82E8	107407	912804	N
Df(3R).7	n/a	Df(3R)ED5020	82A3;82B1	107407	216112	N
Df(3R).8	n/a	Df(3R)ED5142	82B3;82F8	279017	1090602	N
Df(3R).9	7620	Df(3R)Exel6141	82B3;82C4	288150	425261	N
Df(3R).10	n/a	Df(3R)ED5095	82D1;82E8	475606	912804	N
Df(3R).11	n/a	Df(3R)ED5066	82D1;82E4	475606	778401	N
Df(3R).12	7621	Df(3R)Exel6142	82D2;82D6	540103	632530	N
Df(3R).13	**n/a**	**Df(3R)ED5138**	**82D5;82F8**	**606793**	**1090602**	**Y**
Df(3R).15	7622	Df(3R)Exel6143	82E4;82E8	776696	912501	N
Df(3R).16	**n/a**	**Df(3R)ED5147**	**82E8;83A1**	**912839**	**1193523**	**Y**
Df(3R).17	**n/a**	**Df(3R)ED5156**	**82F8;83A4**	**1090652**	**1284571**	**Y**
Df(3R).18	7951	Df(3R)Exel9029	83A2;83A3	1229848	1263156	N
Df(3R).19	**7623**	**Df(3R)Exel6144**	**83A6;83B6**	**1328465**	**1438442**	**Y**

Df(3R).20	**n/a**	**Df(3R)ED5177**	**83B4;83B6**	**1426348**	**1449814**	**Y**
Df(3R).21	**7952**	**Df(3R)Exel7283**	**83B7;83C2**	**1473758**	**1572399**	**Y**
Df(3R).22	**n/a**	**Df(3R)ED5196**	**83B9;83D2**	**1510298**	**1833863**	**Y**
Df(3R).23	7624	Df(3R)Exel6145	83C1;83C4	1542096	1638783	N
Df(3R).24	7953	Df(3R)Exel7284	83C4;83D2	1641743	1833502	N
Df(3R).25	**1984**	**Df(3R)Tpl6**	**83D1-2;84A4-5**	**n/a**	**n/a**	**Y**
Df(3R).26	1982	Df(3R)Tpl3	83D4-5;84A4-5	n/a	n/a	N
Df(3R).27	2393	Df(3R)WIN11	83E1-2;84A4-5	n/a	n/a	N
Df(3R).28	1980	Df(3R)Dfd13	83E3;84A4-5	n/a	n/a	N
Df(3R).29	1907	Df(3R)9A99	83F2-84A1;84B1-2	n/a	n/a	N
Df(3R).30	2172	Df(3R)MAP2	84A1-2;84A4-5	n/a	n/a	N
Df(3R).31	3514	Df(3R)BD5	84A1-2;84B1-2	n/a	n/a	N
Df(3R).32	2173	Df(3R)pb[36L]Antp[5R]	84A1-2;84B2	n/a	n/a	N
Df(3R).33	**1906**	**Df(3R)LIN**	**84A4-5;84B1-2**	**n/a**	**n/a**	**Y**
Df(3R).34	**2013**	**Df(3R)Antp-X1**	**84A4-5;84C2-3**	**n/a**	**n/a**	**Y**
Df(3R).35	2006	Df(3R)Scx2	84A5;84C1-2	n/a	n/a	N
Df(3R).36	**n/a**	**Df(3R)ED7665**	**84B6;84E11**	**2916250**	**3919820**	**Y**
Df(3R).37	n/a	Df(3R)ED5221	84C4;84E11	2954023	3919820	N
Df(3R).38	7625	Df(3R)Exel6146	84C8;84D9	2988384	3317334	N
Df(3R).39	n/a	Df(3R)ED5223	84D9;84E11	3317445	3919820	N
Df(3R).40	7730	Df(3R)Exel6263	84E6;84E13	3792749	3945579	N
Df(3R).41	**n/a**	**Df(3R)ED5230**	**84E6;85A5**	**3803511**	**4478871**	**Y**
Df(3R).42	n/a	Df(3R)ED5220	84E6;84E11	3803511	3919820	N
Df(3R).43	7626	Df(3R)Exel6147	84F6;84F13	4076046	4166658	N
Df(3R).44	n/a	Df(3R)ED5296	84F6;85C3	4076158	4882428	N
Df(3R).45	7627	Df(3R)Exel6148	84F12;85A2	4159516	4303326	N
Df(3R).46	**7628**	**Df(3R)Exel6149**	**85A2;85A5**	**4303326**	**4495369**	**Y**
Df(3R).47	**n/a**	**Df(3R)ED5300**	**85A5;85C3**	**4495323**	**4882428**	**Y**
Df(3R).48	7954	Df(3R)Exel8143	85A5;85B2	4495359	4635805	N
Df(3R).49	7629	Df(3R)Exel6150	85A5;85B6	4495369	4753365	N
Df(3R).50	7725	Df(3R)Exel6258	85B6;85C3	4753365	4878300	N
Df(3R).51	**7630**	**Df(3R)Exel6151**	**85C3;85C11**	**4878300**	**4983814**	**Y**

Df(3R).52	**6756**	**Df(3R)BSC24**	**85C4-9;85D12-14**	**n/a**	**n/a**	**Y**
Df(3R).53	7631	Df(3R)Exel6152	85C11;85D2	4983814	5073164	N
Df(3R).54	**7751**	**Df(3R)Exel6286**	**85D2;85D15**	**5073097**	**5220198**	**Y**
Df(3R).55	7955	Df(3R)Exel9036	85D11;85D11	5152648	5165744	N
Df(3R).56	1931	Df(3R)by10	85D8-12;85E7-F1	n/a	n/a	N
Df(3R).57	1932	Df(3R)by416	85D10-12;85E1-3	n/a	n/a	N
Df(3R).58	1893	Df(3R)by62	85D11-14;85F6	n/a	n/a	N
Df(3R).59	**1937**	**Df(3R)GB104**	**85D12;85E10**	**n/a**	**n/a**	**Y**
Df(3R).60	n/a	Df(3R)ED5429	85D21;85F8	5336047	5874351	N
Df(3R).61	7632	Df(3R)Exel6153	85D21;85E1	5338563	5457581	N
Df(3R).62	7731	Df(3R)Exel6264	85D24;85E5	5376187	5530688	N
Df(3R).63	**7633**	**Df(3R)Exel6154**	**85E9;85F1**	**5619097**	**5754411**	**Y**
Df(3R).64	**7634**	**Df(3R)Exel6155**	**85F1;85F10**	**5754411**	**5915198**	**Y**
Df(3R).65	**7080**	**Df(3R)BSC38**	**85F1-2;86C7-8**	**n/a**	**n/a**	**Y**
Df(3R).66	7732	Df(3R)Exel6265	85F10;85F16	5915198	6015382	N
Df(3R).67	7635	Df(3R)Exel6156	85F16;86B1	6015382	6175785	N
Df(3R).68	7636	Df(3R)Exel6157	86B1;86B2-3	6175785	6209627	N
Df(3R).69	7733	Df(3R)Exel6266	86B2-3;86C2	6213237	6399638	N
Df(3R).70	7637	Df(3R)Exel6158	86C2;86C3	6399638	6464596	N
Df(3R).71	**7638**	**Df(3R)Exel6159**	**86C3;86C7**	**6464596**	**6715088**	**Y**
Df(3R).72	7956	Df(3R)Exel7305	86C6;86C7	6606222	6697995	N
Df(3R).73	**7957**	**Df(3R)Exel7306**	**86C7;86D7**	**6696606**	**6982490**	**Y**
Df(3R).74	n/a	Df(3R)ED5518	86C7;86E16	6710738	7445640	N
Df(3R).75	**n/a**	**Df(3R)ED5514**	**86C7;86E14**	**6710738**	**7394993**	**Y**
Df(3R).76	7958	Df(3R)Exel8152	86D7;86D9	6979586	7026014	N
Df(3R).77	n/a	Df(3R)ED5516	86D10;86E16	7059910	7445640	N
Df(3R).78	7959	Df(3R)Exel7308	86E1;86E8	7069653	7264779	N
Df(3R).79	7962	Df(3R)Exel9018	86E2;86E4	7103606	7178879	N
Df(3R).80	7639	Df(3R)Exel6160	86E4;86E14	7103606	7178879	N
Df(3R).81	7963	Df(3R)Exel8153	86E8;86E14	7261651	7394905	N
Df(3R).82	7743	Df(3R)Exel6276	86E14;86E18	7394904	7495409	N
Df(3R).83	n/a	Df(3R)ED5559	86E14;87B10	7394922	8269757	N

Df(3R).84	**7640**	**Df(3R)Exel6161**	**86E14;86E18**	**7394952**	**7495409**	**Y**
Df(3R).85	**7961**	**Df(3R)Exel8154**	**86E17;86F6**	**7472871**	**7585229**	**Y**
Df(3R).86	7960	Df(3R)Exel7309	86E17;86F1	7541776	7541776	N
Df(3R).87	7964	Df(3R)Exel9019	86F6;86F7	7575337	7590141	N
Df(3R).88	**7965**	**Df(3R)Exel7310**	**86F6;87A1**	**7584271**	**7712793**	**Y**
Df(3R).89	8029	Df(3R)ED5577	86F9;87B13	7654481	8303319	N
Df(3R).90	**n/a**	**Df(3R)ED5558**	**86F9;87B10**	**7654481**	**8269757**	**Y**
Df(3R).91	7642	Df(3R)Exel6163	87A1;87A4	7712866	7824986	N
Df(3R).92	7641	Df(3R)Exel6162	87A1;87B5	7713402	8106825	N
Df(3R).93	7966	Df(3R)Exel7312	87A4;87A7	7803599	7905862	N
Df(3R).94	7967	Df(3R)Exel8155	87A4;87A9	7819284	7939233	N
Df(3R).95	7968	Df(3R)Exel7313	87A9;87B5	7933857	8106492	N
Df(3R).96	7969	Df(3R)Exel7314	87B3;87B8	8061010	8198575	N
Df(3R).97	7643	Df(3R)Exel6164	87B5;87B10	8106825	8268490	N
Df(3R).98	7644	Df(3R)Exel6165	87B5;87B10	8106825	8268490	N
Df(3R).99	7931	Df(3R)Exel7315	87B8;87B9	8194850	8239875	N
Df(3R).100	7970	Df(3R)Exel7316	87B9;87B11	8231675	8274627	N
Df(3R).101	**7932**	**Df(3R)Exel7317**	**87B10;87C3**	**8266959**	**8456337**	**Y**
Df(3R).102	**3355**	**Df(3R)Kar-Sz8**	**87C1-2;87D14-E1**	**n/a**	**n/a**	**Y**
Df(3R).103	7971	Df(3R)Exel8156	87C3;87C5	8456285	8504578	N
Df(3R).104	7645	Df(3R)Exel6166	87C5;87C7	8504578	8546460	N
Df(3R).105	n/a	Df(3R)ED5608	87C7;87D7	8545726	8821416	N
Df(3R).106	7972	Df(3R)Exel7318	87C7;87D5	8549596	8800146	N
Df(3R).107	480	Df(3R)ry27	87D1-2;87F1-2	n/a	n/a	N
Df(3R).108	**1534**	**Df(3R)ry506-85C**	**87D1-2;88E5-6**	**n/a**	**n/a**	**Y**
Df(3R).109	3808	Df(3R)ry75	87D2;87D14-E1	n/a	n/a	N
Df(3R).110	6171	Df(3R)ry619	87D7-9;87E12-F1	n/a	n/a	N
Df(3R).111	7973	Df(3R)Exel8157	87D8;87D10	8838454	8877531	N
Df(3R).112	7646	Df(3R)Exel6167	87D10;87E3	8876908	9084960	N
Df(3R).113	7974	Df(3R)Exel8158	87E3;87E7	9067507	9189980	N
Df(3R).114	7647	Df(3R)Exel6168	87E3;87E8	9105429	9205526	N
Df(3R).115	7975	Df(3R)Exel7320	87E8;87F2	9206766	9369382	N

Df(3R).116	7648	Df(3R)Exel6169	87F2;87F10	9369382	9509692	N
Df(3R).117	n/a	Df(3R)ED5642	87F10;88C2	9509563	10307514	N
Df(3R).118	n/a	Df(3R)ED5622	87F10;88A4	9509563	9809653	N
Df(3R).119	7649	Df(3R)Exel6170	87F10;87F14	9509907	9638553	N
Df(3R).120	7752	Df(3R)Exel6288	87F14;88A4	9638553	9809255	N
Df(3R).121	7650	Df(3R)Exel6171	87F14;88A4	9638639	9809255	N
Df(3R).122	7976	Df(3R)Exel8159	88A4;88B1	9809255	10085129	N
Df(3R).123	7977	Df(3R)Exel7321	88A9;88B1	9951213	10103879	N
Df(3R).124	7734	Df(3R)Exel6267	88B1;88C2	10103460	10307535	N
Df(3R).125	3341	Df(3R)red1	88B1;88D3-4	n/a	n/a	N
Df(3R).126	7978	Df(3R)Exel8160	88C10;88D6	10475121	10701635	N
Df(3R).127	7742	Df(3R)Exel6275	88D1;88D7	10549363	10743994	N
Df(3R).128	7651	Df(3R)Exel6172	88D5;88D7	10643757	10743994	N
Df(3R).129	7652	Df(3R)Exel6173	88D7;88E1	10743994	10920238	N
Df(3R).130	**7979**	**Df(3R)Exel7323**	**88E3;88E12**	**11045834**	**11117494**	**Y**
Df(3R).131	n/a	Df(3R)ED5705	88E12;89A5	11117398	11619536	N
Df(3R).132	**7653**	**Df(3R)Exel6174**	**88F1;88F7**	**11154373**	**11363185**	**Y**
Df(3R).133	**7980**	**Df(3R)Exel7326**	**88F7;89A5**	**11363141**	**11619040**	**Y**
Df(3R).134	**7654**	**Df(3R)Exel6175**	**89A1;89A8**	**11491766**	**11746700**	**Y**
Df(3R).135	7981	Df(3R)Exel8162	89A5;89A8	11618212	11727202	N
Df(3R).136	**7982**	**Df(3R)Exel7327**	**89A8;89B3**	**11727182**	**11867301**	**Y**
Df(3R).137	**7983**	**Df(3R)Exel7328**	**89B1;89B9**	**11835143**	**11983197**	**Y**
Df(3R).137b	3678	Df(3R)sbd45	89B4;89B10	n/a	n/a	N
Df(3R).137c	1920	Df(3R)sbd104	89B5;89C2-7	n/a	n/a	N
Df(3R).138	1467	Df(3R)P115	89B7-8;89E7	n/a	n/a	N
Df(3R).138b		Df(3R)sbd26	89B9-10;89C7-D1	n/a	n/a	N
Df(3R).140	7984	Df(3R)Exel7329	89B14;89B19	12067152	12184315	N
Df(3R).141	**7736**	**Df(3R)Exel6269**	**89B17;89D2**	**12131294**	**12328350**	**Y**
Df(3R).142	7985	Df(3R)Exel7330	89B19;89D2	12177467	12298670	N
Df(3R).143	7986	Df(3R)Exel9055	89C7;89C7	12274903	12279433	N
Df(3R).144	3483	Df(3R)P10	89C1-2;89E1-2	n/a	n/a	N
Df(3R).145	7987	Df(3R)Exel8163	89D2;89D2	12298630	12328350	N

Df(3R).146	**7737**	**Df(3R)Exel6270**	**89D2;89D8**	**12328350**	**12528622**	**Y**
Df(3R).147	**7988**	**Df(3R)Exel8165**	**89E8;89E11**	**12838705**	**12879667**	**Y**
Df(3R).148	**7655**	**Df(3R)Exel6176**	**89E11;89F1**	**12879395**	**12974744**	**Y**
Df(3R).149	**n/a**	**Df(3R)ED5780**	**89E11;90C1**	**12882214**	**13507538**	**Y**
Df(3R).150	n/a	Df(3R)ED5794	90B3;90E4	13365658	13947699	N
Df(3R).152	3010	Df(3R)P14	90C2-D1;91A1-2	n/a	n/a	N
Df(3R).153	**n/a**	**Df(3R)ED5785**	**90C2;90D1**	**13543847**	**13769807**	**Y**
Df(3R).154	3011	Df(3R)Cha7	90F1-F4;91F5	n/a	n/a	N
Df(3R).155	7658	Df(3R)Exel6179	91A5;91B5	14223259	14409970	N
Df(3R).156	**n/a**	**Df(3R)ED2**	**91A5;91F1**	**14224969**	**14922506**	**Y**
Df(3R).157	7659	Df(3R)Exel6180	91B5;91C5	14409970	14566034	N
Df(3R).158	7989	Df(3R)Exel9030	91B5;91B6	14420735	14448184	N
Df(3R).159	7660	Df(3R)Exel6181	91C5;91D5	14566034	14749756	N
Df(3R).160	**n/a**	**Df(3R)ED5911**	**91C5;91F8**	**14568666**	**14991522**	**Y**
Df(3R).161	n/a	Df(3R)ED5938	91D4;92A11	14732373	15467775	N
Df(3R).162	7661	Df(3R)Exel6182	91D5;91E4	14749756	14853107	N
Df(3R).163	7662	Df(3R)Exel6183	91E4;91F8	14853107	14989538	N
Df(3R).164	**n/a**	**Df(3R)ED5942**	**91F12;92B3**	**15052033**	**15660826**	**Y**
Df(3R).165	7663	Df(3R)Exel6184	92A5;92A11	15289196	15467056	N
Df(3R).166	n/a	Df(3R)ED6025	92A11;92E2	15468467	16135258	N
Df(3R).167	7738	Df(3R)Exel6271	92D5;92E2	16030598	16135266	N
Df(3R).168	**7664**	**Df(3R)Exel6185**	**92E2;92F1**	**16135226**	**16376404**	**Y**
Df(3R).169	4962	Df(3R)H-B79	92B3;92F13	n/a	n/a	N
Df(3R).170	**7413**	**Df(3R)BSC43**	**92F7-93A1;93B3-6**	**n/a**	**n/a**	**Y**
Df(3R).171	**7739**	**Df(3R)Exel6272**	**93A7;93B13**	**16783150**	**16938067**	**Y**
Df(3R).172	3340	Df(3R)e-R1	93B6-7;93D2	n/a	n/a	N
Df(3R).173	3357	Df(3R)e-F1	93B6-7;93E1-2	n/a	n/a	N
Df(3R).174	**3013**	**Df(3R)e-BS2**	**93C3-6;93F14-94A1**	**n/a**	**n/a**	**Y**
Df(3R).175	5798	Df(3R)e-GC3	93C6;94A1-4	n/a	n/a	N
Df(3R).176	5805	Df(3R)e-H4	93D1;93F6-8	n/a	n/a	N
Df(3R).178	7665	Df(3R)Exel6186	93E6;93F1	17435102	17536460	N
Df(3R).179	**n/a**	**Df(3R)ED6076**	**93E7;93F14**	**17450191**	**17859514**	**Y**

Df(3R).180	7666	Df(3R)Exel6187	93F1;93F8	17536460	17691795	N
Df(3R).181	7667	Df(3R)Exel6188	93F8;93F14	17691795	17859422	N
Df(3R).182	n/a	Df(3R)ED6085	93F8;94B5	17697681	18404112	N
Df(3R).183	**7668**	**Df(3R)Exel6189**	**93F14;94A2**	**17859422**	**17950445**	**Y**
Df(3R).184	7669	Df(3R)Exel6190	94A2;94A9	17950466	18184665	N
Df(3R).185	**n/a**	**Df(3R)ED6093**	**94A2;94C4**	**17950474**	**18542687**	**Y**
Df(3R).186	7670	Df(3R)Exel6191	94A9;94B2	18184665	18347158	N
Df(3R).187	7740	Df(3R)Exel6273	94B2;94B11	18347158	18483022	N
Df(3R).188	**n/a**	**Df(3R)ED6096**	**94B5;94E7**	**18404059**	**19038348**	**Y**
Df(3R).189	7671	Df(3R)Exel6192	94B11;94D3	18483022	18715446	N
Df(3R).190	n/a	Df(3R)ED6103	94D3;94E9	18714931	19074794	N
Df(3R).191	7672	Df(3R)Exel6193	94D3;94E4	18715437	18991827	N
Df(3R).192	7741	Df(3R)Exel6274	94E4;94E11	18991827	19111693	N
Df(3R).193	**7746**	**Df(3R)Exel6280**	**94E5;94E11**	**19007553**	**19111713**	**Y**
Df(3R).194	**7990**	**Df(3R)Exel9012**	**94E9;94E13**	**19096101**	**19162766**	**Y**
Df(3R).195	**6367**	**Df(3R)slo3**	**94D4-10;96A18**	**n/a**	**n/a**	**Y**
Df(3R).196	7673	Df(3R)Exel6194	94F1;95A4	19201551	19457785	N
Df(3R).197	7674	Df(3R)Exel6195	95A4;95B1	19457785	19540223	N
Df(3R).198	7991	Df(3R)Exel9013	95B1;95B5	19538990	19601223	N
Df(3R).199	7992	Df(3R)Exel9014	95B1;95D1	19589469	19759221	N
Df(3R).200	7675	Df(3R)Exel6196	95C12;95D8	19738513	19847746	N
Df(3R).201	7676	Df(3R)Exel6197	95D8;95E5	19847746	19957689	N
Df(3R).202	n/a	Df(3R)ED6187	95D10;96A7	19868027	20360322	N
Df(3R).203	7677	Df(3R)Exel6198	95E5;95F8	19957689	20087564	N
Df(3R).204	7993	Df(3R)Exel8178	95F8;96A6	20087564	20344004	N
Df(3R).205	7678	Df(3R)Exel6199	95F8;96A2	20087564	20266334	N
Df(3R).206	7948	Df(3R)Exel7357	96A2;96A13	20266334	20467345	N
Df(3R).207	n/a	Df(3R)ED6220	96A7;96C3	20360177	21000152	N
Df(3R).208	**7679**	**Df(3R)Exel6200**	**96A20;96B4**	**20585659**	**20711044**	**Y**
Df(3R).209	**7680**	**Df(3R)Exel6201**	**96C2;96C4**	**20954191**	**21013337**	**Y**
Df(3R).210	**7994**	**Df(3R)Exel9056**	**96C4;96C5**	**21013337**	**21025528**	**Y**
Df(3R).211	2366	Df(3R)XTA1	96B-96D	n/a	n/a	N

Df(3R).212	**7681**	**Df(3R)Exel6202**	**96D1;96E2**	**21109192**	**21330985**	**Y**
Df(3R).213	**7682**	**Df(3R)Exel6203**	**96E2;96E6**	**21330985**	**21452957**	**Y**
Df(3R).214	**5601**	**Df(3R)Espl3**	**96F1;97B1**	**n/a**	**n/a**	**Y**
Df(3R).215	7683	Df(3R)Exel6204	96F9;97A6	21821129	22076527	N
Df(3R).216	**n/a**	**Df(3R)ED6232**	**96F9;97D2**	**21851963**	**22614069**	**Y**
Df(3R).217	**n/a**	**Df(3R)ED6235**	**97B9;97D12**	**22350321**	**22795594**	**Y**
Df(3R).218	n/a	Df(3R)ED6255	97D2;97F1	22614123	23096988	N
Df(3R).219	**7684**	**Df(3R)Exel6205**	**97D12;97E1**	**22790892**	**22885112**	**Y**
Df(3R).220	**7685**	**Df(3R)Exel6206**	**97E1;97E5**	**22885112**	**22972567**	**Y**
Df(3R).222	n/a	Df(3R)ED6265	97E2;98A7	22927346	23394857	N
Df(3R).223	8107	Df(3R)ED6242	97E5;97F1	22955431	23078956	N
Df(3R).224	8106	Df(3R)ED6237	97E5;97F1	22955431	23078633	N
Df(3R).225	7686	Df(3R)Exel6208	97E5;97E11	22972567	23068603	N
Df(3R).226	**2464**	**Df(3R)R38.3**	**97E3-11;98A**	**n/a**	**n/a**	**Y**
Df(3R).227	**3050**	**Df(3R)Sq219**	**97F1-2;98A**	**n/a**	**n/a**	**Y**
Df(3R).228	**7412**	**Df(3R)BSC42**	**98B1-2;98B3-5**	**n/a**	**n/a**	**Y**
Df(3R).229	**7726**	**Df(3R)Exel6259**	**98C4;98D6**	**24142019**	**24416263**	**Y**
Df(3R).230	**7687**	**Df(3R)Exel6209**	**98D6;98E1**	**24416263**	**24490049**	**Y**
Df(3R).231	**7688**	**Df(3R)Exel6210**	**98E1;98F5**	**24490049**	**24805838**	**Y**
Df(3R).232	**7689**	**Df(3R)Exel6211**	**98F5;98F6**	**24805838**	**24879353**	**Y**
Df(3R).233	**430**	**Df(3R)3450**	**98E3;99A6-8**	**n/a**	**n/a**	**Y**
Df(3R).234	n/a	Df(3R)ED6310	98F12;99B2	24953983	25327241	N
Df(3R).235	7690	Df(3R)Exel6212	99A1;99A5	25030264	25103140	N
Df(3R).236	7995	Df(3R)Exel9025	99B10;99B10	25559829	25575231	N
Df(3R).237	**669**	**Df(3R)Dr-rv1**	**99A1-2;99B6-11**	**n/a**	**n/a**	**Y**
Df(3R).238	**5424**	**Df(3R)01215**	**99A6;99C1**	**n/a**	**n/a**	**Y**
Df(3R).239	5091	Df(3R)Ptp99A[R3]	99A7;99A7	n/a	n/a	N
Df(3R).240	**3547**	**Df(3R)127**	**99B5-6;99F1**	**n/a**	**n/a**	**Y**
Df(3R).241	7691	Df(3R)Exel6213	99C5;99D1	25692183	25827755	N
Df(3R).242	1720	Df(3R)ca[nd1]	99B8-10;99B8-10	n/a	n/a	N
Df(3R).243	2352	Df(3R)X3F	99D1-2;99E1	n/a	n/a	N
Df(3R).244	3546	Df(3R)B81	99D3;3Rt	n/a	n/a	N

Df(3R).245	7692	Df(3R)Exel6214	99D5;99E2	25914470	26017969	N
Df(3R).246	**2234**	**Df(3R)R133**	**99E1-5;3Rt**	**n/a**	**n/a**	**Y**
Df(3R).247	2599	Df(3R)tll-g	99F1-2;100B4-5	n/a	n/a	N
Df(3R).248	7693	Df(3R)Exel6215	99F6;99F8	26280966	26378570	N
Df(3R).249	7694	Df(3R)Exel6216	99F6;99F7	26281105	26347557	N
Df(3R).250	**7997**	**Df(3R)Exel7378**	**99F8;100A5**	**26377966**	**26610037**	**Y**
Df(3R).251	**5415**	**DF(3R)tll-e**	**100A2;100C2**	**n/a**	**n/a**	**Y**
Df(3R).252	7918	Df(3R)Exel8194	100A4;100A7	26571483	26703211	N
Df(3R).253	7917	Df(3R)Exel9020	100A4;100A5	26571483	26610037	N
Df(3R).254	7695	Df(3R)Exel6217	100A6;100A7	26635749	26703211	N
Df(3R).255	7727	Df(3R)Exel6260	100A7;100B5	26703211	26984224	N
Df(3R).256	7919	Df(3R)Exel7379	100B2;100B8	26917412	27037034	N
Df(3R).257	7696	Df(3R)Exel6218	100B5;100C1	26984224	27126307	N
Df(3R).258	7697	Df(3R)Exel6219	100C1;100C4	27126307	27277252	N
Df(3R).259	**3369**	**Df(3R)awd-KRB**	**100C;100D**	**n/a**	**n/a**	**Y**
Df(3R).260	**7698**	**Df(3R)Exel6220**	**100D1;100D2**	**27504487**	**27627929**	**Y**
Df(3R).261	**1011**	**Df(3R)faf-BP**	**100D;100F5**	**n/a**	**n/a**	**Y**
Df(3R).262	**5414**	**Df(3R)04661**	**100D2;100F5**	**n/a**	**n/a**	**Y**
Df(3R).263	1452	Df(3R)S1	100F2-3;100F2-3	n/a	n/a	N
Df(3R).264	7747	Df(3R)Exel6282	91B5;91C5	?	?	N

BIBLIOGRAPHY

Akalal, D. B., C. F. Wilson, L. Zong, N. K. Tanaka, K. Ito and R. L. Davis (2006). "Roles for Drosophila mushroom body neurons in olfactory learning and memory." Learn Mem.

Akam, M. (1987). "The molecular basis for metameric pattern in the Drosophila embryo." Development **101**(1): 1-22.

Akam, M. (1998). "Hox genes: from master genes to micromanagers." Curr Biol **8**(19): R676-8.

Akong, K., McCartney, B.M., Peifer, M. (2002). "Drosophila APC2 and APC1 have overlapping roles in the larval brain despite their distinct intracellular localisations." Dev Biol **250**: 71-90.

Alonso, M. C. and C. V. Cabrera (1988). "The *achaete-scute* gene complex of *Drosophila melanogaster* comprises four homologous genes." EMBO J. **7**: 2585-2591.

Artavanis-Tsakonas, S., M. D. Rand and R. J. Lake (1999). "Notch signaling: cell fate control and signal integration in development." Science **284**(5415): 770-6.

Ashburner, M. (1989). *Drosophila*: A laboratory Handbook and Manual. Plainview, NY, Coldspring Harbour Lab. Press.

Bainbridge, S. P. and M. Bownes (1981). "Staging the metamorphosis of Drosophila melanogaster." J Embryol Exp Morphol **66**: 57-80.

Baker, N. E., S. Yu and D. Han (1996). "Evolution of proneural *atonal* expression during distinct regulatory phases in the developing *Drosophila* eye." Curr Biol **6**: 1290-301.

Bate, C. M. (1976). "Embryogenesis of an insect nervous system. I. A map of the thoracic and abdominal neuroblasts in Locusta migratoria." J Embryol Exp Morphol **35**(1): 107-23.

Beadle, G. W., E. L. Tatum and C. W. Clancy (1938). "Food level in relation to rate of development and eye pigmentation in Drosophila." Biol Bull **75**(447-462).

Bello, B., H. Reichert and F. Hirth (2006). "The brain tumor gene negatively regulates neural progenitor cell proliferation in the larval central brain of Drosophila." Development **133**(14): 2639-48.

Bello, B. C., F. Hirth and A. P. Gould (2003). "A pulse of the Drosophila Hox protein Abdominal-A schedules the end of neural proliferation via neuroblast apoptosis." Neuron **37**(2): 209-19.

Berrigan, D. and L. Partridge (1997). "Influence of temperature and activity on the metabolic rate of adult Drosophila melanogaster." Comp Biochem Physiol A Physiol **118**(4): 1301-7.

Betran, E., K. Thornton and M. Long (2002). "Retroposed new genes out of the X in Drosophila." Genome Res **12**(12): 1854-9.

Betschinger, J. and J. A. Knoblich (2004). "Dare to be different: asymmetric cell division in Drosophila, C. elegans and vertebrates." Curr Biol **14**(16): R674-85.

Betschinger, J., K. Mechtler and J. A. Knoblich (2003). "The Par complex directs asymmetric cell division by phosphorylating the cytoskeletal protein Lgl." Nature **422**(6929): 326-30.

Betschinger, J., K. Mechtler and J. A. Knoblich (2006). "Asymmetric segregation of the tumor suppressor brat regulates self-renewal in Drosophila neural stem cells." Cell **124**(6): 1241-53.

Bhat, K. M. (1996). "The patched signaling pathway mediates repression of gooseberry allowing neuroblast specification by wingless during Drosophila neurogenesis." Development **122**(9): 2921-32.

Bhat, K. M. (1999). "Segment polarity genes in neuroblast formation and identity specification during Drosophila neurogenesis." Bioessays **21**(6): 472-85.

Bhat, K. M. and P. Schedl (1997). "Requirement for engrailed and invected genes reveals novel regulatory interactions between engrailed/invected, patched, gooseberry and wingless during Drosophila neurogenesis." Development **124**(9): 1675-88.

Bodenstein, D. (1994). The Postembryonic Development of Drosophila. In *Biology of Drosophila* (ed. M Demerec) pp. 275-367, Cold Spring Harbour Laboratory Press.

Bonini, N. M., W. M. Leiserson and S. Benzer (1993). "The eyes absent gene: genetic control of cell survival and differentiation in the developing Drosophila eye." Cell **72**(3): 379-95.

Booker, R. and J. W. Truman (1987b). "Postembryonic neurogenesis in the CNS of the tobacco hornworm, Manduca sexta. II. Hormonal control of imaginal nest cell degeneration and differentiation during metamorphosis." J Neurosci **7**(12): 4107-14.

Bossing, T., G. Udolph, C. Q. Doe and G. M. Technau (1996). "The embryonic central nervous system lineages of Drosophila melanogaster. I. Neuroblast lineages derived from the ventral half of the neuroectoderm." Dev Biol **179**(1): 41-64.

Bowman, A. B., R. S. Patel-King, S. E. Benashski, J. M. McCaffery, L. S. Goldstein and S. M. King (1999). "Drosophila roadblock and Chlamydomonas LC7: a conserved family of dynein-associated proteins involved in axonal transport, flagellar motility, and mitosis." J Cell Biol **146**(1): 165-80.

Bray, S. J., B. Burke, N. H. Brown and J. Hirsh (1989). "Embryonic expression pattern of a family of Drosophila proteins that interact with a central nervous system regulatory element." Genes Dev **3**(8): 1130-45.

Britton, J. S. and B. A. Edgar (1998). "Environmental control of the cell cycle in Drosophila: nutrition activates mitotic and endoreplicative cells by distinct mechanisms." Development **125**(11): 2149-58.

Broadus, J. and C. Q. Doe (1997). "Extrinsic cues, intrinsic cues and microfilaments regulate asymmetric protein localization in Drosophila neuroblasts." Curr Biol **7**(11): 827-35.

Broadus, J., S. Fuerstenberg and C. Q. Doe (1998). "Staufen-dependent localization of prospero mRNA contributes to neuroblast daughter-cell fate." Nature **391**(6669): 792-5.

Brody, T. and W. F. Odenwald (2000). "Programmed transformations in neuroblast gene expression during Drosophila CNS lineage development." Dev Biol **226**(1): 34-44.

Buenzow, D. E. and R. Holmgren (1995). "Expression of the Drosophila gooseberry locus defines a subset of neuroblast lineages in the central nervous system." Dev Biol **170**(2): 338-49.

Buescher, M., S. L. Yeo, G. Udolph, M. Zavortink, X. Yang, G. Tear and W. Chia (1998). "Binary sibling neuronal cell fate decisions in the Drosophila embryonic central nervous system are nonstochastic and require inscuteable-mediated asymmetry of ganglion mother cells." Genes Dev **12**(12): 1858-70.

Bullock, T. H. and G. A. Horridge (1965). Structure and function in the nervous system of invertebrates. San Fransisco, London: Freeman.

Bump, N. J., M. Hackett, M. Hugunin, S. seshagiri, K. Brady, P. Chen, C. Ferenz, S. Franklin, T. Ghayur, P. Li and e. al. (1995). "Inhibition of ICE family proteases by baculovirus antiproapoptotic protein p35." Science **269**: 1885-1888.

Cai, Y., F. Yu, S. Lin, W. Chia and X. Yang (2003). "Apical complex genes control mitotic spindle geometry and relative size of daughter cells in Drosophila neuroblast and pI asymmetric divisions." Cell **112**(1): 51-62.

Caldwell, M. C. and S. Datta (1998). "Expression of cyclin E or DP/E2F rescues the G1 arrest of trol mutant neuroblasts in the Drosophila larval central nervous system." Mech Dev **79**(1-2): 121-30.

Campos, A. R., D. T. Rosen, S. N. Robinow and K. White (1987). "Molecular analysis of the locus *elav* in *Drosophila Melanogaster:* a gene whose expression is neural specific." Embo J **6**: 425-431.

Campos-Ortega, J. A. (1993a). Early neurogenesis in *Drosophila Melanogaster*. The Development of Drosophila Melanogaster. B. M. and M.-A. A, Cold Spring Harbour Laboratory Press. **II:** 1091-1129.

Campos-Ortega, J. A. (1993b). "Mechanisms of early neurogenesis in Drosophila melongaster." J. Neurobiol. **24**(10): 1305-1327.

Campos-Ortega, J. A. (1997). "Asymmetic division: dynastic intricacies of neuroblast division." Curr Biol **7**(11): R726-8.

Campos-Ortega, J. A. H., V. (1985). The embryonic development of Drosophila Melongaster. Berlin.

Campuzano, S. and J. Modolell (1992). "Patterning of the Drosophila nervous system: the achaete-scute gene complex." Trends Genet **8**(6): 202-8.

Capela, A. and S. Temple (2002). "LeX/ssea-1 is expressed by adult mouse CNS stem cells, identifying them as nonependymal." Neuron **35**(5): 865-75.

Carroll, S. B. (1995). "Homeotic genes and the evolution of arthropods and chordates." Nature **376**(6540): 479-85.

Carroll, S. B., S. D. Weatherbee and J. A. Langeland (1995). "Homeotic genes and the regulation and evolution of insect wing number." Nature **375**(6526): 58-61.

Cattaneo, E. and R. McKay (1990). "Proliferation and differentiation of neuronal stem cells regulated by nerve growth factor." Nature **347**(6295): 762-5.

Caudy, M., H. Vassin, M. Brand, R. Tuma, L. Y. Jan and Y. N. Jan (1988). "*daughterless*, a gene essential for both neurogenesis and sex determination in *Drosophila*, has sequence similarities to *myc* and the *achaete-scute* complex." CELL **55**(1061-1067).

Cayouette, M., A. V. Whitmore, G. Jeffery and M. Raff (2001). "Asymmetric segregation of Numb in retinal development and the influence of the pigmented epithelium." J Neurosci **21**(15): 5643-51.

Cenci, C. and A. P. Gould (2005). "Drosophila Grainyhead specifies late programmes of neural proliferation by regulating the mitotic activity and Hox-dependent apoptosis of neuroblasts." Development **132**(17): 3835-45.

Ceron, J., C. Gonzalez and F. J. Tejedor (2001). "Patterns of cell division and expression of asymmetric cell fate determinants in postembryonic neuroblast lineages of Drosophila." Dev Biol **230**(2): 125-38.

Chan, Y. M., A. Lin, J. McNally, D. Peleg, O. Meyuhas and I. G. Wool (1987). "The primary structure if the rat ribosomal protein L19. A determination from the sequence of nucleotides in a cDNA and from the sequence of amino acids in teh protein." J. Biol. Chem. **262**: 1111-1115.

Chang, T., J. Mazotta, K. Dumstrei, A. Dumitrescu and V. Hartenstein (2001). "Dpp and Hh signaling in the Drosophila embryonic eye field." Development **128**(23): 4691-704.

Chang, T., D. Shy and V. Hartenstein (2003). "Antagonistic relationship between Dpp and EGFR signaling in Drosophila head patterning." Dev Biol **263**(1): 103-13.

Chia, W. and X. Yang (2002). "Asymmetric division of Drosophila neural progenitors." Curr Opin Genet Dev **12**(4): 459-64.

Choi, K. W. and S. Benzer (1994). "Migration of glia along photoreceptor axons in the developing Drosophila eye." Neuron **12**(2): 423-31.

Chotard, C., W. Leung and I. Salecker (2005). "glial cells missing and gcm2 cell autonomously regulate both glial and neuronal development in the visual system of Drosophila." Neuron **48**(2): 237-51.

Chu-LaGraff, Q. and C. Q. Doe (1993). "Neuroblast specification and formation regulated by wingless in the Drosophila CNS." Science **261**(5128): 1594-7.

Church, R. B. (1965). Genetic and biochemical studies of growth in *Drosophila*. Edinburgh, University of Edinburgh.

Cronmiller, C., P. Schedl and T. W. Cline (1989). "Molecular characterisation of *daughterless*, a *Drosophila* sex determination gene with multiple roles in development." Genes Dev **2**: 1666-1676.

Cubas, P., J. F. de Celis, S. Campuzano and J. Modolell (1991). "Proneural clusters of achaete-scute expression and the generation of sensory organs in the Drosophila imaginal wing disc." Genes Dev **5**(6): 996-1008.

Cui, X. and C. Q. Doe (1992). "ming is expressed in neuroblast sublineages and regulates gene expression in the Drosophila central nervous system." Development **116**(4): 943-52.

Curtiss, J. and M. Mlodzik (2000). "Morphogenetic furrow initiation and progression during eye development in *Drosophila*; the roles of decapentaplegic, hedgehog and eyes absent." Development **127**: 1325-36.

Datta, S. (1995). "Control of proliferation activation in quiescent neuroblasts of the Drosophila central nervous system." Development **121**(4): 1173-82.

Datta, S. (1999). "Activation of neuroblast proliferation in explant culture of the Drosophila larval CNS." Brain Res **818**(1): 77-83.

Datta, S. and D. R. Kankel (1992). "l(1)trol and l(1)devl, loci affecting the development of the adult central nervous system in Drosophila melanogaster." Genetics **130**(3): 523-37.

Doe, C. Q. (1992). "Molecular markers for identified neuroblasts and gaglion mother cells in the Drosophila central nervous system." Development **116**: 855-863.

Doe, C. Q. and B. Bowerman (2001). "Asymmetric cell division: fly neuroblast meets worm zygote." Curr Opin Cell Biol **13**(1): 68-75.

Doe, C. Q., Q. Chu-LaGraff, D. M. Wright and M. P. Scott (1991). "The prospero gene specifies cell fates in the Drosophila central nervous system." Cell **65**(3): 451-64.

Doe, C. Q. and C. S. Goodman (1985a). "Early events in insect neurogenesis. I. Development and segmental differences in the pattern of neuronal precursor cells." Dev Biol **111**(1): 193-205.

Doe, C. Q. and C. S. Goodman (1985b). "Early events in insect neurogenesis. II. The role of cell interactions and cell lineage in the determination of neuronal precursor cells." Dev Biol **111**(1): 206-19.

Dumstrei, K., C. Nassif, G. Abbound, A. Aryai and V. Hartenstein (1998). "EGFR sginalling is required for the differentiation and maintenance of neural

progenitors along the dorsal midline of the *Drosophila* embryonic head." Development **125**: 3417-3426.

Dumstrei, K., F. Wang and V. Hartenstein (2003a). "Role of DE-cadherin in neuroblast proliferation, neural morphogenesis, and axon tract formation in Drosophila larval brain development." J Neurosci **23**(8): 3325-35.

Durand, B. R., M. (2000). "A cell intrinsic timer that operates during oligodendrocyte development." Bioessays **22**: 64-71.

Dyer, M. A., F. J. Livesey, C. L. Cepko and G. Oliver (2003). "Prox1 function controls progenitor cell proliferation and horizontal cell genesis in the mammalian retina." Nat Genet **34**(1): 53-8.

Ebens, A. J., H. Garren, B. N. Cheyette and S. L. Zipursky (1993). "The Drosophila anachronism locus: a glycoprotein secreted by glia inhibits neuroblast proliferation." Cell **74**(1): 15-27.

Edenfeld, G., J. Pielage and C. Klambt (2002). "Cell lineage specification in the nervous system." Curr Opin Genet Dev **12**(4): 473-7.

Edlund, T. and T. M. Jessell (1999). "Progression from extrinsic to intrinsic signaling in cell fate specification: a view from the nervous system." Cell **96**(2): 211-24.

Egger, B., J. Q. Boone, N. R. Stevens, A. H. Brand and C. Q. Doe (2007). "Regulation of spindle orientation and neural stem cell fate in the Drosophila optic lobe." Neural Develop **2**: 1.

El Shatoury, H. H. (1956). "Differentiation and metamorphosis of the imaginal optic glomeruli in *Drosophila*." J Embryol Exp Morphol **4**: 240-247.

Fischbach, K. F. (1983). "Neural cell types surviving congenital sensory deprivation in the optic lobes of Drosophila melanogaster." Dev Biol **95**(1): 1-18.

Fischbach, K. F. and G. Technau (1984). "Cell degeneration in the developing optic lobes of the sine oculis and small-optic-lobes mutants of Drosophila melanogaster." Dev Biol **104**(1): 219-39.

Frankfort, B. J. and G. Mardon (2004). "Senseless represses nuclear transduction of Egfr pathway activation." Development **131**(3): 563-70.

Freeman, M. (1996). "Reiterative use of the EGF receptor triggers differentiation of all cell types in the *Drosophila* eye." Cell **87**: 651-660.

Friedrich, M. V., M. Schneider, R. Timpl and S. Baumgartner (2000). "Perlecan domain V of Drosophila melanogaster. Sequence, recombinant analysis and tissue expression." Eur J Biochem **267**(11): 3149-59.

Fuchs, E., T. Tumbar and G. Guasch (2004). "Socializing with the neighbors: stem cells and their niche." Cell **116**(6): 769-78.

Furst, A., Mahowald, A.P. (1985). "Cell division cycle of cultured neural precursor cells from Drosophila." Dev Biol **112**: 467-476.

Gage, F. H. (2000). "Mammalian neural stem cells." Science **287**(5457): 1433-8.

Gage, F. H. (2000). "Mammlian neural stem cells." Science **287**: 1433-1438.

Gallant, P. (2005). "Myc, cell competition, and compensatory proliferation." Cancer Res **65**(15): 6485-7.

Garcia-Bellido, A. (1975). "Genetic control of wing disc development in Drosophila." Ciba Found Symp **0**(29): 161-82.

Garcia-Bellido, A. (1979). "Genetic analysis of the *achaete-scute* system of *Drosophila melanogaster*." Genetics **91**: 491-520.

Garcia-Bellido, A. and J. R. Merriam (1969). "Cell lineage of the imaginal discs in Drosophila gynandromorphs." J Exp Zool **170**(1): 61-75.

Garcia-Bellido, A. and P. Santamaria (1978). "Developmental analysis of the *achaete-scute* system of *Drosophila melanogaster*." Genetics **88**: 469-486.

Gateff, E. (1978). "Malignant neoplasms of genetic origin in Drosophila melanogaster." Science **200**(4349): 1448-59.

Gehring, W. J. (1996). "The master control gene for morphogenesis and evolution of the eye." Genes Cells **1**(1): 11-5.

Ghysen, A. and C. Dambly-Chaudiere (1988). "From DNA to form: the *achaete-scute* complex." Genes Dev **2**: 495-501.

Ghysen, A. and C. Dambly-Chaudiere (1989). "Genesis of the *Drosophila* peripheral nervous system." Trends Genet **5**: 251-255.

Ghysen, A. and C. Dambly-Chaudiere (1990). "Early events in the development of *Drosophila* peripheral nervous system." J. Physiol. (Paris) **84**: 11-20.

Ghysen, A., C. Dambly-Chaudiere, L. Y. Jan and Y. N. Jan (1993). "Cell interactions and gene interactions in peripheral neurogenesis." Genes Dev **7**(5): 723-33.

Giot, L., J. S. Bader, C. Brouwer, A. Chaudhuri, B. Kuang, Y. Li, Y. L. Hao, C. E. Ooi, B. Godwin, E. Vitols, G. Vijayadamodar, P. Pochart, H. Machineni, M. Welsh, Y. Kong, B. Zerhusen, R. Malcolm, Z. Varrone, A. Collis, M. Minto, S. Burgess, L. McDaniel, E. Stimpson, F. Spriggs, J. Williams, K. Neurath, N. Ioime, M. Agee, E. Voss, K. Furtak, R. Renzulli, N. Aanensen, S. Carrolla, E. Bickelhaupt, Y. Lazovatsky, A. DaSilva, J. Zhong, C. A. Stanyon, R. L. Finley, Jr., K. P. White, M. Braverman, T. Jarvie, S. Gold, M. Leach, J. Knight, R. A. Shimkets, M. P. McKenna, J. Chant and J. M. Rothberg (2003). "A protein interaction map of Drosophila melanogaster." Science **302**(5651): 1727-36.

Gonzalez, F., S. Romani, P. Cubas, J. Modolell and S. Campuzano (1989). "Molecular analysis of the asense gene, a member of the achaete-scute complex of Drosophila melanogaster, and its novel role in optic lobe development." Embo J **8**(12): 3553-62.

Gonzalez-Reyes, A., A. Macias and G. Morata (1992). "Autocatalysis and phenotypic expression of Drosophila homeotic gene Deformed: its dependence on polarity and homeotic gene function." Development **116**(4): 1059-68.

Goodman, C. S. and C. Q. Doe (1993). Embryonnic development of the *Drosophila* CNS. In The Development of Drosophila Melanogaster. M. Bate and A. M. Arias, Cold Spring Harbour Laboratory Press. **II:** 1131-1206.

Gould, A., A. Morrison, G. Sproat, R. A. White and R. Krumlauf (1997). "Positive cross-regulation and enhancer sharing: two mechanisms for specifying overlapping Hox expression patterns." Genes Dev **11**(7): 900-13.

Green, P., A. Y. Hartenstein and V. Hartenstein (1993). "The embryonic development of the Drosophila visual system." Cell Tissue Res **273**(3): 583-98.

Greenspan, R. J. (1997). Fly Pushing. The theory and practise of Drosophila genetics, Coldspring Harbours Laboratory Press.

Greenspan, R. J. (2004). Fly pushing: the theory and practice of *Drosophila* genetics. Cold Spring Harbour, Cold Spring Harbour Laboratory Press.

Greenwood, S. and G. Struhl (1999). "Progression of the morphogenetic furrow in the Drosophila eye: the roles of Hedgehog, Decapentaplegic and the Raf pathway." Development **126**(24): 5795-808.

Gritti, A., Frolichsthal-Schoeller, P., Galli, R., Parati, E.A., Cova, L., Pagano, S.F., Bjornson, C.R., Vescovi, A.L. (1999). "Epidermal and fibroblast growth factors behave as mitogenic regulators for a single multiopotent stem cell-like population from the subventricular region of the adult mouse forebrain." J. Neurosci. **19**: 3287-3297.

Hall, P. A. and F. M. Watt (1989). "Stem cells: the generation and maintenance of cellular diversity." Development **106**: 619-633.

Halter, D. A., J. Urban, C. Rickert, S. S. Ner, K. Ito, A. A. Travers and G. M. Technau (1995). "The homeobox gene *repo* is required for the differentiation and maintenance of glia function in the embryonic nervous system of *Drosophila melanogaster*." Development **121**(317-332).

Hanesch, U., K. F. Fischbach and M. Heisenberg (1989). "Neuronal architecture off the central complex in *Drosophila melanogaster*." Cell Tissue Res **257**: 343-366.

Hartenstein, V. and J. A. Campos-Ortega (1984). "Early neurogenesis in wild-type *Drosophila melanogaster*." Roux's Arch. Dev. Biol. **193**: 308-325.

Hay, B. A., T. Wolff and G. M. Rubin (1994). "Expression of baculovirus P35 prevents cell death in *Drosophila*." Development **120**(2121-2129).

Heberlein, U. and K. Moses (1995). "Mechanisms of Drosophila retinal morphogenesis: the virtues of being progressive." Cell **81**(7): 987-90.

Heberlein, U., T. Wolff and G. M. Rubin (1993). "The TGF beta homolog dpp and the segment polarity gene hedgehog are required for propagation of a morphogenetic wave in the Drosophila retina." Cell **75**(5): 913-26.

Heitzler, P., M. Bourouis, L. Ruel, C. Carteret and P. Simpson (1996). "Genes of the Enhancer of split and achaete-scute complexes are required for a regulatory loop between Notch and Delta during lateral signalling in Drosophila." Development **122**(1): 161-71.

Heitzler, P. and P. Simpson (1991). "The choice of cell fate in the epidermis of Drosophila." Cell **64**(6): 1083-92.

Hertweck, H. (1931). "Anatomie und variabilitat des Nervensystems und der Sinnesorgane von *Drosophila melanogaster* (Meigen)." Z Wiss Zool **139**: 559-663.

Hirata, J., H. Nakagoshi, Y. Nabeshima and F. Matsuzaki (1995). "Asymmetric segregation of the homeodomain protein Prospero during Drosophila development." Nature **377**(6550): 627-30.

Hochheimer, A., S. Zhou, S. Zheng, M. C. Holmes and R. Tjian (2002). "TRF2 associates with DREF and directs promoter-selective gene expression in Drosophila." Nature **420**(6914): 439-45.

Hofbauer, A. and J. A. Campos-Ortega (1990). "Proliferation pattern and early differentiation of the optic lobes in *Drosophila melanogaster*." Roux's Arch. Dev. Biol. **198**: 264-274.

Holzbaur, E. L. and R. B. Vallee (1994). "DYNEINS: molecular structure and cellular function." Annu Rev Cell Biol **10**: 339-72.

Honarpour, N., C. Du, J. A. Richardson, R. E. Hammer, X. Wang and J. Herz (2000). "Adult Apaf-1-deficient mice exhibit male infertility." Dev Biol **218**(2): 248-58.

Huang, Z. and S. Kunes (1996). "Hedgehog, transmitted along retinal axons, triggers neurogenesis in the developing visual centers of the Drosophila brain." Cell **86**(3): 411-22.

Huang, Z., B. Z. Shilo and S. Kunes (1998b). "A retinal axon fascicle uses Spitz, an EGF receptor ligand, to construct a synaptic cartridge in the brain of *Drosophila*." Cell **95**: 693-703.

Hummel, T., S. Attix, D. Gunning and S. L. Zipursky (2002). "Temporal control of glial cell migration in the Drosophila eye requires gilgamesh, hedgehog, and eye specification genes." Neuron **33**(2): 193-203.

Ikeshima-Kataoka, H., J. B. Skeath, Y. Nabeshima, C. Q. Doe and F. Matsuzaki (1997). "Miranda directs Prospero to a daughter cell during Drosophila asymmetric divisions." Nature **390**(6660): 625-9.

Isshiki, T. and C. Q. Doe (2004). "Maintaining youth in Drosophila neural progenitors." Cell Cycle **3**(3): 296-9.

Isshiki, T., B. Pearson, S. Holbrook and C. Q. Doe (2001). "Drosophila neuroblasts sequentially express transcription factors which specify the temporal identity of their neuronal progeny." Cell **106**(4): 511-21.

Ito, K. and Y. Hotta (1992). "Proliferation pattern of postembryonic neuroblasts in the brain of Drosophila melanogaster." Dev Biol **149**(1): 134-48.

Ito, K., Urban, J., Technau, G.M. (1995). "Distribution, classification and development or Drosophila glial cells in the late embryonic and early larval ventral nerve cord." Roux's Arch. Dev. Biol. **204**: 284-307.

Ivanov, A. I., A. C. Rovescalli, P. Pozzi, S. Yoo, B. Mozer, H. P. Li, S. H. Yu, H. Higashida, V. Guo, M. Spencer and M. Nirenberg (2004). "Genes required for Drosophila nervous system development identified by RNA interference." Proc Natl Acad Sci U S A **101**(46): 16216-21.

Jacques, T. S., Relvas, J.B., Nishimura, S., Pytela, R., Edwards G.M., Streuli, C.H., Ffrench-Constant, C. (1998). "neural precursor cell migration and division are regulated through different beta integrins." Development **125**: 3167-3177.

Jan, Y. N. and L. Y. Jan (2000). "Polarity in cell division: what frames thy fearful asymmetry?" Cell **100**(6): 599-602.

Jan, Y. N. and L. Y. Jan (2001). "Asymmetric cell division in the Drosophila nervous system." Nat Rev Neurosci **2**(11): 772-9.

Jarman, A. P., E. H. Grell, L. Ackerman, L. Y. Jan and Y. N. Jan (1994). "Atonal is the proneural gene for Drosophila photoreceptors." Nature **369**(6479): 398-400.

Jarman, A. P., Y. Sun, L. Y. Jan and Y. N. Jan (1995). "Role of the proneural gene, atonal, in formation of Drosophila chordotonal organs and photoreceptors." Development **121**(7): 2019-30.

Kaltschmidt, J. A., C. M. Davidson, N. H. Brown and A. H. Brand (2000). "Rotation and asymmetry of the mitotic spindle direct asymmetric cell division in the developing central nervous system." Nat Cell Biol **2**(1): 7-12.

Kambadur, R., K. Koizumi, C. Stivers, J. Nagle, S. J. Poole and W. F. Odenwald (1998). "Regulation of POU genes by castor and hunchback establishes layered compartments in the Drosophila CNS." Genes Dev **12**(2): 246-60.

Kamiya, A., K. Kubo, T. Tomoda, M. Takaki, R. Youn, Y. Ozeki, N. Sawamura, U. Park, C. Kudo, M. Okawa, C. A. Ross, M. E. Hatten, K. Nakajima and A. Sawa (2005). "A schizophrenia-associated mutation of DISC1 perturbs cerebral cortex development." Nat Cell Biol **7**(12): 1167-78.

Kauffmann, R. C., S. Li, P. A. Gallagher, J. Zhang and R. W. Carthew (1996). "Ras1 signaling and transcriptional competence in the R7 cell of Drosophila." Genes Dev **10**(17): 2167-78.

Kilpatrick, T. J. and P. F. Bartlett (1993). "Cloning and growth of multipotential neural precursors: requirements for proliferation and differentiation." Neuron **10**(2): 255-65.

Knoblich, J. A., L. Y. Jan and Y. N. Jan (1995). "Asymmetric segregation of Numb and Prospero during cell division." Nature **377**(6550): 624-7.

Kopan, R. (2002). "Notch: a membrane-bound transcription factor." J Cell Sci **115**(Pt 6): 1095-7.

Kosman, D., Y. T. Ip, M. Levine and K. Arora (1991). "Establishment of the mesoderm-neuroectoderm boundary in the Drosophila embryo." Science **254**(5028): 118-22.

Kraut, R. and J. A. Campos-Ortega (1996). "inscuteable, a neural precursor gene of Drosophila, encodes a candidate for a cytoskeleton adaptor protein." Dev Biol **174**(1): 65-81.

Kraut, R., W. Chia, L. Y. Jan, Y. N. Jan and J. A. Knoblich (1996b). "Role of inscuteable in orienting asymmetric cell divisions in Drosophila." Nature **383**(6595): 50-5.

Kuan, C. Y., K. A. Roth, R. A. Flavell and P. Rakic (2000). "Mechanisms of programmed cell death in the developing brain." Trends Neurosci **23**(7): 291-7.

Kuchinke, U., F. Grawe and E. Knust (1998). "Control of spindle orientation in Drosophila by the Par-3-related PDZ-domain protein Bazooka." Curr Biol **8**(25): 1357-65.

Kulkarni, N. H., A. H. Yamamoto, K. O. Robinson, T. F. Mackay and R. R. Anholt (2002). "The DSC1 channel, encoded by the smi60E locus, contributes to odor-guided behavior in Drosophila melanogaster." Genetics **161**(4): 1507-16.

Kumar, J. P. and K. Moses (2001b). "EGF receptor and Notch signaling act upstream of Eyeless/Pax6 to control eye specification." Cell **104**(5): 687-97.

Kumar, J. P. and K. Moses (2001b). "The EGF receptor and notch signalling pathways control the initiation of the morphogenetic furrow during *Drosophila* eye development." Development **128**: 2689-97.

Lambertsson, A. (1998). "The minute genes in Drosophila and their molecular functions." Adv Genet **38**: 69-134.

Lawrence and S. M. Green (1979b). "Cell lineage in the developing retina of *Drosophila*." Dev Biol **71**: 142-152.

Lee, C. Y., B. D. Wilkinson, S. E. Siegrist, R. P. Wharton and C. Q. Doe (2006). "Brat is a Miranda cargo protein that promotes neuronal differentiation and inhibits neuroblast self-renewal." Dev Cell **10**(4): 441-9.

Lee, T. and L. Luo (1999). "Mosaic analysis with a repressible cell marker (MARCM) for studies of gene function in neuronal morphogenesis." Neuron **22**: 451-461.

Lee, T. and L. Luo (1999b). "Mosaic analysis with a repressible cell marker for studies of gene function in neuronal morphogenesis." Neuron **22**(3): 451-61.

Lee, T. and L. Luo (2001c). "Mosaic analysis with a repressible cell marker (MARCM) for *Drosophila* neural development." Trends Neurosci **24**: 251-4.

Lee, T., C. Winter, S. S. Marticke, A. Lee and L. Luo (2000c). "Essential roles of Drosophila RhoA in the regulation of neuroblast proliferation and dendritic but not axonal morphogenesis." Neuron **25**(2): 307-16.

Leevers, S. J. (2001). "Growth control: invertebrate insulin surprises!" Curr Biol **11**(6): R209-12.

Lehmann, R., U. Dietrich, F. Jimenez and J. A. Campos-Ortega (1981). "Mutations of early neurogenesis in *Drosophila*." Roux's Arch. Dev. Biol. **190**: 226-229.

Lehmann, R., F. Jimenez, U. Dietrich and J. A. Campos-Ortega (1983). "On the phenotype and development of mutants of early neurogenesis in *Drosophila melanogaster*." Roux's Arch. Dev. Biol. **192**: 62-74.

Li, H., D. Harrison, G. Jones, D. Jones and R. L. Cooper (2001). "Alterations in development, behavior, and physiology in Drosophila larva that have reduced ecdysone production." J Neurophysiol **85**(1): 98-104.

Li, L. and W. B. Neaves (2006). "Normal stem cells and cancer stem cells: the niche matters." Cancer Res **66**(9): 4553-7.

Li, L. V., H (2000). "Pan-neural prospero terminated cell proliferation during Drosophila neurogenesis." Genes & Dev. **14**: 147-151.

Li, P., X. Yang, M. Wasser, Y. Cai and W. Chia (1997). "Inscuteable and Staufen mediate asymmetric localization and segregation of prospero RNA during Drosophila neuroblast cell divisions." Cell **90**(3): 437-47.

Lin, D. M. and C. S. Goodman (1994). "Ectopic and increased expresison of Fasciclin II alters motorneuron growth cone guidance." Neuron **13**(507-23).

Lin, H. and T. Schagat (1997). "Neuroblasts: a model for the asymmetric division of stem cells." Trends Genet **13**(1): 33-9.

Lindsley, D. L. Z., G.G. (1992). The Genome of Drosophila Melongaster. New York, New York Academic Press.

Liu, T.-H., Li, L., Vaessin, H. (2002). "Transcription of the Drosophila CKI gene dacapo is regulated by a modular array of cis-regulatory sequences." Mechanisms of development **112**: 25-36.

Liu, Z., R. Steward and L. Luo (2000). "Drosophila Lis1 is required for neuroblast proliferation, dendritic elaboration and axonal transport." Nat Cell Biol **2**(11): 776-83.

Lois, C. and A. Alvarez-Buylla (1993). "Proliferating subventricular zone cells in the adult mammalian forebrain can differentiate into neurons and glia." Proc Natl Acad Sci U S A **90**(5): 2074-7.

Lopez de Heredia, M. and R. P. Jansen (2004). "mRNA localization and the cytoskeleton." Curr Opin Cell Biol **16**(1): 80-5.

Louissaint, A., Jr., S. Rao, C. Leventhal and S. A. Goldman (2002). "Coordinated interaction of neurogenesis and angiogenesis in the adult songbird brain." Neuron **34**(6): 945-60.

Lu, B., L. Ackerman, L. Y. Jan and Y. N. Jan (1999). "Modes of protein movement that lead to the asymmetric localization of partner of Numb during Drosophila neuroblast division." Mol Cell **4**(6): 883-91.

Lu, Y., L. P. Wu and K. V. Anderson (2001). "The antibacterial arm of the drosophila innate immune response requires an IkappaB kinase." Genes Dev **15**(1): 104-10.

Malzacher, P. (1968). "Die embryogeneses des gehirns paurometaboler Insekten. Untersuchungen an *Carausius morosus* und *Periplaneta americana*." A. Morph. Okol. Tiere **62**: 103-161.

Mann, R. S. and G. Morata (2000). "The developmental and molecular biology of genes that subdivide the body of Drosophila." Annu Rev Cell Dev Biol **16**: 243-71.

Mardon, G., N. M. Solomon and G. M. Rubin (1994). "*dachshund* encodes a nuclear protein required for normal eye and leg development in *Drosophila*." Development **120**: 3473-3486.

Martin-Bermudo, M. D., C. Martinez, A. Rodriguez and F. Jimenez (1991). "Distribution and function of the lethal of scute gene product during early neurogenesis in Drosophila." Development **113**(2): 445-54.

Martino, G. and S. Pluchino (2006). "The therapeutic potential of neural stem cells." Nat Rev Neurosci **7**(5): 395-406.

Matsuzaki, F., K. Koizumi, C. Hama, T. Yoshioka and Y. Nabeshima (1992). "Cloning of the Drosophila prospero gene and its expression in ganglion mother cells." Biochem Biophys Res Commun **182**(3): 1326-32.

Maurange, C. and A. P. Gould (2005). "Brainy but not too brainy: starting and stopping neuroblast divisions in Drosophila." Trends Neurosci **28**(1): 30-6.

McDonald, J. A., S. Holbrook, T. Isshiki, J. Weiss, C. Q. Doe and D. M. Mellerick (1998). "Dorsoventral patterning in the Drosophila central nervous system: the vnd homeobox gene specifies ventral column identity." Genes Dev **12**(22): 3603-12.

McGinnis, W. and R. Krumlauf (1992). "Homeobox genes and axial patterning." Cell **68**: 283-302.

McKay, R. (1997). "Stem cells in the central nervous system." Science **276**(5309): 66-71.

Meinertzhagen, I. A. and T. E. Hanson (1993). Chapter 24: The development of the optic lobe. The development of Drosophila melanogaster. M.-A. A. Bate M. Cold Spring Harbor, Cold Spring Harbor Laboratory Press. **2:** 1363-1491.

Melzer, R. R. and H. F. Paulus (1989). "Evolutionswege zum Larvalauge der Insekten - Die Stemmata der hoheren Dipteren und ihre Abwandlung zum BOlwig-Organ." Z. Zool. Syst. Evol. Forsch **27**: 200-245.

Meyerowitz, E. M. and D. R. Kankel (1978). "A genetic analysis of visual system development in *Drosophila melanogaster*." Dev Biol **62**(112-142).

Morata, G. and P. Ripoll (1975). "*Minutes*: mutants autonomously affecting cell division rate in Drosophila." Dev Biol **42**: 211-221.

Morrison, S. J., N. M. Shah and D. J. Anderson (1997a). "Regulatory mechanisms in stem cell biology." Cell **88**(3): 287-98.

Neer, E. J., C. J. Schmidt, R. Nambudripad and T. F. Smith (1994). "The ancient regulatory-protein family of WD-repeat proteins." Nature **371**(6495): 297-300.

Neufeld, T. P., A. F. de la Cruz, L. A. Johnston and B. A. Edgar (1998). "Coordination of growth and cell division in the Drosophila wing." Cell **93**(7): 1183-93.

Newsome, T. P., B. Asling and B. J. Dickson (2000). "Analysis of Drosophila photoreceptor axon guidance in eye-specific mosaics." Development **127**(4): 851-60.

Nolo, R., L. A. Abbott and H. J. Bellen (2000). "Senseless, a Zn finger transcription factor, is necessary and sufficient for sensory organ development in Drosophila." Cell **102**(3): 349-62.

Noveen, A., A. Daniel and V. Hartenstein (2000). "Early development of the *Drosophila* mushroom body: the roles of *eyeless* and *dachshund*." Development **127**: 3475-3488.

Orlando, V. (2003). "Polycomb, epigenomes, and control of cell identity." Cell **112**(5): 599-606.

Ostenfeld, T. and C. N. Svendsen (2003). "Recent advances in stem cell neurobiology." Adv Tech Stand Neurosurg **28**: 3-89.

Palmer, T. D., A. R. Willhoite and F. H. Gage (2000). "Vascular niche for adult hippocampal neurogenesis." J Comp Neurol **425**(4): 479-94.

Panicker, M. and M. S. Rao (2000). Stem cells and Neurogenesis., CSH Press.

Park, Y., C. Rangel, M. M. Reynolds, M. C. Caldwell, M. Johns, M. Nayak, C. J. Welsh, S. McDermott and S. Datta (2003a). "Drosophila perlecan modulates FGF and hedgehog signals to activate neural stem cell division." Dev Biol **253**(2): 247-57.

Parmentier, M. L., D. Woods, S. Greig, P. G. Phan, A. Radovic, P. Bryant and C. J. O'Kane (2000). "Rapsynoid/partner of inscuteable controls asymmetric division of larval neuroblasts in Drosophila." J Neurosci **20**(14): RC84.

Paro, R. (1990). "Imprinting a determined state into the chromatin of Drosophila." Trends Genet **6**(12): 416-21.

Paro, R. (1993). "Mechanisms of heritable gene repression during development of Drosophila." Curr Opin Cell Biol **5**(6): 999-1005.

Pastink, A., E. Heemskerk, M. J. Nivard, C. J. van Vilet and E. W. Vogel (1991). "Mutational specificity of ethyl methanesulphonate in excision-repair-proficient

and -deficient strains of *Drosophila melanogaster*." Mol. Gen. Genet. **2**: 213-218.

Pearson, B. J. and C. Q. Doe (2003). "Regulation of neuroblast competence in Drosophila." Nature **425**(6958): 624-8.

Pearson, B. J. and C. Q. Doe (2004). "Specification of temporal identity in the developing nervous system." Annu Rev Cell Dev Biol **20**: 619-47.

Pereanu, W., D. Shy and V. Hartenstein (2005). "Morphogenesis and proliferation of the larval brain glia in Drosophila." Dev Biol **283**(1): 191-203.

Perez, S. E. and H. Stellar (1996). "Migration of glial cells into retinal axon target field in *Drosophila melanogaster*." J. Neurobiol. **30**: 359-373.

Perez, S. E. and H. Steller (1996). "Migration of glial cells into retinal axon target field in Drosophila melanogaster." J Neurobiol **30**(3): 359-73.

Peterson, C., G. E. Carney, B. J. Taylor and K. White (2002). "reaper is required for neuroblast apoptosis during Drosophila development." Development **129**(6): 1467-76.

Petronczki, M. and J. A. Knoblich (2001). "DmPAR-6 directs epithelial polarity and asymmetric cell division of neuroblasts in Drosophila." Nat Cell Biol **3**(1): 43-9.

Phillis, R., D. Statton, P. Caruccio and R. K. Murphey (1996). "Mutations in the 8 kDa dynein light chain gene disrupt sensory axon projections in the Drosophila imaginal CNS." Development **122**(10): 2955-63.

Pirrotta, V. (1995). "Chromatin complexes regulating gene expression in Drosophila." Curr Opin Genet Dev **5**(4): 466-72.

Poeck, B., S. Fischer, D. Gunning, S. L. Zipursky and I. Salecker (2001). "Glial cells mediate target layer selection of retinal axons in the developing visual system of *Drosophila*." Neuron **29**: 99-113.

Pollock, J. A. and S. NBenzer (1988). "Transcript localisation of four opsin genes in the three visual organs of *Drosophila;* RH2 is ocellus specific." Nature **333**: 779-782.

Pompeiano, M., A. J. Blaschke, R. A. Flavell, A. Srinivasan and J. Chun (2000). "Decreased apoptosis in proliferative and postmitotic regions of the Caspase 3-deficient embryonic central nervous system." J Comp Neurol **423**(1): 1-12.

Porkka, K. P., T. L. Tammela, R. L. Vessella and T. Visakorpi (2004). "RAD21 and KIAA0196 at 8q24 are amplified and overexpressed in prostate cancer." Genes Chromosomes Cancer **39**(1): 1-10.

Potten, C. S. and M. Loeffler (1990). "Stem cells: attributes, cycles, spirals, pitfalls and uncertainties. Lessons for and from the crypt." Development **110**(4): 1001-20.

Poulson, D. F. (1937). "Chromosomal deficiencies and embryonic develipment of *Drosophila melanogaster*." Proc Natl Acad Sci U S A **23**: 133-137.

Poulson, D. F. (1950). Histogenesis, organogenesis and differentiation in the embryo of *Drosophila melanogaster*. Biology of Drosophila. M. Demerec. New York, John Wiley: 168-274.

Power, M. E. (1943). "The effect of reduction in numbers of ommatidia upon the brain of *Drosophila melanogaster*." J. Exp. Zool. **94**: 33-71.

Prokop, A., S. Bray, E. Harrison and G. M. Technau (1998). "Homeotic regulation of segment-specific differences in neuroblast numbers and proliferation in the Drosophila central nervous system." Mech Dev **74**(1-2): 99-110.

Prokop, A. and G. M. Technau (1991). "The origin of postembryonic neuroblasts in the ventral nerve cord of Drosophila melanogaster." Development **111**(1): 79-88.

Prokop, A. and G. M. Technau (1994). "Early tagma-specific commitment of Drosophila CNS progenitor NB1-1." Development **120**(9): 2567-78.

Prokopenko, S. N. and W. Chia (2005). "When timing is everything: role of cell cycle regulation in asymmetric division." Semin Cell Dev Biol **16**(3): 423-37.

Qian, X., S. K. Goderie, Q. Shen, J. H. Stern and S. Temple (1998). "Intrinsic programs of patterned cell lineages in isolated vertebrate CNS ventricular zone cells." Development **125**(16): 3143-52.

Raff, M. C., B. A. Barres, J. F. Burne, H. S. Coles, Y. Ishizaki and M. D. Jacobson (1993). "Programmed cell death and the control of cell survival: lessons from the nervous system." Science **262**(5134): 695-700.

Rangarajan, R., Q. Gong and U. Gaul (1999). "Migration and function of glia in the developing Drosophila eye." Development **126**(15): 3285-92.

Rao, M. S. (1999). "Multipotent and restricted precursors in the central nervous system." Anat Rec **257**(4): 137-48.

Ready, D. F., , T. E. Hanson and S. Benzer (1976). "Development of the Drosophila retina, a neurocrystalline lattice." Dev Biol **53**(2): 217-40.

Reinke, R. and S. L. Zipursky (1988). "Cell-cell interaction in the Drosophila retina: the bride of sevenless gene is required in photoreceptor cell R8 for R7 cell development." Cell **55**(2): 321-30.

Renfranz, P. J. and S. Benzer (1989). "Monoclonal antibody probes discriminate early and late mutant defects in development of the Drosophila retina." Dev Biol **136**(2): 411-29.

Reuter, J. E., T. M. Nardine, A. Penton, P. Billuart, E. K. Scott, T. Usui, T. Uemura and L. Luo (2003). "A mosaic genetic screen for genes necessary for Drosophila mushroom body neuronal morphogenesis." Development **130**(6): 1203-13.

Reynolds, B. A., W. Tetzlaff and S. Weiss (1992). "A multipotent EGF-responsive striatal embryonic progenitor cell produces neurons and astrocytes." J Neurosci **12**(11): 4565-74.

Reynolds, B. A. and S. Weiss (1992). "Generation of neurons and astrocytes from isolated cells of the adult mammalian central nervous system." Science **255**(5052): 1707-10.

Rhyu, M. S., L. Y. Jan and Y. N. Jan (1994). "Asymmetric distribution of numb protein during division of the sensory organ precursor cell confers distinct fates to daughter cells." Cell **76**(3): 477-91.

Riddiford, L. M. (1993). Ch. 15: Hormones and *Drosophila* development. The development of Drosophila melanogaster. M.-A. A. Bate M. Cold Spring Harbor, Cold Spring Harbor Laboratory Press. **2:** 899-939.

Risau, W. (1997). "Mechanisms of angiogenesis." Nature **386**(6626): 671-4.

Robinow, S. and K. White (1988). "The locus *elav* of *Drosophila Melanogaster* is expressed in neurons at all developmental stages." Dev Biol **126**: 294-303.

Rolls, M. M., R. Albertson, H. P. Shih, C. Y. Lee and C. Q. Doe (2003). "Drosophila aPKC regulates cell polarity and cell proliferation in neuroblasts and epithelia." J Cell Biol **163**(5): 1089-98.

Romani, S., S. Campuzano, E. R. Macagno and J. Modolell (1989). "Expression of *achaete* and *scute* genes in *Drosophila* imaginal discs and their function in sensory organ development." Genes Dev **3**: 997-1007.

Satija, R. C. A., V. (1967). "Postembryonic development of the eye and its ganglia of *Drosophila melanogaster*." Res Bull Panjab Univ Sci **18**: 79-93.

Schaefer, M., A. Shevchenko and J. A. Knoblich (2000). "A protein complex containing Inscuteable and the Galpha-binding protein Pins orients asymmetric cell divisions in Drosophila." Curr Biol **10**(7): 353-62.

Schmid, A., A. Chiba and C. Q. Doe (1999). "Clonal analysis of Drosophila embryonic neuroblasts: neural cell types, axon projections and muscle targets." Development **126**(21): 4653-89.

Schmidt (1996).

Schmidt, H., C. Rickert, T. Bossing, O. Vef, J. Urban and G. M. Technau (1997). "The embryonic central nervous system lineages of Drosophila melanogaster. II. Neuroblast lineages derived from the dorsal part of the neuroectoderm." Dev Biol **189**(2): 186-204.

Schober, M., M. Schaefer and J. A. Knoblich (1999). "Bazooka recruits Inscuteable to orient asymmetric cell divisions in Drosophila neuroblasts." Nature **402**(6761): 548-51.

Schulze, S. R., D. A. Sinclair, K. A. Fitzpatrick and B. M. Honda (2005). "A genetic and molecular characterization of two proximal heterochromatic genes on chromosome 3 of Drosophila melanogaster." Genetics **169**(4): 2165-77.

Scott, E. K., T. Lee and L. Luo (2001). "enok encodes a Drosophila putative histone acetyltransferase required for mushroom body neuroblast proliferation." Curr Biol **11**(2): 99-104.

Selleck, S. B. and H. Steller (1991). "The influence of retinal innervation on neurogenesis in the first optic ganglion of Drosophila." Neuron **6**(1): 83-99.

Shen, C. P., L. Y. Jan and Y. N. Jan (1997). "Miranda is required for the asymmetric localization of Prospero during mitosis in Drosophila." Cell **90**(3): 449-58.

Shen, Q., S. K. Goderie, L. Jin, N. Karanth, Y. Sun, N. Abramova, P. Vincent, K. Pumiglia and S. Temple (2004). "Endothelial cells stimulate self-renewal and expand neurogenesis of neural stem cells." Science **304**(5675): 1338-40.

Siegrist, S. E. and C. Q. Doe (2006). "Extrinsic cues orient the cell division axis in *Drosophila* embryonic neuroblasts." Development **133**(3): 529-36.

Skeath, J. B. (1998). "The Drosophila EGF receptor controls the formation and specification of neuroblasts along the dorsal-ventral axis of the Drosophila embryo." Development **125**(17): 3301-12.

Skeath, J. B. (1999). "At the nexus between pattern formation and cell-type specification: the generation of individual neuroblast fates in the Drosophila embryonic central nervous system." Bioessays **21**(11): 922-31.

Skeath, J. B. and S. B. Carroll (1991). "Regulation of achaete-scute gene expression and sensory organ pattern formation in the Drosophila wing." Genes Dev **5**(6): 984-95.

Skeath, J. B., Carroll, S.B. (1992). "regulation of proneural gene expression and cell fate during neuroblast segregation in the drosophila embryo." Development **114**: 939-946.

Skeath, J. B., G. F. Panganiban and S. B. Carroll (1994). "The ventral nervous system defective gene controls proneural gene expression at two distinct steps during neuroblast formation in Drosophila." Development **120**(6): 1517-24.

Skeath, J. B. and S. Thor (2003). "Genetic control of Drosophila nerve cord development." Curr Opin Neurobiol **13**(1): 8-15.

Skeath, J. B., Y. Zhang, R. Holmgren, S. B. Carroll and C. Q. Doe (1995). "Specification of neuroblast identity in the Drosophila embryonic central nervous system by gooseberry-distal." Nature **376**(6539): 427-30.

Slack, C., W. G. Somers, R. Sousa-Nunes, W. Chia and P. M. Overton (2006). "A mosaic genetic screen for novel mutations affecting Drosophila neuroblast divisions." BMC Genet **7**: 33.

Sliter, T. J., V. C. Henrich, R. L. Tucker and L. I. Gilbert (1989). "The genetics of the Dras3-Roughened-ecdysoneless chromosomal region (62B3-4 to 62D3-4) in Drosophila melanogaster: analysis of recessive lethal mutations." Genetics **123**(2): 327-36.

Sommer, L. R., M. (2002). "Neural stem cells and regulation of cell number." Progress in Neurobiology **66**: 1-18.

Song, H., C. F. Stevens and F. H. Gage (2002). "Astroglia induce neurogenesis from adult neural stem cells." Nature **417**(6884): 39-44.

Song, Q. and L. I. Gilbert (1994). "S6 phosphorylation results from prothoracicotropic hormone stimulation of insect prothoracic glands: a role for S6 kinase." Dev Genet **15**(4): 332-8.

Spana, E. P. and C. Q. Doe (1995). "The prospero transcription factor is asymmetrically localized to the cell cortex during neuroblast mitosis in Drosophila." Development **121**(10): 3187-95.

Spana, E. P. and C. Q. Doe (1996). "Numb antagonizes Notch signaling to specify sibling neuron cell fates." Neuron **17**(1): 21-6.

Spradling, A., D. Drummond-Barbosa and T. Kai (2001). "Stem cells find their niche." Nature **414**(6859): 98-104.

Steller, H., K. F. Fischbach and G. M. Rubin (1987). "*disconnected:* a locus required for neuronal pathway formation in the visual system of *Drosophila*." Cell **50**: 1139-1153.

Stemple, D. L. and D. J. Anderson (1992). "Isolation of a stem cell for neurons and glia from the mammalian neural crest." Cell **71**(6): 973-85.

Stern, C. (1954). "Two or three bristles." Am Sci **42**: 213-247.

Strausfeld, N. J. (1976). Atlas of insect brain. Heidelberg, Germany: Springer.

Struhl, G. and A. Adachi (1998). "Nuclear access and action of notch in vivo." Cell **93**(4): 649-60.

Struhl, G. and R. White (1985). "Regulation of the *Ultrabithorax* gene of *Drosophila* by other bithorax complex genes." Cell **43**: 507-519.

Suprenant, K. A. (1993). "Microtubules, ribosomes, and RNA: evidence for cytoplasmic localization and translational regulation." Cell Motil Cytoskeleton **25**(1): 1-9.

Suprenant, K. A., K. Dean, J. McKee and S. Hake (1993). "EMAP, an echinoderm microtubule-associated protein found in microtubule-ribosome complexes." J Cell Sci **104**(2): 445-50.

Suprenant, K. A., L. B. Tempero and L. E. Hammer (1989). "Association of ribosomes with in vitro assembled microtubules." Cell Motil Cytoskeleton **14**(3): 401-15.

Suzuki, T. and K. Saigo (2000). "Transcriptional regulation of atonal required for Drosophila larval eye development by concerted action of eyes absent, sine oculis and hedgehog signaling independent of fused kinase and cubitus interruptus." Development **127**(7): 1531-40.

Tabata, T. and T. B. Kornberg (1994). "Hedgehog is a signaling protein with a key role in patterning Drosophila imaginal discs." Cell **76**(1): 89-102.

Taghert, P. H., C. Q. Doe and C. S. Goodman (1984). "Cell determination and regulation during development of neuroblasts and neurones in grasshopper embryos." Nature **307**: 163-165.

Technau, G. M. and J. A. Campos-Ortega (1985). "Fate mapping in wildtype *Drosophila melanogaster*. II. Injections of horseradish peroxidase in cells of the early gastrula stage." Roux's Arch. Dev. Biol. **194**: 445-454.

Temple, S. (1989). "Division and differentiation of isolated CNS blast cells in microculture." Nature **340**(6233): 471-3.

Temple, S. (2001). "The development of neural stem cells." Nature **414**(6859): 112-7.

Tio, M. and K. Moses (1997). "The Drosophila TGF alpha homolog Spitz acts in photoreceptor recruitment in the developing retina." Development **124**(2): 343-51.

Tio, M., G. Udolph, X. Yang and W. Chia (2001). "cdc2 links the Drosophila cell cycle and asymmetric division machineries." Nature **409**(6823): 1063-7.

Tomlinson, A., D. D. Bowtell, E. Hafen and G. M. Rubin (1987b). "Localization of the sevenless protein, a putative receptor for positional information, in the eye imaginal disc of Drosophila." Cell **51**(1): 143-50.

Tomlinson, A. and D. F. Ready (1987). "Neuronal differentiation in the *Drosophila* ommatidium." Dev Biol **120**: 366-76.

Tropepe, V., Sibilia, M., Ciruna, B.G., Rossant, J., Wagner, E.F., Van der Kooy, D. (1999). "Distinct neural stem cells prolfierate in response to EGF anf FGF in the developing mouse telencephalon." Dev. Biol. **208**: 166-188.

Truman, J. W. (1990). "Metamorphosis of the central nervous system of Drosophila." J Neurobiol **21**(7): 1072-84.

Truman, J. W. and M. Bate (1988). "Spatial and temporal patterns of neurogenesis in the central nervous system of Drosophila melanogaster." Dev Biol **125**(1): 145-57.

Truman, J. W., W. S. Talbot, S. E. Fahrbach and D. S. Hogness (1994). "Ecdysone receptor expression in the CNS correlates with stage-specific responses to ecdysteroids during Drosophila and Manduca development." Development **120**(1): 219-34.

Truman, J. W., B. J. Taylor and T. A. Awad (1993). Formation of the adult nervous system. The Development of *Drosophila Melanogaster*. M. Bate and A. Martinez Arias, Cold Spring Harbour Laboratory Press. **2:** 1245-1275.

Tzolovsky, G., H. Millo, S. Pathirana, T. Wood and M. Bownes (2002). "Identification and phylogenetic analysis of Drosophila melanogaster myosins." Mol Biol Evol **19**(7): 1041-52.

Udolph, G., P. Rath and W. Chia (2001). "A requirement for Notch in the genesis of a subset of glial cells in the Drosophila embryonic central nervous system which arise through asymmetric divisions." Development **128**(8): 1457-66.

Uemura, T., S. Shepherd, L. Ackerman, L. Y. Jan and Y. N. Jan (1989). "numb, a gene required in determination of cell fate during sensory organ formation in Drosophila embryos." Cell **58**(2): 349-60.

Urbach, R., R. Schnabel and G. M. Technau (2003a). "The pattern of neuroblast formation, mitotic domains and proneural gene expression during early brain development in Drosophila." Development **130**(16): 3589-606.

Urbach, R. and G. M. Technau (2003b). "Molecular markers for identified neuroblasts in the developing brain of Drosophila." Development **130**(16): 3621-37.

Urbach, R. and G. M. Technau (2003c). "Segment polarity and DV patterning gene expression reveals segmental organization of the Drosophila brain." Development **130**(16): 3607-20.

Urbach, R. and G. M. Technau (2004). "Neuroblast formation and patterning during early brain development in Drosophila." Bioessays **26**(7): 739-51.

Vaessin, H., M. Brand, L. Y. Jan and Y. N. Jan (1994). "daughterless is essential for neuronal precursor differentiation but not for initiation of neuronal precursor formation in Drosophila embryo." Development **120**(4): 935-45.

Vaessin, H., E. Grell, E. Wolff, E. Bier, L. Y. Jan and Y. N. Jan (1991). "prospero is expressed in neuronal precursors and encodes a nuclear protein that is involved in the control of axonal outgrowth in Drosophila." Cell **67**(5): 941-53.

Van Duin, M., R. Van Marion, K. Vissers, J. E. Watson, W. M. Van Weerden, F. H. Schroder, W. C. Hop, T. H. Van der Kwast, C. Collins and H. Van Dekken (2005). "High-resolution array comparative genomic hybridization of chromosome arm 8q: evaluation of genetic progression markers for prostate cancer." Genes Chromosomes Cancer **44**(4): 438-49.

Villares, R. and C. V. Cabrera (1987). "The *achaete-scute* gene complex of *D. melanogaster:* conserved domains in a subset of genes required for neurogenesis and their homology to *myc*." Cell **50**: 415-424.

Voigt, A., R. Pflanz, U. Schafer and H. Jackle (2002). "Perlecan participates in proliferation activation of quiescent Drosophila neuroblasts." Dev Dyn **224**(4): 403-12.

Von Ohlen, T. and C. Q. Doe (2000). "Convergence of dorsal, dpp, and egfr signaling pathways subdivides the drosophila neuroectoderm into three dorsal-ventral columns." Dev Biol **224**(2): 362-72.

Wakamatsu, Y., T. M. Maynard, S. U. Jones and J. A. Weston (1999). "NUMB localizes in the basal cortex of mitotic avian neuroepithelial cells and modulates neuronal differentiation by binding to NOTCH-1." Neuron **23**(1): 71-81.

Wallace, K., T. H. Liu and H. Vaessin (2000). "The pan-neural bHLH proteins DEADPAN and ASENSE regulate mitotic activity and cdk inhibitor dacapo expression in the Drosophila larval optic lobes." Genesis **26**(1): 77-85.

Watt, F. M. H., B.L. (2000). "Out of Eden: stem cells and theirs niches." Science **287**(1427-1430).

Weiss, J. B., T. Von Ohlen, D. M. Mellerick, G. Dressler, C. Q. Doe and M. P. Scott (1998). "Dorsoventral patterning in the Drosophila central nervous system: the intermediate neuroblasts defective homeobox gene specifies intermediate column identity." Genes Dev **12**(22): 3591-602.

White, K., M. E. Grether, J. M. Abrams, L. Young, K. Farrell and H. Stellar (1994). "Genetic control of programmed cell death in *Drosophila*." Science **264**: 677-683.

White, K. and D. R. Kankel (1978). "Patterns of cell division and cell movement in the formation of the imaginal nervous system of *Drosophila melanogaster*." Dev Biol **65**: 296-321.

White, R. A., Tahaoglu, E., Steller, H. (1996). "Cell killing by the Drosophila gene reaper." Science **271**(5250): 805-807.

Winberg, M. L., S. E. Perez and H. Steller (1992). "Generation and early differentiation of glial cells in the first optic ganglion of Drosophila melanogaster." Development **115**(4): 903-11.

Wodarz, A. and W. B. Huttner (2003). "Asymmetric cell division during neurogenesis in Drosophila and vertebrates." Mech Dev **120**(11): 1297-309.

Wodarz, A., A. Ramrath, A. Grimm and E. Knust (2000). "Drosophila atypical protein kinase C associates with Bazooka and controls polarity of epithelia and neuroblasts." J Cell Biol **150**(6): 1361-74.

Wodarz, A., A. Ramrath, U. Kuchinke and E. Knust (1999). "Bazooka provides an apical cue for Inscuteable localization in Drosophila neuroblasts." Nature **402**(6761): 544-7.

Wolff, T. and D. F. Ready (1991). "Cell death in normal and rough eye mutants of *Drosophila*." Development **113**: 825-839.

Wolff, T. and D. F. Ready (1993). Chapter 22: pattern fomration in the *Drosophila* retina. The development of *Drosophila melanogaster*. M.-A. A. Bate M. Cold Spring Harbor, Cold Spring Harbor Laboratory Press. **2:** 1277-1325.

Wurmser, A. E., T. D. Palmer and F. H. Gage (2004). "Neuroscience. Cellular interactions in the stem cell niche." Science **304**(5675): 1253-5.

Yang, L. and N. E. Baker (2001). "Role of the EGFR/Ras/Raf pathway in specification of photoreceptor cells in the *Drosophila* retina." Development **128**: 1183-1191.

Younossi-Hartenstein, A., C. Nassif, P. Green and V. Hartenstein (1996). "Early neurogenesis of the Drosophila brain." J Comp Neurol **370**(3): 313-29.

Yu, F., Y. Cai, R. Kaushik, X. Yang and W. Chia (2003a). "Distinct roles of Galphai and Gbeta13F subunits of the heterotrimeric G protein complex in the mediation of Drosophila neuroblast asymmetric divisions." J Cell Biol **162**(4): 623-33.

Yu, F., X. Morin, Y. Cai, X. Yang and W. Chia (2000). "Analysis of partner of inscuteable, a novel player of Drosophila asymmetric divisions, reveals two distinct steps in inscuteable apical localization." Cell **100**(4): 399-409.

Zhai, R. G., P. R. Hiesinger, T.-W. Koh, P. Verstreken, K. L. Schulze, Y. Cao, H. Jafar-Nejad, K. K. Norga, H. Pan, V. Bayat, M. P. Greenbaum and H. J. Bellen (2003). "Mapping Drosophila mutations with molecularly defined P element insertions." Proc. Nat. Acad. Sci. USA **19**: 10860-10865.

Zipursky, S. L., T. R. Venkatesh, D. B. Teplow and S. Benzer (1984). "Neuronal development in the Drosophila retina: monoclonal antibodies as molecular probes." Cell **36**(1): 15-26.